TU/e EINDHOVEN UNIVERSITY OF TECHNOLOGY

Activation of demand flexibility for heating systems in buildings

Citation for published version (APA):
Finck, C. J. (Accepted/In press). *Activation of demand flexibility for heating systems in buildings: Real-life demonstration of optimal control for power-to-heat and thermal energy storage*. Eindhoven University of Technology.

Document status and date:
Accepted/In press: 07/12/2021

Document Version:
Publisher's PDF, also known as Version of Record (includes final page, issue and volume numbers)

Please check the document version of this publication:

• A submitted manuscript is the version of the article upon submission and before peer-review. There can be important differences between the submitted version and the official published version of record. People interested in the research are advised to contact the author for the final version of the publication, or visit the DOI to the publisher's website.
• The final author version and the galley proof are versions of the publication after peer review.
• The final published version features the final layout of the paper including the volume, issue and page numbers.

Link to publication

General rights
Copyright and moral rights for the publications made accessible in the public portal are retained by the authors and/or other copyright owners and it is a condition of accessing publications that users recognise and abide by the legal requirements associated with these rights.

• Users may download and print one copy of any publication from the public portal for the purpose of private study or research.
• You may not further distribute the material or use it for any profit-making activity or commercial gain
• You may freely distribute the URL identifying the publication in the public portal.

If the publication is distributed under the terms of Article 25fa of the Dutch Copyright Act, indicated by the "Taverne" license above, please follow below link for the End User Agreement:

www.tue.nl/taverne

Take down policy
If you believe that this document breaches copyright please contact us at:

openaccess@tue.nl

providing details and we will investigate your claim.

Download date: 03. Dez. 2021

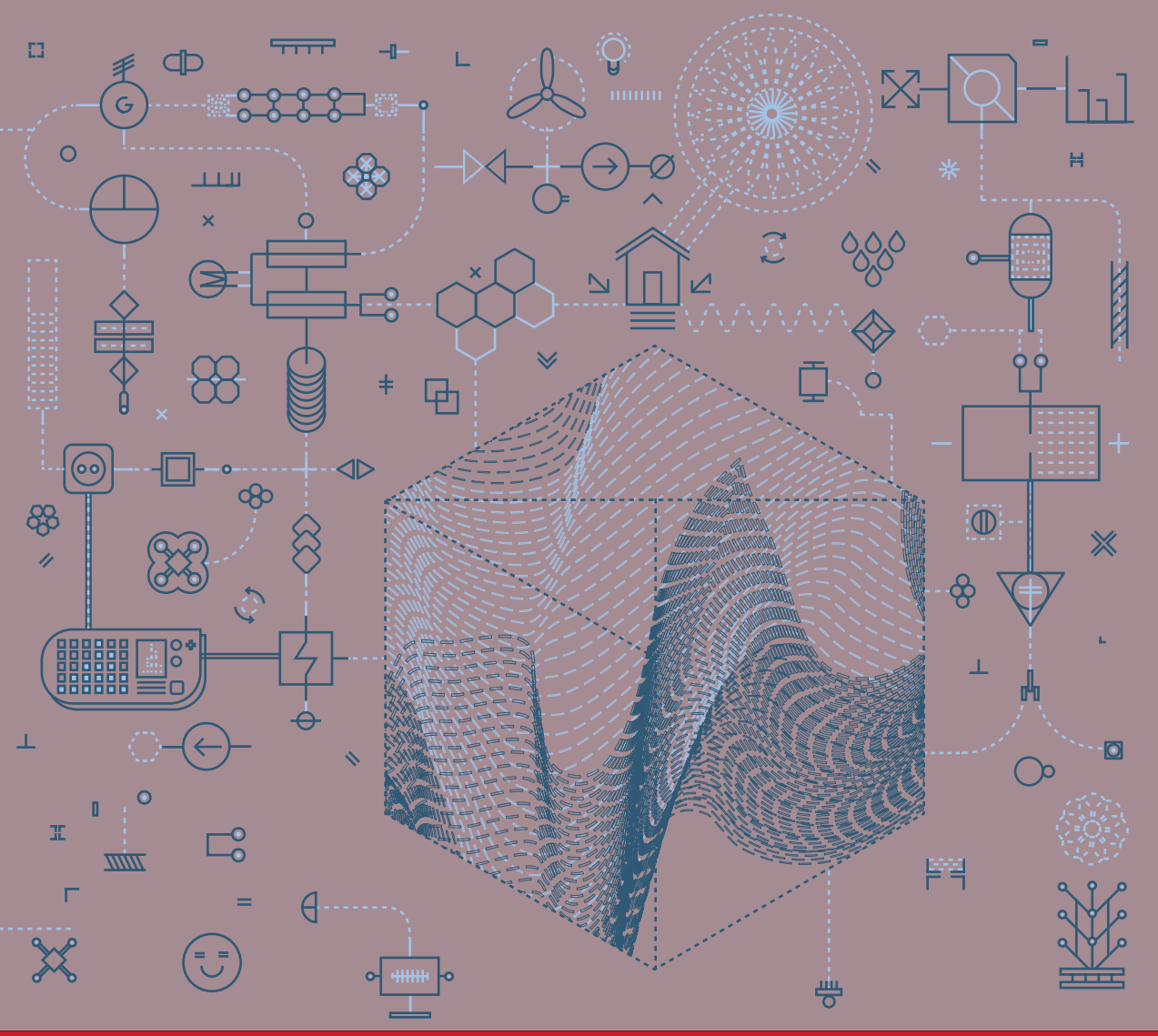

Activation of demand flexibility for heating systems in buildings

REAL-LIFE DEMONSTRATION OF OPTIMAL CONTROL FOR POWER-TO-HEAT AND THERMAL ENERGY STORAGE

Christian Finck

Bouwstenen 328

ACTIVATION OF DEMAND FLEXIBILITY FOR HEATING SYSTEMS IN BUILDINGS

Real-life demonstration of optimal control for power-to-heat and thermal energy storage

PROEFSCHRIFT

ter verkrijging van de graad van doctor aan
de Technische Universiteit Eindhoven, op gezag van
de rector magnificus prof.dr.ir. F.P.T. Baaijens, voor een
commissie aangewezen door het College voor Promoties
in het openbaar te verdedigen
op dinsdag 7 december 2021 om 13:30 uur

door

Christian Johannes Finck

geboren te Halle (Saale), Duitsland

Dit proefschrift is goedgekeurd door de promotoren en de samenstelling van de promotiecommissie is als volgt:

voorzitter:	prof.dr.ir. T.A.M. Salet
1e promotor:	prof.ir. W. Zeiler
copromotor:	dr.ir. R. Li (Technical University of Denmark)
leden:	prof.dr. A. Nieße (Carl von Ossietzky University Oldenburg)
	prof.dr.-ing. habil J. Seifert (TU Dresden)
	prof.dr. H.A. Zondag
	prof.dr. L.C.M. Itard (Technische Universiteit Delft)
	prof.dr.ir. J.L.M. Hensen
reserve:	dr.ir. H.L. Schellen

Het onderzoek of ontwerp dat in dit proefschrift wordt beschreven is uitgevoerd in overeenstemming met de TU/e Gedragscode Wetenschapsbeoefening.

The research presented in this thesis was conducted at Eindhoven University of Technology (TU/e).

A catalogue record is available from Eindhoven University of Technology Library

ISBN: 978-90-386-5418-8

NUR: 955

Bouwstenen: 328

Cover design: Studio Zyklop (www.zyklop.org)

Printed by ADC Nederland

Eindhoven, the Netherlands

@ Christian Finck, 2021

voor

Viki & Alfonsje

Acknowledgements

Whenever you have an opinion on a particular topic, ask yourself: What kind of evidence could convince me to change my mind? If your answer is “There is no evidence that can convince me otherwise,” you are rejecting evidence-based knowledge. While that is acceptable, you should also tell the surgeon about to perform an operation that he can save himself the need to wash his hands (quotation by Vince Ebert and Hans Rosling).

I gratefully thank all the people who have helped me to take a different perspective on my PhD project.

First and foremost, I am deeply indebted to my supervisors dr.ir. Rongling Li and prof.ir. Wim Zeiler. Dear Rongling, you always supported my work and gave me valuable feedback. You helped me to enhance my scientific skills and focus on developing capabilities to complete this thesis. I will remember your encouragement to maintain a positive attitude and aim for the best possible outcome, including publishing in the best journals. Dear Wim, you had a tough time with me as a PhD; when I started the PhD as a former engineer, I had a tendency to discuss solution-oriented approaches. I very much appreciate that you pushed me to work on problem-oriented approaches, so that, ultimately, this PhD contributes to the technical realization of scientific discoveries. I will not forget your advice to continuously question the chosen scientific methods and objectives. To Rongling and Wim, I hope to work with you together in future international collaborations.

Of course, I would like to thank the members of the committee, prof.dr. Astrid Nieße, prof.dr.-ing. habil Joachim Siefert, prof.dr. Herbert Zondag, prof.dr. Laure Itard and prof.dr. Jan Hensen for their feedback and effort to finalize this thesis.

This work was co-funded by Eindhoven University of Technology, BAM Techniek and BAM Energy Systems. Special thanks to BAM including Maarten Hommelberg, Dennis van Goch and Michiel Brink to give this thesis the right direction, especially in the first years.

I also use this opportunity to express gratitude to my former colleagues and friends at the Eindhoven University of Technology, Basar, Katarina, Jacob, Michael, Timi, Kennedy, Gert, Rick, Sanket, Yang and Shalika. Dear Basar and Katarina, we almost worked at the same desk, so there were many funny moments. I was always glad to have you around in the office. Dear Jacob, special thanks to you. You have always been an inspiration to me. We had many fruitful discussions, which made this thesis what it is today.

I would like to recognize the effort of the members of the BPS laboratory, Jan Diepens, Harrie Smulders and Wout van Bommel, for their amazing technical support. Special thanks also to the BPS secretary and Léontine Harmsen for their great administrative support, even for those living abroad.

Furthermore, I want to express my sincere thanks to Triple Solar, Cees Mager, Frank van Maanen and the family of Terence van Buuren. They allowed me to use a residential building for experimental investigations and to test the model predictive controller of the building energy management system under real-life conditions.

This work was the result of the collaboration with research members of the International Energy Agency Energy in Building and Communities Programme Annex 67 under the leadership of Søren Østergaard Jensen. Special thanks to my friends of Annex 67, John Clauß, Pierre Vogler-Finck and Paul Beagon.

Finally, there are not enough words and will never be to express how grateful I am to my wife Viktoria, my son Alfons, my parents Bärbel and Wolfgang, my whole family and my friends in Germany and the Netherlands.

Summary

The world's energy systems are experiencing a transition towards increased renewable integration. As renewable energy generation (such as wind and solar) fluctuates, energy systems require possibilities to enable flexible operations in power supply and demand. On the demand side, it is required that building energy-management systems adapt the energy consumption to fluctuations in supply – the so-called demand response and demand-side management. One of the greatest challenges of demand-side management is the activation of flexibility resources that depend on the availability of flexibility potentials, the technical implementation and control of flexibility, and market penetration of flexibility services. Consequently, the activation of flexibility potentials in energy systems (e.g. building energy systems) is an important milestone in the development and realization of demand-side management.

For building heating systems, this thesis investigates the activation of demand flexibility of power-to-heat conversion and thermal energy storage buffer tanks in the framework of residential and office buildings. Three major case studies are presented:

First, a simulation case study identifies the main dynamic characteristics of demand flexibility of building heating systems, including power-to-heat (heat pumps and electric heating) and thermal energy storage buffer tanks (water, phase change materials, and thermochemical materials). The characteristics of demand flexibility describe the dynamic behaviour and include the amount of energy to be shifted, the power shifting potential (i.e. the evolution of power demand and availability over time), and energy costs as an incentive to regulate demand flexibility. To exploit and control demand flexibility, this case study shows how optimal control strategies can integrate these dynamic characteristics.

Second, an experimental case study applies an artificial neural network – a model predictive controller to optimize demand flexibility, which aims to minimize the operational costs of energy consumption and maximizes self-consumption. The model predictive controller is implemented in a residential heating system to demonstrate that it can be deployed to maximize demand flexibility. This first experimental case study shows that an optimal control framework can integrate many control objectives to maximize demand flexibility, which offers the possibility to regulate energy consumption, on-site generation, grid consumption, and grid feed-in.

Third, another experimental case study is presented that demonstrates the application of a model predictive controller under real-time pricing. Real-time pricing, including day-ahead prices and imbalance prices, is used to test a flexibility service, which offers a dynamic optimization to facilitate the adaption of energy consumption to errors in forecasting renewable energy generation. The flexibility service is validated in a heating system of a detached house with a heat pump and thermal energy storage tanks for domestic hot water and space heating. This study shows that model predictive controllers can activate the demand flexibility of building heating systems through innovative flexibility services.

This thesis presents the successful integration of model-based predictive controllers into real-life applications. This enables the activation of demand flexibility of building heating systems in relation to the power grid and paves the way to accelerate the energy transition towards renewable integration.

Contents

1

Introduction

1.1 Background

"The rise of solar PV and wind power gives unprecedented importance to the flexible operation of power systems in order to keep the lights on" [1]. In the World Energy Outlook 2018 [1], the International Energy Agency (IEA) argues that a radical change of power systems is needed towards flexible operations to achieve reliability and stability for future energy systems. Therefore, it is important to create and use energy system flexibility with new system interconnections, innovative energy storage technologies, and demand-side management (DSM) strategies, including demand response (DR). In DSM and DR, system flexibility is a measure of both supply flexibility and demand flexibility [2].

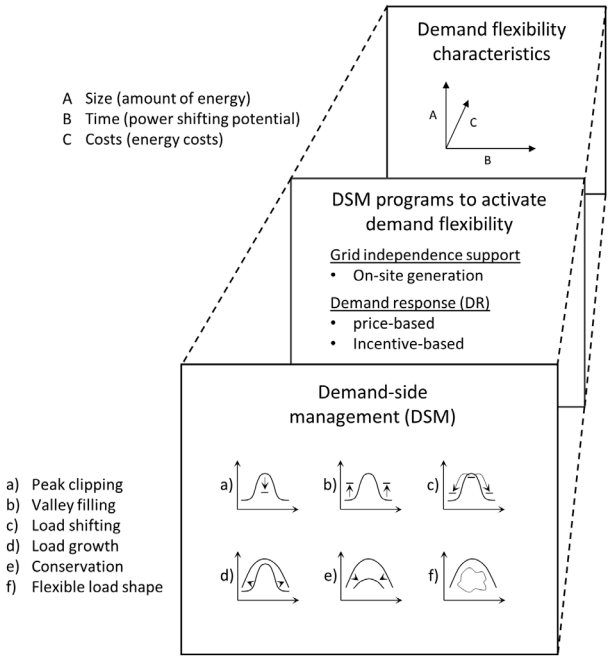

Figure 1.1. Demand flexibility in demand-side management (DSM); layer "DSM" adapted from [2,3]; layer "DSM programs to activate demand flexibility" including demand response (DR) adapted from [4].

For example, power generation units can provide supply flexibility to the power grid by modifying their power output. However, for large amounts of renewable integration, demand flexibility is required to adapt energy demands to fluctuations in supply. Figure 1.1 shows demand flexibility as a feature of system operations in DSM.

Demand flexibility of buildings has become an attractive option to mitigate intermittency issues because buildings account for 30-40% of total energy consumption [5]. Building energy systems can provide potential demand flexibility that relates to the electricity consumption of electric vehicles and smart appliances (e.g. white goods such as washing machines, dishwashers, and refrigerators). Furthermore, power-to-heat systems that convert electrical to thermal power can increase the potential demand flexibility of buildings. In building heating systems, electric heat pumps (HPs) can be used for power-to-heat conversion [6]. The combination of power-to-heat and thermal energy storage (TES) options, such as building thermal mass and TES buffer tanks, including water, phase change materials, and thermochemical materials [7,8], are effective measures to provide demand flexibility.

1.1.1 Demand flexibility of power-to-heat and thermal energy storage

Combinations of HP and TES are an important part of a building's demand flexibility portfolio [9,10]. Unlike less flexible household electrical appliances, such as lighting (i.e. without a battery system), the operation of HPs with TES can be paused and shifted without compromising occupant comfort [11]. However, it is essential to keep the indoor temperature and operative room temperature within comfort boundaries while applying load shifting and providing demand flexibility.

As HP and TES are primary sources of demand flexibility, their technical characteristics and thermal properties affect the load shifting potential. HP systems can be characterized by the following: minimum and maximum capacity, ramping capacity up and down, the maximum change rate of compressor speed, compressors' minimum run and pause time, and the performance coefficient (COP) [10]. TES characteristics comprise the following: storage capacity, charging and discharging rate, charging and discharging temperature levels, and thermal losses [12]. These characteristics are necessary to describe the dynamic behaviour and to quantify the demand flexibility of building energy systems, including HP and TES.

To identify demand flexibility of buildings, including TES systems, an early study investigated the shifting potential of electricity consumption for heating systems [13]. The study determined that the amount of energy to be shifted is an essential characteristic of demand flexibility. In recent studies, the potential of power shifting (i.e. the evolution of power demand and availability over time) has extended the definition of demand flexibility [14–16]. Power shifting was defined as the duration of a shift in power that can be maintained at a given moment in time [14].

In addition to preliminary definitions that exclusively used energy and power to describe flexibility, energy costs were included in the definition of demand flexibility [17]. For example, energy costs were associated with the activation of power shifting of a storage capacity. The costs were presented as cost curves and showed the costs of energy consumption as a function of flexibility, in other words, the amount of energy to be shifted [17]. Consequently, energy costs, the amount of energy, and the power shifting potential are the main characteristics of demand flexibility (Figure 1.1).

1.1.2 Demand flexibility indicators for energy systems in buildings

To provide an accurate measure for demand flexibility, researchers created flexibility indicators (i.e. key performance indicators (KPIs) of demand flexibility) [18,19] (Table 1-1). Flexibility indicators can quantify all possible characteristics of demand flexibility in terms of energy costs, the amount of energy, and the power shifting potential. Researchers, designers, and policymakers can use these flexibility indicators in addition to conventional KPIs (such as total energy consumption, total primary and net energy use, and total costs of energy usage) to determine the overall energy performance of buildings.

Table 1-1. Summary of key performance indicators (KPIs) of demand flexibility, adapted from [18–23].

KPI	Definition	Reference
Available storage capacity	The *amount of energy* shifted during optimal control compared with reference control.	[14]
Grid feed-in	The *amount of energy* generated on-site and exported to the power grid.	[24]
Flexibility (volume shifted)	The *amount (volume) of energy* shifted during an event in which procurement costs are avoided. The load shift is compared with reference control.	[25]
Forced flexibility	The *amount of excess energy* stored during a flexibility event.	[13,15]
Delayed flexibility	The *amount of energy* postponed during a flexibility event. For instance, discharging of TES reduces the grid energy consumption.	[13,15]
Annual mismatch ratio	The annual difference between the *amount of energy* consumed and on-site generation, calculated as an hourly average.	[20]

Peak power generation	The peak *power* of on-site generation normalised by the designed grid connection capacity.	[26]
Peak power load	The peak *power* of energy consumption normalised by the designed grid connection capacity.	[26]
Power shifting capability	The difference between *power* consumption during optimal control and reference control.	[14]
Cost curves	The graphical interpretation of *energy costs* associated with load shifting.	[17]
Cost deviation	The difference between total daily *energy costs* of optimal control and reference control.	[27]
Flexibility factor	The potential shift in energy consumption for heating *from high-price to low-price* periods.	[28]
Flexibility (procurement costs)	The avoided procurement *costs* by applying load shifting.	[25]
Total supply spread	The ratio of *electricity prices and costs* of 1 kWh of a conventional heat generator (boiler) to the costs of 1 kWh of primary energy consumed by cogeneration.	[29]
Storage/Shifting efficiency	The *ratio* between discharging and charging events over an optimal control horizon compared with reference control.	[14,28]
Grid support coefficient	The *ratio* of electricity consumption profiles and generation profiles to a time-resolved reference quantity to express the availability of electricity in the public power grid.	[30]
Self-consumption (supply cover factor)	The *ratio* of direct consumption of on-site generation to the total on-site generation.	[26]
Self-generation (load cover factor)	The *ratio* of direct consumption of on-site generation to the total electrical demand.	[26]
Maximum hourly surplus	The maximum hourly *ratio* of direct consumption of on-site generation to the total electrical demand.	[20]
Maximum hourly deficit	The maximum hourly *ratio* of storage discharging rates compensating direct consumption of on-site generation to the total electrical demand.	[20]

Flexible energy efficiency	The *ratio* of the amount of energy shifted during an event to the rebound energy, which is the amount of energy used outside an event	[21]
Loss of load probability	The *percentage* of time during which the energy consumption is not covered by on-site generation.	[26]
Demand recovery ratio	The *ratio* of energy consumption during a flexibility event to the required minimum energy consumption.	[31]
Generation multiple	The *ratio* of generation peak power to energy consumption peak power.	[26]
Capacity factor	The *ratio* of the amount of energy exchanged with the grid to the nominal connection capacity.	[26]
Dimensioning rate	The *ratio* of the maximum amount of energy exchanged with the grid to the nominal connection capacity.	[26]
Grid control level	The *ratio* of the sum of second and third priority loads (energy consumption) to the total energy consumption.	[32]
Grid interaction index	The *ratio* of energy exchange between building and grid (net energy) to the maximum of net energy for a time interval.	[20,33]

A review of the flexibility indicators (Table 1-1) reveals that KPIs were developed to quantify demand flexibility according to the characteristics of energy costs, the amount of energy, or the power shifting potential. For example, the KPI “the available storage capacity” focuses on load shifting using storage systems whereas the KPI “self-consumption” targets on-site generation. On the other hand, researchers have also aimed to create generic flexibility indicators for building energy systems [34,35]. The flexible performance indicator (FPI) was introduced to capture all relevant parameters of the dynamic interaction in building energy systems [34]. The FPI is calculated as the weighted sum of the response time, the committed power, the recovery time, and the actual energy variation. The weighting factors were assumed constant and retrieved from empirical data.

Indicators of self-consumption of on-site generation have predominated investigations of demand flexibility in buildings [23,36–42]. Furthermore, researchers have shown an increasing interest in evaluating flexibility indicators that present grid-interaction services [23,26,30,36,41,43].

These indicators can help system operators to measure the building to grid interaction and to show the performance of the local grid, including a building's demand flexibility.

Researchers have also become increasingly interested in studying cost-oriented flexibility indicators [44,45]. Cost-oriented flexibility indicators can demonstrate the economic benefit of load shifting and can help system operators to regulate net power exchange between the building and the grid. As these indicators can incorporate time-varying electricity prices, demand flexibility can be facilitated through existing power market mechanisms. For example, power balancing and spot markets offer real-time pricing (RTP) signals to trade electricity between suppliers and consumers. As RTP includes electricity prices, such as day-ahead, intra-day, and imbalance prices, these pricing signals can be used to stimulate load shifting and control demand flexibility [4,46–48].

1.1.3 Control of demand flexibility in buildings

This section discusses the challenges to control demand flexibility. For clarity on the terminology regarding control possibilities for demand flexibility in buildings, the reader is referred to [18].

Control signals for demand flexibility

To activate a building's demand flexibility, system operators provide price-based signals (PBS), such as RTP, time-of-use tariffs (TOU), and critical peak pricing (CPP) [4,46,49]. RTP represents dynamic pricing over the day, whereas TOU and CPP are sets of electricity rates that are constant for several minutes to several hours. Dynamic pricing signals have been used in building energy management systems to study the costs of demand flexibility. An increase of demand flexibility was determined while reducing the total operational electricity costs [49–51]. In [49–51], it was concluded that the use of dynamic pricing signals in building energy management systems results in the activation of a building's demand flexibility. However, it is important to note that a building's differential price responsiveness over the day and hourly pricing variations constitute the degree of demand flexibility [52].

To enable a building's demand flexibility, system operators can also provide incentive-based signals (IBS), which are direct payments to the consumers to adapt their energy consumption [4,49]. Consumers can receive IBS that consist of prices, consumption constraints, and power limitations [46,49]. IBS are, for example, a type of direct load control, curtailable load, and demand-side bidding [49]. For instance, direct load control for short-term flexibility (1 to 30 min of notification time before real-time) was suggested to maintain system reliability [46].

Current DR programs and real-time power markets use direct load control (including IBS) and indirect load control (including PBS). Both IBS and PBS can contribute to regulating a building's energy consumption and demand flexibility [46,49]. To exploit the full potential of buildings' demand flexibility in power markets, researchers investigated strategies to include the provision of demand flexibility into existing real-time markets [53,54]. For example, a demand-side bidding process was investigated to activate flexibility in three different markets: an option market, a spot market, and a flexibility market [53]. The option market trades flexibility capacity days before potential usage, the spot market trades electricity the day-ahead up to 1 h before real-time and the flexibility market achieves close to real-time regulation of flexibility. Through the aggregation of flexibility units, controllable loads, generators, and storages could participate in real-time markets. This was also made possible by simplifications regarding the provision of flexibility by assuming one-way bidding in flexibility markets. Moreover, another recent study investigated a simplification from complex to one-way trading of demand flexibility [54], which suggested the application of one-way trading to a longer trading horizon to provide demand flexibility to real-time markets.

Control objectives for demand flexibility

Through the participation of consumers providing demand flexibility in real-time power markets, the primary objective of consumers was found in minimizing the expected costs of a building's electricity consumption. Recent work on the demand flexibility of buildings has adopted a wider perspective of building performance assessment [55–57]. More precisely, the carbon emissions that originate from energy production can affect a building's energy performance. Therefore, an alternative control signal was investigated – the grid carbon intensity [55–57], which is the amount of CO_2 emitted per unit of energy consumption. Implementing the carbon intensity as a control signal can minimize the CO_2 emissions of energy consumed by buildings [57]. It is important to note that using carbon-based and price-based control signals can lead to conflicting objectives in energy management systems. For example, in northern Europe, hydropower accounts for a large proportion of power generation. Hydropower plants typically operate during periods of high energy demand. As the demand drives the electricity prices, prices of energy consumption remain high throughout periods of high demand, which continue into periods of low CO_2 emissions [58].

The effect of contradicting control objectives on the regulation of demand flexibility was also observed for load shifting of a building's energy consumption while maintaining occupant comfort through advanced control. The control objective included minimizing energy

costs and maintaining thermal comfort. A deviation from thermal comfort boundaries was penalized and it was concluded that providing demand flexibility through load shifting results in a deviation from thermal comfort and, thus, always leads to higher operational costs [17].

The effect of contradicting control objectives was also observed for a combined price-based and self-consumption control [42]. For price-based control, energy consumption was shifted to night-time, whereas for self-consumption, control load shifting was applied during the daytime to maximize on-site generation. It was concluded that both control objectives used the potential demand flexibility. However, the largest peak shaving and lowest grid-interaction were noticed for self-consumption control.

Control methods for demand flexibility

Increasing self-consumption, reducing energy costs, reducing energy consumption, load shifting, and peak shaving are the primary control objectives used to regulate demand flexibility [18,23]. The control of the building energy systems manages the demand flexibility and adapts the electricity consumption accordingly. Early studies applied the simplest control strategy that included a set of rules to regulate a building's energy consumption – the so-called rule-based control (RBC) [19,24]. For example, a proportional-integral controller was used to regulate the temperature set points of floor heating and radiator systems, and demand flexibility was quantified for load shifting [14]. In a recent example, an RBC strategy was applied to adapt the indoor temperature setpoints. The demand flexibility was calculated for load shifting and peak shaving [59]. In another example, RBC was used to study self-consumption of on-site generated PV power [24]. The RBC regulated the amount of energy exchanged between the building and the grid while maximizing self-consumption and minimizing grid feed-in [24]. Studies [14,24,59] showed that RBC is a simple and effective strategy to control the demand flexibility of buildings. Furthermore, RBC strategies have the advantage of robust control and ease of implementation through fixed scheduling [18]. One of the disadvantages of RBC strategies is that they cannot adapt to varying operating conditions. To compensate for this disadvantage, recent work on the demand flexibility of buildings investigated predictive RBC (PRBC) [56,60]. For example, PRBC was used to reduce energy costs, annual CO_2 emissions, and peak load. On the one hand, the PRBC could effectively reduce peak loads using a predefined schedule. On the other hand, the PRBC was not suitable for reducing operational energy costs and CO_2 emissions [56]. In another example, a PRBC was developed that included a sliding schedule and a moving average of temperature setpoints. The developed PRBC resulted in decreased costs of electricity consumption [60]. For RBC and PRBC, however, the major disadvantage is their inability to incorporate time-varying disturbances, complex dynamic control signals, and non-linear and time-varying dynamics, which require more advanced control strategies [18].

Model predictive control (MPC) is an advanced control strategy that can optimize the energy consumption of buildings and implement any time-varying dynamics and disturbances. MPC strategies require formulating an optimal control problem (OCP). The OCP integrates an objective function that can, for example, maximize self-consumption or minimize the total operational energy costs [36]. The MPC solves the OCP and, therefore, a system model is used that anticipates future control actions over the control horizon. The system model implements the objective function, the control signals, the disturbances and the constraints, and predicts the future states over the prediction horizon [18,61]. Studies on buildings' demand flexibility have typically applied a 24 h prediction horizon in MPC formulations [62]. It is important to note that the prediction horizon and the control horizon can differ from each other. While the prediction horizon denotes the computation of MPC's entire time horizon, the control horizon refers to the time of computation of MPC's future control actions [61].

Recently, MPC strategies have been applied to increase the demand flexibility of buildings [45,55]. For example, a co-simulation framework was used to investigate the advantages of MPC over conventional RBC in a residential building. The MPC realized increase demand flexibility while minimizing energy consumption, costs of energy consumption, and CO_2 emissions [55]. In another example, an MPC reduced total electricity costs and improved occupants' comfort. The potential demand flexibility was activated through load shifting of energy consumption from on-peak to off-peak periods of electricity prices [45]. The examples demonstrate that MPC strategies are superior to RBC strategies regarding optimal control of buildings' energy consumption and demand flexibility.

So far, to study MPC in buildings, researchers have focused on simplified system models such as linear state-space models [61], transfer functions, and step response models [63]. Linearization of the model for MPC can be very efficient for online optimization due to the ease of implementation and low computational effort of solving the OCP [61,63]. However, for online optimization, linear system models have shown a low performance in predicting energy consumption. A more detailed MPC modelling approach that incorporates nonlinearities of the energy system can improve prediction performance [61,64].
For online optimization, additionally, a shorter prediction time step can increase the prediction accuracy of MPC [65]. On the other hand, shorter prediction time steps and more complex modelling approaches pose a significant challenge in the computational effort of solving the OCP in MPC.

Due to the high computational complexity of MPC, advanced building control started to focus on the development of reinforcement learning (RL) [18]. In contrast to MPC, RL controllers do not necessarily require employing a system model. The RL controller learns the control actions, including mapping of trial and error interactions between the system and the environment. At each combination of systems states and control actions, RL determines

the feedback, also called reward or reinforcement. For each start and goal of states, the RL controller maximizes the sum of the rewards and obtains the optimal policy of control actions accordingly [18,66]. The optimal policy represents the control objective, such as the costs of energy consumption, and it can be retrieved from model-free and model-based RL. Whereas model-free RL applies simple learning strategies such as look-up tables, model-based RL uses advanced learning strategies such as deep RL to approximate value functions and to receive the optimal policy [18,67]. RL controllers have been applied to investigate the demand flexibility of buildings [68,69]. For example, a model-based RL controller enabled the provision of demand flexibility of a cluster of buildings through Q-learning and extended joint action learning as a policy learning strategy [69]. In another example, a hybrid RL strategy was applied to decrease the energy consumption of domestic hot water production while meeting occupant comfort requirements and increasing demand flexibility through load shifting. The hybrid RL also overcomes one of the main disadvantages of RL, the curse of dimensionality of optimal policy actions. The hybrid RL, therefore, implements a heuristic optimization algorithm for policy learning [68]. Through policy-side learning, the RL controller learns by solving the optimization. Once a combination of systems states, control actions, and optimal policy is learned, the RL controller does not need to solve this optimization problem accordingly. This is the major difference between model-based RL and MPC. As RL and MPC have shown to be superior to RBC strategies, researchers have suggested using these advanced control strategies to regulate demand the flexibility of buildings.

1.2 Objectives and research questions

Load balancing between the power grid and building energy systems requires exploiting the full potential of buildings' demand flexibility. One of the greatest potentials of buildings' demand flexibility lies in building heating systems including power-to-heat and TES, which are characterized by their dynamic behaviour. It is, thus, crucial to include these dynamic characteristics in the control of building energy systems to activate buildings' demand flexibility. As the activation of demand flexibility depends on the chosen control strategy, it is essential to create control methods that can cope with the dynamic behaviour of building energy systems. As optimal control is a promising control strategy that can implement time-varying dynamics and disturbances, the present study examines the following four research questions concerning optimal control of demand flexibility for building heating systems, including power-to-heat and TES:

(1) To exploit the potential of buildings' demand flexibility, control strategies must implement the dynamic characteristics of building energy systems with power-to-heat and TES systems, including water, phase-change materials, and thermochemical materials. Thus far, the dynamic behaviour of power-to-heat and TES systems is not investigated for advanced control such as optimal control of demand flexibility.

How can the main dynamic characteristics of demand flexibility of building heating systems, including power-to-heat and TES, be integrated for optimal control?

(2) To activate demand flexibility in building energy systems, current advanced control strategies integrate only a single control objective, such as costs of energy consumption or thermal comfort. Thus far, there is no uniform formulation to integrate many control objectives into optimal control while maximizing demand flexibility.

What optimal control strategy activates the optimization of demand flexibility while integrating many control objectives?

(3) Optimal control strategies can adapt to time-varying dynamics, disturbances, and real-time pricing. Thus far, optimal control strategies have been extensively investigated in simulation case studies and only a few studies have been validated in experimental case studies. Furthermore, real-time implementations of optimal control methods for demand flexibility have not been designed.

What optimal control method activates online optimization of demand flexibility?

(4) Using real-time pricing from real-time power markets, optimal control methods can enable dynamic optimization of demand flexibility. Until now, real-time power markets use complex price-based trading algorithms such as intra-day pricing to exploit demand flexibility potentials. However, current real-time power markets lack implementation of flexibility services.

What flexibility service creates dynamic optimization of demand flexibility under real-time pricing?

1.3 Research methodology and thesis outline

The previous sections introduced the main challenges to activate demand flexibility of buildings. For demand flexibility of heating systems in buildings, the problem statements were formulated. This section provides further details on the methods that were applied. The methods are described according to the four main research questions:

Research question (1): To identify the characteristics of demand flexibility, a comprehensive literature study of demand flexibility of buildings was performed. All aspects of demand flexibility were extracted from the literature studies. A simulation case study (Chapter 2) identified and quantified the demand flexibility of power-to-heat and TES buffer tanks that include water, phase change materials, and thermochemical materials (Figure 1.2).
To activate TES systems, HP and electric heating were used as power-to-heat. HPs can guarantee a maximum condenser outlet temperature of up to 60 °C [70] or even 70 °C [71], which is ideal for charging buffer tanks that include water and phase change materials. For buffer tanks that include thermochemical materials, we assumed additional electric heating to charge the TES to higher temperatures of up to 120 °C.

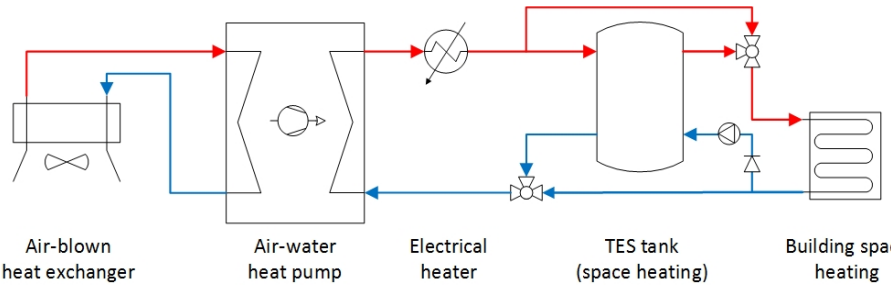

Figure 1.2. Simple process flow diagram of building heating system (simulation case study – Chapter 2).

To enable the full potential of buildings' demand flexibility, the simulation case study implemented an optimal control framework (Figure 1.3). This framework integrated the optimization scheme, the objective function, grid signal support, weather forecasting, and models of the system components. For the TES models, performance maps of TES were introduced to implement the dynamic characteristics of various TES technologies [12].

As the dynamic behaviour of a building's energy system is essential to describe demand flexibility, performance indicators are used to quantify demand flexibility. In the simulation case study, key performance indicators were determined according to the characteristics of demand flexibility in terms of energy costs, the amount of energy, and the power shifting potential.

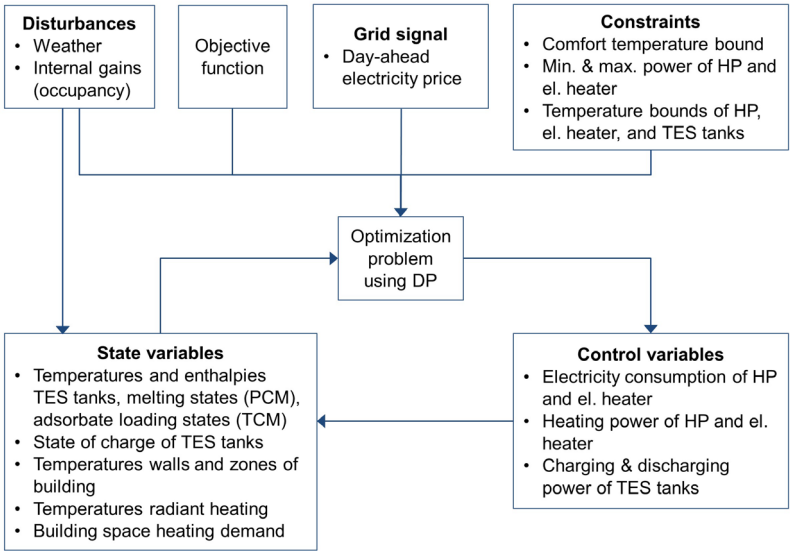

Figure 1.3. Framework of optimal control of building heating system (simulation case study – Chapter 2).

Research question (2): For the activation of buildings' demand flexibility, a comprehensive literature study of control methods, control strategies, and control objectives was performed. Special attention was paid to control objectives implemented in conventional and optimal control strategies to regulate demand flexibility.

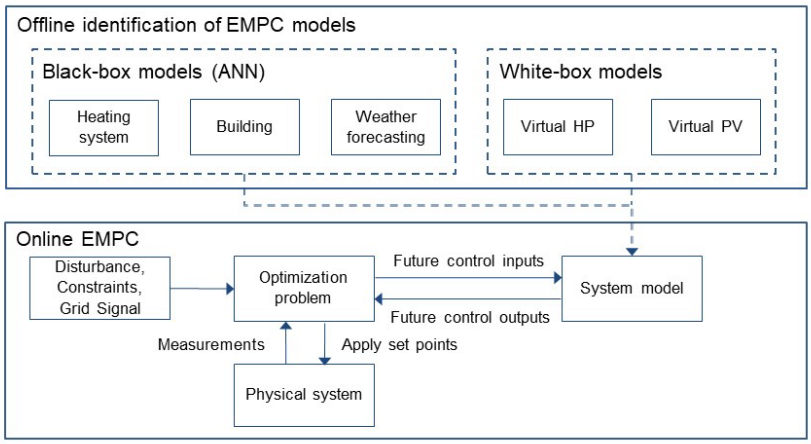

Figure 1.4. Methodological framework of the economic model predictive controller (EMPC) (experimental case study 1 – Chapter 3).

An experimental case study (Chapter 3) was used to introduce a control strategy that maximizes demand flexibility. The control strategy included a new objective function that enables the implementation of many control objectives for demand flexibility. The control strategy was applied in the framework of an economic model predictive controller (EMPC), which consisted of an artificial neural network – model predictive controller (ANN-MPC) (Figure 1.4). The ANN-MPC regulated the building heating system using black-box and white-box modelling. The black-box models identified the building and heating system (i.e. conventional condensing boiler). The white-box models virtually installed PV and HP to simulate onsite renewable generation and power-to-heat to activate buildings' demand flexibility in relation to the power grid. Similar to the previous simulation case study, the first experimental case study integrates key performance indicators to quantify buildings' demand flexibility.

Research question (3): In the first simulation case study and the first experimental case study, an optimal control framework was introduced to establish a system model that can perform fast in an online optimization. The system model was also developed as a plug-and-play solution to integrate different modelling techniques (e.g. black-box, grey-box, and white-box models). In the second experimental case study, the system model (Chapter 4) was comprehensively tested in a real-life application (Chapter 5) for dynamic optimization of demand flexibility of a building heating system that includes power-to-heat (HP) and TES buffer tanks (Figure 1.5).

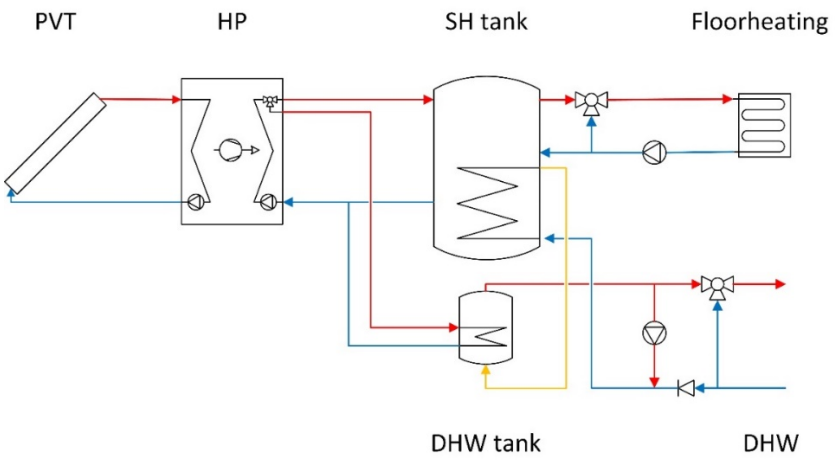

Figure 1.5. Flow diagram of the building heating system (experimental case study 2 – Chapter 4&5).

Research question (4): The second experimental case study (Chapter 5) also introduced a new flexibility service for real-time power markets. The flexibility service consisted of a one-way trading pattern, including day-ahead and imbalance electricity prices. The one-way trading pattern was tested in a real-life application of a building heating system and included HP and TES buffer tanks. Similar to the previous case studies, the second experimental case study integrates key performance indicators to quantify buildings' demand flexibility.

The results of this research are shown in the following four chapters (2-5), which are identical to the journal articles:

- Chapter 2: C. Finck, R. Kramer, R. Li, and W. Zeiler, "Quantifying demand flexibility of power-to-heat and thermal energy storage in the control of building heating systems", Applied Energy 209 (2018):pp. 409-425.
- Chapter 3: C. Finck, R. Li, and W. Zeiler, "Economic model predictive control for demand flexibility of a residential building", Energy 176 (2019):pp. 365-79.
- Chapter 4: C. Finck, R. Li, and W. Zeiler, "Identification of a dynamic system model for a building and heating system including heat pump and thermal energy storage", MethodsX 7 (2020) 100866.
- Chapter 5: C. Finck, R. Li, and W. Zeiler, "Optimal control of demand flexibility under real-time pricing for heating systems in buildings: A real-life demonstration", Applied Energy 263 (2020) 114671.

A comprehensive discussion and conclusion finalize this thesis. The outline of the thesis is presented in Figure 1.6.

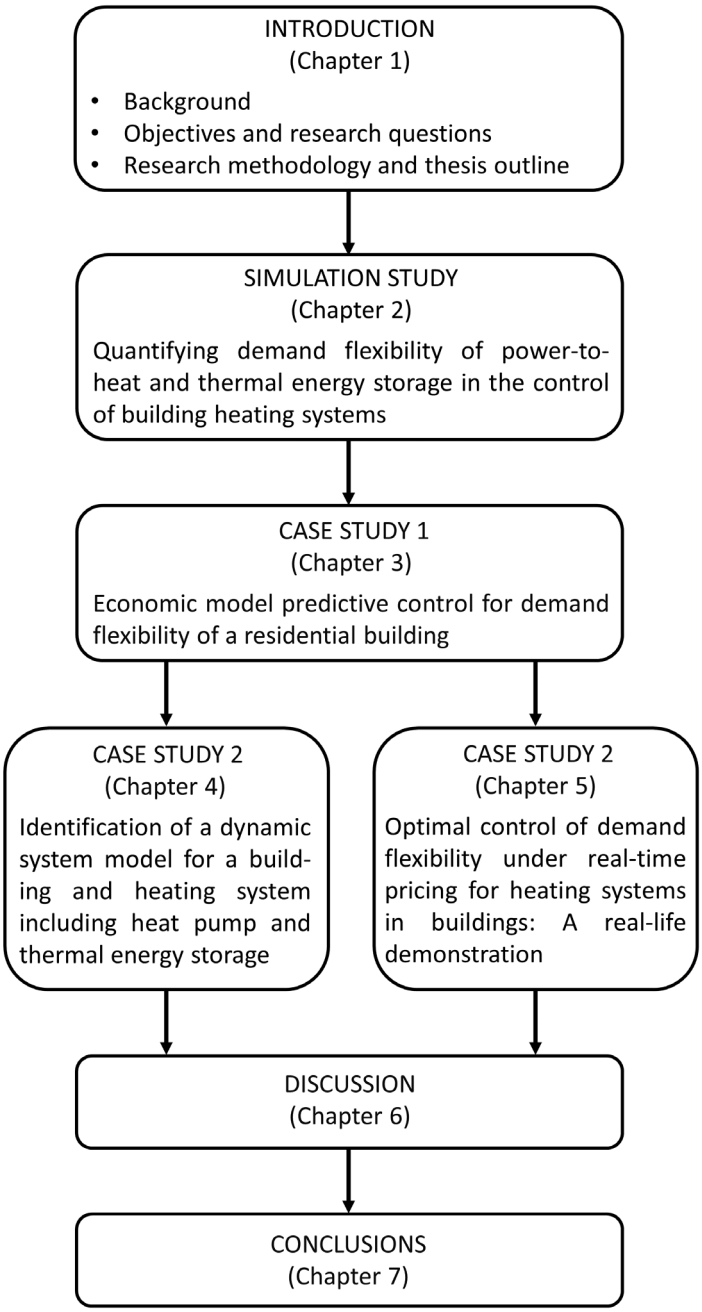

Figure 1.6. Schematic diagram of the thesis.

1.4 References

[1] OECD/IEA. Renewables Information Overview (2018 edition). 2018.

[2] Lund PD, Lindgren J, Mikkola J, Salpakari J. Review of energy system flexibility measures to enable high levels of variable renewable electricity. Renew Sustain Energy Rev 2015;45:785–807. doi:10.1016/j.rser.2015.01.057.

[3] Gelazanskas L, Gamage KAA. Demand side management in smart grid: A review and proposals for future direction. Sustain Cities Soc 2014;11:22–30. doi:10.1016/j.scs.2013.11.001.

[4] Tang H, Wang S, Li H. Flexibility categorization, sources, capabilities and technologies for energy-flexible and grid-responsive buildings: State-of-the-art and future perspective. Energy 2021;219:119598. doi:10.1016/j.energy.2020.119598.

[5] Jensen SØ, Marszal-Pomianowska A, Lollini R, Pasut W, Knotzer A, Engelmann P, et al. IEA EBC Annex 67 Energy Flexible Buildings. Energy Build 2017;155:25–34. doi:10.1016/j.enbuild.2017.08.044.

[6] Salpakari J, Mikkola J, Lund PD. Improved flexibility with large-scale variable renewable power in cities through optimal demand side management and power-to-heat conversion. Energy Convers Manag 2016;126:649–61. doi:10.1016/j.enconman.2016.08.041.

[7] Arteconi A, Hewitt NJ, Polonara F. State of the art of thermal storage for demand-side management. Appl Energy 2012;93:371–89. doi:10.1016/j.apenergy.2011.12.045.

[8] Finck C, Li R, Zeiler W. An optimization strategy for scheduling various thermal energy storage technologies in office buildings connected to smart grid. Energy Procedia, 2015. doi:10.1016/j.egypro.2015.11.105.

[9] Arteconi A, Hewitt NJ, Polonara F. Domestic demand-side management (DSM): Role of heat pumps and thermal energy storage (TES) systems. Appl Therm Eng 2013;51:155–65. doi:10.1016/j.applthermaleng.2012.09.023.

[10] Fischer D, Madani H. On heat pumps in smart grids: A review. Renew Sustain Energy Rev 2017;70:342–57. doi:10.1016/j.rser.2016.11.182.

[11] Vanhoudt D, Geysen D, Claessens B, Leemans F, Jespers L, Van Bael J. An actively controlled residential heat pump: Potential on peak shaving and maximization of self-consumption of renewable energy. Renew Energy 2014;63:531–43. doi:10.1016/j.renene.2013.10.021.

[12] Finck C, Li R, Zeiler W. Performance maps for the control of thermal energy storage. 15th Int Conf Int Build Perform Simul Assoc 2017. doi:10.26868/25222708.2017.238.

[13] Nuytten T, Claessens B, Paredis K, Van Bael J, Six D. Flexibility of a combined heat and power system with thermal energy storage for district heating. Appl Energy 2013;104:583–91. doi:10.1016/j.apenergy.2012.11.029.

[14] Reynders G, Diriken J, Saelens D. Generic characterization method for energy flexibility: Applied to structural thermal storage in residential buildings. Appl Energy 2017;198:192–202. doi:10.1016/j.apenergy.2017.04.061.

[15] Stinner S, Huchtemann K, Müller D. Quantifying the operational flexibility of building energy systems with thermal energy storages. Appl Energy 2016;181:140–54. doi:10.1016/j.apenergy.2016.08.055.

[16] D'hulst R, Labeeuw W, Beusen B, Claessens S, Deconinck G, Vanthournout K. Demand response flexibility and flexibility potential of residential smart appliances: Experiences from large pilot test in Belgium. Appl Energy 2015;155:79–90. doi:10.1016/j.apenergy.2015.05.101.

[17] De Coninck R, Helsen L. Quantification of flexibility in buildings by cost curves - Methodology and application. Appl Energy 2016;162:653–65. doi:10.1016/j.apenergy.2015.10.114.

[18] Finck C, Clauß J, Vogler-Finck P, Beagon P, Zhan K, Kazmi H. Review of applied and tested control possibilities for energy flexibility in buildings. 2018. doi:10.13140/RG.2.2.28740.73609.

[19] Clauß J, Finck C, Vogler-Finck P, Beagon P. Control strategies for building energy systems to unlock demand side flexibility – A review. 15th Int. Conf. Int. Build. Perform. Simul. Assoc., 2017, p. 611–20.

[20] Vigna I, Pernetti R, Pasut W, Lollini R. New domain for promoting energy efficiency: Energy Flexible Building Cluster. Sustain Cities Soc 2018. doi:10.1016/j.scs.2018.01.038.

[21] Kathirgamanathan A, Péan T, Zhang K, De Rosa M, Salom J, Kummert M, et al. Towards standardising market-independent indicators for quantifying energy flexibility in buildings. Energy Build 2020;220:110027. doi:10.1016/j.enbuild.2020.110027.

[22] Bampoulas A, Saffari M, Pallonetto F, Mangina E, Finn DP. A fundamental unified framework to quantify and characterise energy flexibility of residential buildings with multiple electrical and thermal energy systems. Appl Energy 2021;282. doi:10.1016/j.apenergy.2020.116096.

[23] Li H, Wang Z, Hong T, Piette MA. Energy Flexibility of Residential Buildings: A Systematic Review of Characterization and Quantification Methods and Applications. Adv Appl Energy 2021:100054. doi:10.1016/j.adapen.2021.100054.

[24] Salpakari J, Lund P. Optimal and rule-based control strategies for energy flexibility in buildings with PV. Appl Energy 2016;161:425–36. doi:10.1016/j.apenergy.2015.10.036.

[25] Masy G, Georges E, Verhelst C, Lemort V. Smart grid energy flexible buildings through the use of heat pumps and building thermal mass as energy storage in the Belgian context. Sci Technol Built Environ 2015;21:6:800–11. doi:10.1080/23744731.2015.1035590.

[26] Salom J, Marszal AJ, Widén J, Candanedo J, Lindberg KB. Analysis of load match and grid interaction indicators in net zero energy buildings with simulated and monitored data. Appl Energy 2014;136:119–31. doi:10.1016/j.apenergy.2014.09.018.

[27] D'Ettorre F, Rosa M De, Conti P, Testi D, Finn D. Mapping the energy flexibility potential of single buildings equipped with optimally-controlled heat pump, gas boilers and thermal storage. Sustain Cities Soc 2019. doi:10.1016/j.scs.2019.101689.

[28] Le Dréau J, Heiselberg P. Energy flexibility of residential buildings using short term heat storage in the thermal mass. Energy 2016;111:1–5. doi:10.1016/j.energy.2016.05.076.

[29] Piacentino A, Barbaro C. A comprehensive tool for efficient design and operation of polygeneration-based energy μgrids serving a cluster of buildings. Part II: Analysis of the applicative potential. Appl Energy 2013. doi:10.1016/j.apenergy.2012.11.079.

[30] Klein K, Langner R, Kalz D, Herkel S, Henning HM. Grid support coefficients for electricity-based heating and cooling and field data analysis of present-day installations in Germany. Appl Energy 2016. doi:10.1016/j.apenergy.2015.10.107.

[31] Arteconi A, Patteeuw D, Bruninx K, Delarue E, D'haeseleer W, Helsen L. Active demand response with electric heating systems: Impact of market penetration. Appl Energy 2016;177:636–48. doi:10.1016/j.apenergy.2016.05.146.

[32] Ahmadi M, Rosenberger JM, Lee WJ, Kulvanitchaiyanunt A. Optimizing Load Control in a Collaborative Residential Microgrid Environment. IEEE Trans Smart Grid 2015. doi:10.1109/TSG.2014.2387202.

[33] Voss K, Sartori I, Napolitano A, Geier S, Gonzalves H, Hall M, et al. Load Matching and Grid Interaction of Net Zero Energy Building. Proc Build Simul 2011 2011;6:14–6. doi:ISBN: 9870646565101.

[34] Arteconi A, Mugnini A, Polonara F. Energy flexible buildings: A methodology for rating the flexibility performance of buildings with electric heating and cooling systems. Appl Energy 2019;251:113387. doi:10.1016/j.apenergy.2019.113387.

[35] De Groote M, Volt J, Bean F. IS EUROPE READY FOR THE SMART BUILDINGS REVOLUTION? MAPPING SMART-READINESS AND INNOVATIVE CASE STUDIES www.bpie.eu/publication/is-europe-ready-for-the-smart-buildings-revolution/ 2017.

[36] Salpakari J, Lund P. Optimal and rule-based control strategies for energy flexibility in buildings with PV. Appl Energy 2016;161:425–36. doi:10.1016/j.apenergy.2015.10.036.

[37] Aelenei D, Lopes RA, Aelenei L, Gonçalves H. Investigating the potential for energy flexibility in an office building with a vertical BIPV and a PV roof system. Renew Energy 2019. doi:10.1016/j.renene.2018.07.140.

[38] Luthander R, Widén J, Nilsson D, Palm J. Photovoltaic self-consumption in buildings: A review. Appl Energy 2015;142:80–94. doi:10.1016/j.apenergy.2014.12.028.

[39] Sartori I, Napolitano A, Voss K. Net zero energy buildings: A consistent definition framework. Energy Build 2012;48:220–32. doi:10.1016/j.enbuild.2012.01.032.

[40] Widén J. Improved photovoltaic self-consumption with appliance scheduling in 200 single-family buildings. Appl Energy 2014. doi:10.1016/j.apenergy.2014.04.008.

[41] Solano JC, Olivieri L, Caamaño-Martín E. Assessing the potential of PV hybrid systems to cover HVAC loads in a grid-connected residential building through intelligent control. Appl Energy 2017. doi:10.1016/j.apenergy.2017.08.188.

[42] Dar UI, Sartori I, Georges L, Novakovic V. Advanced control of heat pumps for improved flexibility of Net-ZEB towards the grid. Energy Build 2014;69:74–84. doi:10.1016/j.enbuild.2013.10.019.

[43] Zhang S, Huang P, Sun Y. A multi-criterion renewable energy system design optimization for net zero energy buildings under uncertainties. Energy 2016. doi:10.1016/j.energy.2015.11.044.

[44] Liu M, Heiselberg P. Energy flexibility of a nearly zero-energy building with weather predictive control on a convective building energy system and evaluated with different metrics. Appl Energy 2019;233–234:764–75. doi:10.1016/j.apenergy.2018.10.070.

[45] Hu M, Xiao F, Jørgensen JB, Li R. Price-responsive model predictive control of floor heating systems for demand response using building thermal mass. Appl Therm Eng 2019. doi:10.1016/j.applthermaleng.2019.02.107.

[46] Eid C, Codani P, Perez Y, Reneses J, Hakvoort R. Managing electric flexibility from Distributed Energy Resources: A review of incentives for market design. Renew Sustain Energy Rev 2016. doi:10.1016/j.rser.2016.06.008.

[47] Tennet.eu. Onbalansprijssystematiek - Hoe komen de geldstromen tot stand? 2019.

[48] Sharda S, Singh M, Sharma K. Demand side management through load shifting in IoT based HEMS: Overview, challenges and opportunities. Sustain Cities Soc 2021;65:102517. doi:10.1016/j.scs.2020.102517.

[49] De Rosa M, Carragher M, Finn DP. Flexibility assessment of a combined heat-power system (CHP) with energy storage under real-time energy price market framework. Therm Sci Eng Prog 2018. doi:10.1016/j.tsep.2018.10.002.

[50] Pedersen TH, Hedegaard RE, Petersen S. Space heating demand response potential of retrofitted residential apartment blocks. Energy Build 2017;141:158–66. doi:10.1016/j.enbuild.2017.02.035.

[51] Salpakari J, Rasku T, Lindgren J, Lund PD. Flexibility of electric vehicles and space heating in net zero energy houses: an optimal control model with thermal dynamics and battery degradation. Appl Energy 2017. doi:10.1016/j.apenergy.2017.01.005.

[52] Krishnamurthy CKB, Vesterberg M, Böök H, Lindfors A V., Svento R. Real-time pricing revisited: Demand flexibility in the presence of micro-generation. Energy Policy 2018. doi:10.1016/j.enpol.2018.08.024.

[53] Ottesen SØ, Tomasgard A, Fleten SE. Multi market bidding strategies for demand side flexibility aggregators in electricity markets. Energy 2018. doi:10.1016/j.energy.2018.01.187.

[54] Hedegaard RE, Pedersen TH, Petersen S. Multi-market demand response using economic model predictive control of space heating in residential buildings. Energy Build 2017;150. doi:10.1016/j.enbuild.2017.05.059.

[55] Péan T, Costa-Castelló R, Salom J. Price and carbon-based energy flexibility of residential heating and cooling loads using model predictive control. Sustain Cities Soc 2019. doi:10.1016/j.scs.2019.101579.

[56] Clauß J, Stinner S, Sartori I, Georges L. Predictive rule-based control to activate the energy flexibility of Norwegian residential buildings: Case of an air-source heat pump and direct electric heating. Appl Energy 2019;237:500–18. doi:10.1016/J.APENERGY.2018.12.074.

[57] Vogler-Finck PJC, Wisniewski R, Popovski P. Reducing the carbon footprint of house heating through model predictive control – A simulation study in Danish conditions. Sustain Cities Soc 2018. doi:10.1016/j.scs.2018.07.027.

[58] Clauß J, Stinner S, Solli C, Lindberg KB, Madsen H, Georges L. Evaluation method for the hourly average CO2eq. Intensity of the electricity mix and its application to the demand response of residential heating. Energies 2019. doi:10.3390/en12071345.

[59] Foteinaki K, Li R, Heller A, Rode C. Heating system energy flexibility of low-energy residential buildings. Energy Build 2018. doi:10.1016/j.enbuild.2018.09.030.

[60] Alimohammadisagvand B, Jokisalo J, Sirén K. Comparison of four rule-based demand response control algorithms in an electrically and heat pump-heated residential building. Appl Energy 2018;209:167–79. doi:10.1016/j.apenergy.2017.10.088.

[61] Afram A, Janabi-Sharifi F. Theory and applications of HVAC control systems - A review of model predictive control (MPC). Build Environ 2014;72:343–55. doi:10.1016/j.buildenv.2013.11.016.

[62] Péan TQ, Salom J, Costa-Castelló R. Review of control strategies for improving the energy flexibility provided by heat pump systems in buildings. J Process Control 2018. doi:10.1016/j.jprocont.2018.03.006.

[63] Tang R, Wang S. Model predictive control for thermal energy storage and thermal comfort optimization of building demand response in smart grids. Appl Energy 2019. doi:10.1016/j.apenergy.2019.03.038.

[64] Verhelst C, Logist F, Van Impe J, Helsen L. Study of the optimal control problem formulation for modulating air-to-water heat pumps connected to a residential floor heating system. Energy Build 2012. doi:10.1016/j.enbuild.2011.10.015.

[65] Gholamibozanjani G, Tarragona J, Gracia A de, Fernández C, Cabeza LF, Farid MM. Model predictive control strategy applied to different types of building for space heating. Appl Energy 2018;231:959–71. doi:10.1016/j.apenergy.2018.09.181.

[66] Wiering, Marco; van Otterlo M. Reinforcement Learning. vol. 12. 2012. doi:10.1007/978-3-642-27645-3.

[67] Kazmi H, Mehmood F, Lodeweyckx S, Driesen J. Gigawatt-hour scale savings on a budget of zero: Deep reinforcement learning based optimal control of hot water systems. Energy 2018. doi:10.1016/j.energy.2017.12.019.

[68] Kazmi H, D'Oca S, Delmastro C, Lodeweyckx S, Corgnati SP. Generalizable occupant-driven optimization model for domestic hot water production in NZEB. Appl Energy 2016. doi:10.1016/j.apenergy.2016.04.108.

[69] Hurtado LA, Mocanu E, Nguyen PH, Gibescu M, Kamphuis RIG. Enabling Cooperative Behavior for Building Demand Response Based on Extended Joint Action Learning. IEEE Trans Ind Informatics 2018. doi:10.1109/TII.2017.2753408.

[70] Dimplex Technische Daten Luft/Wasser Wärmepumpe LA 18S-TU. 2016.

[71] NIBE. Ground source heat pump NIBE F1155 2019.

2

Quantifying demand flexibility of power-to-heat and thermal energy storage in the control of building heating systems

This chapter has been published as:

C. Finck, R. Kramer, R. Li, and W. Zeiler, “Quantifying demand flexibility of power-to-heat and thermal energy storage in the control of building heating systems”, Applied Energy 209 (2018):pp. 409-425.

Abstract

In the future due to continued integration of renewable energy sources, demand-side flexibility would be required for managing power grids. Building energy systems will serve as one possible source of energy flexibility. The degree of flexibility provided by building energy systems is highly restricted by power-to-heat conversion such as heat pumps and thermal energy storage possibilities of a building. To quantify building demand flexibility, it is essential to capture the dynamic response of the building energy system with thermal energy storage. To identify the maximum flexibility a building’s energy system can provide, optimal control is required. In this paper, optimal control serves to determine in detail demand flexibility of an office building equipped with heat pump, electric heater, and thermal energy storage tanks. The demand flexibility is quantified using different performance indicators that sufficiently characterize flexibility in terms of size (energy), time (power) and costs. To fully describe power flexibility, the paper introduces the instantaneous power flexibility as power flexibility indicator. The instantaneous power flexibility shows the potential power flexibility of TES and power-to-heat in any case of charging, discharging or idle mode. A simulation case study is performed showing that a water tank, a phase change material tank, and a thermochemical material tank integrated with building heating system can be designed to provide flexibility with optimal control.

2.1 Introduction

With the increasing application of distributed energy generation, attuning energy consumption to energy generation has become an attractive mitigation strategy for intermittency issues [1]. The ability to control electrical energy consumption based on power grid incentives is called demand response (DR) [2]. Special attention has been given to the energy consumption of buildings which plays a major role in global energy demand [3]. The DR of buildings is comprised of the ability to control the electricity demand profile [3]. The deviation from the reference demand profile is the demand flexibility of buildings [3,4].

A summary of quantification methods for the energy flexibility of buildings is provided by Lopes et al. [3], in which characterization of energy flexibility refers to a demand increase as negative flexibility and a demand decrease as positive flexibility [5,6]. Nuytten et al. [7] calculated the energy flexibility of a combined heat and power (CHP) system with thermal energy storage (TES) wherein flexibility was related to shifting of the electrical consumption in time, expressed as the number of hours of delayed operation. The authors in [7] introduced the concept of forced and delayed flexibility. With forced flexibility, a period is determined in which a system is forced to store excess energy. Delayed flexibility describes a period in which a system is requested to postpone and reduce energy consumption, for instance, by discharging storage. The method of forced and delayed flexibility provides information about time periods with constant power but does not consider power variations over time. Based on the work of D'hulst et al. [8] and Reynders et al. [9], Stinner et al. [6] introduce power flexibility using power curves, defined as a time-dependent difference between maximum and reference power. Power flexibility is required to determine flexibility towards power grid stabilization. Recent studies about demand flexibility of buildings suggest costs as an additional dimension of flexibility [4,10]. De Coninck et al. [4] use conventional utility rates, including cost curves, associated with costs of flexibility. In the study of [4], flexibility refers to shifts in the power demand of the heating, ventilation, and air conditioning system (HVAC). Le Dreau et al. [10] suggest the flexibility factor as performance indicator measuring the potential flexibility during operation. The flexibility factor considers variable electricity price periods and indicates whether the controlled system is flexible enough to shift the heating demand from high to low-price periods. An overview of flexibility indicators is given by Clauß et al. [11]. The review describes performance indicators that relate to all dimensions of demand flexibility. The review also presents an overview of flexibility indicators that are assumed in conventional and modern, optimal control strategies. Clauß et al. [11] concluded that multiple indicators such as self-consumption, self-generation, flexibility factor, storage capacity, storage efficiency are not yet considered in optimal and model-predictive control.

Potential demand-side flexibility sources have been determined by relevant studies [4–10,12–20]. Electrical power-to-heat and thermal energy storage are identified as effective measures to provide flexibility [18–21]. Building-integrated TES technologies are classified into sensible (e.g. building thermal mass (BTM) and water), latent (e.g. phase change materials (PCM) and ice), and thermochemical materials (TCM) [22]. They can also be categorized as active TES (water, ice, PCM, and TCM tanks) and passive TES (BTM and PCM panels) [23,24]. Thermal energy storage can be an effective solution to attune energy supply and demand, combined with electrical appliances. To activate TES tanks with power-to-heat conversion, the working temperature range of the heat storage medium determines the minimum and maximum flexibility. For water tanks, charging and discharging temperatures in space heating (SH) and domestic hot water (DHW) supply is typically between 21 °C and 95 °C [25]. In the case with charging temperatures higher than 95 °C, it is required that the tank equipment can manage high pressures. The use of thermal oil instead of water as storage medium can compensate for higher temperatures but has a comparably lower heat conductivity and specific heat capacity [25]. Adequate materials used as PCM in SH and DHW are presented by Cabeza [26]. The review describes inorganic and organic PCM with melting points up to 120 °C. TCM systems typically hydrate (discharging) above 40 °C and dehydrate (charging) between 80 – 120 °C [27–30]. Latest advances in TCM development include salt hydrates, such as $CaCl_2 \cdot 6H_20$ or $SrBr_2 \cdot 6H_2O$ with dehydration temperatures down to 52 °C [31]. Furthermore, a regeneration strategy (dehydration) is presented by Mette et al. [32] to enable the dehydration at lower temperatures. The regeneration includes a cascade system in which at least two TCM reactors are required. An experimental case study using zeolite-water as TCM was performed that successfully reduced the dehydration temperature from 180 to 130 °C at similar energy storage capacity [32].

Power-to-heat conversion with heat pumps (HP) is likely the most mature and favourable technology enabling flexibility in smart grid operations. Vanhoudt et al. [12] conducted an experimental study comparing actively controlled heat pumps to common reference installations. By aiming at peak shaving and load shifting due to renewable integration, the study successfully increased self-consumption and decreased grid feed-in. Heat pumps that participate in load matching markets were investigated by Salpakari et al. [20]. A heat pump and water thermal energy storage were successfully integrated into cost-optimal control to provide flexibility for wind and PV integration on an urban level. Considering low-order models for optimal control, the study presented a methodology that can be used as a tool by urban planners to analyse the potential flexibility [20]. Fischer et al. [14] reviewed heat pumps in the context of smart grid integration. The operation of HPs was discussed from a holistic perspective which included typical applied control approaches. Predictive and non-predictive controls were compared and it was concluded that predictive control results in cost optimization but also in an increase in system complexity. Many studies [20,33–36] suggest the application of predictive control and optimal control to enable energy flexibility

of HPs with building integrated TES and for prediction of the dynamic behaviour of the system and system components. In a study by Berkenkamp et al. [37], dynamics of a water tank were integrated into an optimal control framework to outperform non-predictive control. However, due to computational complexity, low-order linear models were preferred above non-linear water tank models [36,38], PCM tank, and TCM tank models [4,13,39–46]. For water tanks, recent studies include more detailed storage models, such as one-dimensional stratification models [37,47,48] to overcome inaccurate flow and return temperature predictions. This study integrates more detailed TES tank models (water tank, PCM tank, and TCM tank) in an optimal control framework to capture the complex storage dynamics that occur in heat transfer and mass transfer processes. The more detailed storage models are required to comprehensively present the demand flexibility of a building heating system with HP, electric heater, and TES tank.

The main aim of this study is to investigate the demand flexibility of power-to-heat conversion with thermal storage regarding all three dimensions of flexibility; size (energy), time (power) and costs. Flexibility indicators are chosen to represent the energy flexibility (available storage capacity, storage efficiency), the power flexibility (power shifting capability), and flexibility regarding costs (flexibility factor). Additionally, a power flexibility indicator is introduced in this paper. The instantaneous power flexibility shows the potential power flexibility of TES and power-to-heat in any case of charging, discharging or idle mode. The instantaneous power flexibility is a crucial parameter for providing grid ancillary services towards the power grid.

Furthermore, a simulation case study was performed to quantify the chosen flexibility indicators and demand flexibility in both reference and optimal control scenarios. For optimal control, a classical control strategy is chosen using day-ahead electricity prices as a control signal for the scheduling of power-to-heat and TES. Day-ahead and intra-day electricity markets are well-established energy markets aimed at matching energy supply and demand. Given that the flexibility relates to supply and demand-side is not yet considered in electricity markets, making a step towards the electricity markets requires identification and quantification methods for supply flexibility and demand flexibility. The methodology presented in this paper is thus essential. Section 2.2 describes the methodology and explains the building heating system. In section 2.2.1, an overview of models used for the building heating system is provided. In section 2.2.2, the models are employed in the framework of reference and optimal control. In section 2.2.3, adequate flexibility indicators are explained. Section 2.3 presents the simulation results and illustrates demand flexibility.

2.2 Methodology

For the study of demand flexibility of building heating systems, a small-scale office building is assumed that is located in the Netherlands. The building heating demand of a typical winter day in March is determined due to internal gains (lighting, computers, and occupants) and external disturbances (weather conditions). The building heating system is equipped with a heat pump, electric heater, air-blown heat exchanger, and a thermal energy storage tank (Figure 2.1).

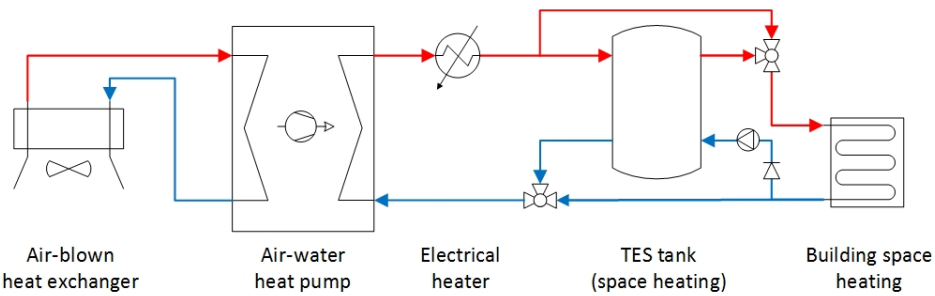

Figure 2.1. Simple process flow diagram of building heating system.

The heat pump and additional electric heating serve as power-to-heat conversion and the thermal storage tank (water tank, PCM tank, and TCM tank) as the source of flexibility. To investigate and compare the flexibility towards the power grid, reference and optimal control in the building heating system are presented. The reference control assumes a typical feed-back controller that uses the heat pump to supply heating. The optimal control integrates the heat pump and optional electric heating with a thermal energy storage tank and aims to optimize the total operational electricity costs. Hourly electricity prices serve as grid signal to optimal control and to optimize flexibility towards the grid. To show the performance of the reference and optimal control scenarios, indicators that relate to demand flexibility are presented.

2.2.1 Modelling

The models of the building heating system are implemented in a simulation framework using MATLAB2016a. For each model, a simulation time step of 1 s was used to solve equations to limit the truncation error of the TES model.

Heat pump model, air-blown heat exchanger model, and electric heater model

The HP model uses a piecewise-linear interpolation function, including the condenser outlet temperature, the evaporation inlet temperature, and the heating capacity of the heat pump to calculate the coefficient of performance (COP), see Figure 2.2. Manufacturer data from Dimplex air-water heat pumps [49] is used to calculate the electrical power consumption and the corresponding COP.

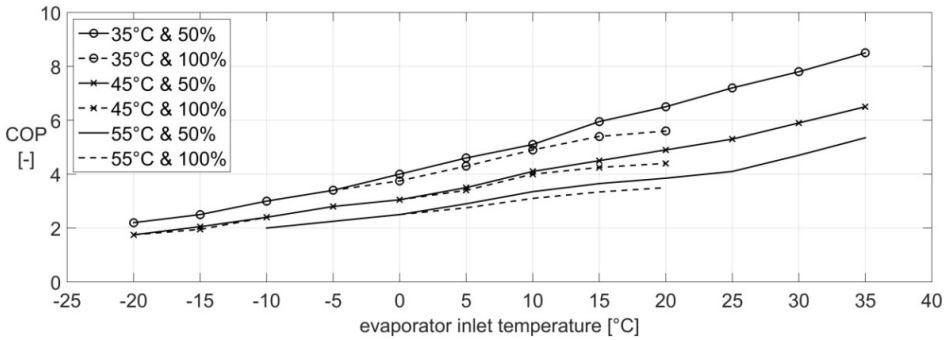

Figure 2.2. Performance of the air-water heat pump (HP). The coefficient of performance (COP) is a function of evaporator inlet temperature for different condenser outlet temperatures (35 °C, 45 °C, 55 °C) and heating capacity of the heat pump (50%, 100%) [49].

The heat exchanger of the HP on the evaporator side is combined with an air-blown heat exchanger. The model of the air-blown heat exchanger assumes that the evaporator inlet temperature is a constant temperature source equal to the ambient air. The HP provides heating to the building and charges the TES tank. The condenser outlet temperature is considered as the inlet temperature of the radiant heaters and the inlet temperature of the TES tank during charging. The HP guarantees a maximum condenser outlet temperature of 60 °C, sufficiently charging water and PCM tanks. To load TCM tanks, temperatures higher than 60 °C are commonly required to activate the desorption process. In this study, the HP is used to preheat the TCM tank to 60 °C. Auxiliary electric heating provides higher charging temperatures. The model for the electric heater assumes that the heating power is equal to the electrical power consumption.

Building model

A small-scale office building model was adopted from [50] with which the Building Resistance-Capacitance Modelling (BRCM) toolbox [51] was used for building modelling. An advanced resistance-capacitance (RC) network represents the building, including internal and external walls, multiple zones, windows, and the ambient environment. The BRCM toolbox uses constant heat transfer values for conduction in walls, convection, and radiation between walls and zones. The BRCM model has been validated with comparison to EnergyPlus. For this study, the BRCM toolbox was modified to simulate radiant heating by integrating the inlet and outlet temperatures of the radiant heater. A two-floor office building (135 m² floor area per floor) with a maximum of eight persons per floor is assumed [50]. The building consists of 7 rooms per floor and is composed of building elements (Table 2-1) containing concrete (0.73 W/(mK), 921 J/(kgK), 1920 kg/m^3) and external mineral insulation (0.04 W/(mK), 830 J/(kgK), 90 kg/m^3).

Table 2-1. The building structure of two-floor office building [50].

Building elements	Materials	Thickness [m]
External wall	Mineral insulation; concrete	0.05; 0.30
Internal wall	Concrete	0.15
Ceiling, floor	Concrete	0.25

Thermal energy storage models

In the models, TES tanks are assumed to be cylindrical vessels. Figure 2.3 shows the design of the water tank, PCM tank, and TCM tank.

The water tank is comprised of a vessel without an internal heat exchanger. The PCM and TCM tank include compartments of packed-bed reactors without any additional electric resistance. The number of compartments is a design decision as can be seen in Figure 2.4. The dimensions of the heat exchangers include the calculation of the pressure drop which is caused by the flow of the heat transfer medium through the internal heat exchanger of the PCM and TCM tank according to Equation 2-1 [52]

$$\Delta p = \left(V_{dot}, d_{tube,HX}, l_{tube,HX}, Pr, Re, Nu\right) \quad (2\text{-}1)$$

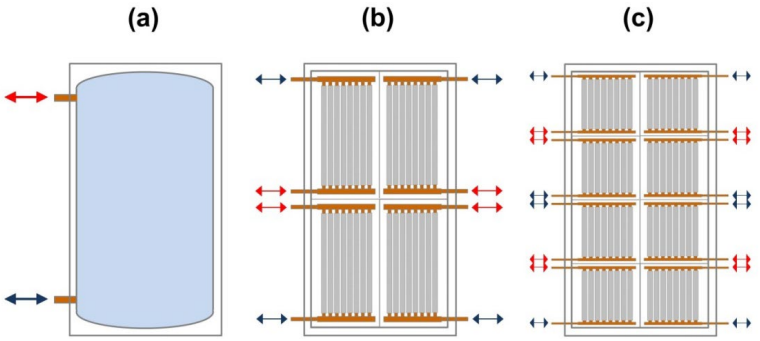

Figure 2.3. Schematic design of thermal energy storage (TES) tanks: (a) water tank; (b) packed-bed phased change material (PCM) tank with four compartments; c) packed-bed thermochemical material (TCM) tank with eight compartments.

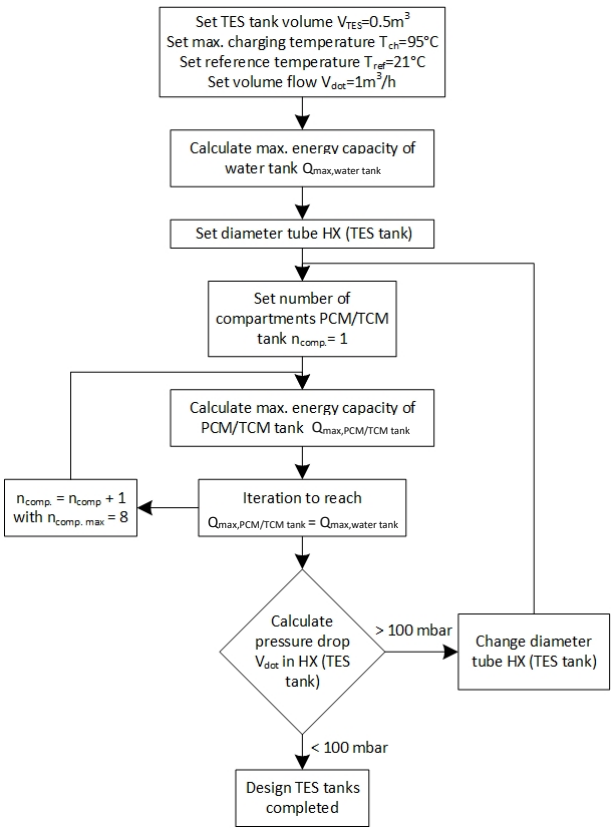

Figure 2.4. Flowchart design decision of TES tanks.

A PCM tank with four compartments and a TCM tank with eight compartments is chosen.

The PCM and TCM reactors consist of vertical copper tubes covered with the heat storage medium. In the reactor, a layer of heat storage medium (PCM or TCM) is applied to the surface of the copper tubes. Because such a layer may be impractical to add, current setups often make use of finned tubes. However, to simplify the simulation of the PCM and TCM layer, the heat exchanger is modelled with a layer of heat storage material. All TES tanks are insulated using a material 0.1 m thick with a thermal conductivity of 0.033 W/(mK) [53].

The heat and mass transfer of the TES tanks is mathematically formulated using a one-dimensional representation. Previous case studies have successfully used the one-dimensional representation of water tanks [54–56], PCM tanks [57,58], and TCM tanks [59,60]. In this case study, the one-dimensional convection-diffusion-reaction equation [61–63] is applied to all TES tanks according to

$$\frac{\partial \theta}{\partial t} = \alpha \frac{\partial^2 \theta}{\partial x^2} - u \frac{\partial \theta}{\partial x} + f(\theta), \qquad 0 \le x \le x_{max}, \qquad t \ge 0, \tag{2-2}$$

$$\theta(x, 0) = f(x), \qquad 0 \le x \le x_{max}, \tag{2-3}$$

$$\theta(0, t) = g(t), \qquad 0 \le t \le t_{max}, \tag{2-4}$$

$$\theta(x_{max}, t) = h(t), \qquad 0 \le t \le t_{max}, \tag{2-5}$$

where $f(\theta)$ is the reaction term, $\theta = \theta(x, t)$ is the dependent variable, α is a positive constant coefficient, u is a positive constant speed, x is the spatial coordinate, t is time, and x_{max} is the range of the spatial domain. Here, f(x), g(t) and h(t) are functions that determine the initial conditions (2-3) and the boundary conditions (2-4, 2-5).

The current study applies a finite difference (FD) method to numerically solve the one-dimensional convection-diffusion equation [55,64,65]. The finite difference method uses an approximation to $\theta = \theta(x, t)$ according to

$$\frac{\partial \theta}{\partial x} \approx \frac{\theta_{i+1} - \theta_i}{\Delta x}, \tag{2-6}$$

$$x_i = (i-1)\Delta x, \qquad i = 1,2,\dots M, \qquad 0 \le x \le x_{max}, \tag{2-7}$$

$$t_n = (n-1)\Delta t, \qquad n = 1,2,\dots N, \qquad 0 \le t \le t_{max}, \tag{2-8}$$

where Δx is the spatial discretization and Δt is the temporal discretization [65].

The simulation model integrates the discrete approximation with the implicit and unconditionally stable Crank-Nicolson [66] scheme which is more accurate than other FD-schemes with respect to the temporal truncation error $O(\Delta t^2)$ [65]. The discrete form of Equation (2-2) is calculated according to

$$\alpha \frac{\partial^2 \theta}{\partial x^2} = \frac{\alpha}{2}\left(\frac{\theta_{i+1}^{n+1} - 2\theta_i^{n+1} + \theta_{i-1}^{n+1}}{\Delta x^2} + \frac{\theta_{i+1}^{n} - 2\theta_i^{n} + \theta_{i-1}^{n}}{\Delta x^2}\right) \tag{2-9}$$

$$a \frac{\partial \theta}{\partial x} = \frac{u}{4}\left(\frac{\theta_{i+1}^{n+1} - \theta_{i-1}^{n+1} + \theta_{i+1}^{n} - \theta_{i-1}^{n}}{\Delta x}\right). \tag{2-10}$$

The convection-diffusion equation can now be written as

$$\frac{\theta_i^{n+1} - \theta_i^n}{\Delta t} = \frac{\alpha}{2}\left(\frac{\theta_{i+1}^{n+1} - 2\theta_i^{n+1} + \theta_{i-1}^{n+1}}{\Delta x^2} + \frac{\theta_{i+1}^{n} - 2\theta_i^{n} + \theta_{i-1}^{n}}{\Delta x^2}\right) - \frac{u}{4}\left(\frac{\theta_{i+1}^{n+1} - \theta_{i-1}^{n+1} + \theta_{i+1}^{n} - \theta_{i-1}^{n}}{\Delta x}\right) + f(\theta_i^n). \tag{2-11}$$

In the following sections, this approach is applied to the water tank, PCM tank, and TCM tank. The main heat and mass transfer effects and their implementations in the numerical solution are described.

Thermal energy storage models - water tank model

The model uses a stratified water tank. For charging, inflow takes place at the top, and outflow at the bottom. In the case of discharging, i.e. providing heating, cold water enters the bottom and leaves through the top (see Figure 2.3). The model includes heat and mass transfer by convection and conduction. A vertical temperature distribution $\partial T/\partial x$ is assumed which depends on the speed of the water flow u and the thermal properties to obtain α according to

$$\frac{\partial T}{\partial t} = \alpha \frac{\partial^2 T}{\partial x^2} - u \frac{\partial T}{\partial x}, \qquad 0 \le x \le x_{max}, \qquad t \ge 0 \tag{2-12}$$

$$\alpha = \frac{\lambda}{\rho c_p}, \tag{2-13}$$

where x is the spatial vertical coordinate and x_{max} is the height of the tank. The speed u is spatially constant and derived from the water volume flow divided by the cross sectional area perpendicular to the volume flow. Table 2-2 shows the properties of the water tank and the water as a heat transfer and storage medium.

Table 2-2. Properties of water as heat storage and heat transfer medium.

Water tank volume [m³]	Volume flow [m³/h]	Density [kg/m³] (303 K)	Specific heat [J/(kgK)] (303 K)	Thermal conductivity [W/(mK)] (303 K)	Max. energy capacity [GJ] deltaT = 74 K
0.5	1	996	4180	0.616	0.15

Thermal energy storage models - phase change material tank model

The water enters the PCM tank and exchanges heat with the PCM layer (Figure 2.3) which melts during charging and, to provide heating, solidifies during discharging. The model uses the enthalpy h of the PCM to implement the melting process in the model. Equation (2-14) shows a one-dimensional formulation for the PCM including heat conduction through the PCM layer [58] according to

$$\rho \frac{\partial h}{\partial \mathrm{t}} = \lambda \frac{\partial^2 T}{\partial x^2}, \qquad 0 \leq x \leq x_{max}, \qquad t \geq 0, \tag{2-14}$$

in which x is the spatial coordinate and x_{max} the thickness of the PCM layer. Table 2-3 presents the properties of the PCM tank. The design of the PCM tank is adapted to the volume and energy capacity of the water tank according to Figure 2.4.

Table 2-3. Properties of the PCM tank.

PCM tank volume [m³]	Number of compart. [-]	Volume flow of heat transfer medium [m³/h]	Diameter of heat exchanger tube [m]	Length of heat exchanger tube per compart. [m]	Thickness of PCM layer [m]	Mass of PCM [kg]	Max. energy capacity [GJ] deltaT = 74 K
0.5	4	1	0.025	35	0.015	511	0.15

Table 2-4 presents the properties of the PCM. $CaCl_2 \cdot 6H_2O$ was chosen as PCM because it melts at 29 °C that is below typical maximum charging temperatures of heat pumps of 60 °C. An overview of PCMs for heat storage application with different melting points can be found in [26,67,68].

Table 2-4. Properties of the PCM ($CaCl_2 \cdot 6H_2O$) [69].

Melting point [°C]	Melting enthalpy [J/kg]	Density [kg/m³]		Specific heat [J/(kgK)]		Thermal conductivity [W/(mK)]	
		Solid	Liquid	Solid	Liquid	Solid	Liquid
29	190.8e03	1710	1530	2200	1400	1.09	0.54

The enthalpy formulation (Equation 2-14) enables the implementation of non-isothermal phase change. Figure 2.5 illustrates the relationship between enthalpy and temperature, highlighting the transition phase between the solid and liquid state of the PCM.

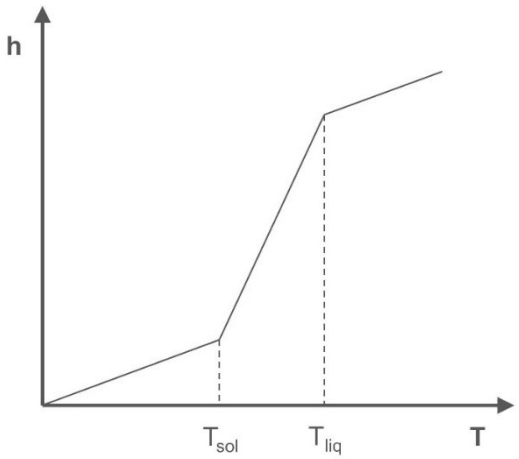

Figure 2.5. Piecewise-linear function h(T) for non-isothermal phase change with the transition temperature T_{sol} between the solid and solid-liquid interface and the transition temperature T_{liq} between the liquid and solid-liquid interface [58].

Non-isothermal phase change is calculated according to [58]

$$h = \begin{cases} c_{p,sol}T & T \leq T_{sol} \\ c_{p,sol}T_{sol} + \dfrac{h_{\Delta liq,sol}(T - T_{sol})}{(T_{liq} - T_{sol})} & T_{sol} < T \leq T_{liq} \\ c_{p,sol}T_{sol} + h_{\Delta liq,sol} + c_{p,liq}T & T > T_{liq} \end{cases}. \quad (2\text{-}15)$$

Furthermore, to simplify the simulations, it is assumed that the PCM is homogenous and isotropic [69] and natural heat convection during the melting process is neglected [70].

Thermal energy storage models - thermochemical material tank model

The model uses a closed TCM unit consisting of the sorption unit (TCM tank) and an evaporator-condenser unit and operates in a vacuum. The TCM tank is a packed-bed reactor in which a sorbent (zeolite13X) desorbs and adsorbs a fluid (water). During desorption, a high-temperature source such as an electric heater serves as a dehydration source. A condenser that is supplied by a low-temperature source, such as ambient air, collects the produced refrigerant (water). During adsorption, the condenser operates as an evaporator. The refrigerant is evaporated and simultaneously adsorbed.

The released heat from the TCM tank can be used for space heating or domestic hot water [29,71]. This study uses zeolite13X-water as a sorption pair because it is one of the most common TCM in current research on component and system design with favourable hydrothermal and mechanical stability and corrosion behaviour [29]. The latest advances in TCM development focus on salt hydrates, such as $Na_2S{\cdot}9H_2O$ with an energy density of up to 3.17 GJ/m^3 [72].The TCM tank model is similar to the PCM tank model (Figure 2.3), but the PCM is replaced by a TCM as the heat storage medium. The evaporator and condenser are assumed to be a constant, low-temperature source. Additional heat exchange for the process of evaporation and condensation is not modelled.

The heat and mass transfer model of the TCM unit includes the diffusion of the refrigerant (water) to and through the adsorbent (zeolite13X), the adsorption process, the heat conduction through the TCM layer, and heat exchange with the heat transfer medium [59,73]. Heat transfer in the adsorbent bed is calculated by

$$\frac{\partial T}{\partial t} = \alpha \frac{\partial^2 T}{\partial x^2} + \frac{H_s}{c_p}\frac{d\bar{q}}{dt}, \qquad 0 \le x \le x_{max}, \qquad t \ge 0, \tag{2-16}$$

moreover, the mass diffusion process through the adsorbent bed is calculated with

$$\frac{\partial m_{ads}}{\partial t} = D \frac{\partial^2 m_{ads}}{\partial x^2} + m_{sorb}\frac{d\bar{q}}{dt}, \qquad 0 \le x \le x_{max}, \qquad t \ge 0, \tag{2-17}$$

where x is the spatial coordinate, x_{max} is the thickness of the TCM layer, and m_{sorb} is the mass of the dry adsorbent. Here, $T = T(x,t)$ describes the temperature distribution affected by the rate of adsorbed refrigerant $d\bar{q}$ and the adsorption enthalpy H_s. $m_{ads} = m_{ads}(x,t)$ represents the adsorbate distribution in the TCM layer affected by the diffusion D of the refrigerant through the adsorbent [59,73]. The average rate of adsorbed refrigerant $d\bar{q}$ is the main driving force during the adsorption process and implemented using the linear driving force (LDF) method according to

$$\frac{d\bar{q}}{dt} = k_m\left(q_{eq} - \bar{q}\right). \tag{2-18}$$

The LDF method accounts for the difference between equilibrium and amount of adsorbate including the mass transfer coefficient k_m [59,73].

This linear driving force is determined by calculating the vapor pressure of water in equilibrium and in solid phase of the dry material (zeolite13X). The equilibrium vapor pressure relates to the condensation and evaporation temperature, because condensation and evaporation model are considered as constant temperature source. The vapor pressure values in equilibrium and in solid phase of the dry material are derived from the Clausius-Clapeyron relation [71] according to

$$\frac{dp}{dT} = \frac{\Delta h_v}{T\Delta v} \cong \frac{p\,\Delta h_v}{RT^2}, \tag{2-19}$$

in which Δh_v is the molar enthalpy, Δv is the molar volume difference of water vapor (also illustrated in Figure 2.6).

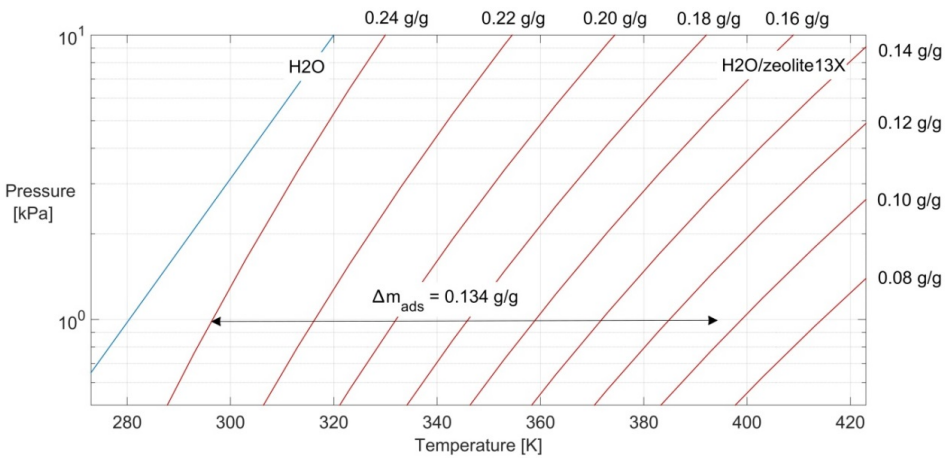

Figure 2.6. Vapor pressure lines for zeolite 13X–water based on data from [74] with, for example, a maximum capacity of 0.24 g/g [75]. Desorption temperature at 120 °C, condensation and evaporation temperature at 10 °C, and adsorption temperature at 20 °C result in a loading difference of 0.134 g/g.

Table 2-5 and Table 2-6 show the properties of the TCM tank and the TCM layer. The design of the TCM tank is adapted to the volume of the water and PCM tank according to Figure 2.4. The energy capacity is 1/3 compared with the water and PCM tank. To reach a larger energy capacity higher charging temperatures than 95 °C are required. Alternatively, a different TCM material can be chosen. However, this study considers zeolite13X-water because all the material properties (Table 2-6) are available.

Table 2-5. Properties of TCM tank.

TCM tank volume [m^3]	Number of compart. [-]	Volume flow of heat transfer medium [m^3/h]	Diameter of heat exchanger tube [m]	Length of heat exchanger tube per compart. [m]	Thickness of TCM layer [m]	Mass of TCM [kg]	Energy capacity [GJ] deltaT = 74K
0.5	8	1	0.025	45	0.005	122	0.05

Table 2-6. Properties of the TCM (zeolite13X-water) [75,76].

Adsorption enthalpy [J/kg]	Density [kg/m^3]	Specific heat [J/(kgK)]	Thermal conductivity [W/(mK)]	Diffusion coefficient [m^2/s]
3.2e06	620	836	0.2	7.5e-09

2.2.2 Control framework

The models of the building heating system are implemented in the framework of reference control, and optimal control and simulations are conducted for the different TES tanks.

Reference control

In the reference control, the HP is used to compensate the heating demand of the building. To identify maximum flexibility, TES tanks are not applied in the reference case. Due to the absence of TES, optimization is not required and a feedback controller (P-controller) is implemented to investigate reference control. The feedback controller regulates the heat pump based on predefined temperature set points $T_{zone,set}$ according to

$$T_{zone,set} = \begin{cases} 15\,℃, & t = 0-6, 19-24 \\ 15\,℃, & t = 6-7 \\ 20\,℃, & t = 7-8, 12-13, 17-19 \\ 21.5\,℃, & t = 8-12, 13-17 \end{cases}. \quad (2\text{-}20)$$

To limit the start-stop cycles of the HP to a maximum of four times per hour, a control time step of 15 min is used. The electricity consumption of the air-blown heat exchanger is not considered.

Optimal control

The optimal control of the building heating system aims to minimize the electricity consumption costs for operating the HP and the electric heater. The control time step of 15 min is identical to reference control. The electricity consumption of the air-blown heat exchanger is as introduced not considered. The cost-optimal control schedules the charging and discharging of either the water tank, the PCM tank, or the TCM tank, by making use of a dynamic optimization routine to predict control actions for 24 hours. Figure 2.7 shows the framework of the optimal control of the building heating system including grid signal, constraints, disturbances, objective function, optimization problem, state variables, and control variables. The grid signal corresponds to hourly day-ahead electricity prices that are taken from the Dutch Amsterdam Power Exchange (APX) power spot market for an average day in March 2016 during the heating period. Disturbances in optimal control estimate internal heating gains and ambient conditions. The occupancy rate ϵ_t is used to model the internal heat gains of lighting systems, computers, and occupants. The occupancy rate refers to the ratio of occupants to the maximum amount of occupants and determines the minimum comfort temperature $T_{zone,min}$ according to:

$$\epsilon_t = \begin{cases} 0, & T_{zone,min} = 15\,℃, & t = 0-6, 19-24 \\ 0.1, & T_{zone,min} = 15\,℃, & t = 6-7 \\ 0.5, & T_{zone,min} = 20\,℃, & t = 7-8, 12-13, 17-19 \\ > 0.7, & T_{zone,min} = 21.5\,℃, & t = 8-12, 13-17 \end{cases}. \quad (2\text{-}21)$$

The occupancy model, which allows the implementation of Markov chains, is adopted from [77]. More information about the occupancy model can be found in a previous case study [50]. However, in this case study, perfect occupancy prediction and ideal weather forecasting are assumed. Figure 2.8 presents the weather data from a small-scale office building located in the Netherlands.

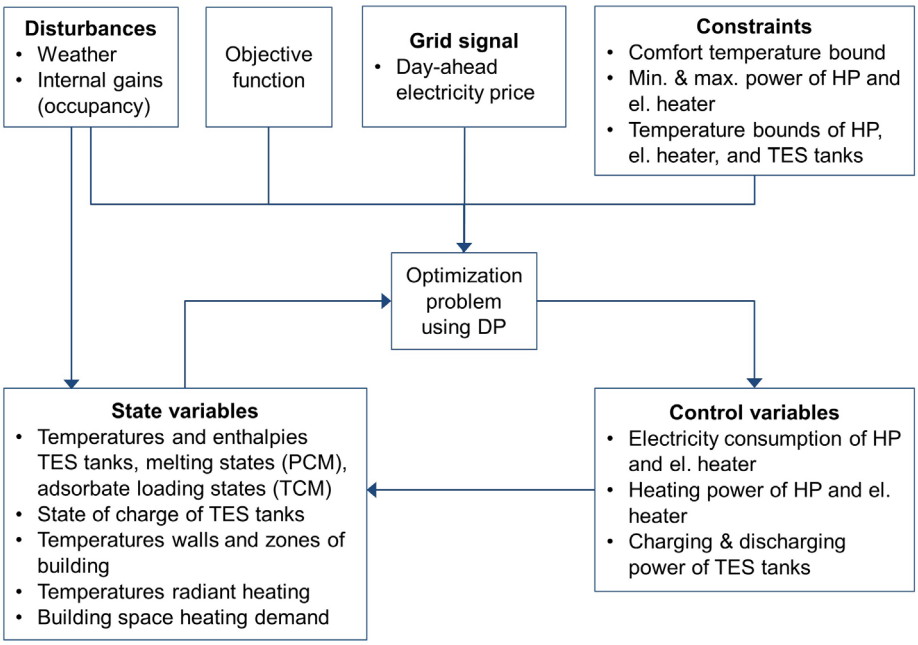

Figure 2.7. Framework of optimal control of building heating system.

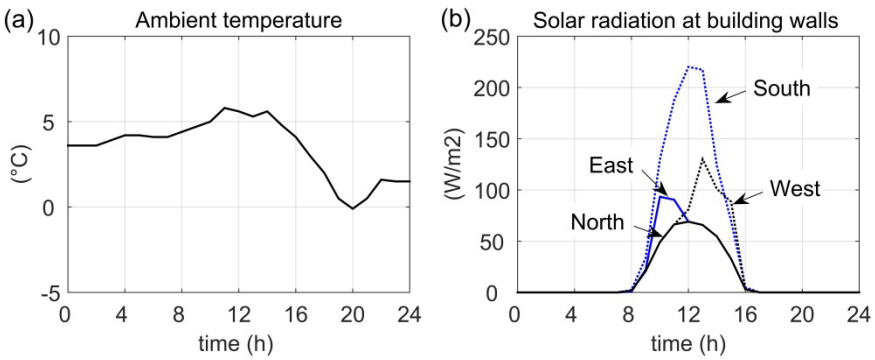

Figure 2.8. Typical meteorological year (TMY) weather data for De Bilt, the Netherlands, 1st of March: (a) ambient temperature, (b) solar radiation at building walls.

The optimal control framework uses the TES tank models integrated with the building heating system as discussed in section 2.2.1. Because the building heating system including TES tanks is inherently non-linear, the optimal control problem is solved using dynamic programming (DP) as optimization methodology. Dynamic programming employs the different TES tank models for reasonable computation times. The basic structure of dynamic programming refers to the Bellman equation [78] according to

$$J(x_0) = \min_{\pi} J_{\pi}(x_0), \tag{2-22}$$

$$J_{\pi}(x_0) = E\left[g_N(x_N) + \sum_{t=0}^{N}(x_t, \mu_t(x_t), \varepsilon_t)\right], \tag{2-23}$$

$$x_{t+1} = f_t(x_t, u_t, \varepsilon_t), \quad t = 0, \dots, N-1, \tag{2-24}$$

$$\text{with } u_t \in U_t(x_t), \ \pi = \{\mu_0, \dots, \mu_{N-1}\}, \ u_t = \mu_t(x_t), \ \mu_t(x_t) \in U_t(x_t) \ \forall \ x_t, \tag{2-25}$$

where f_t describes the building heating system, t the discrete time, N the planning horizon of 24 h, x_t the state variables, u_t the controls variables, U_t the control constraints, ε_t the random parameter (occupancy rate), $J(x_0)$ the optimal cost function, and $J_{\pi}(x_0)$ the expected costs with the policy π at x_0.

Because dynamic programming aims to minimize the electricity consumption costs for operating the HP and the electric heater, the objective function to be minimized consists of the total expected costs for electricity usage. As can be seen in Figure 2.7, the control variables are associated with power consumption and heating power of the HP and electric heater, and the charging and discharging power of the TES tank. DP employs these control options having a vector of discrete states in which:

- HP compensates heating demand of building (no charging and discharging of TES)
- HP compensates heating demand of building and charges TES tank, optionally additional charging of TES tank by electric heating
- HP and/or discharge of TES compensate heating demand of building
- HP and optionally electric heater charge TES tank (no heating demand of building)

The control options are implemented in the DP loop as control decisions which are calculated at each state as can be seen in Figure 2.9.

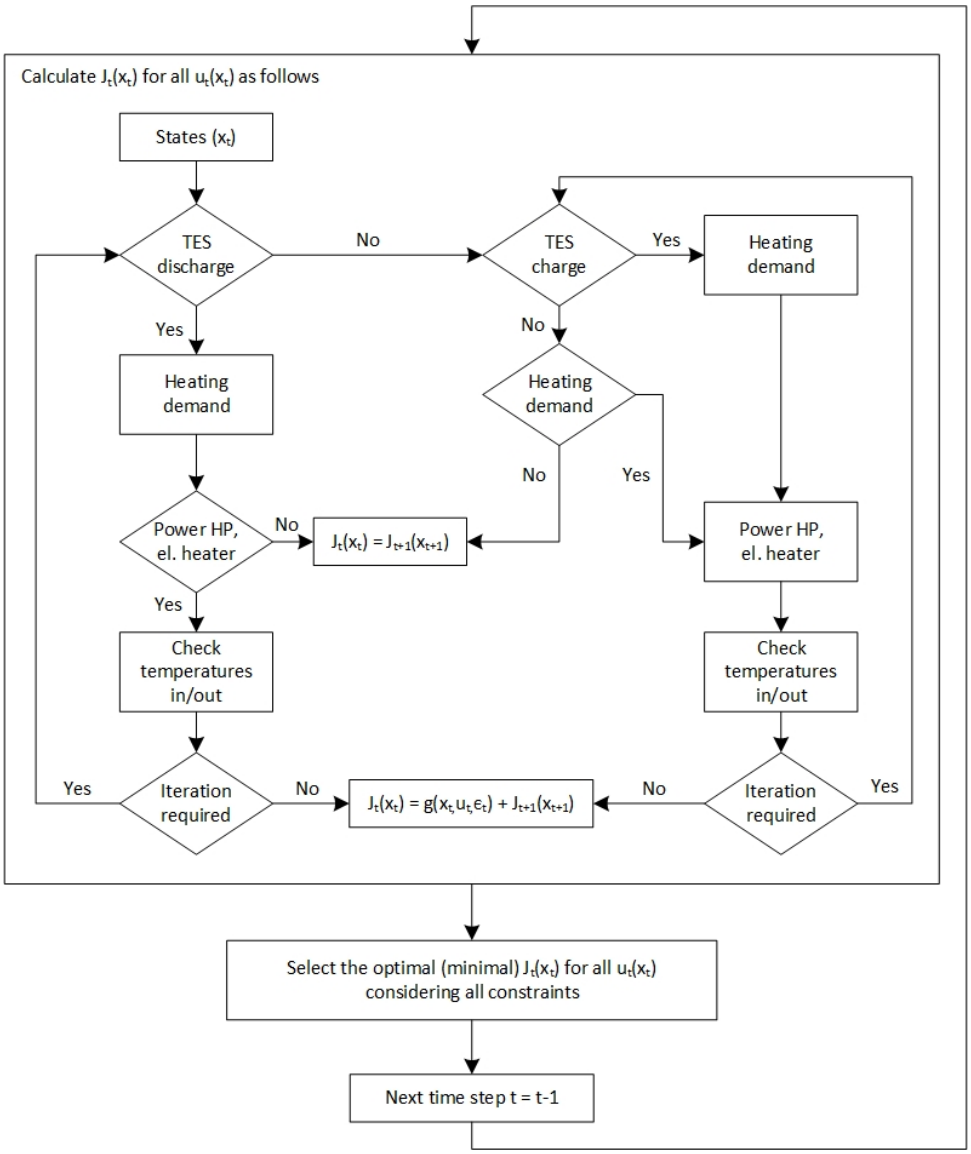

Figure 2.9. Simplified flowchart of control decisions at each state in dynamic programming (DP) optimization loop.

2.2.3 Demand flexibility

Cost-optimal control applies day-ahead electricity prices as grid signal that is crucial information for the optimization. Besides, the forecasting of weather, the predictions of internal heating gains, and the design of the heating system determine the optimal use of building demand flexibility. The amount of flexibility a building heating system can deliver regarding all three dimensions of demand flexibility, size (energy), time (power) and costs, is quantified in corresponding flexibility indicators.

Demand flexibility – energy

In this case study, the indicators, available storage capacity, storage efficiency [15] represent the energy flexibility. Equation (2-26) shows the available storage capacity according to

$$Q_{OC} = \int_{l_{OC\,start}}^{l_{OC\,end}} \left(P_{OC} - P_{Ref}\right) dt, \tag{2-26}$$

where Q_{OC} is the available storage capacity, P_{OC} the heating power, and l_{OC} the duration corresponding to the period of optimal control (OC). The heating demand during reference control is formulated as P_{Ref} [15]. The available storage capacity can be summarized as the amount of energy that is shifted during optimal control. In cost-optimal control, charging and discharging of a TES tank takes place in a control horizon of 24 h. While charging events refer to demand increase as upward heating power $P_{OC,up}$, discharging events represent demand decrease as downward heating power $P_{OC,down}$. The ratio between discharging and charging events over the entire 24 h control horizon is defined as storage efficiency [15] or shifting efficiency [10] η_{OC}. According to Equation (2-27),

$$\eta_{OC} = \frac{\sum_{n_{OC}=1}^{m} \int_{l_{OC,down\,start}}^{l_{OC,down\,end}} \left(P_{OC,down} - P_{Ref}\right) dt}{\sum_{n_{OC}=1}^{m} \int_{l_{OC,up\,start}}^{l_{OC,up\,end}} \left(P_{OC,up} - P_{Ref}\right) dt}, \tag{2-27}$$

the storage efficiency indicates the effective use of the stored heat that compensates HP heating power during optimal control.

Demand flexibility – costs

An energy flexibility indicator that relates to the dimension of electricity costs during operation is the flexibility factor FF [10]. Low electricity and high electricity periods are considered according to

$$FF = \frac{\int_{t_{low\ price\ start}}^{t_{low\ price\ end}} P_{heating}\, dt - \int_{t_{high\ price\ start}}^{t_{high\ price\ end}} P_{heating}\, dt}{\int_{t_{low\ price\ start}}^{t_{low\ price\ end}} P_{heating}\, dt + \int_{t_{high\ price\ start}}^{t_{high\ price\ end}} P_{heating}\, dt}, \tag{2-28}$$

In which $P_{heating}$ is the amount of heating power over low and high-price periods l.
To estimate the different pricing periods, standard deviation is assumed that relates to the electricity prices of the entire 24 h control horizon. Pricing periods that exceed the normal distribution with one standard deviation of -1σ and 1σ account for either low and high price periods. The flexibility factor varies between -1 and 1 whereas -1 correlates to a highly inflexible controlled system and 1 indicates highest desired flexibility.

Demand flexibility – power

Energy flexibility is introduced as the integral of power flexibility which refers to the evolution of heating power during each time step of optimal control. An indicator of power flexibility is the power shifting capability [15] according to

$$P_{\delta} = P_{OC} - P_{Ref}, \tag{2-29}$$

where P_{δ} is the difference between power consumption during optimal control and reference control. For a building heating system with HP, electric heater and TES, the power shifting capability includes thermal (heating) power shifting $P_{\delta,th}$ according to

$$P_{\delta,th} = (P_{OC,th.output\ HP} + P_{OC,th.output\ el.heater}) - (P_{Ref,th.output\ HP} + P_{Ref,th.output\ el.heater}), \tag{2-30}$$

and electrical power shifting $P_{\delta,el}$ due to the electricity consumption of the HP and electric heater,

$$P_{\delta,el} = \left(P_{OC,el.cons.HP} + P_{OC,el.cons.el.heater}\right) - \left(P_{Ref,el.cons.HP} + P_{Ref,el.cons.el.heater}\right). \quad (2\text{-}31)$$

To comprehensively represent the potential power flexibility of TES and power-to-heat, this paper introduces the instantaneous power flexibility. In contrast to the power shifting capability, the instantaneous power flexibility does not require the determination of a reference case and represents the potential flexibility towards the power grid. This is crucial information to provide grid ancillary services of very short (1 ms – 5 min), short (5 min – 1 h), intermediate (1 h – 3 d) and long duration (>3 d) [18]. Because TES systems mostly slowly respond to variations, services to the electricity grid and power market as of min time scale are suitable. Possible services relate to electricity spot markets and load shaping, levelling, peak reduction and congestion management [14,18]. In this case study, the instantaneous power flexibility P_{inst} is presented on a flexibility time step of 1 h and includes electrical instantaneous power flexibility according to

$$P_{inst.el.} = f\left(P_{inst.th.}, COP_{power-to-heat}\right), \quad (2\text{-}32)$$

and thermal instantaneous power flexibility according to

$$P_{inst.th.} = f\left(T_{HT}, \dot{m}_{HT}\right), \quad (2\text{-}33)$$

where T_{HT} is the temperature, and $\dot{m}_{HT}$ is the mass flow of the heat transfer medium that are used to charge or discharge the TES tank. In any case of charging, discharging or idle mode, the instantaneous power flexibility shows the thermal response of TES tanks and the electrical response of power-to-heat devices. The presentation of the thermal response of TES is introduced as performance maps of TES [79]. These maps are developed to show the dynamic behaviour of TES in the control of building energy systems. An example of performance maps of the PCM tank is illustrated in Figure 2.10 and takes into account the properties presented in section 2.2.1.

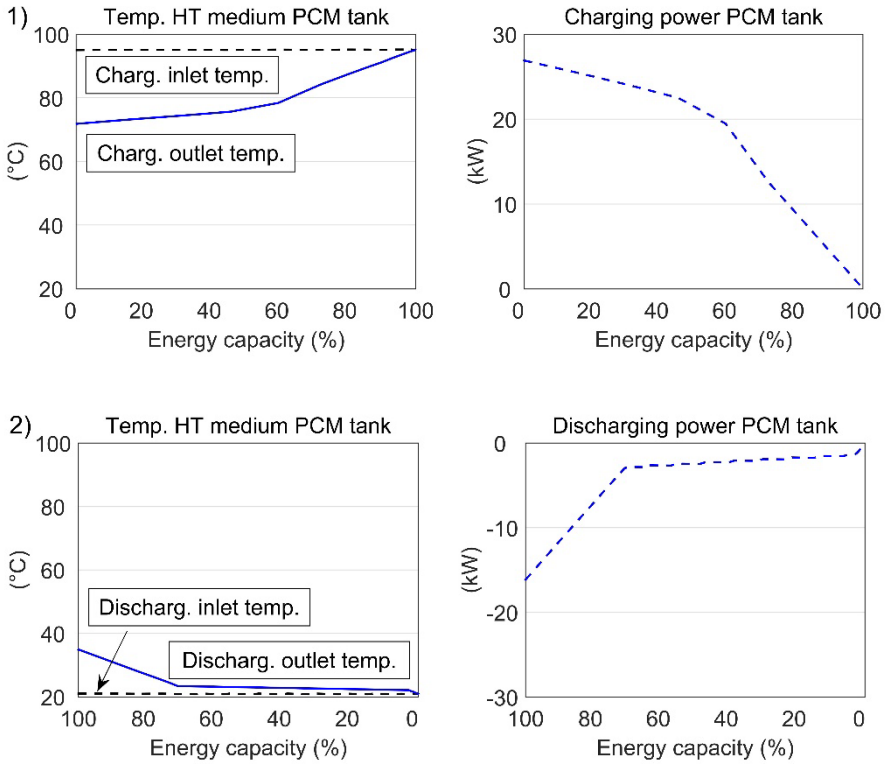

Figure 2.10. Performance maps of the PCM tank. The performance maps show inlet, outlet temperature of the heat transfer (HT) medium over energy capacity and charging/discharging power over energy capacity [79]. The properties of the PCM tank are taken from section 2.2.1 (Thermal energy storage models). The performance maps are illustrated for 1) a charging case in which the PCM tank is charged from 0% (21 °C) to 100% (95 °C), 2) a discharging case in which the PCM tank is discharged from 100% (95 °C) to 0% (21 °C).

In this case study, the performance maps of TES tanks are used to calculate the thermal instantaneous power flexibility. As an example, a charging case is simulated in which the TES tanks are charged with a temperature of 95 °C. Based on the control decisions of cost-optimal control, the thermal and electrical instantaneous power flexibility are simulated for each optimal control time step. The thermal response of TES tanks and the electrical response of power-to-heat devices is shown for a flexibility time step of 1 h. It is to emphasize that the flexibility time step of 1 h is calculated with intermediate steps of 5 min to exclude any starting effects of the first 5 min.

2.3 Results

2.3.1 Reference control

In reference control, the HP compensates the heating demand of the building. As described in section 2.2.2 (Reference control), TES tanks are not considered in the reference case. Figure 2.11 shows the simulation results of the reference control with 15 min control time steps.

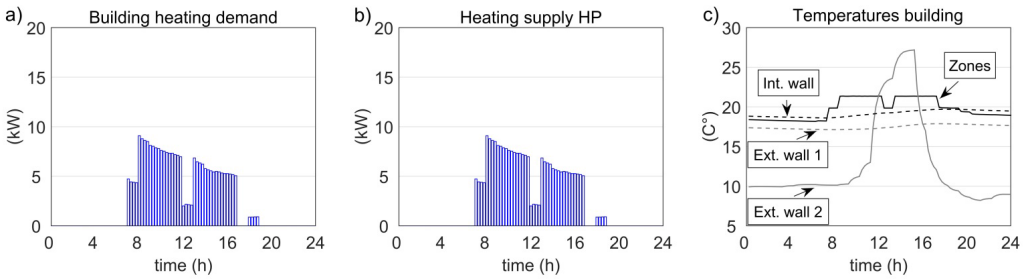

Figure 2.11. Simulation results – reference control, a) building heating consumption, b) heating supply by the HP, and c) temperatures in building including average indoor temperature (zones), average temperature of the concrete of the internal walls (Int. wall), average temperature of the concrete at the inner surface of the external walls (Ext. wall 1), and average temperature of the insulation at the outer surface of the external walls (Ext. wall 2).

The building heating consumption (Figure 2.11a) is identical to the heating supplied by the HP (Figure 2.11b). The resulting average COP is 4.5. As can be seen in Figure 2.11c, the average indoor temperature (zones) is always maintained above the minimum zone temperature set points (Equation 2-20). When the heating power is reduced or heating supply is switched off, the zone temperature drops. For example, between 5 pm and 6 pm, the zone temperature decreases from 21.5 °C to 20 °C. This is due to the lower temperatures of the internal (Int. wall) and external walls (Ext. wall 1) (Figure 2.11c).

2.3.2 Optimal control

In optimal control, HP and TES are used to compensate the heating demand of the building. The heating consumption is similar to the reference case. In contrast to reference control, optimal control applies the use of TES tanks including optimization of charging and discharging. As introduced in section 2.2.2 (Optimal control), optimal operation of TES, HP and electric heater account for minimizing the total operational electricity costs that correspond to hourly APX electricity prices (Figure 2.12).

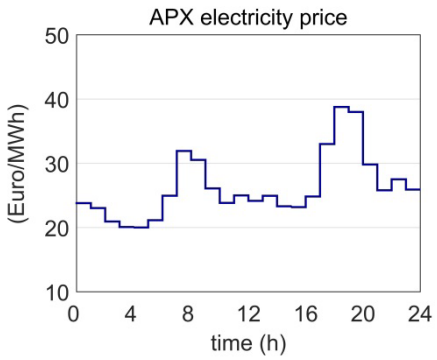

Figure 2.12. Amsterdam Power Exchange (APX) electricity prices from 01.03.2016.

APX prices serve as main grid signal enabling flexibility in the context of cost-optimal control. Figure 2.13 illustrates the simulation results of optimal control with charging and discharging profiles of the water tank, PCM tank, and TCM tank.

It is clear from the nature of optimization that charging the TES tanks takes place when electricity prices are low (2 am – 6 am) whereas discharging is favoured when electricity prices are high (7 am – 9 am). The optimization results show that the TES tanks are charged by the HP only, and no additional electric heating is applied to further increase the charging temperature. Essentially for this particular day, this means that an electric heater with a COP of 1 does not compensate any heating power in high price periods. It can be seen in Figure 2.13 that implementing a water tank achieves highest average charging (+) and discharging (-) power of +7.5 kW and -6.2 kW. It is observed that during some periods of high charging, the maximum thermal output of the HP of 13 kW limits the charging of the water tank. This effect is not observed for the PCM and TCM tank. Compared to the reference case (1.41 €), the water tank achieves highest total operational electricity cost savings of 7.1% (1.31 €), the PCM tank 6.4% (1.32 €), and the TCM tank 2.9% (1.37 €).

The average COP marginally deviates from the reference case with 4.6 (water tank), 4.5 (PCM tank), and 4.6 (TCM tank). As can be seen in Figure 2.13c, the average temperature of the zones is always maintained above the minimum zone temperature set points (Equation 2-21).

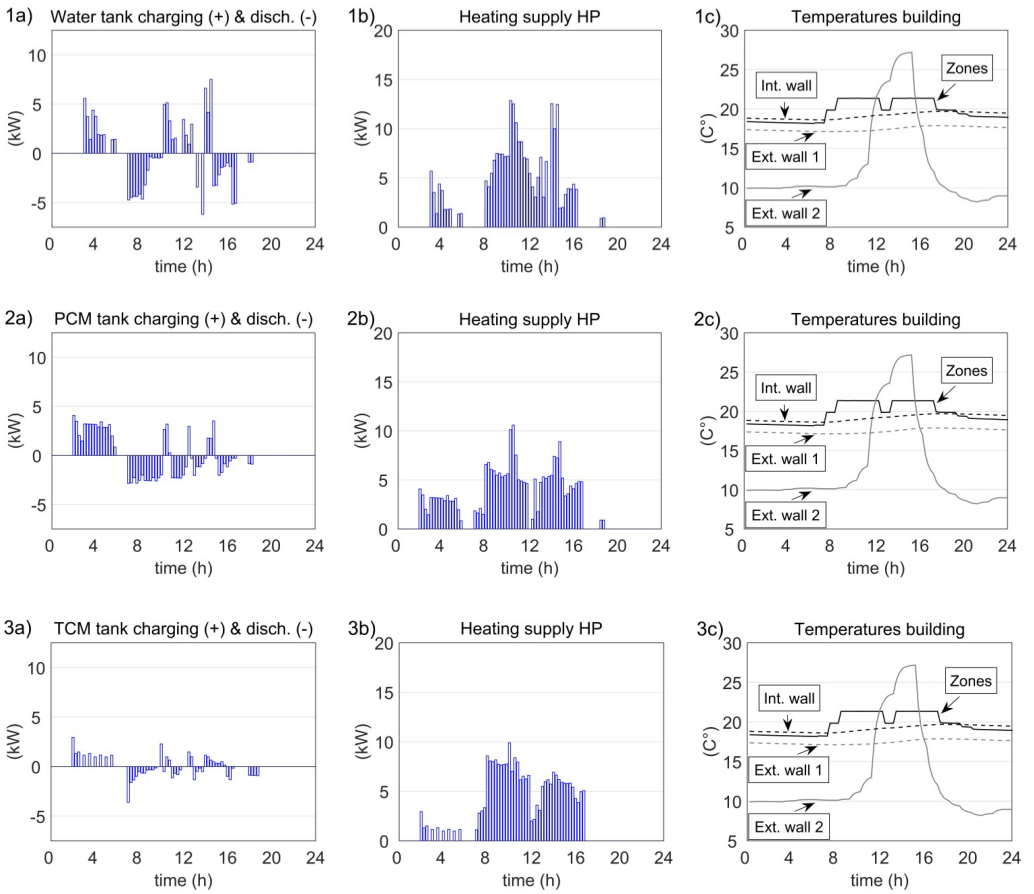

Figure 2.13. Simulation results – optimal control including TES tanks 1) water tank, 2) PCM tank, 3) TCM tank, a) charging and discharging power, b) heating supply by the HP, and c) building temperature including average indoor temperature (zones), average temperature of the concrete of the internal walls (Int. wall), average temperature of the concrete at the inner surface of the external walls (Ext. wall 1), and average temperature of the insulation at the outer surface of the external walls (Ext. wall 2).

2.3.3 Demand flexibility

Demand flexibility – energy

Optimal control achieves cost savings and enables energy flexibility. The results of adequate energy flexibility indicators for the different TES tanks are listed in Table 2-7.

Table 2-7. Simulation results – energy flexibility of different TES tanks comparing optimal control with reference control: available storage capacity Q_{OC} and storage efficiency η_{OC}.

Energy flexibility indicators	Water tank	PCM tank	TCM tank
$Q_{OC,up}$ [kWh]	17.8	15.3	5.9
$Q_{OC,down}$ [kWh]	17.3	14.8	5.6
η_{OC} [-]	0.98	0.97	0.96

The available storage capacity obtains largest values for the water tank. The storage efficiency is almost similar for all the different technologies. The storage efficiency presents the ratio between discharging and charging for the entire control horizon including heat losses. It is to emphasize that the heat losses are low for all TES tanks and < 1% of storage efficiency.

Demand flexibility – costs

The flexibility factor as indicator of flexibility in the dimension of operational costs refers to high and low-price periods. The standard deviation of the daily electricity price serves to determine the high-price periods (Figure 2.14a) and low-price periods (Figure 2.14b). The corresponding flexibility factor is calculated and can be seen in Figure 2.14c. In the reference control, electricity consumption occurs during high price periods which results in a flexibility factor of -1 that is a highly inflexible controlled system. By adding TES tanks and cost-optimal control, the flexibility factor can be increased to 0.15 (TCM tank), 0.67 (PCM tank), and 0.86 (water tank).

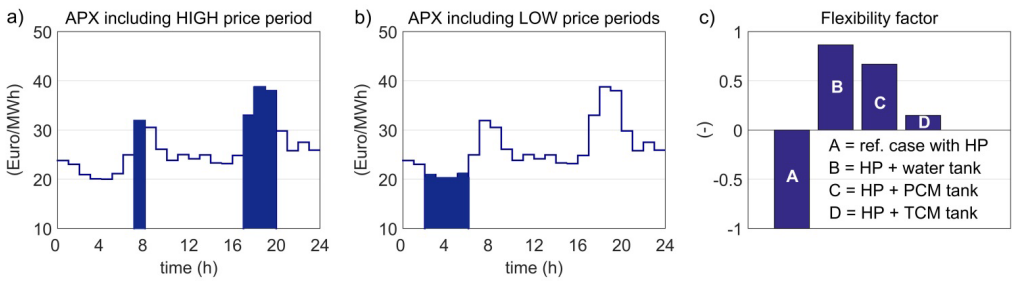

Figure 2.14. Simulation results – flexibility related to operational electricity costs, hourly APX electricity prices including high price periods (a) and low price periods (b), c) flexibility factor of different TES tanks in optimal control compared with reference control.

Demand flexibility – power

The power shifting capability determines the power flexibility in optimal control compared with reference control. The power shifting capability is illustrated in Figure 2.15 indicating the thermal (TES) and electrical (HP) power flexibility. Because optimal control does not result in operations of electric heating, the electric heater is not considered in Figure 2.15.

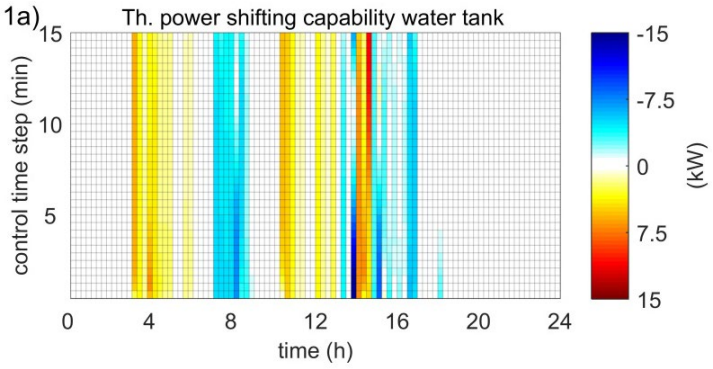

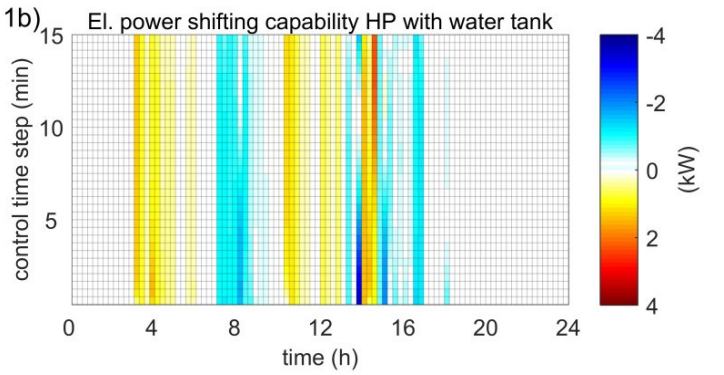
1b)
El. power shifting capability HP with water tank
control time step (min)
time (h)
(kW)
-4
-2
0
2
4

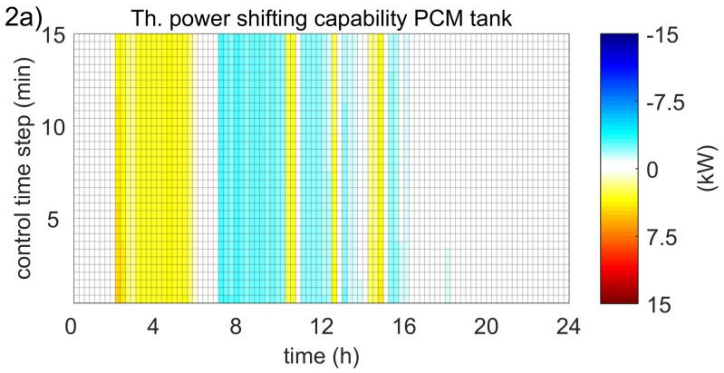
2a)
Th. power shifting capability PCM tank
control time step (min)
time (h)
(kW)
-15
-7.5
0
7.5
15

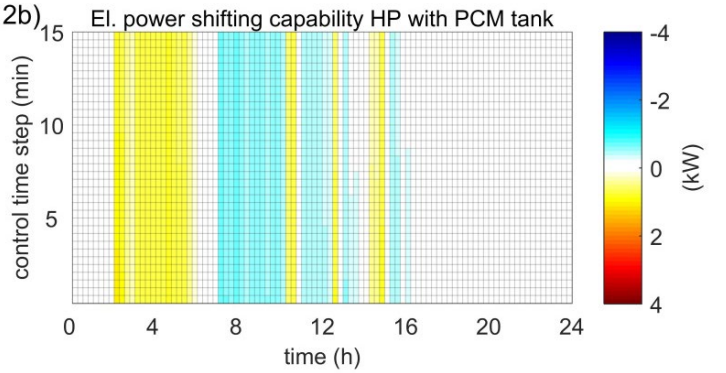
2b)
El. power shifting capability HP with PCM tank
control time step (min)
time (h)
(kW)
-4
-2
0
2
4

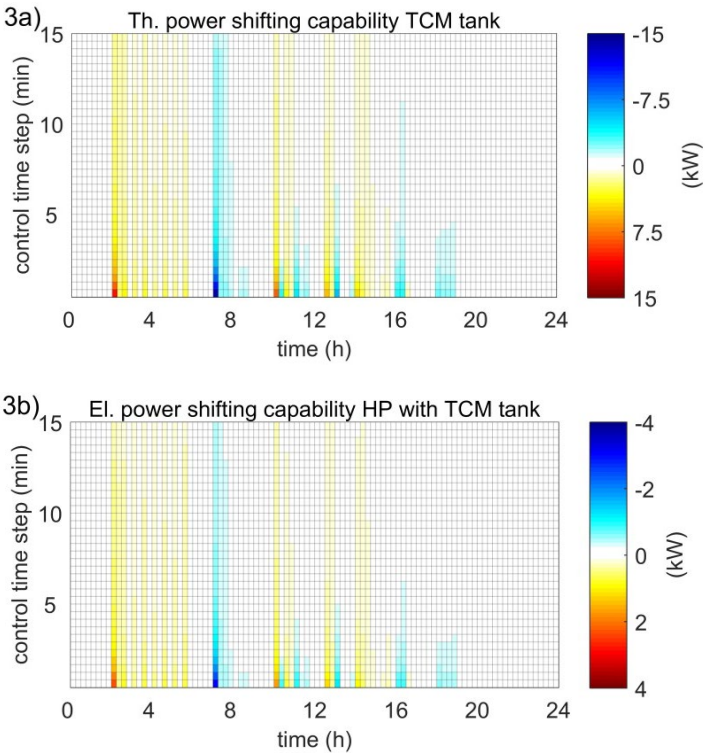

Figure 2.15. Simulation results – power shifting capability comparing the power evolution between optimal and reference control for 1) water tank, 2) PCM tank, 3) TCM tank, a) thermal power shifting capability, b) electrical power shifting capability. The x-axis shows the control horizon of 24 h. The y-axis represents the 15 min control time step. During each control time step the evolving power flexibility is illustrated.

Optimal control of a water tank achieves highest power shifting capability which is identical to the results shown in Figure 2.13-1a) in which the integral of the power flexibility is shown. However, the power shifting capability as shown in Figure 2.15 reveals the detailed dynamic response of the TES. For the water tank, variations of up to 9 kW (one-minute average) during a 15 min control time step of charging and discharging power appear that is due to previous scheduling. It can also be seen that stratification is not established during periods of alternating charging and discharging such as between 13 pm and 15 pm. The PCM tank provides almost constant charging and discharging power during the 15 min control time step that is due to the phase change process in which the PCM gradually melts or solidifies. For the TCM tank, charging and discharging variations during the 15 min time step are the highest among the TES tanks of up to 10 kW (one-minute average). This is because the TCM tank is primarily used as sensible heat storage in which the material quickly heats up and

cools down during low activation temperature during charging (maximum at 47 °C), the proportion of chemical to sensible heat stored is low.

To identify the full flexibility potential of TES and power-to-heat, the instantaneous power flexibility is introduced which gives an insight into the potential power flexibility provided to the power grid. Figure 2.16 shows the hourly potential power flexibility for potential charging of TES using the heat pump and electric heating.

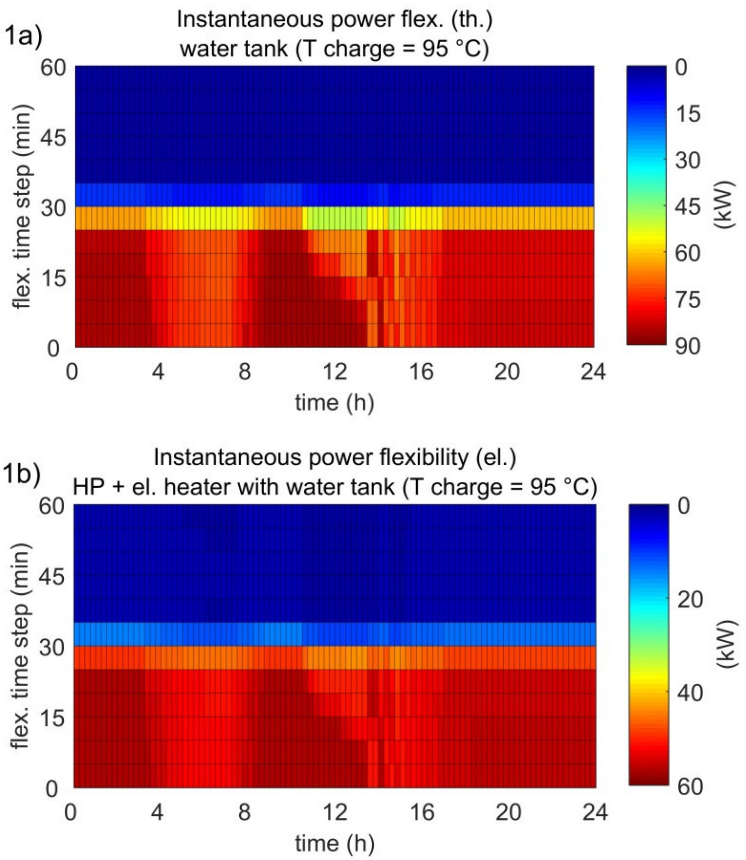

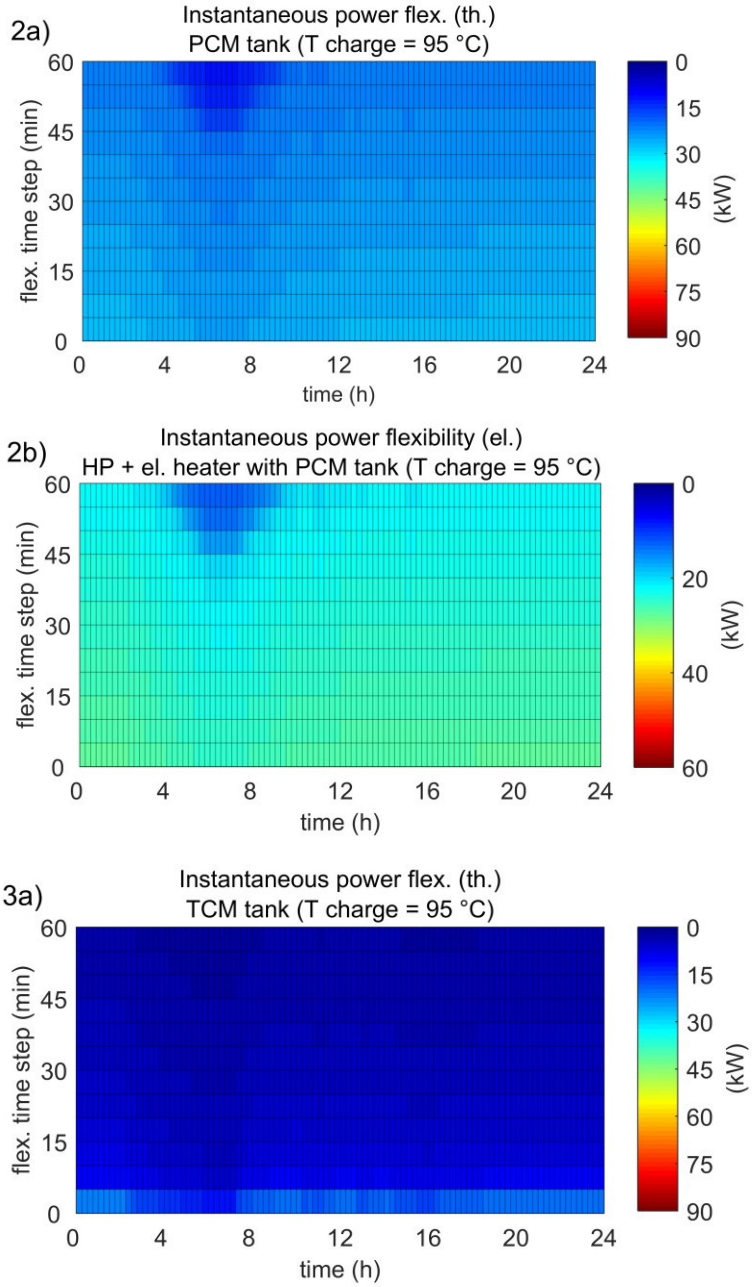
2a)
Instantaneous power flex. (th.)
PCM tank (T charge = 95 °C)
flex. time step (min)
time (h)
(kW)
2b)
Instantaneous power flexibility (el.)
HP + el. heater with PCM tank (T charge = 95 °C)
flex. time step (min)
time (h)
(kW)
3a)
Instantaneous power flex. (th.)
TCM tank (T charge = 95 °C)
flex. time step (min)
time (h)
(kW)

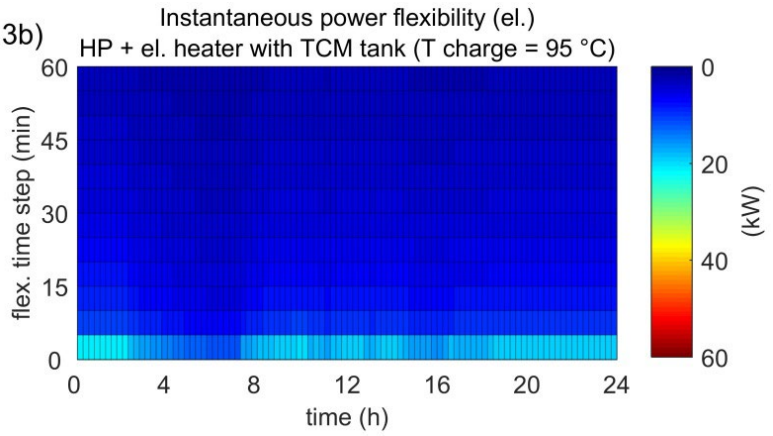

Figure 2.16. Simulation results – instantaneous power flexibility for the charging case of TES with 95 °C based on the results of optimal control; 1) water tank, 2) PCM tank, 3) TCM tank; a) Inst. power flexibility (thermal), b) Inst. power flexibility (electrical). The x-axis shows the control horizon of 24 h. The y-axis represents the flexibility time step of 60 min in which the TES responds to a constant charging temperature of 95 °C. During the 60 min flexibility time step, the evolving power is illustrated at each control time step of the 24 h control horizon.

The instantaneous power flexibility presents the thermal response of TES tanks and related electricity consumption of the HP during charging, discharging and rest mode. In this case study, the instantaneous power flexibility is calculated for charging of 95 °C for one hour and illustrated in Figure 2.16. The simulation results of cost-optimal control serve as an initial condition to determine the instantaneous power flexibility, once cost-optimal control decision is taken but not applied yet. Knowing all information about the instantaneous power flexibility may result in a new control decision. However, it can be seen that the water tank provides the largest thermal instantaneous power flexibility. For example after 12 h of control horizon, charging with 95 °C gives a thermal power that can sustain between 86 and 67 kW for 25 min of flexibility time step. Adequate electrical instantaneous power flexibility of heat pump and electric heater power varies between 57 and 44 kW. At 12 am the water tank can be charged from 12% to 100% of energy capacity after about 45 min of flexibility time step regarding a charging temperature of 95 °C and a reference temperature of 21 °C. The change from 12% to 100% correlates to an energy uptake of about 0.13 GJ. During the entire control horizon of 24 h, it can be seen that the water tank can always be charged with high power. This indicates that for this particular day, optimal control of a water tank only partly uses the available energy capacity. For the PCM, the same results are observed.
At each time step of the entire control horizon of 24 h, the PCM tank can serve as a relatively constant thermal charging source.

For example at 12 am the thermal power can sustain between 27 and 21 kW for 60 min of flexibility time step. Due to the high charging temperature of 95 °C, the maximum temperature difference between PCM tank inlet and outlet is 10 K. Thus, only the electric heater is used to provide electrical instantaneous power flexibility which is similar to the thermal instantaneous power flexibility of 27 – 21 kW. At 12 am the PCM tank can be charged from 7% to 60% of energy capacity after about 60 min of flexibility time step regarding a charging temperature of 95 °C and a reference temperature of 21 °C. The change from 7% to 60% correlates to an energy uptake of 0.09 GJ. The instantaneous power flexibility of the TCM tank is the lowest among the TES tanks. For example at 12 am, charging with 95 °C results in a thermal power of 19 kW in the first 5 min of flexibility time step which is primarily due to the sensible heat stored in the TCM tank. From 5 – 60 min, thermal power decrease gradually from 10 to 3 kW that is due to the chemical energy stored in the TCM tank. The related energy capacity increases from 7% to 69% which is equal to an energy uptake of 0.03 GJ.

2.4 Discussion

Capturing heat and mass transfer dynamics is a prerequisite for determining demand flexibility of TES tanks integrated with building heating systems. To present this dynamic behaviour with sufficient accuracy, TES models were developed based on a one-dimensional approach. The Crank-Nicolson scheme was applied to numerically solve conduction and diffusion for a one-dimensional configuration and reduce the computational effort for simulating TES tanks. The Crank Nicolson approach is a stable, robust, and powerful hybrid FD method. In combination with dynamic programming, Crank Nicolson was introduced and applied to simulate TES tanks in optimal control. The one-dimensional TES models consider simplifications regarding heat and mass transfer. For the packed-bed reactor using PCM, the one-dimensional problem solves the heat and mass transfer through the PCM layer in so far as the enthalpy distribution in the PCM layer is equal for the entire length of the heat exchanger. The PCM model does not include natural convection during the melting process, to facilitate the implementation into the optimization scheme and to reduce computational time. However, recent studies on PCM tanks have shown that natural convection can increase the heat transfer of the PCM in the solid-liquid interface [80–82]. For the packed-bed reactor using TCM, the one-dimensional problem solves the heat and mass transfer through the TCM layer. This simplification includes that the temperature and adsorbate distribution in the TCM layer are equal for the length of the heat exchanger. The one-dimensional approach for the water tank simulates the stratification of temperature segments. However, convection and conduction perpendicular to the height of the water tank are not included. Because previous studies have already successfully used the one-dimensional representation of water tanks [54–56], PCM tanks [57,58], and TCM tanks, for example in [59,60], the dynamic behaviour of the TES tanks is sufficiently represented. However, a validation of the TES tank models using experimental data is recommended. Demand flexibility related to energy is quantified using the performance indicators, storage capacity and storage efficiency. The calculated storage efficiency of the different TES tanks with optimal control is between 96 – 98% achieving a high performance compared to other studies [15].

Demand flexibility related to costs is expressed using the flexibility factor as performance indicator. The flexibility factor is significantly increased by integrating TES tanks with optimal control. A limitation of the flexibility factor as a single indicator is that the results exclude a comparison to different building heating systems in different climate conditions. To overcome this limitation, this study has considered multiple flexibility indicators referring to energy, power, and costs.

Demand flexibility related to power is quantified using the shifting capability as a performance indicator. This indicator describes the difference of power usage between optimal and reference control. Because TES tanks are not considered in the reference control, the power shifting capability is identical to the dynamic response of the TES tanks in optimal control. Because the power shifting capability does not comprehensively represent the potential power flexibility of TES and power-to-heat, this paper has introduced the instantaneous power flexibility as performance indicator which shows the potential power flexibility of TES and power-to-heat in any case of charging, discharging or idle mode. The instantaneous power flexibility is calculated for a time scale of 1 h to determine grid ancillary services of short duration. The results for the power flexibility of TES are obtained with sufficient accuracy because detailed TES models are implemented to capture the complex storage dynamics. It becomes clear that more advanced TES tanks models are required in optimal control because simplified models cannot predict transition periods in which for example stratification in a water tank is not yet established and temperature distribution changes due to increased mixing of water.

In order to determine demand flexibility with TES tanks and power-to-heat, information of flexibility regarding energy, power, and costs have to be considered. It is observed that the water tank and PCM tank achieve highest energy flexibility compared to reference control. All TES tank show different behaviour in the power flexibility. Water tanks can be charged quickly with high charging power and PCM tanks can be constantly charged for a longer time period with adequate charging power. The charging power may be regulated by changing the mass flow of the heat transfer medium that exchanges heat with the TES tank. A variable mass flow may enable more constant charging and discharging, but also introduces an additional operational parameter for optimization which results in an increase of the computational time for cost-optimal control.

2.5 Conclusion

In this study, the demand flexibility of TES tanks integrated with building heating system was determined showing that power-to-heat devices and water tanks, PCM tanks, and TCM tanks can be designed to provide flexibility of short duration (up to 24 h). To investigate the maximum building flexibility towards the power grid, optimal control of TES tanks, HP and electric heater was chosen. Optimal control considers the complexity of the building heating system and enables the integration of weather forecasting and prediction of internal gains. Because current grid signals commonly contain electricity prices, optimal control aims to minimizing the total operational electricity costs. When applying the developed optimal control framework to building energy management systems, real-time signals such as intra-day electricity prices can be implemented. The results of cost-optimal control showed that the water tank and the PCM tank achieve highest cost savings when comparing to reference control. However, no lifetime costs, lifecycle costs, or maintenance costs of the building heating system were assumed. The results of the cost-optimal control also show that the efficient use of electrical energy (COP of the heat pump) is similar to the reference control case. The simulated 24 h are only characteristically for an average day in the spring period and in the Netherlands. As next, different periods of the year and different climate conditions have to be simulated to gain a deeper insight into the system performance. However, this study aimed to determine demand flexibility of TES tanks integrated with building heating system. The demand flexibility is quantified using different performance indicators that sufficiently characterize flexibility in terms of size (energy), time (power) and costs. Energy flexibility with optimal control is expressed using the available storage capacity and storage efficiency indicating that all TES technologies, water tank, PCM tank, TCM tank and power-to-heat can enable energy flexibility towards the power grid. Flexibility related to costs is represented using the flexibility factor that sufficiently determines whether electricity is consumed during low or high electricity price periods. Power flexibility characterizes the evolution of heating power over time. The electrical power flexibility is directly linked to the power grid whereas the thermal flexibility shows the dynamic response of the heating system. The thermal and electrical power shifting capability was calculated to compare optimal control with reference control. However, the power shifting capability cannot be used to quantify the potential power flexibility of TES and power-to-heat in any case of charging, discharging or idle mode. Therefore, this paper has introduced the instantaneous power flexibility. Based on the results of the optimal control the instantaneous power flexibility is quantified for the charging case of 95 °C and a flexibility time step of 60 min.

The identification and quantification of demand flexibility is a crucial step towards electricity markets that can enable flexible energy consumption. Multiple flexibility indicators that relate to all dimensions of demand flexibility in terms of size (energy), time (power) and costs, will serve to determine demand flexibility.

Therefore, it is required to use those flexibility indicators as a measure of the performance of control strategies in addition to conventional performance indicators such as energy consumption, costs, and energy efficiency.

In order to approach the optimization of multiple flexibility indicators in optimal control, future control strategies will implement flexibility indicators in the objective function. As an example, during periods of renewable power fluctuation, a building energy system, including TES, can be requested to increase or decrease power consumption to optimize load following and thus optimize the scheduling of TES and power-to-heat for power flexibility. In order to do that, a flexibility market mechanism must be established that allows to optimize for building demand flexibility.

2.6 Nomenclature

D	effective diffusion
h	specific enthalpy
H_s	adsorption enthalpy
J	optimal cost function
J_π	expected costs referring to policy π
k_m	mass transfer coefficient between evaporator/condenser and adsorber
l	duration
m	number of OC events
m_{ads}	mass adsorbate
n	number
N	planning horizon
p	pressure
P	power
q	adsorbate – amount of refrigerant (water) in the solid phase of dry material (zeolite13X)
Q	capacity
t	time
u	positive constant velocity
u_t	control variables referring to optimal control
U_t	control constraints
V_{dot}	volume flow
x	spatial coordinate referring to the one-dimensional convection-diffusion equation
x_t	state variables referring to optimal control
T	temperature

Greek symbols

α	positive constant coefficient
Δ,δ	difference
ε	random parameter referring to the occupancy rate in optimal control
η	efficiency

θ	dependent variable
λ	thermal conductivity [W/mK]
π	policy
ρ	density [kg/m^3]

Subscripts

ch	charging
comp.	compartments
down	downwards
eq	referred to p as equilibrium
i	referred to x as i-th segment of x
inst	instantaneous
liq	referred to T as liquid
max	maximum
min	minimum
n	referred to t as time step of t
ref	reference
sol	referred to T as solid
up	upwards

Abbreviations

APX	Amsterdam power exchange
BRCM	building resistance-capacitance modelling
BTM	building thermal mass
CHP	combined heat and power
COP	coefficient of performance
DP	dynamic programming
DR	demand response
FD	finite difference
FF	flexibility factor
HP	heat pump
HT	heat transfer

HVAC	heating, ventilation, and air conditioning system
HX	heat exchanger
LDF	linear driving force
OC	optimal control
PCM	phase change material
RC	resistance-capacitance
TCM	thermochemical material
TES	thermal energy storage
TMY	typical meteorological year

2.7 References

[1] Gelazanskas L, Gamage KAA. Demand side management in smart grid: A review and proposals for future direction. Sustain Cities Soc 2014;11:22–30. doi:10.1016/j.scs.2013.11.001.

[2] Ottesen SO, Tomasgard A. A stochastic model for scheduling energy flexibility in buildings. Energy 2015;88:364–76. doi:10.1016/j.energy.2015.05.049.

[3] Lopes RA, Chambel A, Neves J, Aelenei D, Martins J. A Literature Review of Methodologies Used to Assess the Energy Flexibility of Buildings. Energy Procedia 2016;91:1053–8. doi:10.1016/j.egypro.2016.06.274.

[4] De Coninck R, Helsen L. Quantification of flexibility in buildings by cost curves - Methodology and application. Appl Energy 2016;162:653–65. doi:10.1016/j.apenergy.2015.10.114.

[5] Kondziella H, Bruckner T. Flexibility requirements of renewable energy based electricity systems - A review of research results and methodologies. Renew Sustain Energy Rev 2016;53:10–22. doi:10.1016/j.rser.2015.07.199.

[6] Stinner S, Huchtemann K, Müller D. Quantifying the operational flexibility of building energy systems with thermal energy storages. Appl Energy 2016;181:140–54. doi:10.1016/j.apenergy.2016.08.055.

[7] Nuytten T, Claessens B, Paredis K, Van Bael J, Six D. Flexibility of a combined heat and power system with thermal energy storage for district heating. Appl Energy 2013;104:583–91. doi:10.1016/j.apenergy.2012.11.029.

[8] D'hulst R, Labeeuw W, Beusen B, Claessens S, Deconinck G, Vanthournout K. Demand response flexibility and flexibility potential of residential smart appliances: Experiences from large pilot test in Belgium. Appl Energy 2015;155:79–90. doi:10.1016/j.apenergy.2015.05.101.

[9] Reynders G. Quantifying the impact of building design on the potential of structural storage for active demand response in residential buildings. 2015. doi:10.13140/RG.2.1.3630.2805.

[10] Le Dréau J, Heiselberg P. Energy flexibility of residential buildings using short term heat storage in the thermal mass. Energy 2016;111:1–5. doi:10.1016/j.energy.2016.05.076.

[11] Clauß J, Finck C, Vogler-Finck P, Beagon P. Control strategies for building energy systems to unlock demand side flexibility – A review. 15th Int. Conf. Int. Build. Perform. Simul. Assoc., 2017, p. 611–20.

[12] Vanhoudt D, Geysen D, Claessens B, Leemans F, Jespers L, Van Bael J. An actively controlled residential heat pump: Potential on peak shaving and maximization of self-consumption of renewable energy. Renew Energy 2014;63:531–43. doi:10.1016/j.renene.2013.10.021.

[13] Fischer D, Wolf T, Wapler J, Hollinger R, Madani H. Model-based flexibility assessment of a residential heat pump pool. Energy 2017;118:853–64. doi:10.1016/j.energy.2016.10.111.

[14] Fischer D, Madani H. On heat pumps in smart grids: A review. Renew Sustain Energy Rev 2017;70:342–57. doi:10.1016/j.rser.2016.11.182.

[15] Reynders G, Diriken J, Saelens D. Generic characterization method for energy flexibility: Applied to structural thermal storage in residential buildings. Appl Energy 2017;198:192–202. doi:10.1016/j.apenergy.2017.04.061.

[16] Salpakari J, Rasku T, Lindgren J, Lund PD. Flexibility of electric vehicles and space heating in net zero energy houses: an optimal control model with thermal dynamics and battery degradation. Appl Energy 2017. doi:10.1016/j.apenergy.2017.01.005.

[17] Kim YJ, Fuentes E, Norford LK. Experimental Study of Grid Frequency Regulation Ancillary Service of a Variable Speed Heat Pump. IEEE Trans Power Syst 2016;31:3090–9. doi:10.1109/TPWRS.2015.2472497.

[18] Lund PD, Lindgren J, Mikkola J, Salpakari J. Review of energy system flexibility measures to enable high levels of variable renewable electricity. Renew Sustain Energy Rev 2015;45:785–807. doi:10.1016/j.rser.2015.01.057.

[19] Oldewurtel F, Sturzenegger D, Andersson G, Morari M, Smith RS. Towards a standardized building assessment for demand response. Proc IEEE Conf Decis Control 2013:7083–8. doi:10.1109/CDC.2013.6761012.

[20] Salpakari J, Mikkola J, Lund PD. Improved flexibility with large-scale variable renewable power in cities through optimal demand side management and power-to-heat conversion. Energy Convers Manag 2016;126:649–61. doi:10.1016/j.enconman.2016.08.041.

[21] Fischer D, Lindberg KB, Madani H, Wittwer C. Impact of PV and variable prices on optimal system sizing for heat pumps and thermal storage. Energy Build 2016;128:723–33. doi:10.1016/j.enbuild.2016.07.008.

[22] Arteconi A, Hewitt NJ, Polonara F. State of the art of thermal storage for demand-side management. Appl Energy 2012;93:371–89. doi:10.1016/j.apenergy.2011.12.045.

[23] Navarro L, de Gracia A, Colclough S, Browne M, McCormack SJ, Griffiths P, et al. Thermal energy storage in building integrated thermal systems: A review. Part 1. active storage systems. Renew Energy 2016;88:526–47. doi:10.1016/j.renene.2015.11.040.

[24] Navarro L, de Gracia A, Niall D, Castell A, Browne M, McCormack SJ, et al. Thermal energy storage in building integrated thermal systems: A review. Part 2. Integration as passive system. Renew Energy 2016;85:1334–56. doi:10.1016/j.renene.2015.06.064.

[25] Sterner M, Stadler I. Energiespeicher - Bedarf, Technologien, Integration. 2014. doi:10.1007/978-3-642-37380-0.

[26] Cabeza LF, Castell A, Barreneche C, De Gracia A, Fernández AI. Materials used as PCM in thermal energy storage in buildings: A review. Renew Sustain Energy Rev 2011. doi:10.1016/j.rser.2010.11.018.

[27] Cot-Gores J, Castell A, Cabeza LF. Thermochemical energy storage and conversion: A-state-of-the-art review of the experimental research under practical conditions. Renew Sustain Energy Rev 2012. doi:10.1016/j.rser.2012.04.007.

[28] Aydin D, Casey SP, Riffat S. The latest advancements on thermochemical heat storage systems. Renew Sustain Energy Rev 2015. doi:10.1016/j.rser.2014.08.054.

[29] Finck C, Henquet E, van Soest C, Oversloot H, de Jong A-J, Cuypers R, et al. Experimental Results of a 3 kWh Thermochemical Heat Storage Module for Space Heating Application. Energy Procedia 2014;48:320–6. doi:10.1016/j.egypro.2014.02.037.

[30] Zondag H, Kikkert B, Smeding S, Boer R de, Bakker M. Prototype thermochemical heat storage with open reactor system. Appl Energy 2013. doi:10.1016/j.apenergy.2013.01.082.

[31] De Jong AJ, Van Vliet L, Hoegaerts C, Roelands M, Cuypers R. Thermochemical Heat Storage - From Reaction Storage Density to System Storage Density. Energy Procedia 2016;91:128–37. doi:10.1016/j.egypro.2016.06.187.

[32] Mette B, Kerskes H, Drück H, Müller-Steinhagen H. New highly efficient regeneration process for thermochemical energy storage. Appl Energy 2013. doi:10.1016/j.apenergy.2013.01.087.

[33] Masy G, Georges E, Verhelst C, Lemort V. Smart grid energy flexible buildings through the use of heat pumps and building thermal mass as energy storage in the Belgian context. Sci Technol Built Environ 2015;21:6:800–11. doi:10.1080/23744731.2015.1035590.

[34] Arteconi A, Hewitt NJ, Polonara F. Domestic demand-side management (DSM): Role of heat pumps and thermal energy storage (TES) systems. Appl Therm Eng 2013;51:155–65. doi:10.1016/j.applthermaleng.2012.09.023.

[35] Patteeuw D, Bruninx K, Arteconi A, Delarue E, D'haeseleer W, Helsen L. Integrated modeling of active demand response with electric heating systems coupled to thermal energy storage systems. Appl Energy 2015;151:306–19. doi:10.1016/j.apenergy.2015.04.014.

[36] Mikkola J, Lund PD. Modeling flexibility and optimal use of existing power plants with large-scale variable renewable power schemes. Energy 2016;112:364–75. doi:10.1016/j.energy.2016.06.082.

[37] Berkenkamp F, Gwerder M. Hybrid model predictive control of stratified thermal storages in buildings. Energy Build 2014;84:233–40. doi:10.1016/j.enbuild.2014.07.052.

[38] Schütz T, Streblow R, Müller D. A comparison of thermal energy storage models for building energy system optimization. Energy Build 2015. doi:10.1016/j.enbuild.2015.02.031.

[39] Salpakari J, Lund P. Optimal and rule-based control strategies for energy flexibility in buildings with PV. Appl Energy 2016;161:425–36. doi:10.1016/j.apenergy.2015.10.036.

[40] Renaldi R, Kiprakis A, Friedrich D. An optimisation framework for thermal energy storage integration in a residential heat pump heating system. Appl Energy 2017. doi:10.1016/j.apenergy.2016.02.067.

[41] Gambino G, Verrilli F, Canelli M, Russo A, Himanka M, Sasso M, et al. Optimal operation of a district heating power plant with thermal energy storage. Proc. Am. Control Conf., 2016. doi:10.1109/ACC.2016.7525266.

[42] Finck C, Li R, Zeiler W. An optimization strategy for scheduling various thermal energy storage technologies in office buildings connected to smart grid. Energy Procedia, 2015. doi:10.1016/j.egypro.2015.11.105.

[43] Touretzky CR, Salliot AA, Lefevre L, Baldea M. Optimal operation of phase-change thermal energy storage for a commercial building. Proc Am Control Conf 2015;2015-July:980–5. doi:10.1109/ACC.2015.7170861.

[44] Fiorentini M, Wall J, Ma Z, Braslavsky JH, Cooper P. Hybrid model predictive control of a residential HVAC system with on-site thermal energy generation and storage. Appl Energy 2017;187:465–79. doi:10.1016/j.apenergy.2016.11.041.

[45] Verrilli F, Srinivasan S, Gambino G, Canelli M, Himanka M, Del Vecchio C, et al. Model Predictive Control-Based Optimal Operations of District Heating System with Thermal Energy Storage and Flexible Loads. IEEE Trans Autom Sci Eng 2017;14:547–57. doi:10.1109/TASE.2016.2618948.

[46] Touretzky CR, Baldea M. A hierarchical scheduling and control strategy for thermal energy storage systems. Energy Build 2016;110:94–107. doi:10.1016/j.enbuild.2015.09.049.

[47] Fazlollahi S, Becker G, Maréchal F. Multi-objectives, multi-period optimization of district energy systems: II-Daily thermal storage. Comput Chem Eng 2014;71:648–62. doi:10.1016/j.compchemeng.2013.10.016.

[48] Alimohammadisagvand B, Jokisalo J, Kilpeläinen S, Ali M, Sirén K. Cost-optimal thermal energy storage system for a residential building with heat pump heating and demand response control. Appl Energy 2016;174:275–87. doi:10.1016/j.apenergy.2016.04.013.

[49] Dimplex Technische Daten Luft/Wasser Wärmepumpe LA 18S-TU. 2016.

[50] Finck C, Li R, Zeiler W. Operational Load Shaping of Office Buildings Connected to Thermal Energy Storage Using Dynamic Programming. 12th REHVA world Congr.

[51] Sturzenegger D, Gyalistras D, Semeraro V, Morari M, Smith RS. BRCM Matlab Toolbox: Model generation for model predictive building control. Proc Am Control Conf 2014:1063–9. doi:10.1109/ACC.2014.6858967.

[52] H. Recknagel et al. Taschenbuch Heizung + Klimatechnik. Oldenbg Ind München 2006.

[53] Produktkatalog Armacell 2016.

[54] Shukla A, Singh AK, Singh P. A Comparative Study of Finite Volume Method and Finite Difference Method for Convection-Diffusion Problem. Am J Comput Appl Math 2012. doi:10.5923/j.ajcam.20110102.13.

[55] Appadu AR. Numerical solution of the 1D advection-diffusion equation using standard and nonstandard finite difference schemes. J Appl Math 2013;2013. doi:10.1155/2013/734374.

[56] Karahan H. Implicit finite difference techniques for the advection-diffusion equation using spreadsheets. Adv Eng Softw 2006. doi:10.1016/j.advengsoft.2006.01.003.

[57] Lo Brano V, Ciulla G, Piacentino A, Cardona F. Finite difference thermal model of a latent heat storage system coupled with a photovoltaic device: Description and experimental validation. Renew Energy 2014;68:181–93. doi:10.1016/j.renene.2014.01.043.

[58] Hu H, Argyropoulos SA. Mathematical modelling of solidification and melting: A review. Model Simul Mater Sci Eng 1996. doi:10.1088/0965-0393/4/4/004.

[59] Pesaran A, Lee H, Hwang Y, Radermacher R, Chun HH. Review article: Numerical simulation of adsorption heat pumps. Energy 2016;100:310–20. doi:10.1016/j.energy.2016.01.103.

[60] Finck C, Van 't Spijker H, De Jong A-J, Henquet E, Oversloot H, Cuypers R. Design of a modular 3 kWh thermochemical heat storage system for space heating application. 2nd Int. Conf. Sustain. Energy Storage, 2013.

[61] Morton KW. Numerical Solution of Convection-Diffusion Problems. 1996.

[62] Kanzow. Numerik linearer Gleichungssysteme: Direkte und iterative Verfahren. 2005. doi:10.1007/b138019.

[63] Zienkiewicz OC. Numerical computation of internal and external flow vol. 1. Fundamentals of numerical discretisation, C. Hirsch, Wiley, Chichester, 1988, ISBN 0471 917621. Int J Numer Methods Eng 1989. doi:10.1002/nme.1620281016.

[64] Cooper J. Introduction to Partial Differential Equations with MATLAB. 1998. doi:10.1007/978-1-4612-1754-1.

[65] Recktenwald GW. Numerical methods with MATLAB : implementations and applications 2000:786.

[66] Trefethen. numerical ODE/PDE textbook http://people.maths.ox.ac.uk/trefethen/pdetext.html. 1996.

[67] Kenisarin MM. Thermophysical properties of some organic phase change materials for latent heat storage. A review. Sol Energy 2014;107:553–75. doi:10.1016/j.solener.2014.05.001.

[68] Kenisarin M, Mahkamov K. Salt hydrates as latent heat storage materials:Thermophysical properties and costs. Sol Energy Mater Sol Cells 2016;145:255–86. doi:10.1016/j.solmat.2015.10.029.

[69] Mosaffa AH, Garousi Farshi L, Infante Ferreira CA, Rosen MA. Energy and exergy evaluation of a multiple-PCM thermal storage unit for free cooling applications. Renew Energy 2014;68:452–8. doi:10.1016/j.renene.2014.02.025.

[70] Levin PP, Shitzer A, Hetsroni G. Numerical optimization of a PCM-based heat sink with internal fins. Int J Heat Mass Transf 2013;61:638–45. doi:10.1016/j.ijheatmasstransfer.2013.01.056.

[71] De Jong A-J, Trausel F, Finck C, Van Vliet L, Cuypers R. Thermochemical heat storage - System design issues. Energy Procedia, 2014. doi:10.1016/j.egypro.2014.02.036.

[72] Trausel F, De Jong AJ, Cuypers R. A review on the properties of salt hydrates for thermochemical storage. Energy Procedia 2014;48:447–52. doi:10.1016/j.egypro.2014.02.053.

[73] Rindt CCM, Gaastra-Nedea S V. Modeling thermochemical reactions in thermal energy storage systems. Adv. Therm. Energy Storage Syst. Methods Appl., 2015. doi:10.1533/9781782420965.3.375.

[74] Wang Y, LeVan MD. Adsorption equilibrium of carbon dioxide and water vapor on zeolites 5a and 13X and silica gel: Pure components. J Chem Eng Data 2009. doi:10.1021/je800900a.

[75] Sayilgan ŞÇ, Mobedi M, Ülkü S. Effect of regeneration temperature on adsorption equilibria and mass diffusivity of zeolite 13x-water pair. Microporous Mesoporous Mater 2016;224:9–16. doi:10.1016/j.micromeso.2015.10.041.

[76] Leong KC, Liu Y. System performance of a combined heat and mass recovery adsorption cooling cycle: A parametric study. Int J Heat Mass Transf 2006;49:2703–11. doi:10.1016/j.ijheatmasstransfer.2006.01.012.

[77] Dobbs JR, Hencey BM. Predictive HVAC control using a Markov occupancy model. Proc. Am. Control Conf., 2014. doi:10.1109/ACC.2014.6859389.

[78] Bertsekas DP. Dynamic programming and optimal control. Belmont, Mass.: Athena Scientific; 2005.

[79] Finck C, Li R, Zeiler W. Performance maps for the control of thermal energy storage. 15th Int Conf Int Build Perform Simul Assoc 2017. doi:10.26868/25222708.2017.238.

[80] Padovan R, Manzan M. Genetic optimization of a PCM enhanced storage tank for Solar Domestic Hot Water Systems. Sol Energy 2014;103:563–73. doi:10.1016/j.solener.2013.12.034.

[81] Izquierdo-Barrientos MA, Sobrino C, Almendros-Ibáñez JA. Modeling and experiments of energy storage in a packed bed with PCM. Int J Multiph Flow 2016;86:1–9. doi:10.1016/j.ijmultiphaseflow.2016.02.004.

[82] Jmal I, Baccar M. Numerical study of PCM solidification in a finned tube thermal storage including natural convection. Appl Therm Eng 2015;84:320–30. doi:10.1016/j.applthermaleng.2015.03.065.

3

Economic model predictive control for demand flexibility of a residential building

This chapter has been published as:

C. Finck, R. Li, and W. Zeiler, "Economic model predictive control for demand flexibility of a residential building", Energy 176 (2019):pp. 365-379.

Abstract

Future building energy management systems will have to be capable of adapting to variation in the rate of production of energy from renewable sources. Controllers employing a model predictive control (MPC) framework can optimize and schedule energy usage based on the availability of renewably generated energy. In this paper, an MPC using artificial neural networks (ANNs) was implemented in a residential building. The ANN-MPC was successfully tested and demonstrated good performance predicting the building's energy consumption. The controller was then modified to function as an economic MPC (EMPC) to optimize *demand flexibility* (i.e. the ability to adapt energy demands to fluctuations in supply).
The operational costs of energy usage were associated with this demand flexibility, which was represented by three flexibility indicators: flexibility factor, supply cover factor, and load cover factor. The results from a day-long test showed that these flexibility indicators were maximized (flexibility factor ranged from -0.88 to 0.67, supply cover factor from 0.04 to 0.13, and load cover factor from 0.07 to 0.16) when the EMPC controller's demand flexibility was compared to that of a conventional proportional-integral (PI) controller. The EMPC framework for demand flexibility can be used to regulate on-site energy generation, grid consumption, and grid feed-in and can thus serve as a basis for overall optimization of the operation of heating systems to achieve greater demand flexibility.

3.1 Introduction

In Europe, the share of primary energy supply from renewable sources increased to 14.2% in 2016, which was the highest share for renewables among all regions in the Organisation for Economic Co-operation and Development (OECD) [1]. The large proportion of renewables requires added efforts to balance fluctuations and to maintain power quality and grid stability. As additional intermittently available sources of renewable energy – such as wind and solar – are included in the electricity infrastructure, it becomes essential to track and manage the dynamic behaviour of the demand side [2–7]. This ability to adapt to the intermittent availability of energy from renewable sources is called *flexibility*, and applies on both supply and demand sides [2–7]. The relevant literature [2–7] shows that there is a common understanding of the need for flexibility in energy systems. A review by Lund et al. [2], for example, identifies supply and demand flexibility as critical. The concept of demand flexibility is derived from the conventional method of load shifting and implies that demand flexibility should not compromise the quality and continuity of the processes that are consuming energy. DeConinck et al. [4] discussed the flexibility of buildings in terms of the magnitude and duration of load shifting. More precisely, a building's flexibility is described as its ability to deviate from a reference electric load profile [4]. Many studies have investigated the flexibility of buildings and have attempted to derive a common terminology and quantification scheme for building flexibility [7]. In 2015, the International Energy Agency's Energy in Buildings and Communities program launched its Annex 67 Energy Flexible Buildings project with these goals: to develop a common terminology for building's flexibility, to identify key performance indicators for characterising building's flexibility, and to quantify the potential flexibility of different buildings and clusters of buildings [7]. Early results from the Annex 67 project have shown that flexible energy usage in buildings includes different dimensions of flexibility, energy, power, and costs [5,7–9]. To ensure consistency in terminology, the present paper uses the term *demand flexibility* to represent the flexibility of buildings in adapting their energy demands to fluctuations in supply. Further insight into quantifying demand flexibility and its dimensions is provided in section 3.1.1.

The potential for demand flexibility depends on the availability of end-uses that allow for such flexibility, such as electric vehicles and smart domestic appliances [7]. Other major sources of demand flexibility are the thermal and electrical loads for building heating, cooling, and ventilation [7]. To provide flexibility in their demands on the power grid, building heating, ventilation, and air conditioning (HVAC) installations make wide use of electrical power-to-heat systems and thermal energy storage systems [5,10,11]. In buildings, direct heating, combined heat and power systems (CHPs), and heat pumps (HPs) are the most common power-to-heat conversion technologies [9,12–14].

These can be combined with thermal energy storage (TES) options such as building thermal mass, water tanks, phase-change materials, or thermochemical storage systems [5,15].

To increase demand flexibility, recent work has analysed the behaviour of building users [6,16]. The goal of the work is to progress beyond the physical characteristics of buildings, modelling, and measurements and to instead use occupants' perspectives [6]. A survey indicated that 11% of respondents may potentially become flexible in their use of energy. To raise awareness of flexibility among building users, the study [6] suggested, smart-technology adoption should be encouraged, and financial incentives should be provided.

3.1.1 Review of quantification methods and key performance indicators of demand flexibility of buildings

Reynders et al. [8,17] give an overview of methodologies for quantifying demand flexibility of buildings in which they describe three dimensions of demand flexibility: size (energy), time (power), and costs. As an example, in a study by Nuytten et al. [13], energy flexibility is achieved by shifting electricity consumption in time. Reynders et al. [17] quantifies energy flexibility of different residential buildings in Belgium. Structural thermal energy storage has been used as a source of flexibility. Buildings with floor heating have a greater energy storage capacity than buildings with radiator heating. The researchers measured a storage efficiency of between 66% and 85% for non-renovated buildings. Stinner et al. [9] investigated power flexibility and proposed power curves that describe the evolution of power demand and availability over time. By defining a reference case and a maximal power curve, they simulated the maximum power flexibility for a building with CHP, HP, and TES. Junker et al. [18] introduce the flexibility function, which is a dynamic response to the energy consumption of a building. Based on a penalty control signal, the flexibility function represents a power-related flexibility step-response. De Coninck et al. [4] investigated the 3rd dimension of demand flexibility, the costs. They define cost curves for shifting the power demands of a building's HVAC system.

Salpakari et al. [19] investigated cost-optimal control of an HP, an electric boiler, and a water thermal energy storage system in an urban setting. Their simulation case study included low-order models implemented in optimal control indicating that an HP and electric boiler combined with TES can successfully enable load shifting, a reduction of operational costs of energy usage, and an increase in self-consumption (i.e. energy consumption from on-site generation). Operational electricity costs and self-consumption are typical performance indicators used when investigating demand flexibility. The studies by Clauß et al. [20] and Finck et al. [21] provide an overview of key performance indicators used to measure demand flexibility. They pay special attention to flexibility indicators that are used in the control of building energy systems.

They find that conventional indicators such as operational energy costs and level of energy consumption are widely investigated in rule-based, optimal, and model predictive control. Indicators that describe flexibility such as load cover factor (self-generation), supply cover factor (self-consumption), flexibility factor, grid feed-in, available storage capacity, and storage efficiency [4,19,22–26], are primarily studied using rule-based control [20]. Clauß et al. [20] recommended conducting case studies to consider these specific flexibility indicators using optimal control. Péan et al. [27] present a similar conclusion, arguing that flexibility indicators need further investigation within the framework of model predictive control (MPC). Flexibility indicators may consequently be used as performance indicators in the framework of an MPC and economic MPC (EMPC), or even considered as control objective [27].

3.1.2 Review of modelling methods and key performance indicators of MPC implementations in buildings

MPC controllers are becoming more widespread in energy management systems for buildings, because they optimally manage energy consumption through their use of weather forecasting and their prediction of the dynamics of a building's energy system [28–33]. However, they are more complex than conventional controllers, because they must periodically perform an online optimization over a finite time horizon by modelling the entire building energy system. An MPC's prediction performance strongly depends on the modelling approach used to represent the building's energy system. Grey-box and black-box models have been identified as the most appropriate approaches [28]. For grey-box modelling, low-order resistance-capacitance networks are often used, which require less computational effort but exclude nonlinear characteristics [28]. In contrast, black-box models can cope with nonlinear behaviour but require sufficient data sets to be able to identify the dynamics of an energy system [28,34,35]. In recent years, artificial neural networks (ANNs) have been increasingly used as black-box models to represent building energy systems and to predict energy demand [34,36,37]. Afram et al. [34] provide a comprehensive overview of recent and successful implementations of ANNs with MPC, also called ANN-MPC. They find that ANN modelling improved performance of MPC-controlled HVAC subsystems. The use of ANN-MPC in real applications, experimental validations, and comparisons to conventional MPC – including grey-box modelling methods – would help to increase the acceptance of ANN-MPC in buildings. However, Afram et al. [34] conclude that most studies that have applied ANN-MPC have considered residential complexes and commercial buildings rather than residential buildings. Wang et al. [38] reach a similar conclusion, judging that the reason for this may be the lack of monitoring data in residential buildings due to the unavailability of sensors and meters.

There have been few successful demonstrations of MPC implementations in buildings, because the financial benefits of MPC implementation are still smaller than the total costs [39,40]. The main challenges in designing a robust and resilient MPC which can be adapted to different buildings are the consideration of the stochastic nature of disturbances such as weather and occupancy, the effort and cost of modelling methods, and the conflicting nature of control objectives [39,40]. As an example for conflicting control objectives, in an experimental study from Killian et al. [39], optimal control was applied to an office building to minimize the primary energy consumption for heating and cooling while maximizing users' thermal comfort. A similar approach was taken by Viot et al. [41], using an MPC in an office building with a cost function that incorporated comfort (an optimal temperature within a comfort interval) and energy consumption costs. Sturzenegger et al. [42] implemented an office building HVAC system MPC which optimized the costs of operational energy usage and penalized comfort as constraint. Comfort as temperature bounds for MPC implementation was tested by Yu et al. [43], who used a climate chamber to investigate an MPC which minimized energy consumption for heating and cooling. In a study from Fiorentini et al. [30], an MPC was implemented in a residential building to demonstrate that available resources could be deployed to maximize systems efficiency while meeting occupant comfort. It can be noted that experimental investigations of MPC in buildings primarily consider energy costs, energy consumption, thermal comfort, and coefficient of performance (COP) as key performance indicators.

3.1.3 Contribution and outline

From the review of relevant literature it is clear that the development of MPC in buildings needs additional experimental investigation. Furthermore, a comparison of MPC implementations requires a comprehensive analysis of experimental results that show a multitude of performance indicators. This can be accomplished when all conventional indicators are presented, such as energy costs, energy consumption, thermal comfort, and COP. Additionally, to quantify demand flexibility in relation to the power grid, all relevant flexibility indicators need to be determined, so that conventional performance evaluation of MPC can be extended by evaluation of demand flexibility.

This study presents an implementation of MPC in a residential building. The study also shows how flexibility indicators can be associated with the costs of energy usage. Based on this, an EMPC is introduced to optimize demand flexibility. The contributions of this experimental case study can be summarised as follows:

- An ANN-MPC approach is implemented in a residential building and the prediction performance of the ANNs and the ANN-MPC is presented.
- Conventional performance indicators for MPC are determined, which are energy consumption, total cost of operational energy usage, and COP. Thermal comfort is represented by comfort bounds. Accordingly, the maximum and minimum room temperature are implemented as constraints in the MPC framework.
- Demand flexibility indicators are given: the flexibility factor, supply cover factor, and load cover factor.
- The study introduces an EMPC which enables the optimization of performance indicators for demand flexibility and in which the operational costs of energy usage are associated with flexibility indicators.

The outline of the paper is as follows. Section 3.2 explains the methodology and the experimental case study. In section 3.2.1, the test building is described. In section 3.2.2, the MPC framework is presented. Section 3.2.2 (Model identification) provides insight into the identification procedure of black-box modelling using an ANN. The developed ANNs are integrated into the MPC framework. Section 3.2.3 introduces an EMPC for demand flexibility. The formulation of the EMPC includes different objective functions which can optimize the costs of energy usage associated with demand flexibility. The flexibility indicators and conventional performance indicators are also described in section 3.2.3. The MPC framework and the EMPC are tested, and the results are shown in section 3.3.

3.2 Methodology

A Dutch residential building was used as a testbed to conduct the experimental case study of an EMPC approach that optimizes the costs of energy usage associated with demand flexibility. The EMPC was implemented and tested during the heating season, between January and April 2017. The building heating system was equipped with a condensing boiler which distributes heat to radiator circuits. For modelling of the heating system and the building, ANN models were identified from measurements made between January and March 2017. In March and April 2017, the ANN models were validated and implemented in the MPC framework. The validation of the ANN-MPC was conducted based on heating consumption. In April 2017, the MPC was modified to EMPC (Figure 3.1), and photovoltaic (PV) panels were virtually installed at the building to simulate on-site electricity generation. Additionally, an HP was virtually installed to simulate energy conversion from electricity to heating power. The virtual models of PV panels and the HP were implemented in the EMPC.

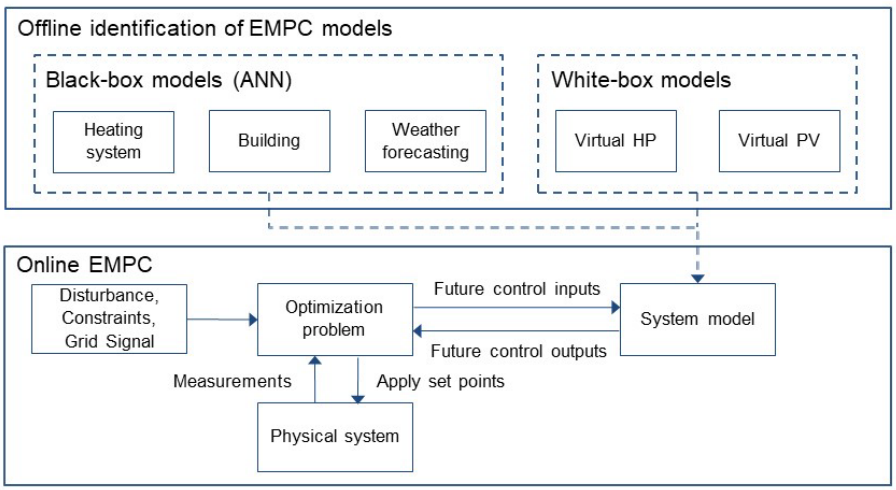

Figure 3.1. Methodological framework of the economic model predictive controller (EMPC).

Thus, the EMPC was simulated and tested with the energy system, including PV panels providing power that could be directly used by the HP and could be fed to the power grid, and an HP which was controlled to provide heating to the building. To investigate the optimization of costs of energy usage associated with demand flexibility, the EMPC assumed (1) the costs of consuming electricity from the grid, (2) the costs of consuming electricity from on-site PV power generation, and (3) the costs delivering electricity from on-site PV

power generation to the grid. Thus, the EMPC incorporates the costs of export of electricity and the costs of electricity consumption in one objective function. Accordingly, the most common indicators representing demand flexibility – the flexibility factor, supply cover factor, and load cover factor [20,21] – can be maximized while using an EMPC implementation that minimizes the total costs of energy usage. Two different EMPC approaches were introduced and tested. The EMPC approach 1 (EMPC1) maximized the flexibility factor and reduced the operational costs of electricity consumption. The EMPC approach 2 (EMPC2) maximized the flexibility factor, supply cover factor, and load cover factor and optimized the costs of electricity consumption from the grid, costs from on-site PV power generation, and costs for grid feed-in.

To simulate electricity consumption from the power grid, hourly day-ahead prices from the Amsterdam Power Exchange (APX) spot market were implemented in the EMPC. The key function of the EMPC approach is that the controller is designed to regulate an HP but, in reality, regulates a condensing boiler. Thus, the controller combines the identified heating system model and the HP model. The heating system model represents heating supplied to the building and the HP model represents the energy conversion from electricity to heating power. The dynamic behaviour of the HP is studied by [44–47]. The major differences to the condensing boiler are variations in the start-up and shut-down phases, which are neglected in this experimental case study to justify the usage of a virtual HP model.

3.2.1 Building description

The dwelling was located in the city of Utrecht, the Netherlands, representing a typical old row house from 1910 (Figure 3.2). During the test period, two persons lived in the dwelling. The dwelling was 75 m^2 with three floors (kitchen on first floor, living room on second, bedroom on third). The building consisted of 25-cm outer and 15-cm inner brick walls. With a 160°[1] and -20° north-south orientation, the house was attached to neighbouring buildings. Due to the shading of the taller neighbouring building in the south, solar gains were limited (Figure 3.2). The windows at -110° and 70° orientation captured solar radiation in the morning and afternoon.

[1] 0° = South orientation; 180° = North orientation; 90° = West orientation; -90° = East orientation

Windows in the living room had 50% single glazing and 50% double glazing; windows in the bedroom and kitchen had single glazing. Due to this large number of single-glazed windows, the thermal loads of the building were higher compared to those of renovated buildings. The annual heating energy usage was about 0.47 GJ/m^2, which was delivered by a gas-fired condensing boiler. During cold periods when heating was required, the room temperature was controlled by one thermostat located on the second floor.

Figure 3.2. Test building located in Utrecht, the Netherlands (left–front view -110° orientation, right–back view 70° orientation).

3.2.2 MPC framework

A model predictive controller was implemented, enabling real-time control with hourly time steps [30,38]. A receding horizon of 12 hours was used for the MPC to regulate room temperature set points. Real-time measurements served as hourly starting points. The controller implemented upper and lower comfort bounds, which were based on occupants' preferences. Due to a deterministic occupancy profile ϵ_t, the room temperature bounds were defined according to

$$T_{room,set} = \begin{Bmatrix} 18 \leq T_{room,set} < 22 \;\; if\; t \in (0{:}00, 8{:}00) \\ 20 \leq T_{room,set} < 22 \;\; if\; t \in (8{:}00, 24{:}00) \end{Bmatrix}, \tag{3-1}$$

and

$$T_{room,set} \in \mathbb{Z}. \quad (3\text{-}2)$$

The windows were closed during the test periods of MPC implementation. The opening of curtains (Cu.) was determined according to

$$Cu.opening = \begin{Bmatrix} Cu. = 0 \ (closed) & if\ t \in (0{:}00, 8{:}00)\&(20{:}00, 24{:}00) \\ Cu. = 1 \quad (open) & if\ t \in (8{:}00, 20{:}00) \end{Bmatrix}, \quad (3\text{-}3)$$

where t is the time (h). Because the MPC performed hourly simulations, a fast optimization strategy was required. Dynamic programming (DP) was used as optimization strategy and carried out in MATLAB. The DP algorithm handled the optimization with sufficient computational times of less than 30 min, because there was only one control variable, which was the average room temperature of the living room. During the computation of the optimization at each control time step, first the duration of computation was estimated, then the simulation was run to predict 12 hours ahead. More information about the DP algorithm can be found in [48].

Data acquisition and processing

The model predictive controller required a modelling and simulation platform and a communication interface to sensors and actuators. All models that were associated with optimal control were implemented in a MATLAB scheme. MATLAB was also used to retrieve data from the sensors and to transfer commands to the thermostat. As middleware between MATLAB and the sensors, microcontrollers were placed in the building to catch information from the sensors and send them to the MATLAB controller. The microcontrollers were Arduino Yun modules that were connected to temperature sensors of type DC95 (thermistors) with an accuracy of 0.1 °C. The temperature sensors measured room temperatures (six sensors placed at 1.20 m height), surface temperatures (three sensors placed at 1.20 m height), radiator temperatures (two sensors attached to radiators), heating return, and heating supply temperatures (two sensors attached to pipes). The constant flow rate of the heating system was determined using an ultrasonic flow meter to have a value of 0.8 m^3/h.

Model identification

Comprehensive data sets were collected from measurements for the modelling of the building envelope, including all thermal zones, and the heating system. Furthermore, historical weather data were used to create the weather forecasting model, which predicted horizontal and global solar radiation and ambient temperature. Weather data and measurement data were used to validate the black-box models that were identified using ANNs. Previous case studies have successfully validated ANNs to identify building dynamics and building heating systems [34–36,49–52] and global and horizontal solar radiation [53–56]. In the present study, three neural networks were identified – an ANN for the building with all thermal zones, an ANN for the heating system, and an ANN for the solar radiation forecasting. All ANNs were developed using the MATLAB Neural Network toolbox. The identification of the ANNs was processed offline (Figure 3.1). Therefore, the data sets from measurements were randomly divided into three data sets which were used for training (70%), validation (15%), and testing (15%). This procedure was repeated more than 100 times. Additionally, for the ANNs of the building and the heating system, a second validation step was performed using a set of unseen data. The performance prediction of the ANNs was statistically estimated by obtaining the root-mean-square error (RMSE), mean absolute error (MAE), mean absolute percentage error (MAPE), coefficient of determination (R^2), and goodness of fit (G) [34,35,51,57–59]. The mathematical description of the performance metrics can be found in the Appendix.

Model identification - weather forecasting

The weather forecasting model predicted ambient temperature and global and horizontal solar radiation. The ambient temperature was retrieved from online forecasting [60] using a local network of 10 weather stations that were located within a radius of 2.5 km [53]. An online MATLAB connection was established, integrating an application programming interface (API) to the website [60]. Because forecasting of solar radiation was typically not provided by local weather forecasting, an ANN was developed to predict short-term solar radiation. The ANN considered for the solar radiation forecasting model was based on a feedforward net-work that consisted of input signals u_i $(i = 1, 2, \dots, n)$, hidden layers, and output signals y_i according to

$$y_i = f\left(\sum_{i=1}^{n} w_{ji} u_i\right). \tag{3-4}$$

In the hidden layer, each neuron j represented a sum of the input signals u_i with a weighting factor w_{ji} and connected to each output y_i [54]. Based on local, historical weather data from the last 10 years [61], the ANN was trained using the input and output variables as shown in Figure 3.3.

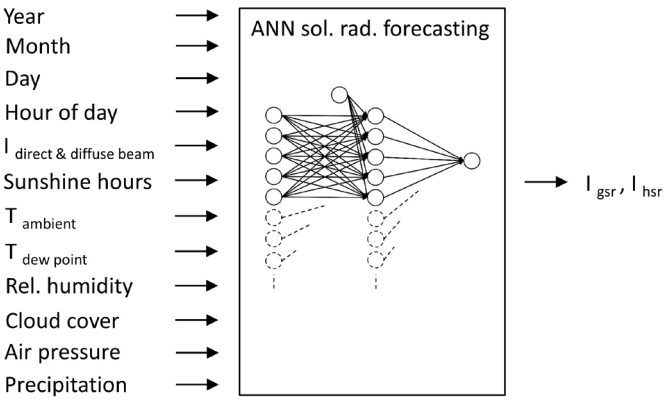

Figure 3.3. Inputs and outputs of artificial neural network (ANN) to obtain the global solar radiation (I_{gsr}) and horizontal solar radiation (I_{hsr}).

Global and horizontal solar radiation include direct and diffuse beam irradiance ($I_{\text{direct \& diffuse beam}}$). Therefore, a simplified clear sky model was used based on the work of Bird et al. [62]. For the ANN of solar radiation forecasting (W/m^2), the best configuration was found with 75 hidden layers, resulting in a RMSE of 25, MAE of 13, MAPE of 0.19, R^2 of 0.98, and G of 0.87, which were in good agreement with results from other studies [55,63,64].

Model identification - building and heating system

The ANNs for the building (building envelope with all thermal zones) and heating system were based on time-series problems that were nonlinear autoregressive with external (exogenous) input (NARX) problems. The NARX was a recurrent dynamic network using feedback connections according to

$$y(t) = f(y(t-1), y(t-2), \dots, y(t-n_y), u(t-1), u(t-2), \dots, u(t-n_u), \quad (3\text{-}5)$$

where $y(t)$ is the output signal and $u(t)$ is the exogenous input variable [65]. Input and output variables of the ANNs are shown in Figure 3.4. During the heating period, only the living room was heated. Thus, the ANN for the building predicted the average thermal-zone temperature T_{room} of the living room, the average surface temperature of the walls $T_{surface}$, and the return temperature of the heating system $T_{heating,\ return}$.

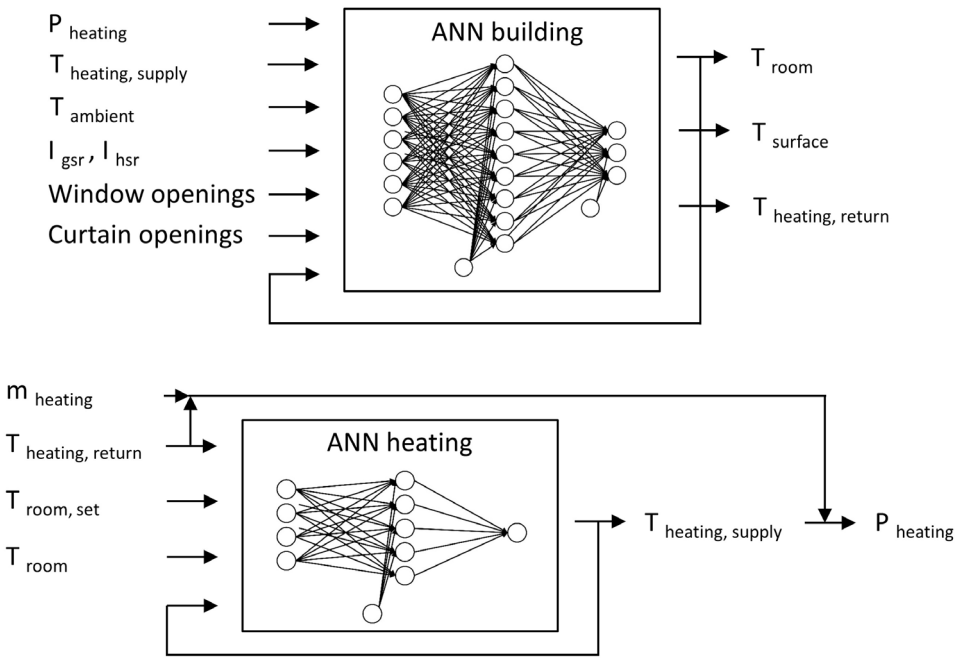

Figure 3.4. Inputs and outputs of artificial neural networks (ANNs) for the building and the heating system.

As can be seen in Figure 3.4, ANN inputs included the opening of windows and curtains. Measures of the opening of windows and curtains were recorded using a survey in which occupants filled in opening and closing times. The ANN for the heating system predicted the heating supply temperature so that the heating power could be calculated according to

$$P_{heating} = f\left(T_{heating,return}\ ;\ T_{heating,supply}; \dot{m}_{heating}\right). \tag{3-6}$$

Measurement data were recorded with 1-s time steps. To train the ANNs, a 3-month data set with Levenberg-Marquardt back-propagation was used. The data set for the identification was quite large compared with other studies, which identified ANNs based on data sets covering ranges of 10 days to 2 months [34,36,49,66]. The developed ANNs were applied to a validation set of unseen data (taken from 16 Mar. 2016 to 25 Mar. 2017), including temperature set point variations. The daily prediction performance is listed in Table 3-1. The best configuration for the ANN building model was with two input delays, two feedback delays, and five hidden layers. For the ANN heating system, the best configuration had two input delays, two feedback delays, and eight hidden layers. The identified ANNs showed a good accuracy compared to the results from other studies that used black-box approaches for building-energy modelling [34–36,49,66].

Table 3-1. Daily performance of ANN models on 10 days of unseen data ($Q = \int P\,dt$, for example $Q_{heating} = \int P_{heating}\,dt$).

ANN model		RMSE	MAE	MAPE	R^2	G
Heating system	$Q_{heating}$ (kWh)	0.14–0.33	0.03–0.10	0.04–0.14	0.98–0.99	0.86–0.95
Building	T_{room} (°C)	0.44–0.66	0.32–0.53	0.01–0.03	0.78–0.89	0.53–0.66
	$T_{surface}$ (°C)	0.18–0.31	0.14–0.25	0.01	0.75–0.88	0.50–0.65
	$T_{heating,\ return}$ (°C)	0.57–0.87	0.40–0.62	0.01–0.02	0.98–0.99	0.88–0.92

3.2.3 Economic MPC (EMPC)

The online EMPC was implemented as shown in Figure 3.5.

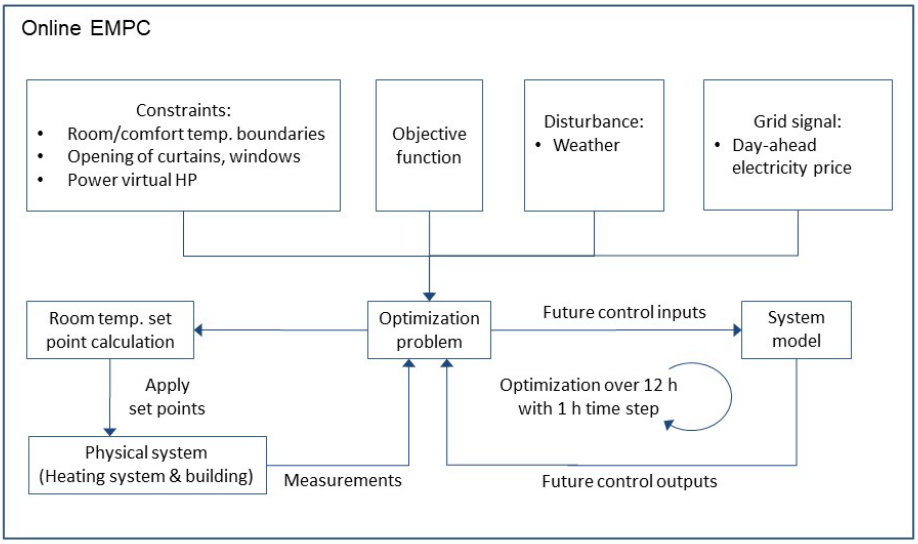

Figure 3.5. Online economic model predictive control (Online EMPC), adapted from Péan et al. [27].

The EMPC approach imposed constraints and incorporated disturbances and control signals into the optimization problem. The control decisions were retrieved from the system model which consists of black-box and white-box models. The black-box models were the ANNs for the building and heating system, and the white-box models virtually simulated the PV panels and the HP. The implementation of the models in the optimization scheme is shown in Figure 3.6.

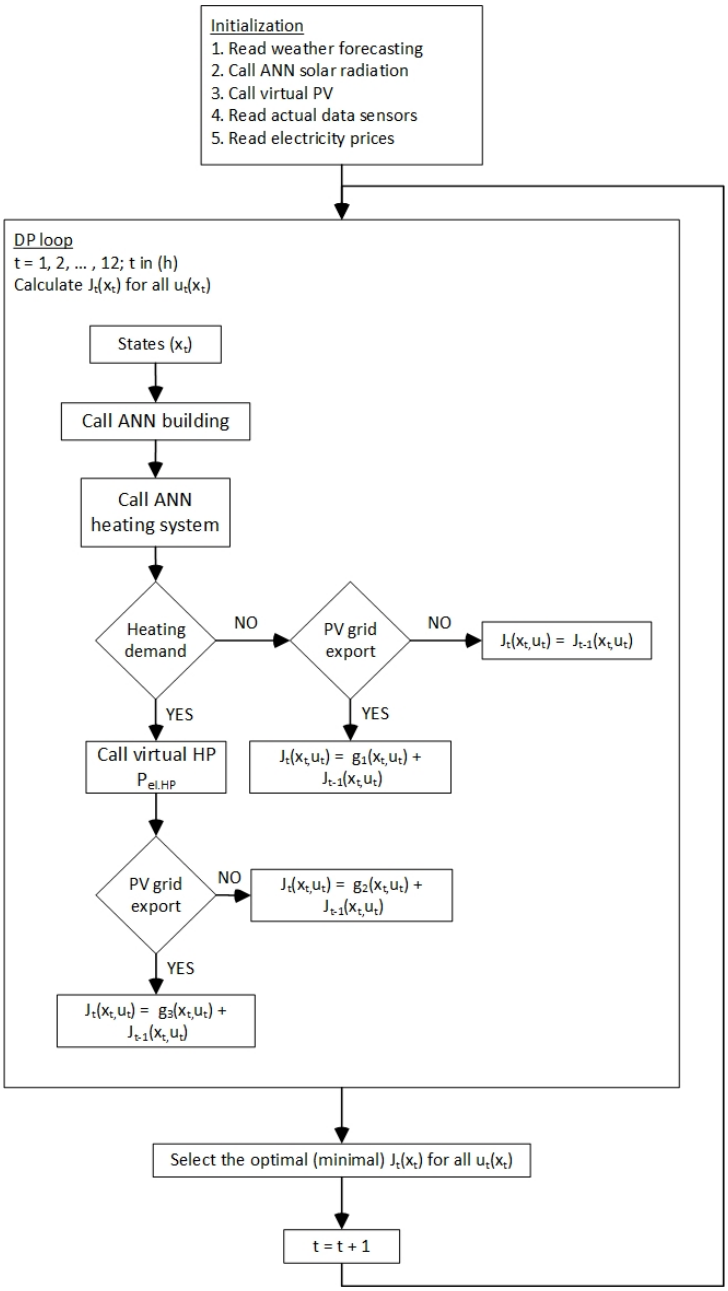

Figure 3.6. Simplified flowchart of optimal control decisions using dynamic programming (DP).

Heat pump (HP) model

The heating power of the HP was limited to 20 kW, which was the maximum heating power of the condensing boiler. The heating supply temperature of the HP reached a maximum of 65 °C, which was the maximum setting for the condensing boiler during the entire test period. The virtual HP was an inverter-controlled air–water HP from NIBE (NIBE2120) [67]. During the learning phase, the condensing boiler was set in Eco mode, which meant that the heating supply temperature was kept as low as possible, providing energy-efficient operation. This control strategy was similar to conventional HP strategies. Thus, the virtual HP model assumed energy-efficient operation which was based on a piecewise linear interpolation function using manufacturers' data (Figure 3.7).

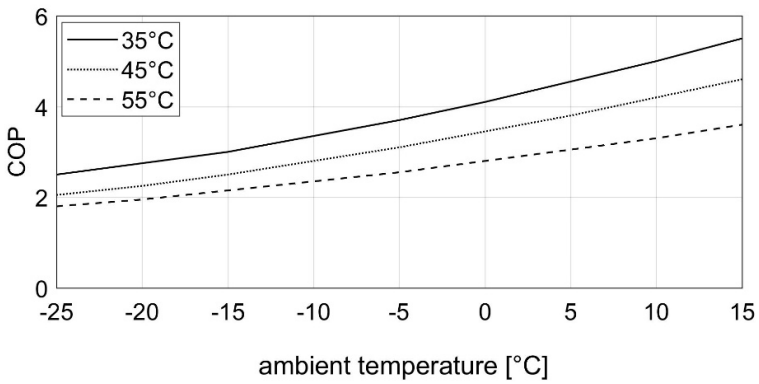

Figure 3.7. Performance of the air–water heat pump (HP); the coefficient of performance (COP) was a function of ambient temperature for different heating supply temperatures [67].

Photovoltaic (PV) model

PV panels were virtually placed on the roof of the building in a west-southwest (WSW) orientation measured 70° from south orientation. As can be seen in Figure 3.2, the roof consisted of two areas with different inclinations: 47.5° and 55°. PV panels were placed in both areas, resulting in a total PV area of about 13 m^2. The chosen PV panels were mono-crystalline, with a nominal power of 300 W per module under standard test conditions (STC), in-plane-irradiation $G_{STC} = 1000\ W/m^2$, and PV module temperature $T_{mod,STC} = 25\ °C$ [68]. The PV model was based on the work of [69,70]. Power generation $P_{el.gen.PV}$ and energy performance of the PV modules $\eta_{el.}$ were implemented in the MPC according to

$$P_{el.gen.PV} = P_{el.STC} \frac{G}{G_{STC}} \eta_{el.}(G', T'), \quad (3\text{-}7)$$

$$\eta_{el.} = 1 + k_1 \, ln \, G' + k_2 \, (ln \, G')^2 + T'(k_3 + k_4 \, ln \, G' + k_5 \, (ln \, G')^2) + k_6 \, T'^2, \quad (3\text{-}8)$$

$$G' = \frac{G}{G_{STC}} \, , \quad (3\text{-}9)$$

and

$$T' = T_{mod} - T_{mod,STC}, \quad (3\text{-}10)$$

where G' and T' are normalized irradiation and temperature. The coefficients $k_1 - k_6$ depended on the type of PV panels and were taken from [69].

Key performance indicators of EMPC

This study presented conventional performance indicators and performance indicators for demand flexibility. The conventional indicators were energy consumption, operational energy costs, and the COP. For energy consumption, the HP used electricity from the grid and from PV panels. Additionally, the amount of heating provided by the HP was presented, and the resulting COP was retrieved according to Figure 3.7. The operational energy costs included (1) the costs of electricity consumption from the grid, (2) the costs related to electricity consumption from on-site PV power generation, and (3) the costs for grid feed-in from on-site PV power generation.

The performance indicators for demand flexibility were the flexibility factor, supply cover factor, and load cover factor. The flexibility factor FF quantified heating energy provided by the HP during low-price and high-price periods for electricity according to

$$FF = \frac{\int_{t_{low\ price\ start}}^{t_{low\ price\ end}} P_{heating} \, dt - \int_{t_{high\ price\ start}}^{t_{high\ price\ end}} P_{heating} \, dt}{\int_{t_{low\ price\ start}}^{t_{low\ price\ end}} P_{heating} \, dt + \int_{t_{high\ price\ start}}^{t_{high\ price\ end}} P_{heating} \, dt}, \quad (3\text{-}11)$$

with

$$-1 \leq FF \leq 1, \quad (3\text{-}12)$$

where $P_{heating}$ is the heating power. A flexibility factor of 1 indicated highest flexibility of the controlled system, and -1 correlated to inflexible energy usage. In the present study, the standard deviation was used to define high- and low-price periods according to [5]. Prices for energy consumption from the grid in periods above one standard deviation of 1σ were considered as high-price periods, and prices in periods below one standard deviation of -1σ were low-price periods.

The degree of local power consumption covered by on-site electricity generation can be calculated using the load-matching indicators supply cover factor and load cover factor [22,25,71]. The supply cover factor γ_{supply} (self-consumption) represents the ratio of direct consumption of PV electricity for heating $P_{el.cons.HP-PV}$ and total PV electricity production $P_{el.gen.PV}$ for a period N according to

$$\gamma_{supply} = \frac{\sum_{t=1}^{N} P_{el.cons.HP-PV}}{\sum_{t=1}^{N} P_{el.gen.PV}}, \tag{3-13}$$

with

$$0 \leq \gamma_{supply} \leq 1. \tag{3-14}$$

The load cover factor γ_{load} (self-generation) represents the ratio of direct consumption of PV electricity for heating $P_{el.cons.HP-PV}$ and total electricity heating demand $P_{el.cons.HP}$ for a period N according to

$$\gamma_{load} = \frac{\sum_{t=1}^{N} P_{el.cons.HP-PV}}{\sum_{t=1}^{N} P_{el.cons.HP}}, \tag{3-15}$$

with

$$0 \leq \gamma_{load} \leq 1. \tag{3-16}$$

EMPC1

EMPC1 was designed to maximize demand flexibility as represented by the flexibility factor. A larger flexibility factor indicated a greater amount of HP-consumed electricity (provided for heating) shifting from high-price periods to low-price periods. The associated costs of energy usage were the costs of electricity consumption from the grid. Thus, EMPC1 attempted to minimize total costs J_{EMPC1} for the HP's operational electricity consumption from the grid $P_{el.cons.HP-grid}$ according to

$$min\, J_{EMPC1} = \sum_{t=1}^{N} \left(C_{el.cons.grid}(t)\, P_{el.cons.HP-grid}(t)\, \Delta t \right);$$

$$N = 12\, h; \quad \Delta t = 1\, h, \qquad (3\text{-}17)$$

where $C_{el.cons.grid}$ is the price of electricity consumption from the grid, which corresponded to hourly day-ahead prices from the APX spot market [5,28,31,32]. Costs related to electricity consumption from on-site PV power generation, and costs for grid feed-in from on-site PV power generation were not considered in EMPC1.

EMPC2

EMPC2 was designed to maximize demand flexibility as represented by the flexibility factor, the supply cover factor, and the load cover factor. As mentioned above, maximizing the flexibility factor can be reached by minimizing the total operational costs of energy consumption from the grid. Maximizing the supply cover factor and load cover factor refers to an increase of self-consumption, or respectively an increase of electrical energy consumed from on-site PV power generation. On-site PV-generated electrical energy not used by the HP was exported to the power grid. Thus, EMPC2 required the inclusion of three different terms: (1) energy consumption from the grid, (2) energy consumption from on-site PV power generation, and (3) energy exported to the grid from on-site PV power generation. By accounting for the operational costs associated with each of these terms, one objective function was created which included costs for electricity consumption from the grid, costs for direct consumption of PV-generated power, and costs for grid feed-in. The study, therefore, introduced an EMPC for demand flexibility which was formulated as a minimization problem according to

$$\begin{aligned} min\, J_{EMPC2} = & \sum_{t=1}^{N} \left(C_{el.cons.grid}(t)\, P_{el.cons.HP-grid}(t)\, \Delta t \right) \\ & + \sum_{t=1}^{N} \left(C_{el.cons.PV}(t)\, P_{el.cons.HP-PV}(t)\, \Delta t \right) \\ & + \sum_{t=1}^{N} \left(C_{el.feed\ in\ grid}(t)\, P_{el.PV\ grid}(t)\, \Delta t \right), \end{aligned}$$

$$N = 12\, h; \quad \Delta t = 1\, h\,, \qquad (3\text{-}18)$$

where $C_{el.cons.grid}$ is the price of electricity consumption from the grid, $C_{el.cons.PV}$ is the price of electricity consumption from on-site PV generation, and $C_{el.feed\ in\ grid}$ is the price of electricity exported to the power grid.

Reference case

A reference case was simulated to evaluate the results of EMPC1 and EMPC2. A 24-h period was simulated using a traditional PI controller according to

$$T_{room,set,ref} = \begin{Bmatrix} T_{room,set,ref} = 18 \;\; if\; t \in (0{:}00, 8{:}00) \\ T_{room,set,ref} = 20 \;\; if\; t \in (8{:}00, 24{:}00) \end{Bmatrix}. \tag{3-19}$$

The results of the reference case simulation were compared to the measured and predicted results of EMPC1 and EMPC2. This comparison gave an indication of the performance of the two EMPC approaches as measured by heating energy consumption, costs for electricity consumption, the HP's COP, and demand flexibility.

3.3 Results

Experiments were carried out at the beginning of April 2017. Experimental results are shown for the validation of the MPC framework (3.3.1) and the application of the EMPC1 and EMPC2 (3.3.2). During the test days, hourly predictions of the ambient temperature were retrieved from local weather stations. Global and horizontal solar radiation was calculated based on the developed forecasting model (ANN sol. rad. forecasting). The MPC results are illustrated below, and measured data are compared to predicted data.

3.3.1 Validation of MPC framework

The model predictive controller was implemented and initially tested on 3 April 2017 between 10:00 and 14:00. During the validation period, solar radiation (W/m^2) and ambient temperature (°C) were measured and predicted. The results of the weather forecasting are illustrated in Figure 3.8. A prediction performance is calculated for ambient temperature (°C) of RMSE = 0.34, MAE = 0.25, and MAPE = 0.02, and for hourly solar radiation (W/m^2) of RMSE = 25, MAE = 20, and MAPE = 0.06.

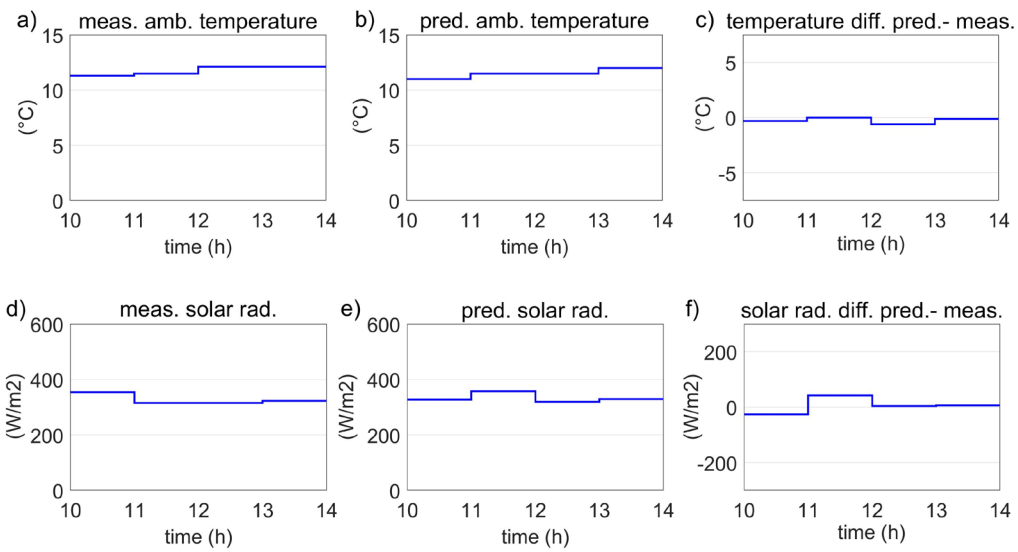

Figure 3.8. Validation of MPC; validation period 10:00 – 14:00; hourly ambient temperature a) measured, b) predicted, and c) difference; hourly solar radiation d) measured, e) predicted, and f) difference.

For the validation period, a constant room temperature set point of 20 °C was chosen. Measured and predicted room temperatures can be found in Figure 3.9. The measured average room temperature varied between 19.4 °C and 20.1 °C, which is in accordance with the temperature range of historical data. The change in average room temperature was due to prevailing weather conditions and the transient interaction of room temperatures and wall temperatures. Using an ANN to simulate the room temperature resulted in a temperature curve that fit well to the measured data. A prediction performance was calculated for room temperature (°C) of RMSE = 0.14, MAE = 0.11, and MAPE = 0.01, and for heating demand (kWh) of RMSE = 0.12, MAE = 0.11, and MAPE = 0.18.

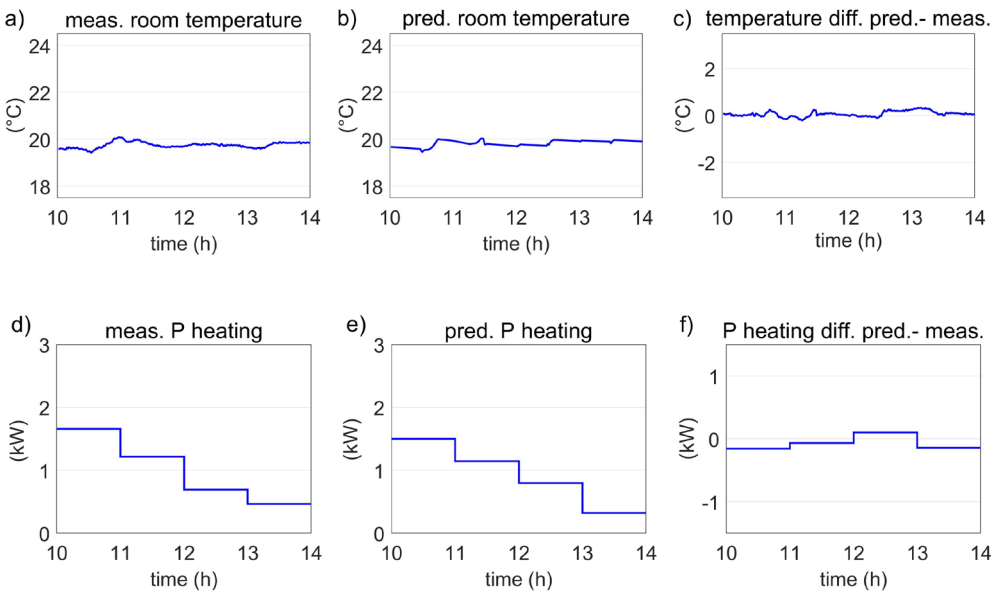

Figure 3.9. Validation of MPC; validation period 10:00 – 14:00; MPC results for a constant temperature set point of 20 °C; average room temperature a) measured, b) predicted, and c) difference; hourly heating demand ($P_{heating}$) d) measured, e) predicted, and f) difference.

3.3.2 EMPC

The MPC framework was modified to two EMPC approaches. Measured and predicted data were collected for a 24-h period (one day), and results were compared for flexibility indicators, daily energy consumption, and total costs of electricity consumption.

EMPC1

EMPC1, designed to maximize the flexibility factor, was implemented and tested on 05 April 2017. The results of hourly predictions and measurements taken for ambient temperature and solar radiation are depicted in Figure 3.10. A prediction performance was calculated for ambient temperature (°C) of RMSE = 0.96, MAE = 0.77, MAPE = 0.07, R^2 = 0.80, G = 0.55 and for the hourly solar radiation (W/m^2) of RMSE = 37, MAE = 24, MAPE = 0.25, R^2 = 0.96 and G = 0.79.

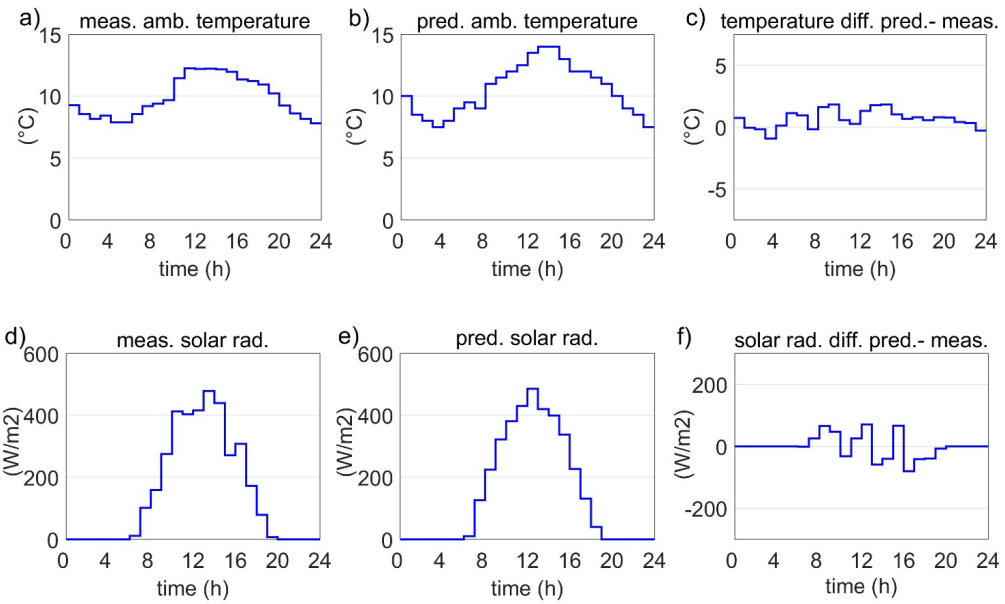

Figure 3.10. EMPC1; hourly ambient temperature a) measured, b) predicted, and c) difference; hourly solar radiation d) measured, e) predicted, and f) difference.

Based on hourly weather forecasting and hourly electricity prices, EMPC1 simulated the optimal control decisions for the operation of the room temperature set points. The results of those control decisions are illustrated in Figure 3.11. A prediction performance was calculated for room temperature (°C) of RMSE = 0.24, MAE = 0.16, MAPE = 0.01, R^2 = 0.89, and G = 0.66 and for heating demand (kWh) of RMSE = 0.26, MAE = 0.17, MAPE = 0.30, R^2 = 0.97, and G = 0.82. Between 5:00 and 6:00, during low-price periods (Figure 3.11b), the HP was scheduled to provide heating to the building (Figure 3.11c). Due to preheating in low-price periods, only minimal heating consumption was required during high-price periods (Figure 3.11a). A summary of the test results using EMPC1 can be found in Table 3-2.

Table 3-2 also lists the results of a simulated reference case using perfect weather prediction and feedback control. The results from EMPC1 indicate that total operational electricity costs were reduced by 7%, and heating demand was increased by 1.5% when measured EMPC1 results were compared to the reference case. However, EMPC1 was designed to maximize the flexibility factor, which increased from -0.89 to 0.42.

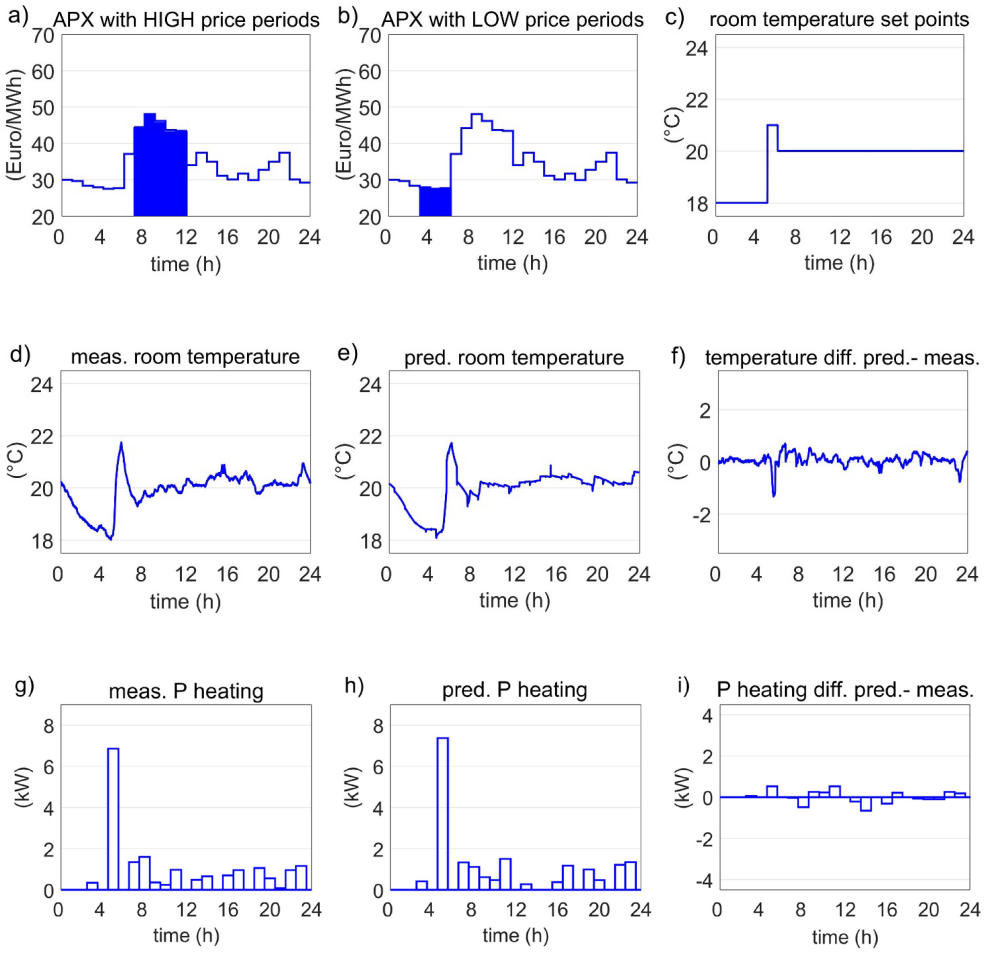

Figure 3.11. EMPC1; Hourly APX electricity prices including a) high-price periods and b) low-price periods; c) hourly room temperature set points; room temperature d) measured, e) predicted, and f) difference; heating demand ($P_{heating}$) g) measured, h) predicted, and i) difference.

Table 3-2. Summary results for EMPC1 ($Q = \int P\, dt$, for example $Q_{heating} = \int P_{heating}\, dt$).

Results	MPC predicted	MPC measured	Reference case
J (Euro cent)	12.43	12.86	13.85
$Q_{heating}$ (kWh)	18.71	18.41	18.15
$Q_{el.cons.HP-grid}$ (kWh)	3.86	3.95	3.50
$Q_{el.cons.HP-PV}$ (kWh)	0.42	0.39	0.46
$Q_{el.gen.PV}$ (kWh)	5.44	5.75	5.75
COP (-)	4.37	4.24	4.58
FF (-)	0.44	0.42	-0.89
γ_{supply} (-)	0.08	0.07	0.08
γ_{load} (-)	0.10	0.09	0.12

EMPC2

EMPC2, designed to maximize the flexibility factor, the supply cover factor, and the load cover factor, was implemented and tested on 11 April 2017. Figure 3.12 shows the results of the weather forecasting and measurement data.

A prediction performance was calculated for ambient temperature (°C) of RMSE = 0.71, MAE = 0.58, MAPE = 0.06, R^2 = 0.94, and G = 0.76 and for hourly solar radiation (W/m^2) of RMSE = 42, MAE = 25, MAPE = 0.25, R^2 = 0.95, and G = 0.76.

In addition to APX electricity prices ($C_{el.cons.grid}(t)$), EMPC2 required the determination of the price of electricity consumed from PV generation ($C_{el.cons.PV}$) and the price of electricity exported to the power grid ($C_{el.feed\ in\ grid}$). For the test day, the electricity prices were assumed according to

$$C_{el.feed\ in\ grid}(t) = -C_{el.cons.grid}(t), \tag{3-20}$$

and

$$C_{el.cons.PV}(t) = -5\left(C_{el.cons.grid}(t)\right). \tag{3-21}$$

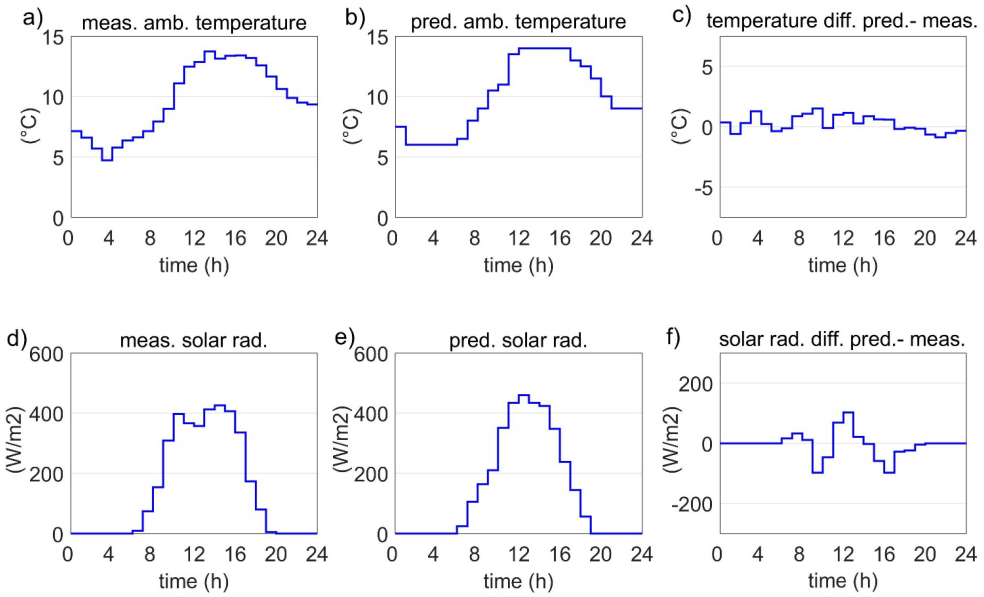

Figure 3.12. EMPC2; hourly ambient temperature a) measured, b) predicted, and c) difference; hourly solar radiation d) measured, e) predicted, and f) difference.

The results of the control decisions of EMPC2 are shown in Figure 3.13. A prediction performance was calculated for room temperature (°C) of RMSE = 0.27, MAE = 0.18, MAPE = 0.01, R^2 = 0.93, and G = 0.73 and for heating demand (kWh) of RMSE = 0.19, MAE = 0.10, MAPE = 0.28, R^2 = 0.99, and G = 0.89. During low-price periods (APX price), the HP provided heating to the building (5:00 – 6:00). Between 15:00 and 17:00 the optimal temperature set point was raised to 22 °C. During this time slot, APX prices were relatively low and PV power generation was relatively high compared to the daily average. Using EMPC2 resulted in increases of flexibility factor from -0.88 to 0.67, supply cover factor from 0.04 to 0.13, and load cover factor from 0.07 to 0.16, as shown in Table 3-3.

Equation 3-20 and 3-21 assume a constant relation between APX electricity prices ($C_{el.cons.grid}(t)$), prices of direct electricity consumption from PV ($C_{el.cons.PV}$) and prices of electricity exported to the power grid ($C_{el.feed\ in\ grid}$). Additional simulations were performed to analyse the effect of price variations. Figure 3.14 illustrates the results of varying $C_{el.cons.PV}/-C_{el.cons.grid}$ between a value of 1 and 15 while keeping $C_{el.feed\ in\ grid} = -C_{el.cons.grid}$ constant.

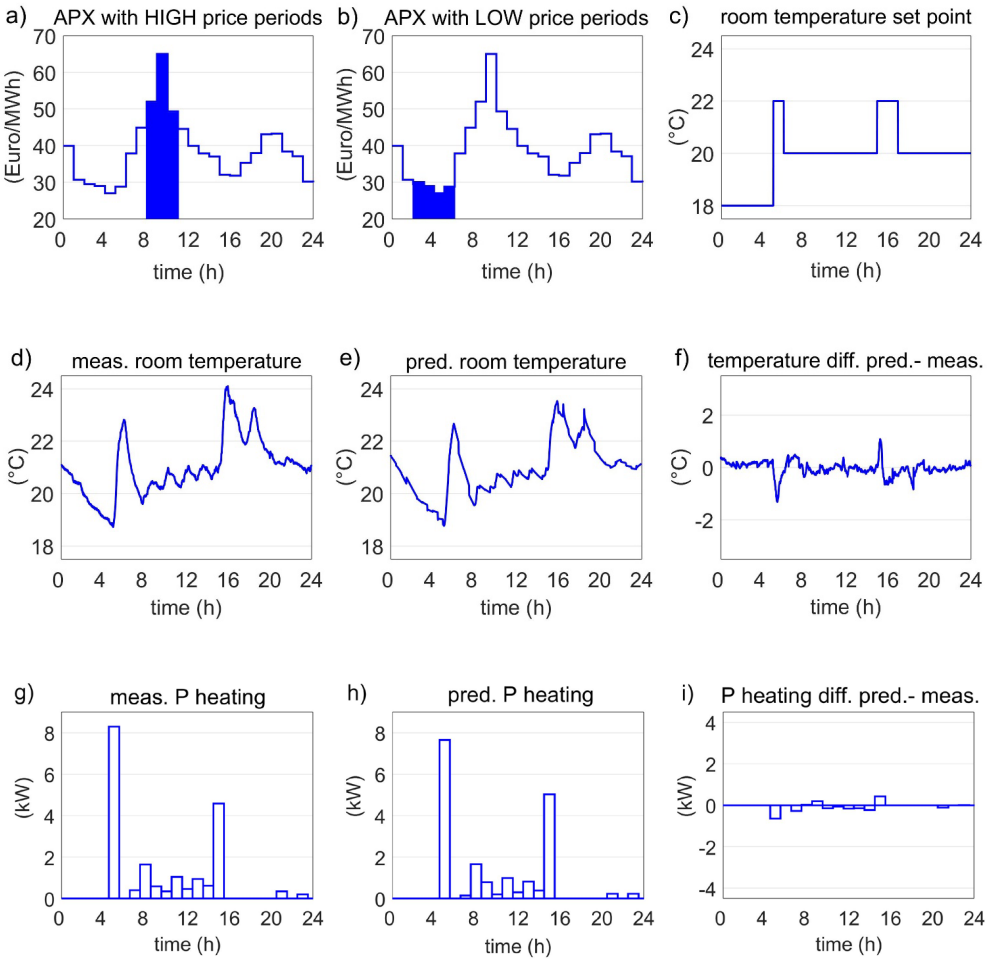

Figure 3.13. EMPC2; Hourly APX electricity prices including a) high-price periods and b) low-price periods; c) hourly room temperature set points; room temperature d) measured, e) predicted, and f) difference; heating demand ($P_{heating}$) g) measured, h) predicted, and i) difference.

Table 3-3. Summary results for EMPC ($Q = \int P\,dt$, for example $Q_{heating} = \int P_{heating}\,dt$).

Results	MPC predicted	MPC measured	Reference case
J (Euro cent)	13.69	13.85	14.28
$Q_{heating}$ (kWh)	19.53	19.33	16.13
$Q_{el.cons.HP-grid}$ (kWh)	4.05	4.25	3.61
$Q_{el.cons.HP-PV}$ (kWh)	0.81	0.82	0.28
$Q_{el.gen.PV}$ (kWh)	7.15	6.56	6.56
COP (-)	4.02	3.76	4.15
FF (-)	0.68	0.67	-0.88
γ_{supply} (-)	0.11	0.13	0.04
γ_{load} (-)	0.17	0.16	0.07

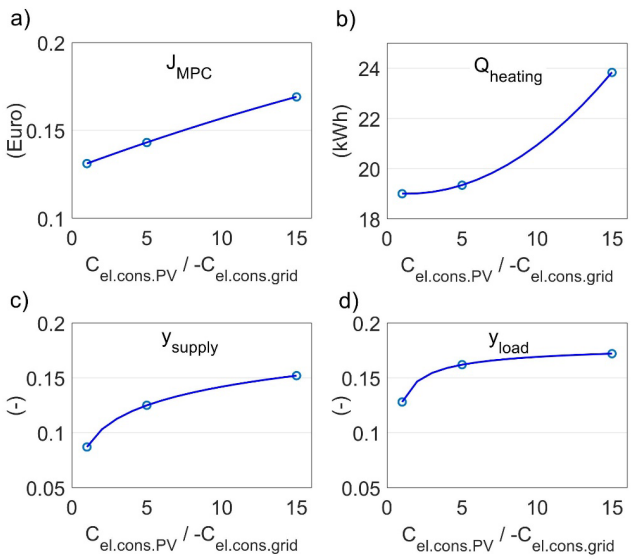

Figure 3.14. EMPC2; Price variations by changing $C_{el.cons.PV}/-C_{el.cons.grid}$ and assuming $C_{el.feed\ in\ grid} = -C_{el.cons.grid}$; a) daily operational electricity costs JEMPC; b) daily heating energy $Q_{heating}$; c) supply cover factor y_{supply} (self-consumption); d) load cover factor y_{supply} (self-generation).

3.4 Discussion

An economic model predictive controller was implemented in a Dutch residential building. This controller included day-ahead electricity prices. The next step will be to incorporate intraday electricity prices to be able to adapt to short-term variations, as recommended by Heldegaard et al. [72]. The EMPC also integrated weather forecasting and prediction of building and heating system dynamics. The EMPC consisted of models using artificial neural networks. ANNs are black-box models which are formulated without using any physical equations. An advantage of ANNs is their ability to deal with nonlinear dynamics. A disadvantage is that they require large data sets for validation. In the present study, four months of measurement data (January–April 2017) were used to identify and validate the black-box models representing the building dynamics and the heating system. A ten-year data set was used to identify the black-box model for forecasting the global and horizontal solar radiation. During the test days, the ANN which forecasts solar radiation (W/m^2) achieved a prediction performance of RMSE of 37–42, MAE of 24–25, MAPE of 0.25, R^2 of 0.95–0.96, and G of 0.76–0.79, which was less accurate than the prediction performance during the validation phase of RMSE = 25, MAE = 13, MAPE = 0.19, R^2 = 0.98, and G = 0.87. The decrease in prediction performance during test days was because of uncertainty in the forecasts of ambient temperature, precipitation, sunshine hours, cloud cover, relative humidity, and air pressure. The forecast of these parameters was retrieved from a professional forecasting service that provided hourly data. A shorter time step for predictions may increase the prediction accuracy [56]. However, shorter prediction time steps require a larger state space for the optimization and thus increase the MPC computational time.

During the EMPC1 test day, no direct solar radiation affected the indoor climate. During the EMPC2 test day, direct solar radiation was observed at 18:00 (Figure 3.13 d, e and f), resulting in a steep increase in room temperature and a reduction of prediction accuracy (delta T of up to 1 K). It is observed that steep, short-term room temperature changes are less accurately predicted (delta T of up to 1.5 K in the first 10 min of heating with set point changes). However, the overall prediction performance for room temperature (°C) of RMSE of 0.24–0.27, MAE of 0.16–0.18, MAPE of 0.01, R^2 of 0.89–0.93, and G of 0.66–0.73 was in good agreement with other studies [34–36,49,66], as was the prediction performance for heating consumption (kWh) of RMSE of 0.19–0.26, MAE of 0.10–0.17, MAPE of 0.28–0.30, R^2 of 0.97–0.99, and G of 0.82–0.89.

During the learning and validation phase of the MPC, the thermal heating power varied between 8 kW and 20 kW, and a maximum of three on/off cycles of the heating system per hour were observed. Compared to conventional HPs in heating systems, the number of on/off cycles is reasonable.

For the future, the number of on/off cycles is less critical when using inverter-controlled HPs that modulate heating power by regulating the compressor speed [27,73]. In the present study, a virtual inverter-controlled HP was assumed and simulated using a regression model which fit manufacturers' data. This modelling approach was sufficient for simulation studies to represent the performance of the HP [74]. For experimental case studies with real HPs, more sophisticated and full dynamic modelling approaches are recommended, for instance approaches using ANNs [74]. A similar conclusion is made for determining realistic performance measures of real PV panels in the control of building energy management systems [75]. The study [75] provides an extensive review of ANNs applied to solar energy systems, including PV. The authors in [75] suggest the use of ANN and machine-learning approaches to solar energy systems to reduce the financial expenses for modelling.

During the learning and validation phase of the MPC, a maximum, virtual PV power of 1 kW was calculated. From Table 3-2 and Table 3-3, it can be seen that the amount of daily electrical energy provided by the virtual PV ($Q_{el.gen.PV}$) was higher than the daily electricity consumption of the virtual HP ($Q_{el.cons.HP}$). In contrast, the calculated self-consumption varied between 7% and 25%. This was primarily because the maximal PV power was always lower than the HP's electrical power consumption. A simple solution could be the installation of an electrical battery that could compensate for this mismatch. The electrical battery could be directly fed by the PV, and the battery's state of charge could be added as state variable to the MPC. An integration into the MPC as an additional control variable is not required.

In the tested MPC, deterministic profiles of occupancy and window and curtain openings were used. Occupants were asked to follow a predefined schedule for opening of windows and curtains during the MPC experimental phase. In a next step, occupants' behaviour will be incorporated using a stochastic approach, as suggested by Wang et al. [16], to consider the uncertainty of energy flexibility that is due to the uncertainty of occupancy.

3.5 Conclusion

In the present paper, an experimental case study was presented of an MPC implemented in a residential building. An ANN-MPC approach was used to represent the dynamical behaviour of the heating systems and the building. Another ANN model was developed for weather forecasting to obtain global and horizontal solar radiation. All ANN models and the ANN-MPC were validated and tested, showing good prediction performance. The application of ANN models can be recommended for future identification of the dynamics of buildings and heating systems and for weather forecasting. The application of ANN-MPC can be recommended as a generic approach for optimal control of energy usage in energy systems in residential buildings. As a next step, it is important to adapt this generic methodology to other residential buildings. Further experimental case studies are required that compare MPC implementations, including performance evaluation of conventional and flexibility indicators.

This paper also introduced an EMPC approach to optimize demand flexibility. For this approach, operational costs of energy usage were associated with demand flexibility, which was represented by these flexibility indicators: flexibility factor, supply cover factor, and load cover factor. The operational costs were (1) the costs of consuming electricity from the grid, (2) the costs of consuming electricity from on-site PV power generation, and (3) the costs delivering electricity from on-site PV power generation to the grid. By taking into account the operational costs of energy usage, one objective function can be created, and demand flexibility can be optimized. As an example, assuming positive prices for electricity consumption from the grid, negative prices for electricity consumption from on-site PV generation, and negative prices for grid feed-in from on-site PV power generation resulted in an increase of flexibility factor, supply cover factor (self-consumption), and load cover factor (self-generation). This generic approach offers the possibility to regulate on-site generation, grid consumption, and grid feed-in. The methodology can be adapted to flexibility indicators which are associated with the costs of energy usage.

3.6 Appendix – Performance metrics

i is the sample number, n is the total number of samples, e is the estimated data, o is the output, $\bar{o}$ is the mean output

Root-Mean-Square Error

$$RMSE = \sqrt{\frac{1}{n}\sum_{i=1}^{n}(e_i - o_i)^2}$$

Mean Absolute Error

$$MAE = \frac{1}{n}\sum_{i=1}^{n}|e_i - o_i|$$

Mean Absolute Percentage Error

$$MAPE = \frac{1}{n}\sum_{i=1}^{n}\left|\frac{|e_i - o_i|}{o_i}\right|$$

Coefficient of Determination

$$R^2 = 1 - \frac{\sum_{i=1}^{n}(o_i - e_i)^2}{\sum_{i=1}^{n}(o_i - \bar{o})^2}$$

Goodness of Fit

$$G = 1 - \frac{\sqrt{\sum_{i=1}^{n}(e_i - o_i)^2}}{\sqrt{\sum_{i=1}^{n}\left(o_i - \frac{1}{n}\sum_{i=1}^{n}o_i\right)^2}}$$

3.7 References

[1] International Energy Agency, Renewables information: Overview, 2017. http://www.iea.org/publications/freepublications/publication/RenewablesInformation2017Overview.pdf.

[2] P.D. Lund, J. Lindgren, J. Mikkola, J. Salpakari, Review of energy system flexibility measures to enable high levels of variable renewable electricity, Renew. Sustain. Energy Rev. 45 (2015) 785–807. doi:10.1016/j.rser.2015.01.057.

[3] L. Gelazanskas, K.A.A. Gamage, Demand side management in smart grid: A review and proposals for future direction, Sustain. Cities Soc. 11 (2014) 22–30. doi:10.1016/j.scs.2013.11.001.

[4] R. De Coninck, L. Helsen, Quantification of flexibility in buildings by cost curves - Methodology and application, Appl. Energy. 162 (2016) 653–665. doi:10.1016/j.apenergy.2015.10.114.

[5] C. Finck, R. Li, R. Kramer, W. Zeiler, Quantifying demand flexibility of power-to-heat and thermal energy storage in the control of building heating systems, Appl. Energy. 209 (2018) 409–425. doi:10.1016/j.apenergy.2017.11.036.

[6] R. Li, G. Dane, C. Finck, W. Zeiler, Are building users prepared for energy flexible buildings?—A large-scale survey in the Netherlands, Appl. Energy. 203 (2017). doi:10.1016/j.apenergy.2017.06.067.

[7] S.Ø. Jensen, A. Marszal-Pomianowska, R. Lollini, W. Pasut, A. Knotzer, P. Engelmann, A. Stafford, G. Reynders, IEA EBC Annex 67 Energy Flexible Buildings, Energy Build. 155 (2017) 25–34. doi:10.1016/j.enbuild.2017.08.044.

[8] G. Reynders, R. Amaral Lopes, A. Marszal-Pomianowska, D. Aelenei, J. Martins, D. Saelens, Energy flexible buildings: An evaluation of definitions and quantification methodologies applied to thermal storage, Energy Build. (2018). doi:10.1016/j.enbuild.2018.02.040.

[9] S. Stinner, K. Huchtemann, D. Müller, Quantifying the operational flexibility of building energy systems with thermal energy storages, Appl. Energy. 181 (2016) 140–154. doi:10.1016/j.apenergy.2016.08.055.

[10] J. Salpakari, P. Lund, Optimal and rule-based control strategies for energy flexibility in buildings with PV, Appl. Energy. 161 (2016) 425–436. doi:10.1016/j.apenergy.2015.10.036.

[11] D. Vanhoudt, D. Geysen, B. Claessens, F. Leemans, L. Jespers, J. Van Bael, An actively controlled residential heat pump: Potential on peak shaving and maximization of self-consumption of renewable energy, Renew. Energy. 63 (2014) 531–543. doi:10.1016/j.renene.2013.10.021.

[12] D. Fischer, H. Madani, On heat pumps in smart grids: A review, Renew. Sustain. Energy Rev. 70 (2017) 342–357. doi:10.1016/j.rser.2016.11.182.

[13] T. Nuytten, P. Moreno, D. Vanhoudt, L. Jespers, A. Solé, L.F. Cabeza, Comparative analysis of latent thermal energy storage tanks for micro-CHP systems, Appl. Therm. Eng. 59 (2013) 542–549. doi:10.1016/j.applthermaleng.2013.06.023.

[14] J. Clauß, S. Stinner, I. Sartori, L. Georges, Predictive rule-based control to activate the energy flexibility of Norwegian residential buildings: Case of an air-source heat pump and direct electric heating, Appl. Energy. 237 (2019) 500–518. doi:10.1016/J.APENERGY.2018.12.074.

[15] A. Arteconi, N.J. Hewitt, F. Polonara, State of the art of thermal storage for demand-side management, Appl. Energy. 93 (2012) 371–389. doi:10.1016/j.apenergy.2011.12.045.

[16] A. Wang, R. Li, S. You, Development of a data driven approach to explore the energy flexibility potential of building clusters, Appl. Energy. 232 (2018) 89–100. doi:10.1016/j.apenergy.2018.09.187.

[17] G. Reynders, J. Diriken, D. Saelens, Generic characterization method for energy flexibility: Applied to structural thermal storage in residential buildings, Appl. Energy. 198 (2017) 192–202. doi:10.1016/j.apenergy.2017.04.061.

[18] R.G. Junker, A.G. Azar, R.A. Lopes, K.B. Lindberg, G. Reynders, R. Relan, H. Madsen, Characterizing the energy flexibility of buildings and districts, Appl. Energy. 225 (2018) 175–182. doi:10.1016/j.apenergy.2018.05.037.

[19] J. Salpakari, J. Mikkola, P.D. Lund, Improved flexibility with large-scale variable renewable power in cities through optimal demand side management and power-to-heat conversion, Energy Convers. Manag. 126 (2016) 649–661. doi:10.1016/j.enconman.2016.08.041.

[20] J. Clauß, C. Finck, P. Vogler-Finck, P. Beagon, Control strategies for building energy systems to unlock demand side flexibility – A review, in: 15th Int. Conf. Int. Build. Perform. Simul. Assoc., 2017: pp. 611–620.

[21] C. Finck, J. Clauß, P. Vogler-Finck, P. Beagon, K. Zhan, H. Kazmi, Review of applied and tested control possibilities for energy flexibility in buildings, 2018. doi:10.13140/RG.2.2.28740.73609.

[22] J. Salom, A.J. Marszal, J. Widén, J. Candanedo, K.B. Lindberg, Analysis of load match and grid interaction indicators in net zero energy buildings with simulated and monitored data, Appl. Energy. 136 (2014) 119–131. doi:10.1016/j.apenergy.2014.09.018.

[23] G. Masy, E. Georges, C. Verhelst, V. Lemort, Smart grid energy flexible buildings through the use of heat pumps and building thermal mass as energy storage in the Belgian context, Sci. Technol. Built Environ. 21:6 (2015) 800–811. doi:10.1080/23744731.2015.1035590.

[24] J. Le Dréau, P. Heiselberg, Energy flexibility of residential buildings using short term heat storage in the thermal mass, Energy. 111 (2016) 991–1002. doi:10.1016/j.energy.2016.05.076.

[25] R. Luthander, J. Widén, D. Nilsson, J. Palm, Photovoltaic self-consumption in buildings: A review, Appl. Energy. 142 (2015) 80–94. doi:10.1016/j.apenergy.2014.12.028.

[26] G. Reynders, Quantifying the impact of building design on the potential of structural storage for active demand response in residential buildings, 2015. doi:10.13140/RG.2.1.3630.2805.

[27] T.Q. Péan, J. Salom, R. Costa-Castelló, Review of control strategies for improving the energy flexibility provided by heat pump systems in buildings, J. Process Control. (2018). doi:10.1016/j.jprocont.2018.03.006.

[28] Y. Zong, G.M. Böning, R.M. Santos, S. You, J. Hu, X. Han, Challenges of implementing economic model predictive control strategy for buildings interacting with smart energy systems, Appl. Therm. Eng. 114 (2017) 1476–1486. doi:10.1016/j.applthermaleng.2016.11.141.

[29] D. Lindelöf, H. Afshari, M. Alisafaee, J. Biswas, M. Caban, X. Mocellin, J. Viaene, Field tests of an adaptive, model-predictive heating controller for residential buildings, Energy Build. 99 (2015) 292–302. doi:10.1016/j.enbuild.2015.04.029.

[30] M. Fiorentini, J. Wall, Z. Ma, J.H. Braslavsky, P. Cooper, Hybrid model predictive control of a residential HVAC system with on-site thermal energy generation and storage, Appl. Energy. 187 (2017) 465–479. doi:10.1016/j.apenergy.2016.11.041.

[31] C.R. Touretzky, M. Baldea, Integrating scheduling and control for economic MPC of buildings with energy storage, J. Process Control. 24 (2014) 1292–1300. doi:10.1016/j.jprocont.2014.04.015.

[32] J. Ma, S.J. Qin, T. Salsbury, Application of economic MPC to the energy and demand minimization of a commercial building, J. Process Control. 24 (2014) 1282–1291. doi:10.1016/j.jprocont.2014.06.011.

[33] H. Huang, L. Chen, E. Hu, A new model predictive control scheme for energy and cost savings in commercial buildings: An airport terminal building case study, Build. Environ. 89 (2015) 203–216. doi:10.1016/j.buildenv.2015.01.037.

[34] A. Afram, F. Janabi-Sharifi, A.S. Fung, K. Raahemifar, Artificial neural network (ANN) based model predictive control (MPC) and optimization of HVAC systems: A state of the art review and case study of a residential HVAC system, Energy Build. 141 (2017) 96–113. doi:10.1016/j.enbuild.2017.02.012.

[35] A. Afram, F. Janabi-Sharifi, Black-box modeling of residential HVAC system and comparison of gray-box and black-box modeling methods, Energy Build. 94 (2015) 121–149. doi:10.1016/j.enbuild.2015.02.045.

[36] H. Huang, L. Chen, E. Hu, A neural network-based multi-zone modelling approach for predictive control system design in commercial buildings, Energy Build. 97 (2015) 86–97. doi:10.1016/j.enbuild.2015.03.045.

[37] J. Reynolds, Y. Rezgui, A. Kwan, S. Piriou, A zone-level, building energy optimisation combining an artificial neural network, a genetic algorithm, and model predictive control, Energy. 151 (2018) 729–739. doi:10.1016/j.energy.2018.03.113.

[38] Z. Wang, R.S. Srinivasan, A review of artificial intelligence based building energy use prediction: Contrasting the capabilities of single and ensemble prediction models, Renew. Sustain. Energy Rev. 75 (2017) 796–808. doi:10.1016/j.rser.2016.10.079.

[39] M. Killian, M. Kozek, Implementation of cooperative Fuzzy model predictive control for an energy-efficient office building, Energy Build. (2018). doi:10.1016/j.enbuild.2017.11.021.

[40] M. Killian, M. Kozek, Ten questions concerning model predictive control for energy efficient buildings, Build. Environ. 105 (2016) 403–412. doi:10.1016/j.buildenv.2016.05.034.

[41] H. Viot, A. Sempey, L. Mora, J.C. Batsale, J. Malvestio, Model predictive control of a thermally activated building system to improve energy management of an experimental building: Part II - Potential of predictive strategy, Energy Build. (2018). doi:10.1016/j.enbuild.2018.04.062.

[42] D. Sturzenegger, D. Gyalistras, M. Morari, R.S. Smith, Model Predictive Climate Control of a Swiss Office Building: Implementation, Results, and Cost-Benefit Analysis, IEEE Trans. Control Syst. Technol. (2016). doi:10.1109/TCST.2015.2415411.

[43] N. Yu, S. Salakij, R. Chavez, S. Paolucci, M. Sen, P. Antsaklis, Model-based predictive control for building energy management: Part II – Experimental validations, Energy Build. (2017). doi:10.1016/j.enbuild.2017.04.027.

[44] A. Floss, S. Hofmann, Optimized integration of storage tanks in heat pump systems and adapted control strategies, Energy Build. 100 (2015) 10–15. doi:10.1016/j.enbuild.2015.01.009.

[45] E. Fuentes, D.A. Waddicor, J. Salom, Improvements in the characterization of the efficiency degradation of water-to-water heat pumps under cyclic conditions, Appl. Energy. 179 (2016) 778–789. doi:10.1016/j.apenergy.2016.07.047.

[46] M. Uhlmann, S.S. Bertsch, Theoretical and experimental investigation of startup and shutdown behavior of residential heat pumps, Int. J. Refrig. 35 (2012) 2138–2149. doi:10.1016/j.ijrefrig.2012.08.008.

[47] M. Qu, Y. Fan, J. Chen, T. Li, Z. Li, H. Li, Experimental study of a control strategy for a cascade air source heat pump water heater, Appl. Therm. Eng. 110 (2017) 835–843. doi:10.1016/j.applthermaleng.2016.08.176.

[48] D.P. Bertsekas, Dynamic programming and optimal control, Athena Scientific, Belmont, Mass., 2005.

[49] A. Garnier, J. Eynard, M. Caussanel, S. Grieu, Predictive control of multizone heating, ventilation and air-conditioning systems in non-residential buildings, Appl. Soft Comput. J. 37 (2015) 847–862. doi:10.1016/j.asoc.2015.09.022.

[50] P.M. Ferreira, A.E. Ruano, S. Silva, E.Z.E. Conceição, Neural networks based predictive control for thermal comfort and energy savings in public buildings, Energy Build. 55 (2012) 238–251. doi:10.1016/j.enbuild.2012.08.002.

[51] S.M.C. Magalhães, V.M.S. Leal, I.M. Horta, Modelling the relationship between heating energy use and indoor temperatures in residential buildings through Artificial Neural Networks considering occupant behavior, Energy Build. 151 (2017) 332–343. doi:10.1016/j.enbuild.2017.06.076.

[52] A.E. Ruano, E.M. Crispim, E.Z.E. Conceição, M.M.J.R. Lúcio, Prediction of building's temperature using neural networks models, Energy Build. 38 (2006) 682–694. doi:10.1016/j.enbuild.2005.09.007.

[53] B. Amrouche, X. Le Pivert, Artificial neural network based daily local forecasting for global solar radiation, Appl. Energy. 130 (2014) 333–341. doi:10.1016/j.apenergy.2014.05.055.

[54] M.H. Al Al Shamisi, A.H. Assi, H.A.N. Hejase, Using MATLAB to develop artificial neural network models for predicting global solar radiation in Al Ain City – UAE, Eng. Educ. Res. Using MATLAB. (2011) 219–238. doi:10.1104/pp.17.01693.

[55] R.H. Inman, H.T.C. Pedro, C.F.M. Coimbra, Solar forecasting methods for renewable energy integration, Prog. Energy Combust. Sci. 39 (2013) 535–576. doi:10.1016/j.pecs.2013.06.002.

[56] M. Diagne, M. David, P. Lauret, J. Boland, N. Schmutz, Review of solar irradiance forecasting methods and a proposition for small-scale insular grids, Renew. Sustain. Energy Rev. 27 (2013) 65–76. doi:10.1016/j.rser.2013.06.042.

[57] Z. Afroz, T. Urmee, G.M. Shafiullah, G. Higgins, Real-time prediction model for indoor temperature in a commercial building, Appl. Energy. (2018). doi:10.1016/j.apenergy.2018.09.052.

[58] A. Afram, A.S. Fung, F. Janabi-Sharifi, K. Raahemifar, Development of an accurate gray-box model of ubiquitous residential HVAC system for precise performance prediction during summer and winter seasons, Energy Build. (2018). doi:10.1016/j.enbuild.2018.04.038.

[59] G. Mustafaraj, J. Chen, G. Lowry, Thermal behaviour prediction utilizing artificial neural networks for an open office, Appl. Math. Model. (2010). doi:10.1016/j.apm.2010.02.014.

[60] The Weather Company, Weather Forecast & Reports - Long Range & Local | Wunderground | Weather Underground. https://www.wunderground.com/ (accessed January 10, 2019).

[61] KNMI climate data, KNMI - Koninklijk Nederlands Meteorologisch Instituut. http://www.knmi.nl (accessed January 10, 2019).

[62] R.E. Bird, R.L. Hulstrom, Simplified clear sky model for direct and diffuse insolation on horizontal surfaces, 1981. doi:10.2172/6510849.

[63] A.G.R. Vaz, B. Elsinga, W.G.J.H.M. van Sark, M.C. Brito, An artificial neural network to assess the impact of neighbouring photovoltaic systems in power forecasting in Utrecht, the Netherlands, Renew. Energy. 85 (2016) 631–641. doi:10.1016/j.renene.2015.06.061.

[64] A.K. Yadav, S.S. Chandel, Solar radiation prediction using Artificial Neural Network techniques: A review, Renew. Sustain. Energy Rev. 33 (2014) 772–781. doi:10.1016/j.rser.2013.08.055.

[65] MathWorks - Deep Learning Toolbox - Modeling and Prediction with NARX and Time-Delay Networks. https://www.mathworks.com (accessed January 10, 2019).

[66] E. Žáčeková, Z. Váňa, J. Cigler, Towards the real-life implementation of MPC for an office building: Identification issues, Appl. Energy. 135 (2014) 53–62. doi:10.1016/j.apenergy.2014.08.004.

[67] NIBE, Air/water heat pump NIBE F2120, 2017. https://www.nibe.eu/en-eu/products/heat-pumps/air-water-heat-pumps/NIBE-F2120-34 (accessed January 16, 2019).

[68] Solar Fabrik - Photovoltaic modules. https://www.solar-fabrik.de/downloads (accessed January 10, 2019).

[69] T. Huld, R. Gottschalg, H.G. Beyer, M. Topič, Mapping the performance of PV modules, effects of module type and data averaging, Sol. Energy. 84 (2010) 324–338. doi:10.1016/j.solener.2009.12.002.

[70] D. Fischer, K.B. Lindberg, H. Madani, C. Wittwer, Impact of PV and variable prices on optimal system sizing for heat pumps and thermal storage, Energy Build. 128 (2016) 723–733. doi:10.1016/j.enbuild.2016.07.008.

[71] I. Sartori, A. Napolitano, K. Voss, Net zero energy buildings: A consistent definition framework, Energy Build. 48 (2012) 220–232. doi:10.1016/j.enbuild.2012.01.032.

[72] R.E. Hedegaard, T.H. Pedersen, S. Petersen, Multi-market demand response using economic model predictive control of space heating in residential buildings, Energy Build. 150 (2017). doi:10.1016/j.enbuild.2017.05.059.

[73] T. Dengiz, P. Jochem, W. Fichtner, Demand response with heuristic control strategies for modulating heat pumps, Appl. Energy. 238 (2019) 1346–1360. doi:10.1016/j.apenergy.2018.12.008.

[74] C.P. Underwood, Heat pump modelling, Elsevier Ltd, 2016. doi:10.1016/B978-0-08-100311-4.00014-5.

[75] A.H. Elsheikh, S.W. Sharshir, M. Abd Elaziz, A.E. Kabeel, W. Guilan, Z. Haiou, Modeling of solar energy systems using artificial neural network: A comprehensive review, Sol. Energy. 180 (2019) 622–639. doi:10.1016/j.solener.2019.01.037.

4

Identification of a dynamic system model for a building and heating system including heat pump and thermal energy storage

This chapter has been published as:

C. Finck, R. Li, and W. Zeiler, “Identification of a dynamic system model for a building and heating system including heat pump and thermal energy storage”, MethodsX 7 (2020): 100866.

Abstract

Controllers employing optimal control strategies will pave the way to enable flexible operations in future power grids. As buildings will increasingly act as prosumers in future power grids, optimal control of buildings’ energy consumption will play a major role in providing flexible operations. Optimal controllers such as model predictive controller are able to manage buildings’ operations and to optimize their energy consumption. For online optimization, model predictive controller require a model of the energy system. The more accurate the system model represents the system dynamics, the more accurate the model predictive controller predicts the future states of the energy system while optimizing its energy consumption. In this article, a system model is presented that can be used in online MPC, including dynamic programming as optimization strategy. The system model is validated using a building and heating system, including heat pump and thermal energy storage. The following bullet points summarize the main requirements for the configuration of the system model:

- The system model performs fast with low computational effort in less than 1s
- The system model can be implemented in online MPC
- The system model accurately represents the dynamic behaviour

4.1 Method details

To implement large amounts of renewable energy sources, power systems are required to change towards flexible operations. One possible source of flexible operations is the energy consumption of buildings, as buildings account for a large proportion of total energy consumption [1]. To adapt the energy consumption of buildings to fluctuations in supply, innovative control strategies are needed that enable flexible operations and optimally manage the energy consumption.

Controllers employing optimal control strategies are for example model predictive controller (MPC) [2]. To optimize the energy consumption, the MPC integrates a model of the building energy system. This system model implements disturbances (for example the weather forecasting) and predicts the future states of the building energy system [3,4]. So far, simplified system models such as resistance-capacitance (RC) network models have been predominantly used to study MPC in buildings. The RC models represent the building and heating system and are often validated offline. For online MPC, models of the building and heating system are converted to continuous-time state-space models via model linearization [4,5]. The use of linear modelling for online optimization is due to their ease of implementation and their low computational effort [4,5]. Linear models, however, have shown a low performance in predicting the energy consumption of buildings because they are not able to represent the complex and dynamic interactions within building energy systems [4,6].

To make a step towards application of MPC in building energy systems, models of building energy systems need to be developed for online optimization that, 1) can accurately predict the energy consumption, 2) can perform fast with low computational effort, 3) can fit into online optimization schemes. Furthermore, if the same system model can be used in both, offline validation and online optimization, then model reduction (state-space linearization of the model) for MPC is obsolete.

In this article, a detailed system model is presented that can be used in online MPC [7]. For the MPC, the system model is configured to fit into a dynamic programming scheme as optimization strategy. The MPC modelling approach, thus, does not require any model reduction for online optimization because the developed system model can be used for both offline validation and online optimization.

For offline validation, the datasets of non-time-series data were randomly divided into three datasets (training, validation, and testing). For time-series black-box modelling, the identification – including training (70%), validation (15%), and testing (15%) – was done in a so-called series-parallel architecture using standard backpropagation.

After identification, the nonlinear autoregressive with external (exogenous) input (NARX) model was transformed into a multi-step-ahead prediction network. The performance of all models of the system components was tested using a dataset of unseen data. For each of the models, the procedure was repeated more than 100 times to obtain the best performance.

For offline and online validation, model performance of the system and the system components was calculated using root mean square error (RMSE), mean absolute error (MAE), mean absolute percentage error (MAPE), coefficient of determination (R^2), and goodness of fit (G) [2,8–13]. The mathematical descriptions of the performance metrics can be found in Appendix I.

For online implementation, additionally, the system model is configured to perform fast with low computational effort and to accurately predict the dynamics of the system components. It is noted that the developed system model provides a plug-and-play solution to integrate models of the system components.

The aim of this study is to identify a dynamic system model of the building and heating system. This is why the study firstly presents the system model and the experimental set up, including data acquisition and processing. Then modelling and validation of the system components is described, and finally the application of the system model for online optimization is discussed.

4.1.1 Experimental setup and system modelling

We tested and modelled a low energy house, which was located in the Netherlands. Between November 2017 and April 2018, measurement data were recorded for the building and heating system, including occupants' domestic hot water profile and the heating demand. The heating system of the building consisted of a heat pump (HP), a photovoltaic thermal solar collector (PVT), a space heating (SH) tank, and a domestic hot water (DHW) tank. Table 4-1 lists the properties of the building and heating system. For the system model, the SH demand is simulated that was an integrated floor heating system throughout the entire building. Furthermore, a stochastic modelling approach for the DHW demand is implemented that was retrieved from the stochastic behaviour of occupants. Figure 4.1 shows the system model of the building and the heating system that is illustrated as process flow diagram. Figure 4.2 illustrates the system model that is implemented in an MPC framework. We, therefore, defined the models of the weather forecasting, the HP, the SH tank, the SH demand, the DHW tank, and the DHW demand as the system components.

Table 4-1. Properties of the building and heating system.

Building and heating system	Properties
Detached house	Total floor area = 345 m^2 Annual heating energy consumption = 55.6 kWh/m^2
HP	NIBE F1155-16 Nominal heating output = 16 kW
PVT	TripleSolar with a total area = 30 m^2
SH tank	Volume = 1000 L Insulation thickness = 0.2 m Insulation thermal conductivity = 0.07 W/(mK)
DHW tank	Volume = 300 L Insulation thickness = 0.05 m Insulation thermal conductivity = 0.07 W/(mK)

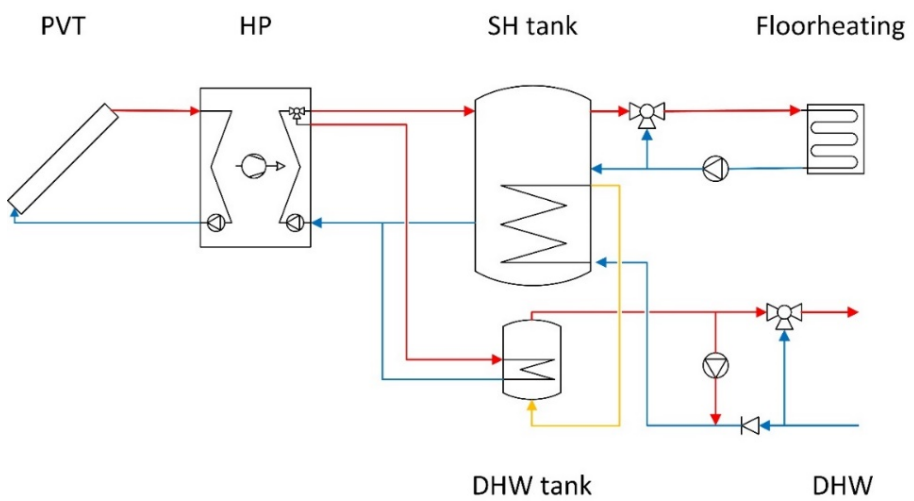

Figure 4.1. Process flow diagram of the building heating system.

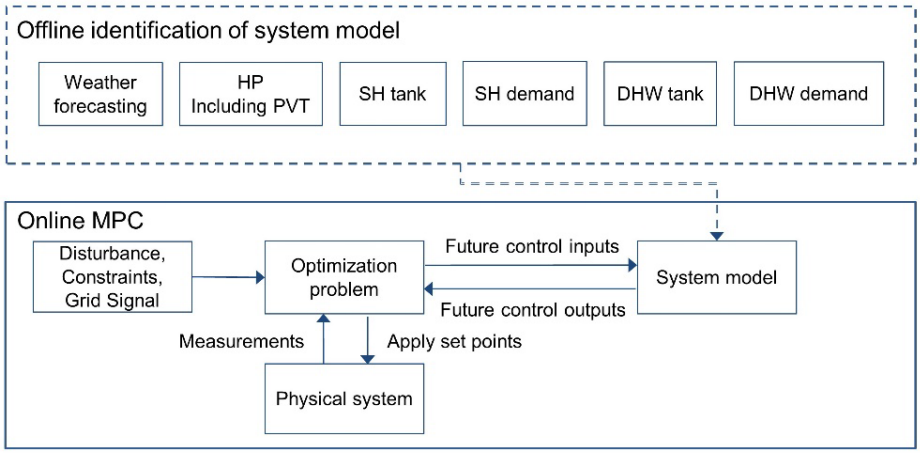

Figure 4.2. Methodological framework of the system model implemented in online MPC.

For acquisition of measurement data, the HP was equipped with sensors that measured temperatures in the upper third of each tank. The HP also had sensors for the ambient temperature and the supply and return temperatures of the evaporator and condenser circuits. A DT80-dataTaker data logger was installed for this project to capture all DHW and SH tank supply and return temperatures along with measurements at two heights in the DHW tank and three heights in the SH tank. Temperature sensors for the data logger and the heat pump were Negative-Temperature-Coefficient thermistors with a tolerance of 5% (accuracy of 0.1 °C at 20 °C). Flow meters were also installed to provide information on fluid flow rates in the HP evaporator and condenser circuits and the floor heating circuit and to measure tap water demand. The Huba-Control flow meters measured in a range between 0.5 and 150 L/min with +/- 2% accuracy. The experimental setup also included an electricity meter from Imbema-Controls to measure energy consumption by the HP. Electricity consumption values were issued via pulse outputs of 1000 imp/kWh to the data logger. The electricity that was generated by the PVT was not measured because the current systems directly fed electricity into the power grid.

Measurement data were recorded with a 1-min time step and submitted to a MATLAB controller (Figure 4.3). MATLAB 2017a was used for the processing of data. To exchange information with the heat pump, a Modbus Remote-Terminal-Unit was installed, which enabled the use of Modbus as a communication protocol. Modbus is widely used in building management systems because this message structure is reliable for bi-directional communication of data.

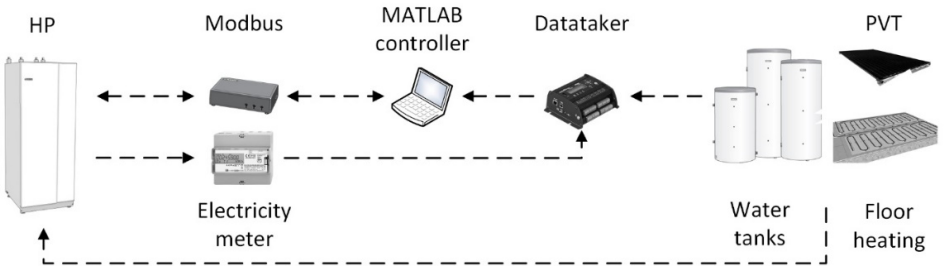

Figure 4.3. Communication infrastructure for the building heating system.

4.1.2 Weather forecasting model

Short-term weather forecasting included forecasting of global and horizontal solar radiation and ambient temperature. The local ambient temperature was obtained from professional online forecasting [14]. An application programming interface between the forecasting service and the MATLAB controller was created to retrieve real-time forecasting of the ambient temperature. Forecasting of the global and horizontal solar radiation was implemented by designing a feedforward artificial neural network (ANN) that had been successfully applied in a previous case study [2]. The ANN integrated the input signals including year, month, day, hour of day, sunshine hours, ambient temperature, dew point temperature, relative humidity, cloud cover factor, air pressure, precipitation, and direct and diffuse beam irradiance [2]. To obtain the direct and diffuse beam irradiance, a simplified clear sky model was used, which was developed by Bird et al. [15]. For weather forecasting, the ANN was trained, validated, and tested using a weather data set of 7 years (2011–2017) of hourly data [16]. For the hourly forecasting of solar radiation $I_{gsr-hsr}$ (W/m^2), the best configuration was found with 50 hidden layers, resulting in an RMSE of 22, MAE of 12, MAPE of 0.19, R^2 of 0.99, and G of 0.88, which were in good agreement with results from other studies [2,17–19].

4.1.3 SH tank model

For the SH tank, grey-box and black-box models are typically applied to online optimization. For optimal control, grey-box models are one-node capacity models [20–24] or one-dimensional multi-node models [20,25–27]. Black-box models include, for example, ANN [10,28], transfer function, state-space (SS) or autoregressive exogenous [8] models. However, because of the lack of experimental MPC implementations, none of the grey-box or black-box SH tank models have shown superior performance.

In the present study, four SH tank models were developed, then the prediction performance of these models using measurement data was tested, and finally the best performing model to be integrated into the system model for online MPC was chosen. The developed SH tank models were a one-node (capacity), a multi-node (multi-layer), a time-series ANN (recurrent dynamic network), and a discrete-time SS model. The SH tank models were designed to predict supply temperatures (SH demand, HP, and DHW tank) (Figure 4.1) and internal SH tank temperatures. The latter was used to calculate degree minutes ($°m$) (parameter to regulate SH tank charging). Table 4-2 shows the results of the prediction performance (supply temperatures in °C) of the different SH tank models.

Table 4-2. Prediction performance of SH tank models (supply temperatures in °C) during the identification procedure.

SH tank models		RMSE	MAE	MAPE	R^2	G
Grey-box	One-node	2.65	2.19	0.06	0.57	0.36
	Multi-node	1.24	0.88	0.02	0.91	0.70
Black-box	ANN	1.61	0.83	0.03	0.62	0.38
	SS	4.43	2.98	0.09	0.23	0.12

The best performing SH tank model was the multi-node model (Table 4-2), which was thus chosen to be integrated into the system model for online MPC. The reason for the variability in prediction performances may be the presence of three inlet and outlet ports, which leads to high model complexity. In the multi-node model, the complexity is represented by 30 layers, which is the best configuration that was found. This multi-layer configuration was based on the one-dimensional convection-diffusion-reaction equation [26,27,29,30] (Equation 4-1, 4-2, 4-3). Heat transfer through convection and conduction was simulated according to

$$\frac{\partial T_{SH}}{\partial t} = \alpha \frac{\partial^2 T_{SH}}{\partial z^2} - v_{SH} \frac{\partial T_{SH}}{\partial z} + \gamma (P_{HX\,SH} - P_{loss\,SH}), \quad 0 \le z \le z_{max}, \quad t \ge 0, \tag{4-1}$$

$$\alpha = \frac{\lambda}{\rho c_p}, \tag{4-2}$$

$$\gamma = \frac{1}{\rho c_p}, \tag{4-3}$$

where $\partial T_{SH}/\partial z$ is the vertical temperature distribution, z is the spatial vertical coordinate, and z_{max} is the height of the SH tank. The speed of water flow v_{SH} was calculated as flow rate divided by the cross-sectional area perpendicular to the water flow. The flow rate depended on the operating mode, which included charging and discharging. For Equation 4-1, inlet temperatures during charging (HP circuit) and discharging (floor heating circuit) were implemented as Dirichlet boundary conditions. According to inflow and outflow positions of the HP and floor heating circuits, the vertical temperature array z was divided into multiple sections. For each section of z, a virtual layer was added at both ends to represent inlet and outlet temperatures for charging and discharging the SH tank.
The SH tank was also used for preheating tap water through an immersed heat exchanger coil. The heat exchange $P_{HX\,SH}$ between the SH tank and tap water (to the DHW tank) was implemented as a source term in Equation 4-1 according to

$$\begin{aligned} P_{HX\,SH} &= \frac{c_p\,\rho\,A_{HX\,SH}\,v_{DHW}}{V_{SH}}\left(T_{HX\,SH\,out} - T_{HX\,SH\,in}\right) \\ &= \frac{c_p\,\rho\,A_{HX\,SH}\,v_{DHW}}{V_{SH}}\left(T_{SH} - T_{HX\,SH\,in}\right)\left[1 - e^{-\frac{h_{HX\,SH}\,S\,L}{c_p\,\rho\,A_{HX\,SH}\,v_{DHW}}}\right], \end{aligned} \tag{4-4}$$

where $A_{HX\,SH}, L,$ and S are the cross-sectional area, the length, and the circumference of the heat exchanger, respectively. $h_{HX\,SH}$ is the heat exchange coefficient, which depends on the speed of the heat exchanger fluid v_{DHW} [29,31]. Equation 4-1 also included the heat loss of the SH tank $P_{loss\,SH}$ to the ambient environment T_{amb} according to

$$P_{loss\,SH} = \frac{h_{amb\,SH} A_{amb\,SH}\,(T_{SH} - T_{amb})}{V_{SH}}, \tag{4-5}$$

where $A_{amb\,SH}$ is the surface area of the SH tank, and $h_{amb\,SH}$ is the heat exchange coefficient between SH tank and ambient environment. Equation 4-1 was solved numerically using the combination of a Crank–Nicolson scheme [26,29,30,32] for the diffusion problem and an upwind scheme [33] for the convection problem. Additionally, the upwind scheme was used to solve mixing effects that resulted from temperature inversion in the SH tank.

The combination of the Crank–Nicolson scheme and the upwind scheme successfully established the simulation of thermal stratification, charging, and discharging.

4.1.4 SH demand model

The space heating demand comes from the floor heating system that extracts heat from the SH tank. The SH demand model was a black-box model that was developed using the Neural Network Toolbox in MATLAB. Previous case studies successfully applied ANNs for prediction of space heating demand [34]. Amasyali et al. [34] provided a comprehensive review of ANNs to forecast the energy consumption of residential and non-residential buildings, concluding that there was a lack of studies of residential buildings that considered hourly prediction of energy demand. In one of the few studies, Chou et al. [35] reported that in addition to support vector regression, ANN can play a major role in predicting hourly heating and cooling loads.

In the present study, an ANN is created to solve a time-series problem which was a NARX problem. A NARX model is a recurrent dynamic network using feedback connections according to

$$i(t) = f(i(t-1), i(t-2), \dots, i(t-n_i), w(t-1), w(t-2), \dots, w(t-n_w)), \quad (4\text{-}6)$$

where $i(t)$ is the output signal, and $w(t)$ represents the exogenous input variables [36]. The ANN simulated the heating demand based on the input variables: ambient temperature, global and horizontal solar radiation, supply temperature to floor heating, and time of day. The room temperature set points were excluded as ANN input signals because set points were kept at a constant value of 21.5 °C. The best configuration for the heating demand (kWh) was found with three input delays, three feedback delays, and a hidden layer size of 20, resulting in an hourly performance with an RMSE of 2.2, MAE of 1.3, MAPE of 0.18, R2 of 0.94, and G of 0.77.

4.1.5 DHW tank model

The model of the DHW buffer tank was conceived as a grey-box capacity model which represented a fully-mixed one-node model [21,37–39]. The purpose of the DHW tank model was to predict future average temperatures. The evolution of the average temperature T_{DHW} (°C) was represented according to

$$\rho V_{DHW} \frac{dT_{DHW}}{dt} = P_{HP\ DHW} - P_{tapwater\ DHW} - P_{loss\ DHW}\ , \quad (4\text{-}7)$$

where $P_{HP\ DHW}$ is the heat delivered by the heat pump, $P_{tapwater\ DHW}$ is the heat extracted by tap water usage, and $P_{loss\ DHW}$ is the heat loss to the ambient environment. The DHW tank model was identified (T_{DHW} in °C) as showing a good prediction performance with an RMSE of 0.90, MAE of 0.74, MAPE of 0.01, R2 of 0.83, and G of 0.60, which were comparable to results of other studies [40,41].

4.1.6 DHW demand model

The DHW demand model was a discrete-time Markov chain model for tap water demand. Markov chains represent random processes and are used to predict stochastic behaviour, such as tap water demand [42,43], wind power generation [44], and occupancy presence [45,46]. In this study, the stochastic behaviour of tap water is represented by a time-homogeneous Markov chain $\{Y_t\}$ for $t > 0$ and the states $a_b \in S_{ab}$ with

$$X(Y_{t+1} = b \mid Y_t = a, Y_{t-1} = a_{t-1}, \dots, Y_0 = a_0) = X(Y_{t+1} = b \mid Y_t = a) = X_{ab}. \quad (4\text{-}8)$$

The Markov chain was associated with a probability transition matrix X in which X_{ab} denoted the probability of moving from state a to state b with $X_{ab} = X(y_t = b \mid y_{t-1} = a)$ [47]. The DHW demand model used a row vector of probabilities of tap water usage $x[t]$ with $x_b[t] = X(Y_t = b)$, which evolved according to

$$x[t] = x[t-1]X. \quad (4\text{-}9)$$

Real-time measurements were used to determine $x[0]$ at each control time step. Furthermore, continuous measurements of tap water usage served to create the transition probability X. Tap water flow measurement data were averaged over a time step of 15 min and implemented in the online optimization. A distinction was made between tap water demand on weekdays and weekends [43]. For example, during the week, at 8:30 the probability of changing from state a to b was

$$X = \begin{bmatrix} 0 & 0 & 0 & 0 & 1 & 0 & 0 & 0 \\ 0 & 0 & 1 & 0 & 0 & 0 & 0 & 0 \\ 0 & 0 & 0 & 0 & 0 & 0 & 0 & 1 \\ 0 & 0 & 1 & 0 & 0 & 0 & 0 & 0 \\ 0 & 0 & 0 & 0 & 0 & 0 & 0 & 1 \\ 0 & 0 & 0 & 0 & 0 & 0 & 0 & 1 \\ 0 & 0 & 0 & 0 & 0 & 0 & 0 & 1 \\ 0 & 0 & 0 & 0 & 0 & 0 & 0 & 1 \end{bmatrix},$$

where $a, b \in [0, 1, 2, \dots, 7]$ represents the minimum and maximum water flow in L/min. The identified tap water demand model (L/min) performed with an RMSE of 0.60, MAE of 0.25, MAPE of 0.03, R2 of 0.40, and G of 0.22. The DHW demand $P_{tapwater\ DHW}$ was calculated using the tap water demand, average DHW tank temperature, and inlet DHW tank temperature.

4.1.7 HP model

The water-to-water HP extracted heat from the PVT system and charged the SH tank and the DHW tank. Unsteady PVT operating conditions (HP source) and water thermal storage tank conditions (HP sink) required that the HP continuously adapt its electricity consumption. A summary of the measurements, including performance data such as coefficient of performance (COP), is given in Appendix II. The HP's energy efficiency varied during start-up and shut-down moments and during phases of partial load, especially at low compressor speeds [48]. To sufficiently capture the dynamic behaviour of the HP, Underwood et al. [48] suggested fully dynamic modelling, which likely requires artificial intelligence methods. Mathioulakis et al. [49] proposed the use of ANNs for HP performance prediction. In the present study, an ANN is developed (Figure 4.4) which was a NARX based on Equation 4-6. The ANN predicted the electricity consumption of the HP. Control of the HP β had three modes: charging DHW tank β_{DHW}, charging SH tank β_{SH}, and idle mode. The best configuration for electricity consumption P_{HP} was found with three input delays, three feedback delays, and a hidden layer size of 20, resulting in an hourly performance ($Q_{HP} = \int P_{HP}\, dt$) (kWh) with an RMSE of 0.15, MAE of 0.09, MAPE of 0.15, R2 of 0.92, and G of 0.72.

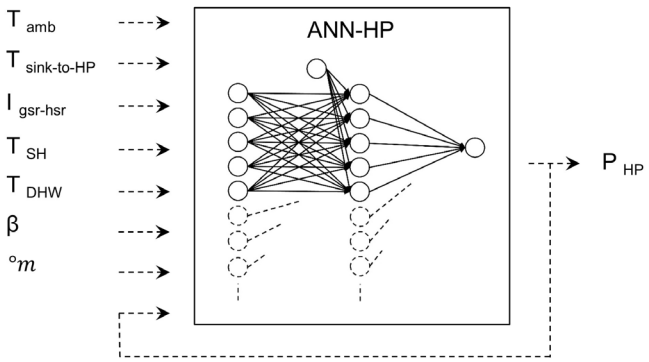

Figure 4.4. Artificial neural network (ANN) to obtain the electricity consumption of the HP (P_{HP}) based on the ambient temperature (T_{amb}), temperature of DHW and SH return to the HP ($T_{sink-to-HP}$), global and horizontal solar radiation ($I_{gsr-hsr}$), SH tank temperature for HP control (T_{SH}), DHW tank temperature for HP control (T_{DHW}), control output (β), and degree minutes ($°m$).

4.2 Method validation

The system model was integrated into an online MPC that used dynamic programming as optimization method. In the original research article [7] (Chapter 5), a prediction performance of HPs electricity consumption of RMSE between 0.17 kWh and 0.22 kWh was achieved, which is an improvement against prior studies [34].

The system model, furthermore, performed fast with low computational effort. For the computation of the system model, a computational time of less than 1s was achieved using MATLAB and an industrial box-PC with Intel core i7-6700TE processor and RAM8GB-DDR4. For the optimization method, assuming a state space of 1200 decisions, the current system model thus can be simulated within 20 min of computational time.

4.3 Conclusion

We developed a system model of a building and heating system, including models of the weather forecasting, the SH tank, the SH demand, the DHW tank, the DHW demand, and the HP. The models of the system components were validated offline using measurement data between November 2017 and April 2018.

The current system model implements various modelling techniques for the system components. The modelling techniques were chosen to accurately represent the dynamic behaviour of the system components. It is noted that the system model was configured to act as a plug-and-play solution, which means that the models of the components can be replaced in case that more accurate and faster performing models of the components are developed.

In the following Chapter 5, the system model is used in the framework of optimal control of demand flexibility under real-time pricing.

4.4 Appendix I – Performance metrics

i is the sample number, n is the total number of samples, e is the estimated data point, o is the output, and $\bar{o}$ is the mean output.

Root Mean Square Error

$$RMSE = \sqrt{\frac{1}{n}\sum_{i=1}^{n}(e_i - o_i)^2}$$

Mean Absolute Error

$$MAE = \frac{1}{n}\sum_{i=1}^{n}|e_i - o_i|$$

Mean Absolute Percentage Error

$$MAPE = \frac{1}{n}\sum_{i=1}^{n}\left|\frac{|e_i - o_i|}{o_i}\right|$$

Coefficient of Determination

$$R^2 = 1 - \frac{\sum_{i=1}^{n}(o_i - e_i)^2}{\sum_{i=1}^{n}(o_i - \bar{o})^2}$$

Goodness of Fit

$$G = 1 - \frac{\sqrt{\sum_{i=1}^{n}(e_i - o_i)^2}}{\sqrt{\sum_{i=1}^{n}\left(o_i - \frac{1}{n}\sum_{i=1}^{n}o_i\right)^2}}$$

4.5 Appendix II – Experimental data for heat pump

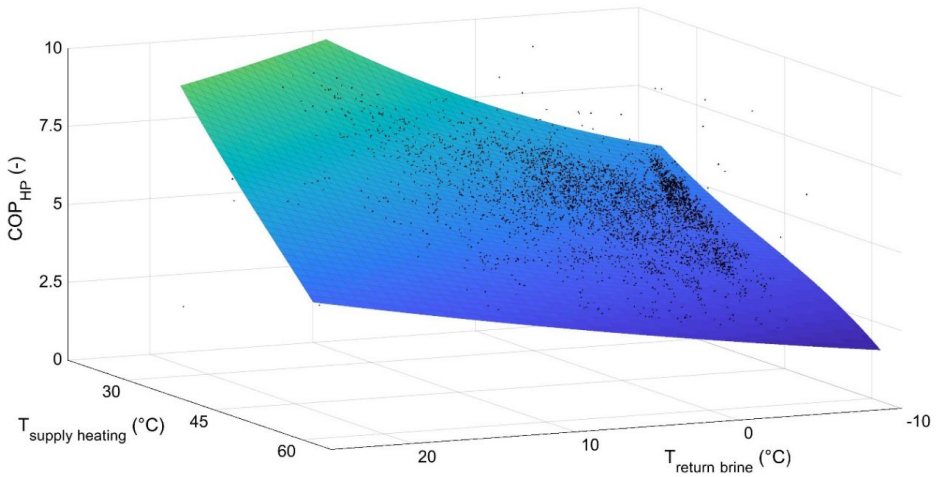

Experimental data for heat pump $COP_{HP} = f(T_{supply\ heating}, T_{return\ brine})$; curve fitting of experimental data using a polynomial fitting curve ($R^2 = 0.89$, RMSE = 0.36).

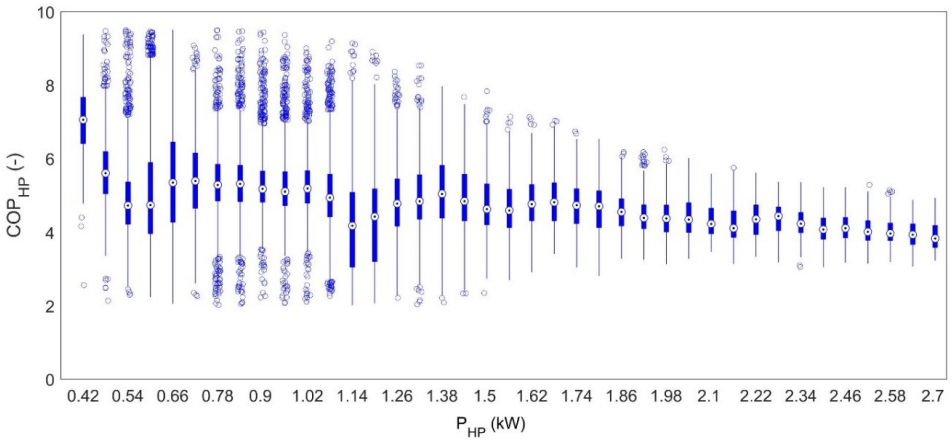

Experimental data for heat pump COP_{HP} vs. P_{HP}; the heat pump regulates the electricity consumption of the compressor according to $P_{HP\ min} = 0.42$ kW, $P_{HP\ max} = 2.7$ kW, and $\Delta P_{HP} = 0.06$ kW; box plots for $P_{HP\ min} \leq P_{HP} \leq P_{HP\ max}$.

4.6 References

[1] Jensen SØ, Marszal-Pomianowska A, Lollini R, Pasut W, Knotzer A, Engelmann P, et al. IEA EBC Annex 67 Energy Flexible Buildings. Energy Build 2017;155:25–34. doi:10.1016/j.enbuild.2017.08.044.

[2] Finck C, Li R, Zeiler W. Economic model predictive control for demand flexibility of a residential building. Energy 2019;176:365–79. doi:10.1016/j.energy.2019.03.171.

[3] Finck C, Clauß J, Vogler-Finck P, Beagon P, Zhan K, Kazmi H. Review of applied and tested control possibilities for energy flexibility in buildings. 2018. doi:10.13140/RG.2.2.28740.73609.

[4] Afram A, Janabi-Sharifi F. Theory and applications of HVAC control systems - A review of model predictive control (MPC). Build Environ 2014;72:343–55. doi:10.1016/j.buildenv.2013.11.016.

[5] Tang R, Wang S. Model predictive control for thermal energy storage and thermal comfort optimization of building demand response in smart grids. Appl Energy 2019. doi:10.1016/j.apenergy.2019.03.038.

[6] Verhelst C, Logist F, Van Impe J, Helsen L. Study of the optimal control problem formulation for modulating air-to-water heat pumps connected to a residential floor heating system. Energy Build 2012. doi:10.1016/j.enbuild.2011.10.015.

[7] Finck C, Li R, Zeiler W. Optimal control of demand flexibility under real-time pricing for heating systems in buildings: A real-life demonstration. Appl Energy 2020;263.

[8] Afram A, Janabi-Sharifi F. Black-box modeling of residential HVAC system and comparison of gray-box and black-box modeling methods. Energy Build 2015;94:121–49. doi:10.1016/j.enbuild.2015.02.045.

[9] Afroz Z, Urmee T, Shafiullah GM, Higgins G. Real-time prediction model for indoor temperature in a commercial building. Appl Energy 2018. doi:10.1016/j.apenergy.2018.09.052.

[10] Afram A, Janabi-Sharifi F, Fung AS, Raahemifar K. Artificial neural network (ANN) based model predictive control (MPC) and optimization of HVAC systems: A state of the art review and case study of a residential HVAC system. Energy Build 2017;141:96–113. doi:10.1016/j.enbuild.2017.02.012.

[11] Afram A, Fung AS, Janabi-Sharifi F, Raahemifar K. Development of an accurate gray-box model of ubiquitous residential HVAC system for precise performance prediction during summer and winter seasons. Energy Build 2018. doi:10.1016/j.enbuild.2018.04.038.

[12] Mustafaraj G, Chen J, Lowry G. Thermal behaviour prediction utilizing artificial neural networks for an open office. Appl Math Model 2010. doi:10.1016/j.apm.2010.02.014.

[13] Magalhães SMC, Leal VMS, Horta IM. Modelling the relationship between heating energy use and indoor temperatures in residential buildings through Artificial Neural Networks considering occupant behavior. Energy Build 2017;151:332–43. doi:10.1016/j.enbuild.2017.06.076.

[14] The Weather Company. Weather Forecast & Reports - Long Range & Local | Wunderground | Weather Underground. https://www.wunderground.com/ (accessed January 10, 2019).

[15] Bird RE, Hulstrom RL. Simplified clear sky model for direct and diffuse insolation on horizontal surfaces. 1981. doi:10.2172/6510849.

[16] KNMI climate data. KNMI - Koninklijk Nederlands Meteorologisch Instituut. http://www.knmi.nl (accessed January 10, 2019).

[17] Inman RH, Pedro HTC, Coimbra CFM. Solar forecasting methods for renewable energy integration. Prog Energy Combust Sci 2013;39:535–76. doi:10.1016/j.pecs.2013.06.002.

[18] Vaz AGR, Elsinga B, van Sark WGJHM, Brito MC. An artificial neural network to assess the impact of neighbouring photovoltaic systems in power forecasting in Utrecht, the Netherlands. Renew Energy 2016;85:631–41. doi:10.1016/j.renene.2015.06.061.

[19] Yadav AK, Chandel SS. Solar radiation prediction using Artificial Neural Network techniques: A review. Renew Sustain Energy Rev 2014;33:772–81. doi:10.1016/j.rser.2013.08.055.

[20] Schütz T, Streblow R, Müller D. A comparison of thermal energy storage models for building energy system optimization. Energy Build 2015. doi:10.1016/j.enbuild.2015.02.031.

[21] D'Ettorre F, Conti P, Schito E, Testi D. Model predictive control of a hybrid heat pump system and impact of the prediction horizon on cost-saving potential and optimal storage capacity. Appl Therm Eng 2019;148:524–35. doi:10.1016/j.applthermaleng.2018.11.063.

[22] Zhang Y, Zhang T, Wang R, Liu Y, Guo B. Optimal operation of a smart residential microgrid based on model predictive control by considering uncertainties and storage impacts. Sol Energy 2015;122:1052–65. doi:10.1016/j.solener.2015.10.027.

[23] Gambino G, Verrilli F, Canelli M, Russo A, Himanka M, Sasso M, et al. Optimal operation of a district heating power plant with thermal energy storage. Proc. Am. Control Conf., 2016. doi:10.1109/ACC.2016.7525266.

[24] Finck C, Li R, Zeiler W. An optimization strategy for scheduling various thermal energy storage technologies in office buildings connected to smart grid. Energy Procedia, 2015. doi:10.1016/j.egypro.2015.11.105.

[25] Berkenkamp F, Gwerder M. Hybrid model predictive control of stratified thermal storages in buildings. Energy Build 2014;84:233–40. doi:10.1016/j.enbuild.2014.07.052.

[26] Finck C, Li R, Kramer R, Zeiler W. Quantifying demand flexibility of power-to-heat and thermal energy storage in the control of building heating systems. Appl Energy 2018;209:409–25. doi:10.1016/j.apenergy.2017.11.036.

[27] Touretzky CR, Baldea M. Integrating scheduling and control for economic MPC of buildings with energy storage. J Process Control 2014;24:1292–300. doi:10.1016/j.jprocont.2014.04.015.

[28] Amarasinghe K, Wijayasekara D, Carey H, Manic M, He D, Chen WP. Artificial neural networks based thermal energy storage control for buildings. IECON 2015 - 41st Annu. Conf. IEEE Ind. Electron. Soc., 2015. doi:10.1109/IECON.2015.7392953.

[29] Logie WR, Frank E. A Transient Immersed Coil Heat Exchanger Model. J Sol Energy Eng 2013;135:041006. doi:10.1115/1.4023928.

[30] Finck C, Li R, Zeiler W. Performance maps for the control of thermal energy storage. 15th Int Conf Int Build Perform Simul Assoc 2017. doi:10.26868/25222708.2017.238.

[31] De Jong A-J, Trausel F, Finck C, Van Vliet L, Cuypers R. Thermochemical heat storage - System design issues. Energy Procedia, 2014. doi:10.1016/j.egypro.2014.02.036.

[32] Recktenwald GW. Finite-Difference Approximations to the Heat Equation. Cl Notes 2004. doi:10.1109/IJCNN.2011.6033441.

[33] Recktenwald G. One Dimensional Convection : Interpolation Models for CFD The Convection-Diffusion Equation. Mater Eng 2006.

[34] Amasyali K, El-Gohary NM. A review of data-driven building energy consumption prediction studies. Renew Sustain Energy Rev 2018;81:1192–205. doi:10.1016/j.rser.2017.04.095.

[35] Chou JS, Bui DK. Modeling heating and cooling loads by artificial intelligence for energy-efficient building design. Energy Build 2014. doi:10.1016/j.enbuild.2014.07.036.

[36] MathWorks - Deep Learning Toolbox - Modeling and Prediction with NARX and Time-Delay Networks. https://www.mathworks.com (accessed January 10, 2019).

[37] Ruusu R, Cao S, Manrique Delgado B, Hasan A. Direct quantification of multiple-source energy flexibility in a residential building using a new model predictive high-level controller. Energy Convers Manag 2019;180:1109–28. doi:10.1016/j.enconman.2018.11.026.

[38] Verrilli F, Srinivasan S, Gambino G, Canelli M, Himanka M, Del Vecchio C, et al. Model Predictive Control-Based Optimal Operations of District Heating System with Thermal Energy Storage and Flexible Loads. IEEE Trans Autom Sci Eng 2017;14:547–57. doi:10.1109/TASE.2016.2618948.

[39] Renaldi R, Kiprakis A, Friedrich D. An optimisation framework for thermal energy storage integration in a residential heat pump heating system. Appl Energy 2017. doi:10.1016/j.apenergy.2016.02.067.

[40] Mongibello L, Bianco N, Di Somma M, Graditi G. Experimental Validation of a Tool for the Numerical Simulation of a Commercial Hot Water Storage Tank. Energy Procedia, 2017. doi:10.1016/j.egypro.2017.03.917.

[41] Afram A, Janabi-Sharifi F. Gray-box modeling and validation of residential HVAC system for control system design. Appl Energy 2015. doi:10.1016/j.apenergy.2014.10.026.

[42] Gagliardi F, Alvisi S, Kapelan Z, Franchini M. A probabilistic short-termwater demand forecasting model based on the Markov chain. Water (Switzerland) 2017;9:7–14. doi:10.3390/w9070507.

[43] Fischer D, Wolf T, Scherer J, Wille-Haussmann B. A stochastic bottom-up model for space heating and domestic hot water load profiles for German households. Energy Build 2016. doi:10.1016/j.enbuild.2016.04.069.

[44] Arasteh F, Riahy GH. MPC-based approach for online demand side and storage system management in market based wind integrated power systems. Int J Electr Power Energy Syst 2019;106:124–37. doi:10.1016/j.ijepes.2018.09.041.

[45] Widén J, Nilsson AM, Wäckelgård E. A combined Markov-chain and bottom-up approach to modelling of domestic lighting demand. Energy Build 2009. doi:10.1016/j.enbuild.2009.05.002.

[46] Dobbs JR, Hencey BM. Predictive HVAC control using a Markov occupancy model. Proc Am Control Conf 2014:1057–62. doi:10.1109/ACC.2014.6859389.

[47] Yin GG, Zhang Q. Discrete-time markov chains: Two-time-scale methods and applications. 2009. doi:10.1007/b138226.

[48] Underwood CP. Heat pump modelling. Elsevier Ltd; 2016. doi:10.1016/B978-0-08-100311-4.00014-5.

[49] Mathioulakis E, Panaras G, Belessiotis V. Artificial neural networks for the performance prediction of heat pump hot water heaters. Int J Sustain Energy 2018;37:173–92. doi:10.1080/14786451.2016.1218495.

5

Optimal control of demand flexibility under real-time pricing for heating systems in buildings: A real-life demonstration

This chapter has been published as:

C. Finck, R. Li, and W. Zeiler, "Optimal control of demand flexibility under real-time pricing for heating systems in buildings: A real-life demonstration", Applied Energy 263 (2020): 114671.

Abstract

The identification, quantification, and control of demand flexibility is the major challenge for future grid operations and requires innovative methods and new control strategies. Optimal control strategies such as economic model predictive control have gained attention in building energy management systems. The present experimental case study demonstrates the application of an economic model predictive controller under real-time pricing, including day-ahead prices and imbalance prices. For real-time prices in balancing and spot markets, we introduce a method that presents a flexibility service to provide demand flexibility for a notification time of $1\ h < t < t_{day\ end}$ in advance. The flexibility service can be used as an ancillary service for innovative flexibility markets. The flexibility service includes a dynamic modification of the day-ahead prices to enable the adaption of energy consumption to errors in forecasting of renewable energy generation. The developed method was tested under real-life conditions, which also included the stochastic behaviour of occupants and the dynamic behaviour of the building and heating system. During the test periods, the controller managed the total operational costs of the heat pump's electricity consumption and achieved a prediction performance of Root Mean Square Error between 0.17 and 0.22 kWh. To show the provision of demand flexibility, key performance indicators were quantified according to the categories 1) energy and power, 2) energy efficiency, and 3) energy costs. We introduce this categorization to present the benefits of using flexibility indicators along with conventional performance indicators in real-life applications.

5.1 Introduction

The transformation of the world's energy systems is driven by the rapid growth of renewable energy sources such as wind and solar. In 2017, renewable sources increased to 14.3% of the primary energy supply among European regions, according to the Organisation for Economic Cooperation and Development [1]. However, the integration of renewable energy into power grids creates challenges in balancing fluctuations and ensuring reliable grid operations. A radical change of power systems towards flexible operations on both supply and demand sides can satisfy the needs for reliable and robust energy networks [2]. As buildings account for a large proportion of energy consumption, demand flexibility of buildings represents a major potential source of flexibility [3]. In 2015, Annex 67 was initiated under the International Energy Agency's Energy in Buildings and Communities program to characterize building flexibility and to identify potential flexibility of single buildings and building clusters. Annex 67 also aims to provide building flexibility metrics by defining performance indicators for use in comparing buildings, including various energy systems [3]. Annex 67 has investigated the flexibility of multiple applications – for example, residential and non-residential buildings with energy systems including heat pumps (HPs), electric heating, structural storage, and thermal energy storage (TES) tanks.

One of the earliest Annex 67 studies presented the potential flexibility of the structural thermal mass of residential building stock using rule-based control [4]. The authors showed that structural storage capacity contributes to heating flexibility. They also emphasized that larger power shifting can result in a decrease in storage efficiency. The performance indicators from [4] were adopted in a study using a residential building with an HP, electric heating, and TES [5]. The authors in [5] optimized the charging and discharging of TES tanks using model predictive control (MPC) and day-ahead electricity prices. The main conclusion of that study was that TES tanks with water, phase-change materials, or thermochemical materials can be designed to provide short-term flexibility (up to 24 h) in an MPC framework. In [6], an MPC framework was investigated for heating and cooling using an HP and the structural storage of a residential building. The authors concluded that MPC controllers have great potential to increase flexibility by using time-varying electricity prices and carbon intensity. In [7], economic MPC (EMPC) was successfully applied in a residential building with an HP and structural storage. The experimental case study showed that demand flexibility can be optimized by associating operational electricity costs with performance indicators for demand flexibility. These examples from Annex 67 demonstrate that MPC strategies can enable the full potential of demand flexibility. However, only one of these studies was an experimental investigation of optimal control for demand flexibility [7]. This may be because of the lack of common metrics for demand flexibility to track control performance indicators and control signals.

5.1.1 Literature review of flexibility indicators for control of energy systems in buildings

Clauβ et al. [8] classify performance indicators for the control of building energy systems into flexibility indicators and conventional indicators. The latter represent, for example, energy consumption, costs of energy consumption, and CO_2 emissions. In examining flexibility indicators, early studies quantified demand flexibility in the framework of rule-based control (RBC) (Table 5-1). Recently, flexibility indicators have gained more attention in optimal control (OC) of residential and office buildings that include energy systems with electrical batteries, electric heating, and TES tanks (Table 5-1).

Table 5-1. Overview of flexibility indicators applied in optimal control (OC) and rule-based control (RBC).

Categories	Flexibility indicators	OC	RBC
Energy and power	Available storage capacity	[5]	[4,9,10]
	Power-shifting capability	[5]	[4,9,11,12]
	Grid feed-in	[13]	
	Instantaneous power flexibility	[5]	
	Self-consumption/-generation	[7]	[13,14]
	Grid support coefficient		[15]
Energy efficiency	Storage/shifting efficiency	[5]	[4,9,16]
Energy costs	Flexibility factor	[5–7,17]	[11,16]
	Cost curves	[18]	
	Cost deviation	[19]	

Table 5-1 shows that flexibility indicators in OC and RBC can be classified in terms of size (energy) and time (power), energy efficiency, and energy costs. Likewise, conventional performance indicators can be allocated to their respective categories: for example, energy consumption (energy), coefficient of performance (energy efficiency), and costs of energy consumption (energy costs). The categorization can help in identifying adequate key performance indicators (KPIs) for control. However, a question from this brief review remains: How can real-life applications benefit from the quantification of flexibility indicators for control?

5.1.2 Literature review of control signals to enable demand flexibility in buildings

System operators and aggregators provide incentive-based and price-based control signals to enable flexible operations of building energy management systems [20,21]. Incentive-based signals support direct load management in which the central actor regulates the load. To ensure reliable grid management, direct load control for frequency and voltage control is likely to be required as a short-term flexibility service, which regulates the electricity system from seconds to several minutes in advance. For longer notification times, balancing markets (up to 1 h) and spot markets (up to 48 h) have been established, which can include both incentive-based and price-based signals. When electricity prices are used, the building energy management system receives time-varying price signals and adapts electricity consumption accordingly. One variable pricing scheme, for example, is real-time pricing (RTP), which typically consists of day-ahead prices and intra-day prices [21]. Day-ahead prices aim to schedule the energy consumption for the next day. To compensate for imbalances from the day-ahead market, intra-day prices are traded during the day of operation. In spot markets, electricity prices are being traded and disseminated up to 5 minutes in advance [22]. However, power imbalances are caused by differences between commercial trade schedules and measurements of electrical power injected into and taken from the electricity grid. In the Netherlands, therefore, the Transmission-System-Operator (TSO) provides imbalance prices, which act as a competitive product in the balancing market [23].

To date, only a few studies have used RTP signals to determine demand flexibility in building energy systems. Those studies mainly incorporate day-ahead electricity prices from power spot markets [5–7,13–17]. Based on these time-varying prices, the studies quantified flexibility indicators that represent demand flexibility as shown in Table 5-1.

Recent work on demand flexibility has considered alternative control signals such as the grid carbon intensity [6,24,25], which is defined as the proportion of CO_2 emitted per unit of energy consumption [25]. Carbon intensity as a control signal can serve to minimize CO_2 emissions of buildings. The authors in [25] argued that the usage of carbon-based signals and price-based signals can lead to conflicting control objectives; for example, cost-optimal control using price-based signals does not reduce the yearly CO_2 footprint of buildings compared with optimization of CO_2 emissions. We must emphasize that the authors in [25] focused on a yearly evaluation of buildings' flexibility rather than concentrating on short-term balancing and spot markets. As for these short-term markets for demand flexibility, a question remains: Can building energy systems provide short-term demand flexibility in balancing and spot markets?

5.1.3 Main contributions and outline

To increase integration of renewables into power systems, we need to create a common metric for demand flexibility. A review of relevant literature reveals that the determination of demand flexibility of buildings strongly depends on the chosen control strategy, control signals, and KPIs. Optimal control – or more precisely MPC and EMPC – were found to be the most advanced control strategies that can provide various control objectives and can include a multitude of control signals. However, only a few studies have implemented MPC and EMPC in buildings as part of experimental investigations.

This study demonstrates the use of EMPC in regulating demand flexibility of a building. We use the building heating system, including HP and TES, to provide demand flexibility in relation to the power grid. The contributions of this experimental case study are summarized as follows:

- An EMPC strategy is applied to a heating system of a residential building. A variety of techniques are used to model the components of the heating system. We introduce a method to determine the prediction performance of different models within an EMPC framework.
- Conventional KPIs and KPIs for demand flexibility are classified in terms of size (energy) and time (power), energy efficiency, and energy costs. For KPIs of energy efficiency, additionally, we introduced KPIs that refer to the effective utilization of available sources such as HP and TES. The KPIs are presented for use in EMPC validation.
- We introduce a method that enables the control of demand flexibility in balancing and spot markets using day-ahead prices and imbalance prices. Day-ahead prices are modified during the day of operation to provide a flexibility service. The flexibility service can be used as an ancillary service for flexibility markets (for example provided by EPEX SPOT) and enables dynamic optimization of demand flexibility.

The main advantage of this flexibility service is the implementation of a simple one-way trading mechanism, which enables the use of more detailed MPC approaches with moderate computational effort of solving the OCP. In this study, the EMPC optimization algorithm is solved once per hour of operation.

The outline of this paper is as follows. Section 5.2 presents the methodological framework of the experimental case study. In 5.2.1, the experimental set up in a detached house is described. In 5.2.2, a method is introduced to control demand flexibility using day-ahead and imbalance prices. The developed method requires an EMPC formulation (5.2.4), which is validated (5.2.5) and compared with conventional RBC (5.2.3).

The performance evaluations of RBC and EMPC are described in section 5.2.6, including determination of conventional KPIs and KPIs for demand flexibility. The results of the experimental case study, including performance evaluation of RBC and EMPC, are presented in section 5.3. Finally, section 5.4 discusses the main contributions of this case study, and section 5.5 provides concluding remarks and recommendations for future research.

5.2 Methodology

For the experimental case study of demand flexibility in real-time power markets, a detached house was used that was located in Amstelveen, the Netherlands. During the test period, a family of four lived in the house. Occupants' domestic hot water profile and the heating demand were measured between November 2017 and April 2018 under real-life conditions. Measurement data were also recorded for the building heating system, including the HP and TES tanks. During this period, three different controllers were analysed: one standard RBC and two EMPC strategies (EMPC1 and EMPC2). The RBC utilized constant temperature set points for the TES tanks. The EMPC strategies determined the optimal trajectory of temperature set points of TES tanks by scheduling the electricity consumption of the HP based on optimized operational electricity costs. Real-time electricity prices were included in the optimization. The OC was designed to meet occupant comfort requirements and to enable demand-oriented flexibility. The order of magnitude of demand flexibility was quantified by KPIs that contained information about energy and power, energy efficiency, and energy costs.

5.2.1 Experimental setup

Experiments were performed in a detached house that had been built in 2017 (Figure 5.1). The low-energy house had a total floor area of 345 m^2 on four levels and was designed to achieve an annual heating energy consumption of 55.6 kWh/m^2.

The heating system of the test building was equipped with a water-to-water HP that charged the TES tanks for domestic hot water (DHW) and space heating (SH) (Figure 5.2). Control of the HP β had three modes: charging DHW tank β_{DHW}, charging SH tank β_{SH}, and idle mode. The HP was of type F1155-16 from NIBE with an inverter-controlled compressor [26]. The HP had a nominal heating output of 16 kW (according to EN 14825) and a maximal supply temperature of 70 °C. Low-temperature heat on the evaporator side of the HP was generated by a highly efficient photovoltaic thermal solar collector (PVT) from TripleSolar [27]. A total 20 m^2 of PVT panels were installed on the roof facing south, and an additional 10 m^2 of PVT panels were placed on the property of the house. The 300-L DHW tank had insulation that was 0.05 m thick with a thermal conductivity of 0.07 W/(mK). A thermostatic three-way valve regulated the temperature of the tap water, with a maximum setting of 60 °C. Space heating was supplied by an integrated floor heating system throughout the entire building. Thermostats regulated the indoor temperature on each level. When space heating was demanded, the SH tank was discharged, and a thermostatic three-way valve regulated the temperature of floor heating to a maximum of 35 °C. The 1,000-L SH tank was insulated using a material 0.2 m thick with thermal conductivity of 0.07 W/(mK). This tank was designed to provide efficient charging and discharging by establishing thermal stratification

[28–30]. Thermal stratification could be disrupted, however, because during operation colder water entered the upper part of the tank, resulting in downward fluid motion with convective mixing [28,30]. To maintain a vertical temperature gradient, pipe connections were configured as can be seen in Figure 5.2. Cold tap water entered the bottom of the SH tank, passed through an immersed heat ex-changer coil, and left from the middle of the SH tank to the DHW tank. From the SH tank, low-temperature heat was provided to the floor heating loop.

Figure 5.1. Test building near Amstelveen, the Netherlands, during the construction phase in summer 2017 (top); photovoltaic thermal solar collector (PVT) from TripleSolar on the roof of the building (bottom).

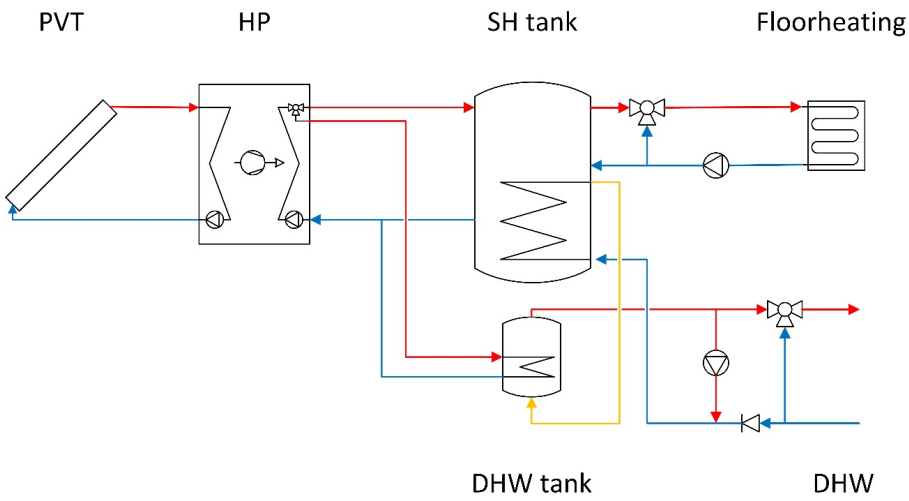

Figure 5.2. Process flow diagram of the building heating system.

We created a MATLAB controller (MATLAB 2017) that retrieved real-time measurement data from the heating system and regulated the energy consumption of the HP. A more detailed description of the MATLAB controller, including acquisition and processing of measurement data, can be found in Chapter 4.

5.2.2 Real-time pricing

To manage power supply and demand, system operators have established power spot markets in which suppliers and consumers trade electricity. Current power spot markets offer RTP, including day-ahead and intra-day prices. In the Netherlands, the TSO also provides imbalance prices, which act as a competitive product in the balancing market. We used a one-way pattern, including hourly day-ahead prices, to optimize the energy consumption for the next day and hourly imbalance prices to optimize the energy consumption for the next hour (one hour of notification time before real-time). The hourly day-ahead prices $c_{day-ahead}$ were retrieved from the Amsterdam-Power-eXchange spot market, and imbalance prices c_{imb} were used from Tennet, a Dutch electricity TSO.

To be able to participate in spot markets for a notification time of $1\ h < t < t_{day\ end}$, a flexibility service was developed that can be used as an ancillary service. The idea of the flexibility service was to compensate for variations in renewable energy generation for a notification time of $1\ h < t < t_{day\ end}$. The flexibility service makes it possible to adapt to errors in the forecasting of renewable energy generation.

For example, weather forecasting estimates peak solar power at a certain moment within the day of operation. For this moment, optimal planning of control actions is required to provide demand flexibility. A flexibility service, therefore, is offered towards this moment of peak solar power. In this study, hourly forecasting of global and horizontal solar radiation was used to estimate the peak hour during the day. For this peak hour, it was assumed that $c_{day-ahead} = 0$. Based on this assumption, $c_{day-ahead}$ was modified to create a dynamic pricing plan ($c_{mod\ day-ahead}$) and enable a dynamic optimization of demand flexibility. Figure 5.3 shows the results of an example test day, including standard day-ahead price ($c_{day-ahead}$) and the modification of the day-ahead price ($c_{mod\ day-ahead}$).

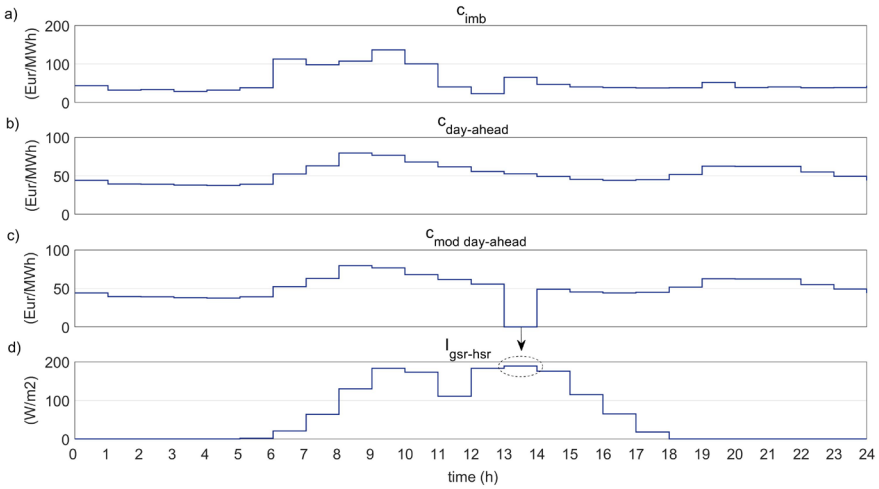

Figure 5.3. A real-time electricity pricing plan on 26.03.2018 including a) imbalance prices c_{imb}, b) day-ahead prices $c_{day-ahead}$, c) modified day-ahead prices $c_{mod\ day-ahead}$, and d) global and horizontal solar radiation $I_{gsr-hsr}$. During the peak of solar power supply, $c_{mod\ day-ahead} = 0$.

The different control strategies incorporated the following assumptions and steps:

- In RBC, day-ahead and imbalance prices were not used.
- EMPC1 included c_{imb} and $c_{day-ahead}$. *First*, EMPC1 determined a unique energy consumption profile (24-h plan) for the next day. *Second*, during the EMPC1 test day, hourly c_{imb} were implemented to optimize the energy consumption for the next hour.

- EMPC2 included c_{imb} and $c_{mod\ day-ahead}$. *First*, EMPC2 determined an energy consumption profile for the next day. *Second*, during the test day, hourly intra-day prices were used to optimize the energy consumption for the next hour. *Third*, day-ahead prices were modified to optimize the energy consumption profile and to enable dynamic optimization of demand flexibility for a notification time of $1\ h < t < t_{day\ end}$.

5.2.3 RBC

Rules-based control was used for the heat pump and regulated the temperature of the SH and DHW tanks using temperature set points. The RBC retrieved measurements from one sensor located in the upper third of each tank. Charging of the DHW tank took priority over charging of the SH tank. When the measured DHW tank temperature fell below the lower bound of 42 °C, charging was requested from the HP. The charging process was stopped at the upper bound temperature of 52 °C. Regulation of the SH tank charging was based on degree minutes ($°m$) using

$$°m = \int (T_{SH} - T_{SH\ set})\, dt, \tag{5-1}$$

with

$$°m \leq 100, \tag{5-2}$$

where T_{SH} is the measured SH tank temperature, and $T_{SH\ set}$ is the default temperature set point of 34 °C. The charging process of the SH tank started when $°m$ fell below a value of -60. The HP compressor stopped the charging process at $°m = 0$.

5.2.4 EMPC

The EMPC framework enabled optimal control of the building heating system with hourly optimization time steps [5,32,33]. During each control time step, real-time measurements served as the starting point for online optimization. The EMPC framework exploited a receding horizon of a full day (24-h period). In EMPC, optimal control decisions were implemented as diagrammed in Figure 5.4.

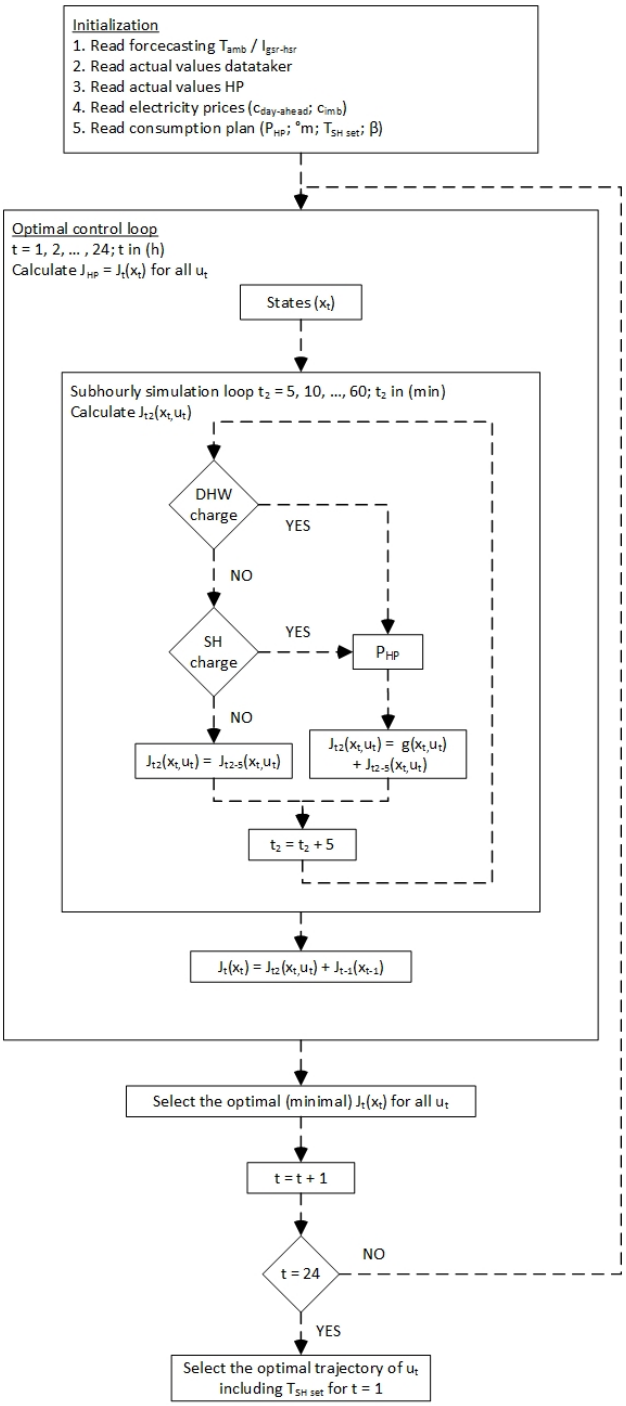

Figure 5.4. Simplified flowchart of optimal control decisions.

An optimal control problem (OCP) was formulated to minimize the total costs of electricity usage of the HP $J_{HP}(x)$. The state variables x integrated temperatures and fluid flow within the building heating system referring to the HP, DHW tank, DHW demand, SH tank, and SH demand. The control variables u included temperature set points of the DHW tank and SH tank. As with the RBC, charging of the DHW tank had priority over charging of the SH tank. The charging decision for the DHW tank was either ON or OFF. The OCP decision variable included the temperature set point $T_{SH\ set}$ of the SH tank. To reduce the computational effort of solving the OCP, a two-step approximation method was applied to the decision state of $T_{SH\ set}$. The optimal control trajectory of $T_{SH\ set}$ was generated in less than 20 min of computational time.

The first approximation step determined the state space with $T_{SH\ set}(t) \in [34, 36, 38, \dots, 50]$, which included a temperature step of 2 °C. This temperature step was chosen in accordance with early measurements where hourly temperature variations of the SH tank of ≥ 2 °C were observed. The minimum $T_{SH\ set}$ of 34 °C was identical to the reference control to meet occupant comfort requirements. Due to the safety requirements of the test set-up, a maximum $T_{SH\ set}$ of 50 °C was chosen. The second approximation step was the reduction of the number of possible decision states at each optimization time step as shown in Algorithm 1.

Algorithm 1. Procedure to perform the 2nd step of the approximation of control decision states.

---

for *each decision* $u(t)$ $\quad //T_{SH\ set}(t-1)\ to\ T_{SH\ set}(t)$

  if $t = \{1, 2\}$ $\quad //For\ EMPC1\ \&\ EMPC2$

    $T_{SH\ set\ min} \leq T_{SH\ set}(t) \leq T_{SH\ set\ max}$

  elseif $c_{day-ahead}(t) \neq c_{mod\ day-ahead}(t)$ ||

    $c_{mod\ day-ahead}(t-1) \neq c_{mod\ day-ahead}(t-1)$ $\quad //For\ \ EMPC2$

    $T_{SH\ set\ min} \leq T_{SH\ set}(t) \leq T_{SH\ set\ max}$

  else

    $\Delta T_{SH\ set} = T_{SH\ set}(t) - T_{SH\ set}(t-1)$

    $-4 \leq \Delta T_{SH\ set} \leq 4$ $\quad //For\ EMPC1\ \&\ EMPC2$

  end

end

During EMPC1 and EMPC2 optimization, when c_{imb} was used, the optimal set point $T_{SH\ set}(t)$ could change between 34 °C and 50 °C at $t = \{1,2\}$. For EMPC2, the optimal set point $T_{SH\ set}(t)$ could also change between $T_{SH\ set\ min}$ and $T_{SH\ set\ max}$ for modified day-ahead prices. To investigate the effect of day-ahead prices on the variations of the optimal temperature set point, we used the day-ahead prices between January and March 2018 to calculate the optimal temperature set points. It was observed that the set point varied by maximally +/- 4 °C. For EMPC1 and EMPC2, therefore, in decision states in which no modified day-ahead prices were assumed, hourly set point changes were limited to a maximum change of 4 °C.

It is important to note that, in contrast to RBC, EMPC implemented the possibility of stopping the charging of the SH tank when $T_{SH\ set}$ changed. In particular, if $T_{SH\ set}(t) \leq T_{SH\ set}(t-1)\ \&\&\ T_{SH\ set}(t) < T_{SH}(t-1)$, $^{\circ}m$ for the HP was set to zero. For example, when $T_{SH\ set}(t)$ changed from 50 °C to 34 °C, while $T_{SH\ set}(t) < T_{SH}(t-1)$, charging was disabled by setting $^{\circ}m = 0$. EMPC1 and EMPC2 applied the minimization of operational costs J_{HP} in a rolling horizon control framework with $t \in \{1, 2, \dots, N\}$ and $N = 24$. For each control time step, the cost function $J_{HP}(t)$ was calculated according to Algorithm 2.

Algorithm 2. Procedure to calculate the cost function $J_{HP}(t)$.

---

for *each decision* $u(t)$ $\qquad$ $//T_{SH\ set}(t-1)\ to\ T_{SH\ set}(t)$

$//For\ \ EMPC1$

if $t = 1$

$$J_{HP}(t) = \left(c_{day-ahead}(t)\ P_{HP}(t)\ \Delta t + \ c_{imb}\left(P_{HP}(t) - \ P_{HP\ 24h\ plan}(t)\right)\Delta t\right)$$

else

$$J_{HP}(t) = \ \left(c_{day-ahead}(t)\ P_{HP}(t)\ \Delta t\right)$$

end

$//For\ \ EMPC2$

if $t = 1$

$$J_{HP}(t) = \left(c_{mod\ day-ahead}(t)\ P_{HP}(t)\ \Delta t + \ c_{imb}\left(P_{HP}(t) - \ P_{HP\ mod\ 24h\ plan}(t)\right)\Delta t\right)$$

else

$$J_{HP}(t) = \ \left(c_{mod\ day-ahead}(t)\ P_{HP}(t)\ \Delta t\right)$$

end

end

In Algorithm 2, P_{HP} is the electricity consumption of the HP, and $P_{HP\ 24h\ plan}$ is the scheduled electricity consumption for the next day (24-h plan) based on day-ahead prices. For both forms of EMPC, during each control time step, c_{imb} was used to calculate a control decision, which could result in a deviation from the scheduled power plan $P_{HP\ 24h\ plan}$ at $t = 1$. For EMPC1, $P_{HP\ 24h\ plan}$ was determined on the day before using $c_{day-ahead}$. For EMPC2, $P_{HP\ 24h\ plan}$ was calculated a day ahead and could change at each control time step $P_{HP\ mod\ 24h\ plan}$ due to the consideration of flexibility assuming $c_{mod\ day-ahead}$.

The EMPC framework integrated a system model of the building and heating system, which consisted of the models of system components (weather forecasting, SH tank, SH demand, DHW tank, DHW demand, and HP) [31]. The PVT system as the heat source of the HP was considered in the HP model. Table 5-2 shows the models of the system components that were implemented as system model in the EMPC framework. All models of the system components were identified offline. A detailed description of the identification procedure can be found in Chapter 4.

Table 5-2. Modelling characteristics of the system components implemented in the EMPC framework [31].

System components	Modelling technique	Model characteristics	Model output
Weather forecasting	Black-box model	Feedforward artificial neural network (ANN)	Global and horizontal solar radiation
SH tank	Grey-box model	Multi-node model with 30 vertical layers including 3 inlet and 3 outlet ports	Supply temperatures (SH demand, HP, and DHW tank), internal SH tank temperatures
SH demand	Black-box model	Time-series ANN that is a nonlinear autoregressive with external (exogenous) input model	Heating demand
DHW tank	Grey-box model	Fully-mixed one-node (capacity) model	Average DHW tank temperature
DHW demand	Black-box model	Discrete-time Markov chain model	Tap water demand
HP including PVT	Black-box model	Time-series ANN that is a nonlinear autoregressive with external (exogenous) input model	Electricity consumption of the HP

5.2.5 EMPC validation

The EMPC performance was obtained in three validation steps: (1) RBC, (2) EMPC1, and (3) EMPC2. In (1), the standard RBC regulated the electricity consumption of the HP, while the EMPC predicted the dynamic behaviour of the controlled system without interaction between EMPC and HP. In (2) and (3), EMPC1 and EMPC2 solved the optimal control problem of $T_{SH\ set}$ and regulated on/off control of charging of the DHW tank. To determine the performance of the EMPC, the predictions of the electricity consumption of the HP ($Q_{HP} = \int P_{HP}\, dt$) were compared using the performance metrics root mean square error (RMSE), mean absolute error (MAE), mean absolute percentage error (MAPE), coefficient of determination (R^2), and goodness of fit (G) [7,34–39]. The mathematical descriptions of the performance metrics can be found in Appendix I.

The EMPC performance and the overall EMPC prediction error were the result of the prediction performance of the models of the system components (weather forecasting, SH tank, SH demand, DHW tank, DHW demand, and HP). To identify EMPC's modelling performance, the EMPC was recalculated using the experimental results from (1) RBC, (2) EMPC1, and (3) EMPC2. For example, to retrieve the performance of the HP model, the EMPC was simulated using experimental results of the HP's input parameters, which are SH tank output, DHW tank output, and weather forecasting. In a second example, to determine the prediction performance of the SH tank model, experimental results of SH tank input parameters and experimental results of HPs input parameters from the DHW tank and weather forecasting were used. In this second example, an overall prediction error was first calculated, which included the SH tank model and the HP model. Then, to determine the individual prediction error of the SH tank model, the fractional error Δs_n was calculated according to [40]

$$\Delta e = \sqrt{\left(\frac{\partial e}{\partial s_1}\Delta s_1\right)^2 + \cdots + \left(\frac{\partial e}{\partial s_n}\Delta s_n\right)^2}, \tag{5-3}$$

where Δe is the absolute error, and $\Delta s_1, \ldots, \Delta s_n$ are the fractional errors that result from the different models of the system components $s_1, \ldots, s_n$. In the present study, the fractional errors of the models for weather forecasting, SH tank, SH demand, DHW tank, DHW demand, and HP were taken from the RMSE.

5.2.6 Evaluation of control strategies

The three different control strategies, RBC, EMPC1, and EMPC2, were tested on a daily basis, and the results were analysed. To correctly assess the test results of these control strategies, environmental conditions such as ambient temperature T_{amb} and global and horizontal solar radiation $I_{gsr-hsr}$ were summarized on a daily basis. Furthermore, for the test days, the running mean ambient temperature $T_{rm\ amb}$ was calculated according to

$$T_{rm\ amb} = (1 - \alpha_{rm})\{T_{d-1\ amb} + \alpha_{rm}\ T_{d-2\ amb} + \alpha_{rm}{}^{2}\ T_{d-3\ amb} \dots\}, \tag{5-4}$$

which is a weighted running mean of the series of previous days that is simplified according to

$$T_{rm\ amb} = (1 - \alpha_{rm})\ T_{d-1\ amb} + \ \alpha_{rm}\ T_{rm-1\ amb}, \tag{5-5}$$

where $T_{d-m\ amb}$ is the daily running mean ambient temperature of the previous days with $m = 1$ for the day before and so on, and α_{rm} is a constant between 0 and 1, recommended to be 0.8 [41]. $T_{rm\ amb}$ was used to identify the normalized daily electricity consumption of the HP $Q_{HP\ norm}$ according to

$$Q_{HP\ norm} = f(T_{rm\ amb}, I_{gsr-hsr}). \tag{5-6}$$

Identification of $Q_{HP\ norm}$, was retrieved in MATLAB from a regression function, which was obtained from RBC test days. Likewise, the normalized daily operational electricity costs $J_{HP\ norm}$ was identified with a regression function according to

$$J_{HP\ norm} = f(Q_{HP\ norm}, T_{rm\ amb}, Q_{gsr-hsr}). \tag{5-7}$$

To compare the performance of the three control strategies (RBC, EMPC1, and EMPC2), conventional KPIs and KPIs for demand flexibility were defined. The KPIs were categorized into three domains – energy and power, energy efficiency, and energy costs – and are shown in Table 5-3.

Table 5-3. Key performance indicators (KPIs) for RBC, EMPC1, and EMPC2.

KPIs	Energy and Power	Energy efficiency	Energy costs
Conventional	$Q_{HP\ SH}$	$COP_{HP\ SH}$	J_{HP}
	$Q_{HP\ DHW}$	$COP_{HP\ DHW}$	$J_{HP}/J_{HP\ norm}$
	$Q_{HP}/Q_{HP\ norm}$		
Demand flexibility	$P_{inst\ HP\ SH}$	$\varepsilon_{cap\ HP}$	FF
	$P_{inst\ SH}$	$\varepsilon_{cap\ SH}$	

KPIs – energy and power

The electricity consumption of the HP ($Q_{HP} = \int P_{HP}\, dt$) is a classical KPI. For the current experimental setup, the HP's electricity consumption was measured for charging the SH tank ($Q_{HP\ SH}$) and charging the DHW tank ($Q_{HP\ DHW}$). The calculation of the ratio ($Q_{HP}/Q_{HP\ norm}$) compared the HP's electricity consumption under EMPC and RBC. The instantaneous power flexibility was simulated to identify the demand flexibility of the HP ($P_{inst\ HP\ SH}$) and the SH tank ($P_{inst\ SH}$). When using the instantaneous power flexibility as a KPI, it is possible to completely identify the demand flexibility. The instantaneous power flexibility is defined as the evolution of electrical power and heating power during a flexibility event [5]. For example, during low price periods of $c_{day-ahead}$, an increase of demand flexibility is requested. In the present study, for EMPC2, which included $c_{mod\ day-ahead}$, the evolution of electrical power of the HP with the SH tank ($P_{inst\ HP\ SH}$) and the evolution of the charging power of the SH tank ($Q_{inst\ SH}$) were simulated. In the results, we illustrated the instantaneous power flexibility $P_{inst\ HP\ SH}$ and $Q_{inst\ SH}$ to show the major importance of this flexibility indicator.

KPIs – energy efficiency

Conventional KPIs are primarily used to identify energy efficiency issues such as the coefficient of performance (COP) of the HP, which was determined for the charging of the SH tank ($COP_{HP\ SH}$) and the DHW tank ($COP_{HP\ DHW}$). Additionally, we developed efficiency indicators for demand flexibility, which refer to the effective utilization of available sources such as the HP and the SH tank. We introduce the effective utilization of the capacity of the SH tank ($\varepsilon_{cap\ SH\ tank}$) according to

$$\varepsilon_{cap\ SH\ tank} = \frac{\max_{t \epsilon N} Q_{SH}(t)}{Q_{SH\ max}}, \tag{5-8}$$

where $Q_{SH\ max}$ is the maximum storage capacity, which refers to the amount of heat stored in the SH tank at $T_{SH\ max}$ of 50 °C. The effective utilization of the capacity of the HP ($\varepsilon_{cap\ HP}$) is introduced according to

$$\varepsilon_{cap\ HP} = \frac{\max_{t \epsilon N} P_{HP}(t)}{P_{HP\ max}}, \tag{5-9}$$

where $P_{HP\ max}$ is the maximum nominal power of the HP, which is retrieved from experimental data as shown in Appendix II.

KPIs – energy costs

Conventional KPIs and KPIs for demand flexibility integrate operational costs of electricity consumption of the HP. The total operational cost of the HP's electricity consumption (J_{HP}) is a classical KPI. The calculation of the ratio ($J_{HP}/J_{HP\ norm}$) gave a comparison of the HP's operational costs under EMPC and RBC. It should be emphasized that $J_{HP\ norm}$ was calculated based on $c_{day-ahead}$.

The flexibility factor (FF) was calculated to identify demand flexibility. The flexibility factor presented the potential shift in energy consumption for heating from high-price to low-price periods [5,7,16]. In the present study, the flexibility factor was simulated for the energy consumption of the HP to compensate for the heating demand of the SH tank according to

$$FF = \left(\frac{\int_{t_{c_{day-ahead}^{start}_{low}}}^{t_{c_{day-ahead}^{end}_{low}}} P_{HP\ SH}\ dt - \int_{t_{c_{day-ahead}^{start}_{high}}}^{t_{c_{day-ahead}^{end}_{high}}} P_{HP\ SH}\ dt}{\int_{t_{c_{day-ahead}^{start}_{low}}}^{t_{c_{day-ahead}^{end}_{low}}} P_{HP\ SH}\ dt + \int_{t_{c_{day-ahead}^{start}_{high}}}^{t_{c_{day-ahead}^{end}_{high}}} P_{HP\ SH}\ dt} + \frac{\int_{t_{c_{imb}^{start}_{low}}}^{t_{c_{imb}^{end}_{low}}} P_{HP\ SH}\ dt - \int_{t_{c_{imb}^{start}_{high}}}^{t_{c_{imb}^{end}_{high}}} P_{HP\ SH}\ dt}{\int_{t_{c_{imb}^{start}_{low}}}^{t_{c_{imb}^{end}_{low}}} P_{HP\ SH}\ dt + \int_{t_{c_{imb}^{start}_{high}}}^{t_{c_{imb}^{end}_{high}}} P_{HP\ SH}\ dt} \right) / 2, \tag{5-10}$$

with

$$-1 \leq FF \leq 1\,, \tag{5-11}$$

where FF of -1 represents an inflexible and FF of 1 a highly flexible system. Similar to previous studies [5,7], the standard deviation served to determine low- and high-price periods of $c_{day-ahead}$ and c_{imb}. A standard deviation above 1σ defined high-price periods, whereas a standard deviation below -1σ was used to indicate low-price periods.

5.3 Results

During the measurement period between November 2017 and April 2018, experiments were carried out to test the performance of the applied EMPC framework. The EMPC performance was obtained from three validation steps, (1) RBC, (2) EMPC1, and (3) EMPC2, which are shown in section 5.3.1. Performance data of EMPC validation were broken down by different models of the EMPC framework, as illustrated in section 5.3.1 (EMPC's modelling performance). In section 5.3.2, the three control strategies are compared according to the performance indicators of energy and power, energy efficiency, and energy costs. For all test cases, identical imbalance prices (c_{imb}) and day-ahead prices ($c_{day-ahead}$) were assumed (Figure 5.5). For EMPC2, $c_{day-ahead}$ was modified to create a dynamic pricing plan including $c_{mod\ day-ahead}$.

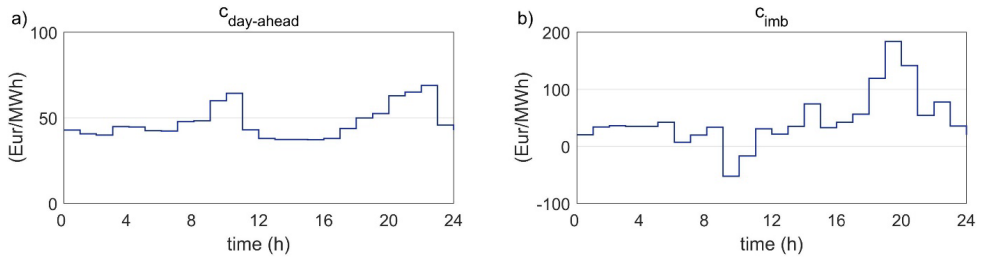

Figure 5.5. Real-time pricing including a) day-ahead prices ($c_{day-ahead}$) and b) imbalance prices (c_{imb}) used for validation steps (1) RBC, (2) EMPC1, and (3) EMPC2.

5.3.1 EMPC validation

RBC

The first step in validating the EMPC was performed on 26 March 2018. The conventional RBC was applied to regulate the heating system with a constant SH tank temperature set point ($T_{SH\ set}$) of 34 °C (Figure 5.6a), which resulted in a low number of on/off cycles of the HP: three cycles for charging the SH tank (β_{SH}) (Figure 5.6b) and two cycles for charging the DHW tank (β_{DHW}) (Figure 5.6c). Figure 5.6 also shows the results of the predicted and the measured electricity consumption of the HP (P_{HP}). The prediction performance was calculated for ($Q_{HP} = \int P_{HP}\, dt$) (kWh) with RMSE = 0.17, MAE = 0.13, MAPE = 0.28, R^2 = 0.91, and G = 0.71.

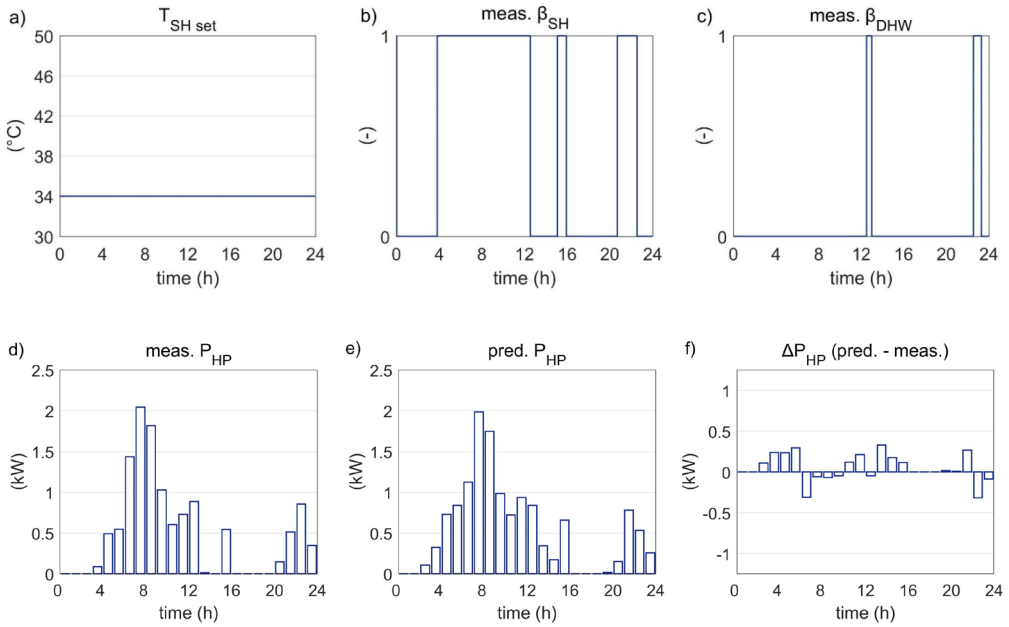

Figure 5.6. RBC experimental results for 26.03.2018: a) temperature set point for the SH tank $T_{SH\ set}$, b) control output charging the SH tank (β_{SH}), and c) control output charging the DHW tank (β_{DHW}). Electricity consumption of the HP (P_{HP}) d) measured and e) predicted and f) the difference between predicted and measured.

EMPC1

The EMPC1 strategy was applied on 05 April 2018 and incorporated real-time pricing ($c_{day-ahead}$ and c_{imb}) as illustrated in Figure 5.5. For EMPC1, we assumed static day-ahead prices $c_{day-ahead}$. The results of the control decisions of EMPC1 are shown in Figure 5.7a. Between 9:00 and 10:00, when c_{imb} reached negative values, $T_{SH\ set}$ was changed to the maximum setting of 50 °C to enable high power to the HP, which charged the SH tank. As can be seen in Figure 5.7b, applying EMPC1 resulted in an increase in the number of on/off cycles for charging the SH tank, which are almost twice the number of cycles with RBC. This was because °m were set to zero at $T_{SH\ set}(t) \leq T_{SH\ set}(t-1)$ && $T_{SH\ set}(t) < T_{SH}(t-1)$. The results of the predicted and measured P_{HP} are shown in Figure 5.7d-f. The prediction performance was calculated for ($Q_{HP} = \int P_{HP}\, dt$) (kWh) with RMSE = 0.22, MAE = 0.13, MAPE = 0.27, R^2 = 0.85, and G = 0.62.

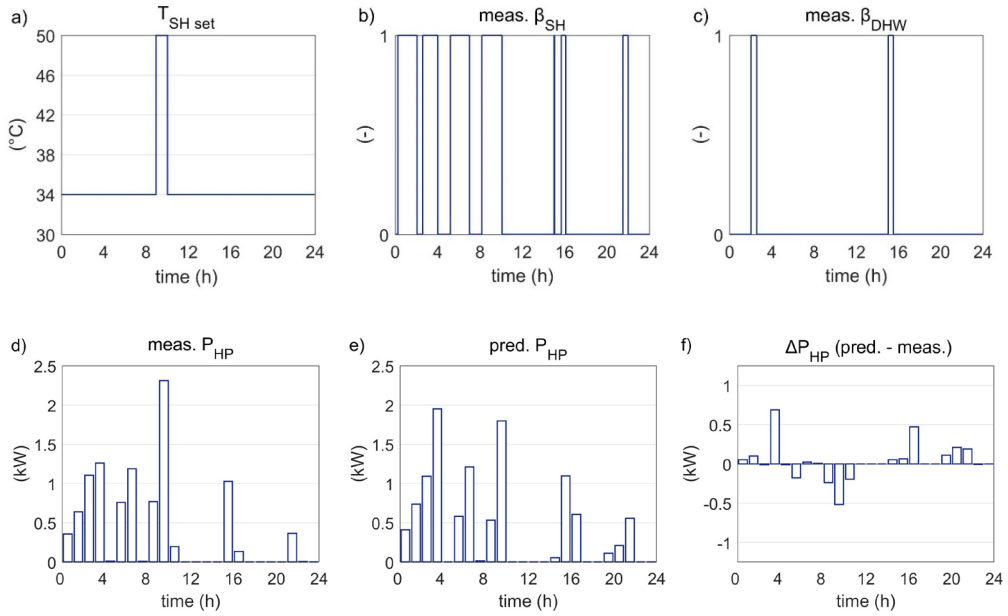

Figure 5.7. EMPC1 experimental results for 05.04.2018: a) temperature set point for the SH tank $T_{SH\,set}$, b) control output charging the SH tank (β_{SH}), and c) control output charging the DHW tank (β_{DHW}). Electricity consumption of the HP (P_{HP}) d) measured and e) predicted and f) the difference between predicted and measured.

EMPC2

Real-time pricing, including $c_{day-ahead}$ and c_{imb}, was implemented in EMPC2 and tested on 01 April 2018. A modified day-ahead price $c_{mod\,day-ahead}$ was used, which related to the forecasting of one daily peak of global and horizontal solar radiation (Figure 5.8). As shown in Figure 5.8, between 14:00 and 15:00, the daily hourly peak of solar radiation was observed, and $c_{mod\,day-ahead}$ was set to zero. The results of the control decisions of EMPC2 are shown in Figure 5.9a. Between 9:00 and 10:00, when c_{imb} reached a daily minimum, the HP provided maximum power for charging the SH tank with $T_{SH\,set} = 50$ °C. It was also observed that during the daily peak of solar radiation with $c_{mod\,day-ahead} = 0$, the HP charged the SH tank with $T_{SH\,set} = 46$ °C. It can be noticed that 2 hours before the peak of solar radiation, $T_{SH\,set}$ was changed to 38 °C. EMPC2 changed this set point to provide the best charging conditions for the peak hour (2 hours later), during which maximum charging was requested. The results of the predicted and measured P_{HP} are shown in Figure 5.9d-f. The prediction performance was calculated for ($Q_{HP} = \int P_{HP}\,dt$) (kWh) with RMSE = 0.22, MAE = 0.16, MAPE = 0.31, R^2 = 0.87, and G = 0.64.

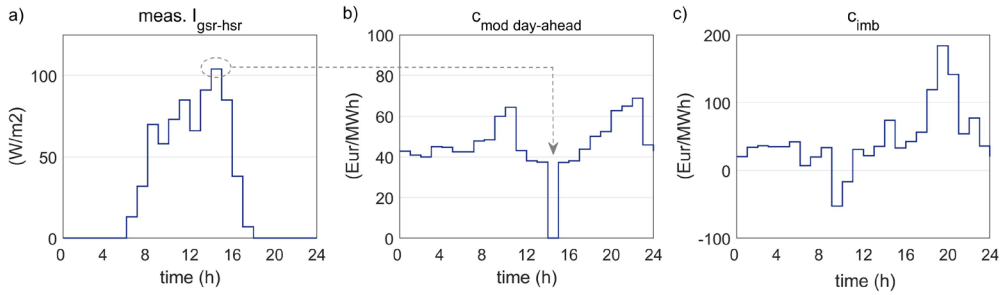

Figure 5.8. EMPC2 experimental results for 01.04.2018: a) measured $I_{gsr-hsr}$, b) $c_{mod\ day-ahead}$, c) c_{imb}. $c_{mod\ day-ahead}$ was set to zero during predicted and measured peak of $I_{gsr-hsr}$.

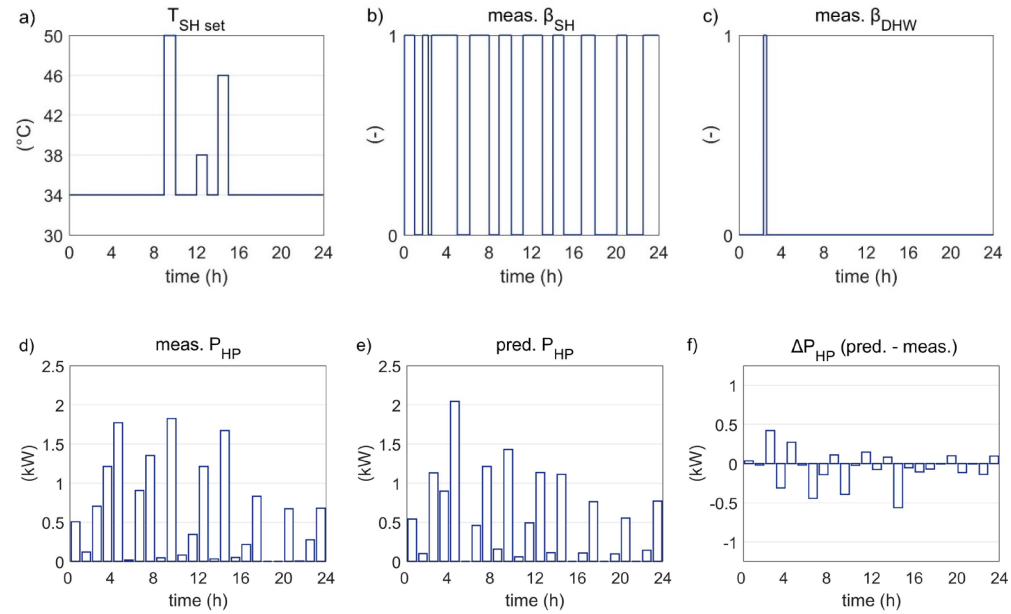

Figure 5.9. EMPC2 experimental results for 01.04.2018: a) temperature set point for the SH tank $T_{SH\ set}$, b) control output charging the SH tank (β_{SH}), and c) control output charging the DHW tank (β_{DHW}). Electricity consumption of the HP (P_{HP}) d) measured and e) predicted and f) the difference between predicted and measured.

EMPC's modelling performance

Previous sections showed the results of the prediction performance of P_{HP} during test days for RBC, EMPC1, and EMPC2. The overall prediction performance of Q_{HP} was a result of the performance of the different models implemented in the EMPC framework. The fractional prediction error for each of these models was calculated according to Equation 5-3 and is shown in Figure 5.10 as the percentage of the absolute error (RMSE) of the testing days for RBC, EMPC1, and EMPC2.

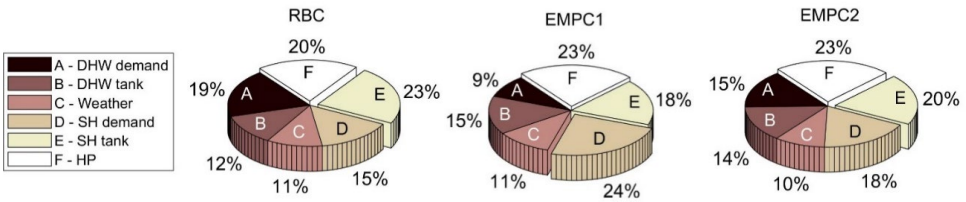

Figure 5.10. EMPC's modelling performance under RBC, EMPC1, and EMPC2. The fractional prediction error of each model (weather forecasting, SH tank, SH demand, DHW tank, DHW demand, and HP) is shown as the percentage of the absolute error (RMSE) for RBC, EMPC1, and EMPC2.

In Figure 5.10, the two models responsible for the largest fraction of the prediction error for each test day are highlighted (exploded view). During RBC and EMPC2 testing days, the largest fractional errors were calculated for the HP model and the SH tank model, whereas during the EMPC1 test day, the largest fractional prediction errors were obtained for the HP model and the SH demand model.

5.3.2 Evaluation of control strategies

From the test results of the different control strategies (RBC, EMPC1, and EMPC2), KPIs were calculated for energy and power, energy efficiency, and energy costs. The environmental conditions for the three testing days are summarized in Table 5-4.

Table 5-4. Experimental results – environmental conditions.

Control strategy	T_{amb} (°C)	$T_{rm\ amb}$ (°C)	$I_{gsr-hsr}$ (kWh/m^2)
RBC	4.8	4.9	1.4
EMPC1	6.5	6.5	1.2
EMPC2	5.1	5.3	0.6

Experimental results of environmental conditions and KPIs of control established a benchmark for comparing performances of the different control strategies, as detailed in the following sections.

KPIs – energy and power

The HP charged the SH and DHW tanks. The HP's electricity consumption (Q_{HP}) for charging the SH ($Q_{HP\ SH}$) and DHW tanks ($Q_{HP\ DHW}$) for the three testing days was measured, and the ratio of $Q_{HP}/Q_{HP\ norm}$ was calculated (Table 5-5). For EMPC1, Q_{HP} increased by 4%. We could not conclude, however, that EMPC1 resulted in greater energy consumption than RBC, because the 4% Q_{HP} increase was within the regression error of 5%. In contrast, the HP's electricity consumption under EMPC2 increased by 9%.

Table 5-5. KPIs for control strategies - energy and power.

Control strategy	$Q_{HP\ SH}$ (kWh)	$Q_{HP\ DHW}$ (kWh)	Q_{HP} (kWh)	$Q_{HP\ norm}$ (kWh)	$\left(\frac{Q_{HP}}{Q_{HP\ norm}} - 1\right)$
RBC	10.6	1.4	12.0	12.0	-
EMPC1	8.9	1.2	10.1	9.7	+ 4%
EMPC2	13.9	0.4	14.3	13.1	+ 9%

In EMPC2, real-time pricing, including $c_{mod\ day-ahead}$, was introduced to offer a dynamic pricing plan for the next 24 hours so as to be able to continuously adapt the energy consumption profile. Additionally, the $c_{mod\ day-ahead}$ was set to zero according to the daily peak of solar radiation, which occurred between 14:00 and 15:00 (Figure 5.8).

During this period, EMPC2 forced the HP to provide maximum charging power to the SH tank. The instantaneous power flexibility was calculated to illustrate the provision of maximum charging power during a flexibility time step Δt_{flex} of 60 min (Figure 5.11). It can be seen in Figure 5.11 that during the flexibility event ($c_{mod\ day-ahead} = 0$), between 14:00 and 15:00, the HP provided high charging power to the SH tank ($P_{inst\ SH}$) of up to 13.8 kW (Figure 5.11a) driven by great electricity consumption by the HP ($P_{inst\ HP\ SH}$) of up to 2.5 kW (Figure 5.11b). It was observed that between 14:00 and 15:00 it took about 50 minutes of Δt_{flex} to increase $P_{inst\ HP\ SH}$ to above 2 kW. This was due to the primary control of the HP's compressor, which was regulated based on °m, as the °m value decreased, the $P_{inst\ HP\ SH}$ value increased.

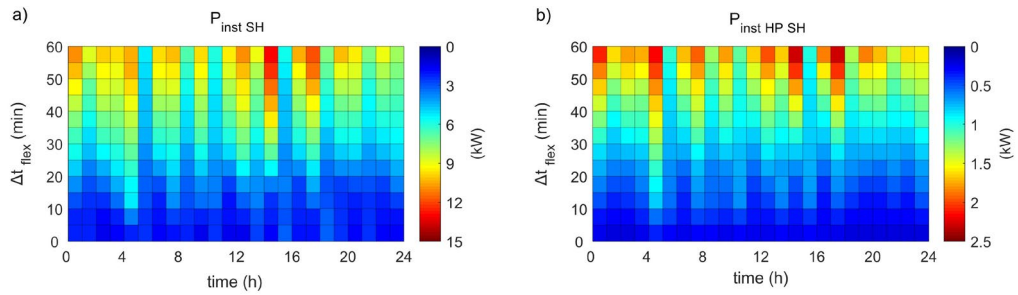

Figure 5.11. Instantaneous power flexibility for charging the SH tank using the HP under EMPC2: a) thermal instantaneous power flexibility of the SH tank ($P_{inst\ SH}$) and b) electrical instantaneous power flexibility of the HP with the SH tank ($P_{inst\ HP\ SH}$). The x-axis shows the control horizon of EMPC2. The y-axis represents the flexibility time step (Δt_{flex}) of 60 min in which the HP can charge the SH tank, assuming a maximum set point of $T_{SH\ set} = 50$ °C.

KPIs – energy efficiency

The HP electricity consumption and the heating power provided to the SH and DHW tanks were measured. Accordingly, the HP's efficiency was calculated for charging the SH tank ($COP_{HP\ SH}$) and the DHW tank ($COP_{HP\ DHW}$) (Table 5-6). Experimental results showed that this heating system worked efficiently, with a $COP_{HP\ SH}$ between 5.9 and 6.4 and a $COP_{HP\ DHW}$ between 3.3 and 4.0, which were in accordance with theoretical assumptions from manufacturer's data. An overview of experimental data on the HP's efficiency is shown in Appendix II. For all control strategies, $COP_{HP\ SH}$ was higher than $COP_{HP\ DHW}$, which was due to higher charging temperatures for the DHW tank than for the SH tank. Table 5-6 also lists effective utilization of capacity of the SH tank ($\varepsilon_{cap\ SH\ tank}$) and effective utilization of capacity of the HP ($\varepsilon_{cap\ HP}$). It can be seen from Table 5-6 that EMPC increases effective utilization of the capacity of both the HP and the SH tank.

Table 5-6. KPIs for control strategies – energy efficiency.

Control strategy	$COP_{HP\ SH}$	$COP_{HP\ DHW}$	$\varepsilon_{cap\ HP}$	$\varepsilon_{cap\ SH\ tank}$
RBC	5.9	3.9	0.78	0.49
EMPC1	6.4	4.0	0.91	0.60
EMPC2	6.1	3.3	0.96	0.56

KPIs – energy costs

For the control strategies EMPC1 and EMPC2, the total costs of electricity usage (J_{HP}) were calculated according to Algorithm 2. In the same way it was for EMPC1, the total cost for RBC was retrieved using $c_{day-ahead}$ and c_{imb}. Table 5-7 lists J_{HP} and shows the ratio $J_{HP}/J_{HP\ norm}$, which indicates that the use of EMPC reduces the total operational costs of electricity consumption. For RBC, a decrease of J_{HP} compared to $J_{HP\ norm}$ was due to the consideration of c_{imb} and $c_{day-ahead}$. To create $J_{HP\ norm}$, only $c_{day-ahead}$ was used. The application of EMPC also improved demand flexibility in terms of costs, as can be seen in an increase of the flexibility factor (FF) compared to RBC.

Table 5-7. KPIs for control strategies – costs.

Control strategy	J_{HP} (€)	$\left(\frac{J_{HP}}{J_{HP\ norm}} - 1\right)$	FF
RBC	0.58	- 2%	0.07
EMPC1	0.42	- 15%	0.27
EMPC2	0.61	- 12%	0.37

5.4 Discussion

The experimental results showed an energy-efficient operation of the heating system, including HP and TES. It was observed that the performance of the heating system was in good agreement with the results from other studies, which used heating systems in office buildings and residential buildings, including HP combined with PCM and TCM tanks [5], HP and fan coils, radiators, and air-handling units [18], HP in combination with CHP [42], and CHP combined with TES [20].

During the test days, the overall performance in predicting HP electricity consumption was between 0.17 and 0.22 kWh as measured by RMSE; this is an improvement over results in other studies [43]. For performance in predicting Q_{HP}, the largest fractional prediction errors were determined for the HP model (20–23%) and the SH tank model (18–23%). The HP was modelled as an ANN – more precisely, a recurrent dynamic network with feedback connections – using T_{amb} and $I_{gsr-hsr}$ as input variables for modelling the evaporator side. A detailed approach to modelling the evaporator circuit could increase the prediction performance but also would require an additional model of the PVT system.

For the SH tank, the presence of three inlet and outlet ports meant a more complex model was required. A multi-node grey-box model was configured, which outperformed ANN and state-space black-box models. In the case of the black-box models, this was because the measurement data did not sufficiently reflect all possible cases of different states of the SH tank. The use of a fast, high performing multi-node grey-box model in an EMPC/MPC framework is recommended for the SH tank.

For modelling SH demand, ANN black-box models have already shown good prediction performance [7,43]. In the present study, SH demand was predicted by applying a recurrent dynamic network, which resulted in a fractional prediction error of 15–24%. To improve the prediction performance of heating, cooling or energy load profiles for buildings, black-box modelling approaches such as support vector machines, deep neural networks, or combined models including ensemble and improved models [44] could be further investigated.

The use of a one-node grey-box model (capacity model) of the DHW tank resulted in a fractional prediction error of 12–15%, indicating that there is still room for improvement. We recommend that future applications use multi-node grey-box models even for well-mixed DHW tanks.

To identify DHW demand, Markov chains were applied, showing a fractional prediction error of 9–19%. To improve performance in predicting DHW demand profiles, black-box modelling approaches such as support vector machines [45] could be further investigated.

For the weather forecasting model, online forecasting was combined with a feedforward network (an ANN) to forecast solar radiation. A fractional prediction error of 10–11% showed that this model performs well and can be recommended for the use in an EMPC/MPC framework. For a possible performance improvement, a shorter time step for predictions could be used [7,46], however, this would lead to a larger state space regarding OCP formulation of EMPC.

We compared the performances of EMPC and RBC using conventional indicators and indicators for demand flexibility. These performance indicators were categorized into three domains: energy and power, energy efficiency, and energy costs. This categorization emphasizes the necessity of quantifying demand flexibility indicators according to the following benefits:

1. Performance indicators in the category of *energy costs* can be included in the formulation of OCP [7]. This makes it possible to optimize demand flexibility by creating a cost function, which incorporates operational costs of energy usage that are associated with demand flexibility [7].
2. Performance indicators in the category of *energy and power* can provide detailed information about energy consumption in relation to the power grid. For example, the flexibility indicator *instantaneous power flexibility* presents the evolution of electrical power and heating power during a requested flexibility event [5].
3. Performance indicators in the category of *energy efficiency* can be used to identify performance issues of the current energy system. For example, in the present study, we introduced a measure of the effective utilization of SH tank capacity. We determined a maximum value of 0.6 across all control strategies, which implies that the current SH tank is oversized for the request of demand flexibility under RTP. We note that for the retrofitting of the current system or the design of new systems, a comprehensive overview is required of all *efficiency* indicators, such as the COP of the HP.

We used a one-way trading pattern, including dynamic day-ahead prices and imbalance prices. In contrast to complex trading mechanisms using intra-day pricing, this one-way trading mechanism can be simply implemented in an EMPC framework and enables dynamic optimization of demand flexibility. Recent studies have investigated complex trading and simple one-way trading mechanisms for demand flexibility. In [47], a simulation study served to investigate intra-day trading of transient building load. The study concluded that one-hour intra-day trading can bring economic benefits. The authors in [47] suggested a simple one-way trading pattern that could also be adapted to longer trading horizons. Integrating flexible demand into current trading markets was also investigated by [48].

The simulation study [48] showed that above a certain ratio of flexible consumers, the current trading mechanism can hinder correct predictions of energy consumption. The authors in [48] suggested more direct control of flexible demand. In [21], authors argued that direct control of flexible demand can increase the reliability of demand-side actions caused by fluctuating prices in trading markets. These authors [21] suggest direct control for flexibility provision of 1 to 30 min before real-time and the use of pricing markets and/or trading markets for longer notification times. In a simulation study [49], hourly RTP and CO_2 intensity were integrated as weighted sums into an MPC's cost function. The study [49] found that optimal control can integrate a trade-off between cost optimization and CO_2 emissions, which can be directly linked to renewable energy sources. To facilitate renewable integration, there are several approaches to control demand flexibility. However, these control approaches have to fit into existing electricity markets or have to lead to innovative flexibility markets [50] such as local flexibility markets [51].

5.5 Conclusion

We developed and demonstrated an economic model predictive controller to optimally manage the total operational costs of electricity consumption of a heat pump in a house. The experiments were performed in a residential building with a hydraulic heating system, an HP, and TES tanks. During the test periods, the stochastic behaviour of occupants was implemented in the EMPC. The EMPC also included different modelling techniques of the system components (weather forecasting, the SH tank, the SH demand, the DHW tank, the DHW demand, and the HP). We introduced a methodology to determine the fractional prediction error of all models applied in the EMPC framework. We recommend measuring the fractional prediction error to assess the impact of modelling techniques on EMPC prediction performance. The overall performance in predicting the HPs electricity consumption was a result of the prediction errors of the different models. The study realized good performance at predicting HP energy consumption.

The performance of EMPC and RBC were compared by quantifying conventional indicators and flexibility indicators. We introduced a categorization of indicators according to 1) energy and power, 2) energy efficiency, and 3) energy costs. This categorization helps to make clear the benefits of using flexibility indicators in real-life applications. Those benefits include 1) detailed information on demand flexibility in relation to the power grid, 2) demand flexibility for retrofitting and design of new energy systems, and 3) optimal control of demand flexibility. We also introduced KPIs in the category of energy efficiency to measure the effective utilization of available sources such as HP and TES.

A building heating system, including HP and TES, was used to demonstrate the provision of demand flexibility for real-time power markets. We introduced a flexibility service that can be used as an ancillary service for flexibility markets. The flexibility service is based on a dynamic modification of day-ahead prices. This modification was used to adapt energy consumption to errors in the forecasting of renewable energy generation. To facilitate renewable integration and control demand flexibility, the introduced methodology is one possible solution that fits into flexibility markets. However, demand flexibility was dynamically optimized using a notification time of $1\ h < t < t_{day\ end}$. For shorter-term provision of demand flexibility where $t < 1\ h$, we suggest investigating direct control of demand flexibility to ensure reliable grid operations. Eventually, a combination of direct control (incentive-based) and price-based control of demand flexibility will create robust energy networks, which are of vital importance for the integration of renewable sources.

5.6 Appendix I – Performance metrics

i is the sample number, n is the total number of samples, e is the estimated data point, o is the output, and $\bar{o}$ is the mean output.

Root Mean Square Error

$$RMSE = \sqrt{\frac{1}{n}\sum_{i=1}^{n}(e_i - o_i)^2}$$

Mean Absolute Error

$$MAE = \frac{1}{n}\sum_{i=1}^{n}|e_i - o_i|$$

Mean Absolute Percentage Error

$$MAPE = \frac{1}{n}\sum_{i=1}^{n}\left|\frac{|e_i - o_i|}{o_i}\right|$$

Coefficient of Determination

$$R^2 = 1 - \frac{\sum_{i=1}^{n}(o_i - e_i)^2}{\sum_{i=1}^{n}(o_i - \bar{o})^2}$$

Goodness of Fit

$$G = 1 - \frac{\sqrt{\sum_{i=1}^{n}(e_i - o_i)^2}}{\sqrt{\sum_{i=1}^{n}\left(o_i - \frac{1}{n}\sum_{i=1}^{n}o_i\right)^2}}$$

5.7 Appendix II – Experimental data for heat pump

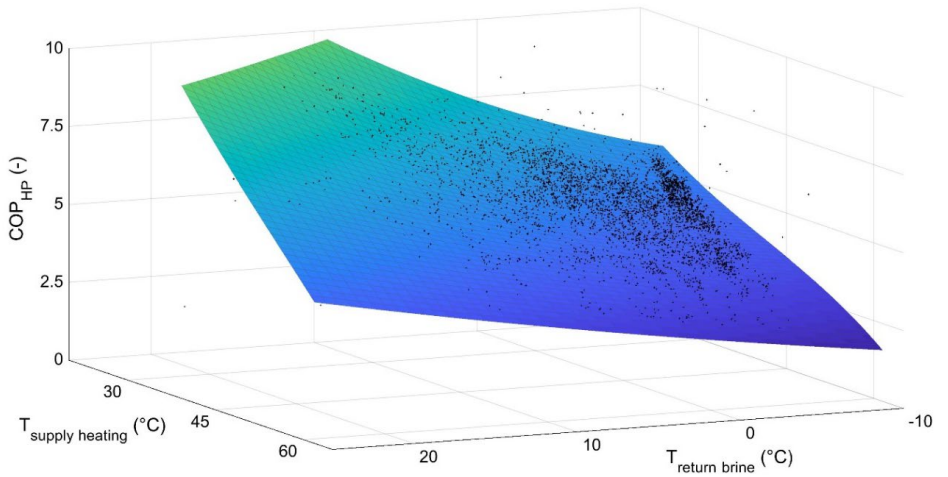

Experimental data for heat pump $COP_{HP} = f(T_{supply\ heating}, T_{return\ brine})$; curve fitting of experimental data using a polynomial fitting curve ($R^2 = 0.89$, RMSE = 0.36).

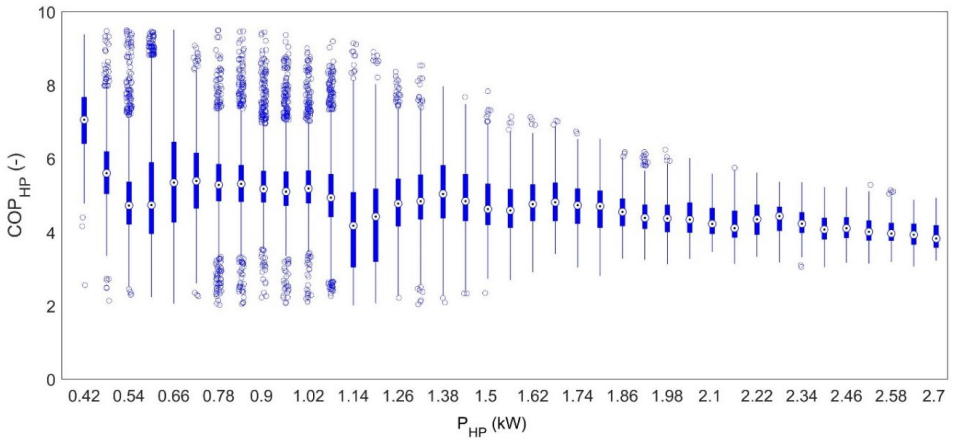

Experimental data for heat pump COP_{HP} vs. P_{HP}; the heat pump regulates the electricity consumption of the compressor according to $P_{HP\ min} = 0.42$ kW, $P_{HP\ max} = 2.7$ kW, and $\Delta P_{HP} = 0.06$ kW; box plots for $P_{HP\ min} \leq P_{HP} \leq P_{HP\ max}$.

5.8 References

[1] OECD/IEA. Renewables Information Overview (2018 edition). 2018.

[2] IEA. 2018 World Energy Outlook: Executive Summary. 2018.

[3] Jensen SØ, Marszal-Pomianowska A, Lollini R, Pasut W, Knotzer A, Engelmann P, et al. IEA EBC Annex 67 Energy Flexible Buildings. Energy Build 2017;155:25–34. doi:10.1016/j.enbuild.2017.08.044.

[4] Reynders G, Diriken J, Saelens D. Generic characterization method for energy flexibility: Applied to structural thermal storage in residential buildings. Appl Energy 2017;198:192–202. doi:10.1016/j.apenergy.2017.04.061.

[5] Finck C, Li R, Kramer R, Zeiler W. Quantifying demand flexibility of power-to-heat and thermal energy storage in the control of building heating systems. Appl Energy 2018;209:409–25. doi:10.1016/j.apenergy.2017.11.036.

[6] Péan T, Costa-Castelló R, Salom J. Price and carbon-based energy flexibility of residential heating and cooling loads using model predictive control. Sustain Cities Soc 2019. doi:10.1016/j.scs.2019.101579.

[7] Finck C, Li R, Zeiler W. Economic model predictive control for demand flexibility of a residential building. Energy 2019;176:365–79. doi:10.1016/j.energy.2019.03.171.

[8] Clauß J, Finck C, Vogler-Finck P, Beagon P. Control strategies for building energy systems to unlock demand side flexibility – A review. 15th Int. Conf. Int. Build. Perform. Simul. Assoc., 2017, p. 611–20.

[9] Balint A, Kazmi H. Determinants of energy flexibility in residential hot water systems. Energy Build 2019. doi:10.1016/j.enbuild.2019.02.016.

[10] Foteinaki K, Li R, Heller A, Rode C. Heating system energy flexibility of low-energy residential buildings. Energy Build 2018. doi:10.1016/j.enbuild.2018.09.030.

[11] Liu M, Heiselberg P. Energy flexibility of a nearly zero-energy building with weather predictive control on a convective building energy system and evaluated with different metrics. Appl Energy 2019;233–234:764–75. doi:10.1016/j.apenergy.2018.10.070.

[12] Wang A, Li R, You S. Development of a data driven approach to explore the energy flexibility potential of building clusters. Appl Energy 2018;232:89–100. doi:10.1016/j.apenergy.2018.09.187.

[13] Salpakari J, Lund P. Optimal and rule-based control strategies for energy flexibility in buildings with PV. Appl Energy 2016;161:425–36. doi:10.1016/j.apenergy.2015.10.036.

[14] Aelenei D, Lopes RA, Aelenei L, Gonçalves H. Investigating the potential for energy flexibility in an office building with a vertical BIPV and a PV roof system. Renew Energy 2019. doi:10.1016/j.renene.2018.07.140.

[15] Klein K, Langner R, Kalz D, Herkel S, Henning HM. Grid support coefficients for electricity-based heating and cooling and field data analysis of present-day installations in Germany. Appl Energy 2016. doi:10.1016/j.apenergy.2015.10.107.

[16] Le Dréau J, Heiselberg P. Energy flexibility of residential buildings using short term heat storage in the thermal mass. Energy 2016;111:1–5. doi:10.1016/j.energy.2016.05.076.

[17] Hu M, Xiao F, Jørgensen JB, Li R. Price-responsive model predictive control of floor heating systems for demand response using building thermal mass. Appl Therm Eng 2019. doi:10.1016/j.applthermaleng.2019.02.107.

[18] De Coninck R, Helsen L. Quantification of flexibility in buildings by cost curves - Methodology and application. Appl Energy 2016;162:653–65. doi:10.1016/j.apenergy.2015.10.114.

[19] D'Ettorre F, Rosa M De, Conti P, Testi D, Finn D. Mapping the energy flexibility potential of single buildings equipped with optimally-controlled heat pump, gas boilers and thermal storage. Sustain Cities Soc 2019. doi:10.1016/j.scs.2019.101689.

[20] De Rosa M, Carragher M, Finn DP. Flexibility assessment of a combined heat-power system (CHP) with energy storage under real-time energy price market framework. Therm Sci Eng Prog 2018. doi:10.1016/j.tsep.2018.10.002.

[21] Eid C, Codani P, Perez Y, Reneses J, Hakvoort R. Managing electric flexibility from Distributed Energy Resources: A review of incentives for market design. Renew Sustain Energy Rev 2016. doi:10.1016/j.rser.2016.06.008.

[22] epexspot.com. Intraday lead time overview 2019. https://www.epexspot.com/en/product-nfo/intradaycontinuous/intraday_lead_time.

[23] Tennet.eu. Onbalansprijssystematiek - Hoe komen de geldstromen tot stand? 2019.

[24] Clauß J, Stinner S, Sartori I, Georges L. Predictive rule-based control to activate the energy flexibility of Norwegian residential buildings: Case of an air-source heat pump and direct electric heating. Appl Energy 2019;237:500–18. doi:10.1016/J.APENERGY.2018.12.074.

[25] Vogler-Finck PJC, Wisniewski R, Popovski P. Reducing the carbon footprint of house heating through model predictive control – A simulation study in Danish conditions. Sustain Cities Soc 2018. doi:10.1016/j.scs.2018.07.027.

[26] NIBE. Ground source heat pump NIBE F1155 2019.

[27] TripleSolar. Technische documentatie warmtepomppanelen / PVT 2019.

[28] Han YM, Wang RZ, Dai YJ. Thermal stratification within the water tank. Renew Sustain Energy Rev 2009. doi:10.1016/j.rser.2008.03.001.

[29] Schütz T, Streblow R, Müller D. A comparison of thermal energy storage models for building energy system optimization. Energy Build 2015. doi:10.1016/j.enbuild.2015.02.031.

[30] Chandra YP, Matuska T. Stratification analysis of domestic hot water storage tanks: A comprehensive review. Energy Build 2019. doi:10.1016/j.enbuild.2019.01.052.

[31] Finck C, Li R, Zeiler W. Identification of a dynamic system model for a building and heating system including heat pump and thermal energy storage. MethodsX 2020:100866. doi:10.1016/j.mex.2020.100866.

[32] Fiorentini M, Wall J, Ma Z, Braslavsky JH, Cooper P. Hybrid model predictive control of a residential HVAC system with on-site thermal energy generation and storage. Appl Energy 2017;187:465–79. doi:10.1016/j.apenergy.2016.11.041.

[33] Wang Z, Srinivasan RS. A review of artificial intelligence based building energy use prediction: Contrasting the capabilities of single and ensemble prediction models. Renew Sustain Energy Rev 2017;75:796–808. doi:10.1016/j.rser.2016.10.079.

[34] Afram A, Janabi-Sharifi F. Black-box modeling of residential HVAC system and comparison of gray-box and black-box modeling methods. Energy Build 2015;94:121–49. doi:10.1016/j.enbuild.2015.02.045.

[35] Afroz Z, Urmee T, Shafiullah GM, Higgins G. Real-time prediction model for indoor temperature in a commercial building. Appl Energy 2018. doi:10.1016/j.apenergy.2018.09.052.

[36] Afram A, Janabi-Sharifi F, Fung AS, Raahemifar K. Artificial neural network (ANN) based model predictive control (MPC) and optimization of HVAC systems: A state of the art review and case study of a residential HVAC system. Energy Build 2017;141:96–113. doi:10.1016/j.enbuild.2017.02.012.

[37] Afram A, Fung AS, Janabi-Sharifi F, Raahemifar K. Development of an accurate gray-box model of ubiquitous residential HVAC system for precise performance prediction during summer and winter seasons. Energy Build 2018. doi:10.1016/j.enbuild.2018.04.038.

[38] Mustafaraj G, Chen J, Lowry G. Thermal behaviour prediction utilizing artificial neural networks for an open office. Appl Math Model 2010. doi:10.1016/j.apm.2010.02.014.

[39] Magalhães SMC, Leal VMS, Horta IM. Modelling the relationship between heating energy use and indoor temperatures in residential buildings through Artificial Neural Networks considering occupant behavior. Energy Build 2017;151:332–43. doi:10.1016/j.enbuild.2017.06.076.

[40] Taylor J. Introduction to Error Analysis, the Study of Uncertainties in Physical Measurements, 2nd Edition. Publ by Univ Sci Books 1997.

[41] Dansk Standard DS/EN 15251. Indoor environmental input parameters for design and assessment of energy performance of buildings addressing indoor air quality, thermal environment, lighting and acoustics. 2007.

[42] Salata F, Golasi I, Domestico U, Banditelli M, Lo Basso G, Nastasi B, et al. Heading towards the nZEB through CHP+HP systems. A comparison between retrofit solutions able to increase the energy performance for the heating and domestic hot water production in residential buildings. Energy Convers Manag 2017. doi:10.1016/j.enconman.2017.01.062.

[43] Amasyali K, El-Gohary NM. A review of data-driven building energy consumption prediction studies. Renew Sustain Energy Rev 2018;81:1192–205. doi:10.1016/j.rser.2017.04.095.

[44] Bourdeau M, Zhai X qiang, Nefzaoui E, Guo X, Chatellier P. Modeling and forecasting building energy consumption: A review of data-driven techniques. Sustain Cities Soc 2019. doi:10.1016/j.scs.2019.101533.

[45] Cao S, Hou S, Yu L, Lu J. Predictive control based on occupant behavior prediction for domestic hot water system using data mining algorithm. Energy Sci Eng 2019:1–19. doi:10.1002/ese3.341.

[46] Diagne M, David M, Lauret P, Boland J, Schmutz N. Review of solar irradiance forecasting methods and a proposition for small-scale insular grids. Renew Sustain Energy Rev 2013;27:65–76. doi:10.1016/j.rser.2013.06.042.

[47] Hedegaard RE, Pedersen TH, Petersen S. Multi-market demand response using economic model predictive control of space heating in residential buildings. Energy Build 2017;150. doi:10.1016/j.enbuild.2017.05.059.

[48] Kühnlenz F, Nardelli PHJ, Karhinen S, Svento R. Implementing flexible demand: Real-time price vs. market integration. Energy 2018;149:550–65. doi:10.1016/j.energy.2018.02.024.

[49] Dahl Knudsen M, Petersen S. Demand response potential of model predictive control of space heating based on price and carbon dioxide intensity signals. Energy Build 2016;125:196–204. doi:10.1016/j.enbuild.2016.04.053.

[50] Kohlhepp P, Harb H, Wolisz H, Waczowicz S, Müller D, Hagenmeyer V. Large-scale grid integration of residential thermal energy storages as demand-side flexibility resource: A review of international field studies. Renew Sustain Energy Rev 2019. doi:10.1016/j.rser.2018.09.045.

[51] EPEX Spot. Trading on EPEX SPOT 2019-2020 2018.

6

Discussion

At the beginning of this research, the International Energy Agency – Energy in Buildings and Communities program initiated Annex 67 "Energy Flexible Buildings". A major objective of Annex 67 was to develop a common terminology and definition of "Energy flexibility in buildings" [1]. While all participants agreed that the development of energy flexibility in buildings would mitigate intermittency issues of renewable energy resources, there was no common agreement on the terminology of energy flexibility in buildings. To date, a comprehensive characterization of energy flexibility [2], an overview of example studies [3], and alternative formulations of energy flexibility, which are demand-side flexibility [4] and demand flexibility [5], have been developed. In this study, the term "demand flexibility" is used to describe the potential energy flexibility of buildings. This is because a building's flexibility is characterized by its size (amount of energy), time (power shifting potential), and costs (energy costs) (Figure 1.1 – Chapter 1) [6,7]. Therefore, exclusively using "energy flexibility" offers an inadequate description of a building's flexibility.

In this work, the demand flexibility of building heating systems, including power-to-heat and thermal energy storage, was investigated. The results and limitations of these investigations were presented in the previous four chapters. Here, the answers to the research questions as formulated in Chapter 1 are discussed:

(1) *How can the main dynamic characteristics of demand flexibility of building heating systems, including power-to-heat and TES, be integrated for optimal control?*

The main dynamic characteristics of TES include storage capacity, charging and discharging rates, and thermal losses. To provide demand flexibility of TES systems (buffer tanks including water, phase change materials, and thermochemical materials), the heat and mass transfer dynamics were captured using performance maps [8]. These performance maps were used in the framework of optimal control, and they show the dynamic characteristics of energy and power, and efficiency. Based on performance maps, grey-box and black-box TES models were created for use in optimal control. The grey-box models were retrieved from the one-dimensional convection-diffusion-reaction equation. The black-box models included, for example, time-series recurrent dynamic networks.

As shown in Chapter 2, in the first simulation case study of power-to-heat and TES buffer tanks, a finite-difference method (the Crank-Nicolson scheme) was implemented, which is a numerical solution to the one-dimensional equation. The Crank-Nicolson scheme was applied to grey-box models of TES buffer tanks that include water, phase change materials, and thermochemical materials, and integrated into an optimal control framework. The Crank-Nicolson scheme was chosen because it provides stable, robust, and fast modelling with low computational effort.

Chapter 4 and Chapter 5 present the second experimental case study, where the Crank-Nicolson scheme was integrated into the optimal control framework to model the water buffer tank. During validation of the water tank model, it was found that the simulations insufficiently represented the mixing effect that resulted from temperature inversion. Based on this observation, a numerical solution was created for online optimization that included a combination of the Crank-Nicolson scheme for the diffusion problem and an upwind scheme for the convection problem. This one-dimensional multi-node model of the water buffer tank outperformed the grey-box one-node (capacity) model and black-box models such as time-series recurrent dynamic networks and discrete-time state-space models. For the performance of black-box models, it was observed that learning strategies play an important role in establishing training and validation data. For example, a training and validation data set of six months was used, which is commonly a rich dataset. Nevertheless, the measurement data did not include all possible cases of different states of the water buffer tank model (TES).

The charging of TES systems strongly depends on the characteristics of power-to-heat devices such as HPs that can be represented by the minimum and maximum capacity, and the ramping capacity up and down. To implement the HP's characteristics into the framework of optimal control, in the second experimental case study, a black-box model was created that was an artificial neural network (a nonlinear autoregressive with an external input model). The black-box model performed well during validation and online optimization because the measurement data sufficiently captured all possible cases of different states for the HP. A well-performing HP model is needed to successfully test the developed optimal control strategy because the optimal control problem includes HPs' electricity consumption. To regulate the electricity usage of the HP, a soft control was implemented using HPs' degree minutes to be controlled. Degree minutes are the difference between the actual and setpoint temperature of TES. Regulating HPs' degree minutes was found to be a robust method for online optimization without interrupting HPs primary compressor control.

To integrate the dynamic characteristics of HP and TES into optimal control (online-optimization), it was concluded that grey-box modelling approaches perform best for TES buffer tanks and black-box modelling approaches perform best for HPs. For future implementations of model-based optimal control, the following strategy is recommended:

First, determine a learning strategy to capture all relevant states of building energy system components. It was noted that it is essential to focus on all possible cases of states of building energy system components rather than focusing on a certain measurement period.

Second, create black-box models for building energy system components. If it is not possible to measure all relevant cases, develop detailed and fast-performing grey-box models.

Third, if black-box models are developed, additionally, create simplified grey-box models that offer online validation of the black-box models. During online optimization, if the results of the black-box model are greater than a threshold (deviation of performance criteria), the simplified grey-box model is used for online optimization to prevent inaccurate predictions during unlearned situations.

(2) *What optimal control strategy activates the optimization of demand flexibility while integrating many control objectives?*

Optimizing demand flexibility is associated with optimizing load shifting, peak shaving, energy consumption, costs of energy consumption, self-consumption, CO_2 emissions, and thermal comfort. For optimal control, most researchers investigated one of these control objectives [9,10]. A few research studies implemented many control objectives and found that they can contradict each other. For example, minimizing energy consumption can lead to discomfort [11,12]. For multi-objective optimization, the effect of contradicting objectives is not new and has been solved using methods such as Pareto optimal solutions. Examples of Pareto optimization were found for the investigation of thermal comfort and energy consumption [13] or thermal comfort and energy costs of buildings [12,14]. As a result, a Pareto front can visualize all possible solutions, including the best compromise based on the decision-maker's criteria. Thus, the Pareto method can include many control aspects in one objective function.

To optimize demand flexibility, in this thesis, a different approach to the Pareto method was used. An objective function was introduced, where each term associates operational costs of energy usage with demand flexibility. For example, in the first experimental case study (Chapter 3), the costs of consuming electricity from the grid, the costs of consuming electricity from on-site PV power generation, and the costs of delivering electricity from on-site PV power generation to the grid were integrated into one objective function of the model predictive controller. The demand flexibility was optimized for contradicting objectives such as self-consumption and grid feed-in. However, this method is only applicable to control objectives that aim to optimize the use of energy, such as load shifting, peak shaving, total energy consumption, self-consumption, and CO_2 emissions. The method is not applicable to optimize thermal comfort, because indicators to quantify thermal comfort, such as the predicted mean vote, exclude the use of energy. To meet thermal comfort requirements in optimal control using model predictive control, it is recommended to integrate boundary conditions of an acceptable range of indoor temperature, moisture, and air velocity.

(3) *What optimal control method activates online optimization of demand flexibility?*

Rule-based control strategies cannot incorporate time-varying disturbances, complex dynamic control signals, and non-linear and time-varying dynamics. To compensate for this drawback, an optimal control strategy was created, which was applied in both experimental case studies. The optimal control problem was formulated in an MPC framework that consisted of a dynamic system model of the building and heating systems and implemented dynamic programming as the optimization method. Applying approximations to the dynamic programming scheme reduced the state and decisions space and, thus, reduced the computational effort of solving the optimal control problem.

For the experimental case studies, it was shown, that the MPC resulted in greater total operational energy consumption, which was the daily electricity consumption of the HP. In the first experimental case study HPs electricity consumption increased by 13% (0.5 kWh for $EMPC1_{Chapter3}$) and 18% (0.6 kWh for $EMPC2_{Chapter3}$). In the second experimental case study, the MPC increased HPs electricity consumption by 4% (0.4 kWh for $EMPC1_{Chapter5}$) and 9% (1.2 kWh for $EMPC2_{Chapter5}$). For the total costs of HPs electricity consumption, the MPC, which was an economic MPC (EMPC), always realized cost savings. In the first experimental case study, costs of HPs electricity usage decreased by 7% (1.0 Euro cent for $EMPC1_{Chapter3}$) and 3% (0.4 Euro cent for $EMPC2_{Chapter3}$). In the second experimental case study, cost savings of HPs electricity usage were achieved by 15% (6.0 Euro cent for $EMPC1_{Chapter5}$) and 12% (7.0 Euro cent for $EMPC2_{Chapter5}$). Recent studies on MPC in building heating systems also concluded that minimizing buildings' total operational costs of energy consumption can result in an increase of total energy consumption [15,16]. The studies also showed that an increase of energy consumption and activation of demand flexibility corresponds to building's differential price responsiveness over the day and hourly pricing variations [15–17]. Thus, real-time markets, which trade day-ahead, intra-day and imbalance electricity prices can stimulate load shifting and constitute the degree of demand flexibility [18–21].

Moreover, in this work, the MPC framework was developed to maximize demand flexibility. In the first experimental case study, the flexibility factor (key performance indicator of demand flexibility) was improved from -0.9 to 0.4 for $EMPC1_{Chapter3}$ and from -0.9 to 0.7 for $EMPC2_{Chapter3}$. In the second experimental case study the flexibility factor was increased from 0.1 to 0.3 for $EMPC1_{Chapter5}$ and 0.1 to 0.4 for $EMPC2_{Chapter5}$. In Chapter 2 (first simulation case study), additionally, it was shown that different TES technologies can maximize demand flexibility in optimal control (flexibility factor of 0.15 for the TCM tank, of 0.67 for the PCM tank and of 0.86 for the water buffer tank compared to a reference situation without TES of -1).

Thus far, there are still barriers to building adoption of MPC implementation, which primarily relates to the willingness to use MPC. The first argument is that MPC is not robust and may violate building energy systems or breach energy contracts. In the present second experimental case study, HPs' primary control was not used. Instead, the HPs' secondary control (i.e. soft control) was used and temperature setpoints were overwritten by MPC results. In case of inactivity of the MPC, HPs' settings were reset to initial conditions, which indicates that this MPC is robust and reliable. The second argument is that MPC requires engineering effort for constructing a system model, which increases MPC investment costs. This may be true for MPC applications where a system model is constructed from the ground up. In the present experimental case studies, a system model (plug-and-play model) and optimization strategy were developed that were highly flexible to adapt to different situations, including new system components, and consequently reduces investment costs. The third argument is that additional sensors to measure relevant parameters must be installed. This is only partly true because current implementations of smart home devices and appliances provide a range of sensors, which, in case of accessibility, can be used in data analysis to enable MPC.

(4) What flexibility service creates dynamic optimization of demand flexibility under real-time pricing?

To enable flexible operations of building energy management systems, system operators provide pricing signals via balancing and spot markets. Thus far, these complex trading mechanisms have been a computational burden to real-life applications of optimal control, because online optimization in building energy management systems must be solved during each negotiation phase. Furthermore, complex trading mechanisms hinder correct predictions of a building's energy consumption above a certain ratio of flexible consumers [22]. To facilitate the implementation of advanced control, such as optimal control, a flexibility service was developed for existing balancing markets, spot markets, and flexibility markets [23] such as local flexibility markets [24]. The developed flexibility service (Chapter 5) includes a one-way trading mechanism and paves the way for increased application of optimal control by reducing computational effort in online optimization. This flexibility service aims to adapt energy consumption to errors in the forecasting of renewable energy generation. Preferential targets of application are price-based spot markets where dynamic modification of day-ahead prices provides dynamic optimization of demand flexibility for a notification time of $1\ h < t < t_{\text{day end}}$. In addition to spot markets, the flexibility service may be also applied to reserve markets. Recent studies emphasize the value of demand flexibility in reserve markets [25,26]. As reserve markets aim to maintain capacities for unforeseeable events, the flexibility service facilitates the provision of capacities to the power grid as a condition of its dynamic optimization.

More precisely, the flexibility service can ensure a minimum available capacity through its dynamic modification of day-ahead prices. However, current spot markets and reserve markets are separated to provide additional security [27,28].

In addition to the four research questions, this work also categorized flexibility indicators for use in real-life applications and control of building energy systems. The categorization comprises 1) energy and power, 2) energy efficiency, and 3) energy costs. These categories show the different characteristics of demand flexibility. The benefits of associating flexibility indicators with these categories include the following:

1) information about power profiles and their integral (area below the curve), which is the amount of energy that can be provided to the power grid
2) efficiency curves provide detailed information on retrofitting and design of new energy systems
3) information about operational costs affecting optimal control of energy systems.

Flexibility indicators assigned to one of the categories can compare the specific characteristic of demand flexibility and quantify the dynamic behaviour of building energy systems and their components. Researchers have attempted to aggregate these characteristics in a single generic indicator. For example, the flexible performance indicator was introduced, which consists of a weighing sum of the response time, the committed power, the recovery time, and the actual energy variation [29]. In another example, a generic indicator was developed in which demand flexibility is considered as one aspect to enable smart building technologies (i.e. the smart-ready built environment indicator) [30,31]. The smart-ready built environment indicator and the flexible performance indicator were both designed to provide information to policymakers and investors. However, these flexibility indicators are less suitable to quantify demand flexibility in the control of building energy systems that include online optimization because these generic flexibility indicators consist of performance weights that are average values of characteristics such as the response time. As performance weights neglect the dynamic effects of buildings' energy systems, real-life implementations require specific flexibility indicators to control demand flexibility.

Thus far, indicators that quantify flexibility in the framework of optimal control integrate reference scenarios and reference curves, which are derived from the acceptable thermal comfort. Those reference curves have been retrieved from measurement data. To determine reference curves in real-life applications, all possible reference cases need to be measured. Alternatively, reference curves can also be quantified using standardized energy consumption data.

In this thesis, reference curves were simulated to quantify demand flexibility for optimal control. As shown in Chapter 3, in periods with optimal control, the system model predicted reference curves of minimum comfort, which were simulated at the beginning of the day for the following 24 hours. While this is one possible solution, it assumes that reference curves are simulated each day for 24 hours. Using such a static approach to determine reference curves may lead to inaccurate predictions of reference scenarios. A more flexible approach through, for example, innovative performance indicators, may improve quantification of demand flexibility for optimal control.

In this work, the instantaneous power flexibility indicator was defined, which quantifies demand flexibility to the power grid in the absence of reference data. The instantaneous power flexibility presents the evolution of power during flexibility events, which is retrieved from performance maps that fully capture the dynamic behaviour of system components such as TES. Optimal control implements these dynamic characteristics and maximizes load shifting using TES. As load shifting is crucial to provide flexibility to the power grid, for instance, in situations to mitigate errors in solar and wind power forecasting, the instantaneous power flexibility recalls details of the discrete features of load shaping, such as energy and power. To quantify the instantaneous power flexibility, reference curves from conventional controllers are not required. Instead, performance maps were included for different cases such as charging and discharging of TES using power-to-heat. Thus, the instantaneous power flexibility represents performance maps for all possible flexibility events and can visualize optimal control results, including maximizing load shaping. To determine the instantaneous power flexibility, the dynamic behaviour of the building energy system needs to be predicted, which requires a system model. In this study, the system models performed in model-based predictive control frameworks and included both grey-box and black-box modelling. As other optimal control strategies, such as reinforcement learning, do not necessarily employ a system model, the quantification of the instantaneous power flexibility is restricted by the mapping of learned control actions. Advanced model-based reinforcement learning may compensate for this drawback.

The instantaneous power flexibility can be classified as “energy and power”. Efficiency values cannot be retrieved from this indicator. To quantify energy-efficient operations for demand flexibility, this work introduced the effective utilization of power-to-heat and TES. The effective utilization is the ratio of the maximum capacity during operation to the upper capacity limit. Reference curves are not required to quantify the effective utilization. The determination of effective utilization can result in adequate actions for retrofitting and redesign of building energy systems. It is noted that those results strongly depend on results of optimal control decisions, including control signals such as real-time pricing.

6.1 References

[1] Jensen SØ, Marszal-Pomianowska A, Lollini R, Pasut W, Knotzer A, Engelmann P, et al. IEA EBC Annex 67 Energy Flexible Buildings. Energy Build 2017;155:25–34. doi:10.1016/j.enbuild.2017.08.044.

[2] International Energy Agency - Energy in Buildings and Communities Programme. Principles of Energy Flexible Buildings. 2019.

[3] International Energy Agency - Energy in Buildings and Communities Programme. Examples of Energy Flexibility in Buildings. 2019.

[4] Aduda KO, Labeodan T, Zeiler W, Boxem G, Zhao Y. Demand side flexibility: Potentials and building performance implications. Sustain Cities Soc 2016. doi:10.1016/j.scs.2016.02.011.

[5] Lund PD, Lindgren J, Mikkola J, Salpakari J. Review of energy system flexibility measures to enable high levels of variable renewable electricity. Renew Sustain Energy Rev 2015;45:785–807. doi:10.1016/j.rser.2015.01.057.

[6] Reynders G, Diriken J, Saelens D. Generic characterization method for energy flexibility: Applied to structural thermal storage in residential buildings. Appl Energy 2017;198:192–202. doi:10.1016/j.apenergy.2017.04.061.

[7] Reynders G, Amaral Lopes R, Marszal-Pomianowska A, Aelenei D, Martins J, Saelens D. Energy flexible buildings: An evaluation of definitions and quantification methodologies applied to thermal storage. Energy Build 2018. doi:10.1016/j.enbuild.2018.02.040.

[8] Finck C, Li R, Zeiler W. Performance maps for the control of thermal energy storage. 15th Int Conf Int Build Perform Simul Assoc 2017. doi:10.26868/25222708.2017.238.

[9] Finck C, Clauß J, Vogler-Finck P, Beagon P, Zhan K, Kazmi H. Review of applied and tested control possibilities for energy flexibility in buildings. 2018. doi:10.13140/RG.2.2.28740.73609.

[10] Li H, Wang Z, Hong T, Piette MA. Energy Flexibility of Residential Buildings: A Systematic Review of Characterization and Quantification Methods and Applications. Adv Appl Energy 2021:100054. doi:10.1016/j.adapen.2021.100054.

[11] De Coninck R, Helsen L. Quantification of flexibility in buildings by cost curves - Methodology and application. Appl Energy 2016;162:653–65. doi:10.1016/j.apenergy.2015.10.114.

[12] Martell M, Rodríguez F, Castilla M, Berenguel M. Multiobjective control architecture to estimate optimal set points for user comfort and energy saving in buildings. ISA Trans 2020;99:454–64. doi:10.1016/j.isatra.2019.10.006.

[13] Li X, Malkawi A. Multi-objective optimization for thermal mass model predictive control in small and medium size commercial buildings under summer weather conditions. Energy 2016;112:1194–206. doi:10.1016/j.energy.2016.07.021.

[14] Cui Y, Geng Z, Zhu Q, Han Y. Review: Multi-objective optimization methods and application in energy saving. Energy 2017;125:681–704. doi:10.1016/j.energy.2017.02.174.

[15] Golmohamadi H, Guldstrand Larsen K, Gjøl Jensen P, Riaz Hasrat I. Optimization of power-to-heat flexibility for residential buildings in response to day-ahead electricity price. Energy Build 2021;232:110665. doi:10.1016/j.enbuild.2020.110665.

[16] Hu M, Xiao F, Jørgensen JB, Li R. Price-responsive model predictive control of floor heating systems for demand response using building thermal mass. Appl Therm Eng 2019. doi:10.1016/j.applthermaleng.2019.02.107.

[17] Krishnamurthy CKB, Vesterberg M, Böök H, Lindfors A V., Svento R. Real-time pricing revisited: Demand flexibility in the presence of micro-generation. Energy Policy 2018. doi:10.1016/j.enpol.2018.08.024.

[18] Eid C, Codani P, Perez Y, Reneses J, Hakvoort R. Managing electric flexibility from Distributed Energy Resources: A review of incentives for market design. Renew Sustain Energy Rev 2016. doi:10.1016/j.rser.2016.06.008.

[19] Tennet.eu. Onbalansprijssystematiek - Hoe komen de geldstromen tot stand? 2019.

[20] Tang H, Wang S, Li H. Flexibility categorization, sources, capabilities and technologies for energy-flexible and grid-responsive buildings: State-of-the-art and future perspective. Energy 2021;219:119598. doi:10.1016/j.energy.2020.119598.

[21] Sharda S, Singh M, Sharma K. Demand side management through load shifting in IoT based HEMS: Overview, challenges and opportunities. Sustain Cities Soc 2021;65:102517. doi:10.1016/j.scs.2020.102517.

[22] Kühnlenz F, Nardelli PHJ, Karhinen S, Svento R. Implementing flexible demand: Real-time price vs. market integration. Energy 2018;149:550–65. doi:10.1016/j.energy.2018.02.024.

[23] Kohlhepp P, Harb H, Wolisz H, Waczowicz S, Müller D, Hagenmeyer V. Large-scale grid integration of residential thermal energy storages as demand-side flexibility resource: A review of international field studies. Renew Sustain Energy Rev 2019. doi:10.1016/j.rser.2018.09.045.

[24] EPEX Spot. Trading on EPEX SPOT 2019-2020, 2018.

[25] Roos A, Bolkesjø TF. Value of demand flexibility on spot and reserve electricity markets in future power system with increased shares of variable renewable energy. Energy 2018;144:207–17. doi:10.1016/j.energy.2017.11.146.

[26] Salpakari J, Rasku T, Lindgren J, Lund PD. Flexibility of electric vehicles and space heating in net zero energy houses: an optimal control model with thermal dynamics and battery degradation. Appl Energy 2017. doi:10.1016/j.apenergy.2017.01.005.

[27] Federal Ministry for Economic Affairs and Energy - Germany. Electricity Market of the Future 2020. https://www.bmwi.de/Redaktion/EN/Dossier/electricity-market-of-the-future.html.

[28] Netztransparenz.de. Kapazitätsreserve 2020. https://www.netztransparenz.de/EnWG/Kapazitaetsreserve.

[29] Arteconi A, Mugnini A, Polonara F. Energy flexible buildings: A methodology for rating the flexibility performance of buildings with electric heating and cooling systems. Appl Energy 2019;251:113387. doi:10.1016/j.apenergy.2019.113387.

[30] De Groote M, Volt J, Bean F. IS EUROPE READY FOR THE SMART BUILDINGS REVOLUTION? MAPPING SMART-READINESS AND INNOVATIVE CASE STUDIES www.bpie.eu/publication/is-europe-ready-for-the-smart-buildings-revolution/ 2017.

[31] VITO. Summary of State of Affairs in 2nd Technical Support Study on the smart readiness indicator for buildings. 2019.

7

Conclusions

This thesis demonstrated the application of demand flexibility (i.e. energy flexibility) of power-to-heat and thermal energy storage in real-life including the essential steps of identification, quantification, and activation of demand flexibility. *First*, to identify demand flexibility, it required to describe in detail the main characteristics of demand flexibility of power-to-heat and thermal energy storage for optimal control. *Second*, to quantify demand flexibility, adequate performance indicators were used. Furthermore, performance indicators were developed for the use in optimal control. *Third*, to activate demand flexibility, optimal control methods were developed and tested for building heating systems including power-to-heat and thermal energy storage.

An optimal controller was introduced, which was an MPC framework that implemented predictions of time-varying dynamics of building and heating systems, weather forecasting and grid signal support. Because heating systems including HP and TES mostly slowly respond to variations, grid signal support was investigated for a time scale between 5 min and 1 d. To provide potential flexibility in relation to the power grid, the MPC framework included price-based signals (i.e. price-based demand response) that were day-ahead and imbalance electricity prices. This makes it possible to participate in real-time markets such as balancing markets, spot-markets and flexibility markets. For example, spot markets trade electricity the day-ahead up to 1 h before real-time and flexibility markets achieve close to real-time regulation of flexibility.

The activation of buildings' demand flexibility in real-time markets depends on the availability of flexibility, the technical implementation of flexibility and market penetration of flexibility services. To date, researchers have developed strategies to deploy flexibility in real-time power markets. However, many studies have neglected technical implementations and lack validations through experimental investigations.

This thesis demonstrated the activation of buildings' demand flexibility in real-time markets through experimental investigations. In the first experimental case study, a control method was introduced and tested (testing period of one day) to maximize demand flexibility in an optimal control framework. An objective function was created, where operational costs of energy usage were associated with demand flexibility. This makes it possible to include control objectives such as load shifting, peak shaving, energy consumption, self-consumption, grid feed-in, and CO_2 emissions. As the developed control method requires including various pricing signals, the system operator needs to provide these pricing signals to the building's energy management system. In the second experimental case study, to activate buildings' demand flexibility in real-time markets, a one-way price-based flexibility service was developed that can be used in balancing, spot, flexibility and reserve markets. This flexibility service was tested (testing period of one day) and validated in an experimental case study where demand flexibility was dynamically optimized using the MPC framework.

The building's energy management system implemented the MPC and the one-way trading process. The absence of negotiation phases could speed up the real-life application of the MPC. For future applications and implementations into existing markets, the one-way trading process may stimulate system operators to develop new learning strategies for power forecasting.

This thesis made the step towards activation of demand flexibility of building heating systems in relation to the power grid through real-life investigations. To activate flexibility in energy systems, more attention must be paid to real-life applications of optimal control and the development of innovative flexibility services as these services are crucial steps towards flexible electricity markets and flexibility markets. Consequently, establishing flexibility markets, including advanced control strategies, is a major milestone in the development of demand response strategies and demand-side management programs.

Future research

The successful integration of model-based predictive controllers into real-life applications can encourage other researchers to develop and apply innovative control solutions. For optimal control, it is noted that researchers primarily use simplified modelling techniques. In this thesis, complex and fast performing modelling techniques were developed and integrated into an optimal control framework. One may say that optimal control requires complex modelling techniques and that simplified modelling techniques are not suitable for optimal control. This may be true for real-life applications that require a high prediction performance. However, what quality of prediction performance is required to provide robust and reliable optimal control of buildings' demand flexibility in relation to the power grid? Therefore, innovative benchmarking methods are needed for optimal control of buildings' demand flexibility.

This study investigated the demand flexibility of power-to-heat and thermal energy storage in relation to the power grid. The demand flexibility of short duration (up to 24 h) was determined for TES systems (buffer tanks including water, phase change materials, and thermochemical materials). As these TES systems can also be designed to store thermal energy of intermediate and long duration (> 24 h), demand flexibility can be provided for a prediction horizon of > 24 h. Consequently, can building energy systems implement short-term, mid-term and seasonal thermal storage capacities to provide demand flexibility? And how can advanced control methods such as optimal control regulate building energy systems including short-term, mid-term and seasonal storage? One possible solution may be the combination of short-term water buffer tanks and seasonal thermochemical heat storage. Seasonal storage can be used during periods with high demand and low rate of production from renewable sources. During these periods the seasonal storage can be discharged by the water buffer tank, which on one hand can exploit the storage capacity of the thermochemical reactor and on the other hand, can provide short-term demand flexibility. As short-term flexibility in relation to the power grid can also be provided by power-to-X such as power-to-gas or electrical batteries, the scheduling of different storage technologies will depend on the availability of renewable sources, the technical implementation of storage technologies, and the availability of flexibility service and markets. Therefore, research activities must focus on real-life implementations and optimal control of different storage technologies.

List of figures

List of tables

List of publications

International journals

C. Finck, R. Li, W. Zeiler, "Optimal control of demand flexibility under real-time pricing for heating systems in buildings: A real-life demonstration", Applied Energy 263 (2020): 114671. https://doi.org/10.1016/j.apenergy.2020.114671

C. Finck, R. Li, and W. Zeiler, "Identification of a dynamic system model for a building and heating system including heat pump and thermal energy storage", MethodsX 7 (2020): 100866. https://doi.org/10.1016/j.mex.2020.100866

C. Finck, R. Li, and W. Zeiler, "Economic model predictive control for demand flexibility of a residential building", Energy 176 (2019): pp. 365-379. https://doi.org/10.1016/j.energy.2019.03.171

C. Finck, R. Kramer, R. Li, and W. Zeiler, "Quantifying demand flexibility of power-to-heat and thermal energy storage in the control of building heating systems", Applied Energy 209 (2018): pp. 409-425. https://doi.org/10.1016/j.apenergy.2017.11.036

R. Li, G. Dane, C. Finck, W. Zeiler, "Are building users prepared for energy flexible buildings?—A large-scale survey in the Netherlands", Applied Energy 203 (2017): pp. 623-634. https://doi.org/10.1016/j.apenergy.2017.06.067

C. Finck, R. Li, W. Zeiler, "An optimization strategy for scheduling various thermal energy storage technologies in office buildings connected to smart grid", Energy Procedia 78 (2015): pp. 806-811. https://doi.org/10.1016/j.egypro.2015.11.105

International reports

A. Santos, B. Jørgensen, H. Kazmi, R. Ruusu, A. Hasan, T. Péan, Y. Zhou, S. Cao, Y. Yu, J. Clauß, R. Junker, C. Finck, D. Christantoni, D. Finn, A. Derakhtenjani, J. Candanedo, A. Athienitis, A. Kathirgamanathan, "Control strategies and algorithms for obtaining energy flexibility in buildings" IEA EBC Annex 67 (2019). https://annex67.org/media/1898/control-strategies.pdf

S. Jensen, J. Parker, P. Engelmann, A. Marszal, H. Johra, T. Weiss, T. Péan, A. Derakhtenjani, J. Candanedo, A. Athienitis, E. Mlecnik, I. De Jaeger, D. Saelens, H. Kazmi, I. Vigna, M. Lovati, R. Pernetti, R. Lollini, Y. Yu, K. Klein, L. Frison, Y. Zhou, S. Cao, J. Le Dréau, L. Aelenei, S. O'Connell, M. Kean, D. Aelenei, K. Zhang, J. Meulemans, M. Brennenstuhl, M. Yadack, U. Eicker, K. Foteinaki, R. Junker, R. Li, C. Finck, S. Mohammadi, F. Wang, A. Kathirgamanathan, D. Christantoni, D. Finn, F. D'Ettorre, K. Murphy, M. De Rosa, M. Saffari, E. Mangina, M. Hall,

A. Santos, K. Arendt, G. Reynders, R. Ruusu, A. Hasan, “Examples of Energy Flexibility in Buildings”, IEA EBC Annex 67 (2019). https://annex67.org/media/1921/examples-of-energy-flexibility-in-buildings.pdf

C. Finck, J. Clauß, P. Vogler-Finck, P. Beagon, K. Zhan, H. Kazmi, “Review of applied and tested control possibilities for energy flexibility in buildings”, IEA EBC Annex 67 (2018). doi:10.13140/RG.2.2.28740.73609, https://annex67.org/media/1551/review-of-applied-and-tested-control-possibilities-for-energy-flexibility-in-buildings-technical-report-annex67.pdf

Conference proceedings

C. Finck, R. Li, W. Zeiler, “Performance maps for the control of thermal energy storage”, 15th Int Conf Int Build Perform Simul Assoc (2017)

J. Clauß, C. Finck C, P. Vogler-Finck, P. Beagon, “Control strategies for building energy systems to unlock demand side flexibility – A review”, 15th Int Conf Int Build Perform Simul Assoc (2017)

C. Finck, R. Li, W. Zeiler, “Operation of heat pumps for smart grid integrated buildings with thermal energy storage”, IEA Heat Pump Conference (2017)

C. Finck, R. Li, “Operational load shaping of office buildings connected to thermal energy storage using dynamic programming”, Proc. 12th REHVA World congress CLIMA2016 (2016) Vol. 10 Pap. 70

National journals

C. Finck, G. Boxem, W. Zeiler, “Thermische opslagtechnieken in gebouwen”, TVVL Magazine (2015)

Curriculum Vitae

Christian Finck was born on 27.09.1979 in Halle (Saale), Germany. After graduating as industrial & business engineer in 2007 at Martin-Luther-University in Halle/Wittenberg, Germany, he worked as an energy engineer, researcher and scientist at Technische Universität Berlin, Germany and Netherlands Organisation for Applied Scientific Research (TNO), the Netherlands. In 2014 he started a PhD project at Building Services at Eindhoven University of Technology, the Netherlands. Since 2020, he has been working on sustainable building systems and applications of artificial intelligence in renewable energy systems.

Bouwstenen is een publicatiereeks
van de Faculteit Bouwkunde,
Technische Universiteit Eindhoven.
Zij presenteert resultaten van
onderzoek en andere activiteiten op
het vakgebied der Bouwkunde,
uitgevoerd in het kader van deze
Faculteit.

Bouwstenen en andere proefschriften van de
TU/e zijn online beschikbaar via:
https://research.tue.nl/

Reeds verschenen in de serie
Bouwstenen

nr 1
Elan: A Computer Model for Building Energy Design: Theory and Validation
Martin H. de Wit
H.H. Driessen
R.M.M. van der Velden

nr 2
Kwaliteit, Keuzevrijheid en Kosten: Evaluatie van Experiment Klarendal, Arnhem
J. Smeets
C. le Nobel
M. Broos
J. Frenken
A. v.d. Sanden

nr 3
Crooswijk: Van 'Bijzonder' naar 'Gewoon'
Vincent Smit
Kees Noort

nr 4
Staal in de Woningbouw
Edwin J.F. Delsing

nr 5
Mathematical Theory of Stressed Skin Action in Profiled Sheeting with Various Edge Conditions
Andre W.A.M.J. van den Bogaard

nr 6
Hoe Berekenbaar en Betrouwbaar is de Coëfficiënt k in x-ksigma en x-ks?
K.B. Lub
A.J. Bosch

nr 7
Het Typologisch Gereedschap: Een Verkennende Studie Omtrent Typologie en Omtrent de Aanpak van Typologisch Onderzoek
J.H. Luiten

nr 8
Informatievoorziening en Beheerprocessen
A. Nauta
Jos Smeets (red.)
Helga Fassbinder (projectleider)
Adrie Proveniers
J. v.d. Moosdijk

nr 9
Strukturering en Verwerking van Tijdgegevens voor de Uitvoering van Bouwwerken
ir. W.F. Schaefer
P.A. Erkelens

nr 10
Stedebouw en de Vorming van een Speciale Wetenschap
K. Doevendans

nr 11
Informatica en Ondersteuning van Ruimtelijke Besluitvorming
G.G. van der Meulen

nr 12
Staal in de Woningbouw, Korrosie-Bescherming van de Begane Grondvloer
Edwin J.F. Delsing

nr 13
Een Thermisch Model voor de Berekening van Staalplaatbetonvloeren onder Brandomstandigheden
A.F. Hamerlinck

nr 14
De Wijkgedachte in Nederland: Gemeenschapsstreven in een Stedebouwkundige Context
K. Doevendans
R. Stolzenburg

nr 15
Diaphragm Effect of Trapezoidally Profiled Steel Sheets: Experimental Research into the Influence of Force Application
Andre W.A.M.J. van den Bogaard

nr 16
Versterken met Spuit-Ferrocement: Het Mechanische Gedrag van met Spuit-Ferrocement Versterkte Gewapend Betonbalken
K.B. Lubir
M.C.G. van Wanroy

nr 17
De Tractaten van Jean Nicolas Louis Durand
G. van Zeyl

nr 18
Wonen onder een Plat Dak: Drie Opstellen over Enkele Vooronderstellingen van de Stedebouw
K. Doevendans

nr 19
Supporting Decision Making Processes: A Graphical and Interactive Analysis of Multivariate Data
W. Adams

nr 20
Self-Help Building Productivity: A Method for Improving House Building by Low-Income Groups Applied to Kenya 1990-2000
P. A. Erkelens

nr 21
De Verdeling van Woningen: Een Kwestie van Onderhandelen
Vincent Smit

nr 22
Flexibiliteit en Kosten in het Ontwerpproces: Een Besluitvormingondersteunend Model
M. Prins

nr 23
Spontane Nederzettingen Begeleid: Voorwaarden en Criteria in Sri Lanka
Po Hin Thung

nr 24
Fundamentals of the Design of Bamboo Structures
Oscar Arce-Villalobos

nr 25
Concepten van de Bouwkunde
M.F.Th. Bax (red.)
H.M.G.J. Trum (red.)

nr 26
Meaning of the Site
Xiaodong Li

nr 27
Het Woonmilieu op Begrip Gebracht: Een Speurtocht naar de Betekenis van het Begrip 'Woonmilieu'
Jaap Ketelaar

nr 28
Urban Environment in Developing Countries
editors: Peter A. Erkelens
George G. van der Meulen (red.)

nr 29
Stategische Plannen voor de Stad: Onderzoek en Planning in Drie Steden
prof.dr. H. Fassbinder (red.)
H. Rikhof (red.)

nr 30
Stedebouwkunde en Stadsbestuur
Piet Beekman

nr 31
De Architectuur van Djenné: Een Onderzoek naar de Historische Stad
P.C.M. Maas

nr 32
Conjoint Experiments and Retail Planning
Harmen Oppewal

nr 33
Strukturformen Indonesischer Bautechnik: Entwicklung Methodischer Grundlagen für eine 'Konstruktive Pattern Language' in Indonesien
Heinz Frick arch. SIA

nr 34
Styles of Architectural Designing: Empirical Research on Working Styles and Personality Dispositions
Anton P.M. van Bakel

nr 35
Conjoint Choice Models for Urban Tourism Planning and Marketing
Benedict Dellaert

nr 36
Stedelijke Planvorming als Co-Produktie
Helga Fassbinder (red.)

nr 37
Design Research in the Netherlands
editors: R.M. Oxman
M.F.Th. Bax
H.H. Achten

nr 38
Communication in the Building Industry
Bauke de Vries

nr 39
Optimaal Dimensioneren van Gelaste Plaatliggers
J.B.W. Stark
F. van Pelt
L.F.M. van Gorp
B.W.E.M. van Hove

nr 40
Huisvesting en Overwinning van Armoede
P.H. Thung
P. Beekman (red.)

nr 41
Urban Habitat: The Environment of Tomorrow
George G. van der Meulen
Peter A. Erkelens

nr 42
A Typology of Joints
John C.M. Olie

nr 43
Modeling Constraints-Based Choices for Leisure Mobility Planning
Marcus P. Stemerding

nr 44
Activity-Based Travel Demand Modeling
Dick Ettema

nr 45
Wind-Induced Pressure Fluctuations on Building Facades
Chris Geurts

nr 46
Generic Representations
Henri Achten

nr 47
Johann Santini Aichel: Architectuur en Ambiguiteit
Dirk De Meyer

nr 48
Concrete Behaviour in Multiaxial Compression
Erik van Geel

nr 49
Modelling Site Selection
Frank Witlox

nr 50
Ecolemma Model
Ferdinand Beetstra

nr 51
Conjoint Approaches to Developing Activity-Based Models
Donggen Wang

nr 52
On the Effectiveness of Ventilation
Ad Roos

nr 53
Conjoint Modeling Approaches for Residential Group preferences
Eric Molin

nr 54
Modelling Architectural Design Information by Features
Jos van Leeuwen

nr 55
A Spatial Decision Support System for the Planning of Retail and Service Facilities
Theo Arentze

nr 56
Integrated Lighting System Assistant
Ellie de Groot

nr 57
Ontwerpend Leren, Leren Ontwerpen
J.T. Boekholt

nr 58
Temporal Aspects of Theme Park Choice Behavior
Astrid Kemperman

nr 59
Ontwerp van een Geïndustrialiseerde Funderingswijze
Faas Moonen

nr 60
Merlin: A Decision Support System for Outdoor Leisure Planning
Manon van Middelkoop

nr 61
The Aura of Modernity
Jos Bosman

nr 62
Urban Form and Activity-Travel Patterns
Daniëlle Snellen

nr 63
Design Research in the Netherlands 2000
Henri Achten

nr 64
Computer Aided Dimensional Control in Building Construction
Rui Wu

nr 65
Beyond Sustainable Building
editors: Peter A. Erkelens
Sander de Jonge
August A.M. van Vliet
co-editor: Ruth J.G. Verhagen

nr 66
Das Globalrecyclingfähige Haus
Hans Löfflad

nr 67
Cool Schools for Hot Suburbs
René J. Dierkx

nr 68
A Bamboo Building Design Decision Support Tool
Fitri Mardjono

nr 69
Driving Rain on Building Envelopes
Fabien van Mook

nr 70
Heating Monumental Churches
Henk Schellen

nr 71
Van Woningverhuurder naar Aanbieder van Woongenot
Patrick Dogge

nr 72
Moisture Transfer Properties of Coated Gypsum
Emile Goossens

nr 73
Plybamboo Wall-Panels for Housing
Guillermo E. González-Beltrán

nr 74
The Future Site-Proceedings
Ger Maas
Frans van Gassel

nr 75
Radon transport in Autoclaved Aerated Concrete
Michel van der Pal

nr 76
The Reliability and Validity of Interactive Virtual Reality Computer Experiments
Amy Tan

nr 77
Measuring Housing Preferences Using Virtual Reality and Belief Networks
Maciej A. Orzechowski

nr 78
Computational Representations of Words and Associations in Architectural Design
Nicole Segers

nr 79
Measuring and Predicting Adaptation in Multidimensional Activity-Travel Patterns
Chang-Hyeon Joh

nr 80
Strategic Briefing
Fayez Al Hassan

nr 81
Well Being in Hospitals
Simona Di Cicco

nr 82
Solares Bauen: Implementierungs- und Umsetzungs-Aspekte in der Hochschulausbildung in Österreich
Gerhard Schuster

nr 83
Supporting Strategic Design of Workplace Environments with Case-Based Reasoning
Shauna Mallory-Hill

nr 84
ACCEL: A Tool for Supporting Concept Generation in the Early Design Phase
Maxim Ivashkov

nr 85
Brick-Mortar Interaction in Masonry under Compression
Ad Vermeltfoort

nr 86
Zelfredzaam Wonen
Guus van Vliet

nr 87
Een Ensemble met Grootstedelijke Allure
Jos Bosman
Hans Schippers

nr 88
On the Computation of Well-Structured Graphic Representations in Architectural Design
Henri Achten

nr 89
De Evolutie van een West-Afrikaanse Vernaculaire Architectuur
Wolf Schijns

nr 90
ROMBO Tactiek
Christoph Maria Ravesloot

nr 91
External Coupling between Building Energy Simulation and Computational Fluid Dynamics
Ery Djunaedy

nr 92
Design Research in the Netherlands 2005
editors: Henri Achten
Kees Dorst
Pieter Jan Stappers
Bauke de Vries

nr 93
Ein Modell zur Baulichen Transformation
Jalil H. Saber Zaimian

nr 94
Human Lighting Demands: Healthy Lighting in an Office Environment
Myriam Aries

nr 95
A Spatial Decision Support System for the Provision and Monitoring of Urban Greenspace
Claudia Pelizaro

nr 96
Leren Creëren
Adri Proveniers

nr 97
Simlandscape
Rob de Waard

nr 98
Design Team Communication
Ad den Otter

nr 99
Humaan-Ecologisch Georiënteerde Woningbouw
Juri Czabanowski

nr 100
Hambase
Martin de Wit

nr 101
Sound Transmission through Pipe Systems and into Building Structures
Susanne Bron-van der Jagt

nr 102
Het Bouwkundig Contrapunt
Jan Francis Boelen

nr 103
A Framework for a Multi-Agent Planning Support System
Dick Saarloos

nr 104
Bracing Steel Frames with Calcium Silicate Element Walls
Bright Mweene Ng'andu

nr 105
Naar een Nieuwe Houtskeletbouw
F.N.G. De Medts

nr 106 and 107
Niet gepubliceerd

nr 108
Geborgenheid
T.E.L. van Pinxteren

nr 109
Modelling Strategic Behaviour in Anticipation of Congestion
Qi Han

nr 110
Reflecties op het Woondomein
Fred Sanders

nr 111
On Assessment of Wind Comfort by Sand Erosion
Gábor Dezsö

nr 112
Bench Heating in Monumental Churches
Dionne Limpens-Neilen

nr 113
RE. Architecture
Ana Pereira Roders

nr 114
Toward Applicable Green Architecture
Usama El Fiky

nr 115
Knowledge Representation under Inherent Uncertainty in a Multi-Agent System for Land Use Planning
Liying Ma

nr 116
Integrated Heat Air and Moisture Modeling and Simulation
Jos van Schijndel

nr 117
Concrete Behaviour in Multiaxial Compression
J.P.W. Bongers

nr 118
The Image of the Urban Landscape
Ana Moya Pellitero

nr 119
The Self-Organizing City in Vietnam
Stephanie Geertman

nr 120
A Multi-Agent Planning Support System for Assessing Externalities of Urban Form Scenarios
Rachel Katoshevski-Cavari

nr 121
Den Schulbau Neu Denken, Fühlen und Wollen
Urs Christian Maurer-Dietrich

nr 122
Peter Eisenman Theories and Practices
Bernhard Kormoss

nr 123
User Simulation of Space Utilisation
Vincent Tabak

nr 125
In Search of a Complex System Model
Oswald Devisch

nr 126
Lighting at Work: Environmental Study of Direct Effects of Lighting Level and Spectrum on Psycho-Physiological Variables
Grazyna Górnicka

nr 127
Flanking Sound Transmission through Lightweight Framed Double Leaf Walls
Stefan Schoenwald

nr 128
Bounded Rationality and Spatio-Temporal Pedestrian Shopping Behavior
Wei Zhu

nr 129
Travel Information: Impact on Activity Travel Pattern
Zhongwei Sun

nr 130
Co-Simulation for Performance Prediction of Innovative Integrated Mechanical Energy Systems in Buildings
Marija Trčka

nr 131
Niet gepubliceerd

nr 132
Architectural Cue Model in Evacuation Simulation for Underground Space Design
Chengyu Sun

nr 133
Uncertainty and Sensitivity Analysis in Building Performance Simulation for Decision Support and Design Optimization
Christina Hopfe

nr 134
Facilitating Distributed Collaboration in the AEC/FM Sector Using Semantic Web Technologies
Jacob Beetz

nr 135
Circumferentially Adhesive Bonded Glass Panes for Bracing Steel Frame in Façades
Edwin Huveners

nr 136
Influence of Temperature on Concrete Beams Strengthened in Flexure with CFRP
Ernst-Lucas Klamer

nr 137
Sturen op Klantwaarde
Jos Smeets

nr 139
Lateral Behavior of Steel Frames with Discretely Connected Precast Concrete Infill Panels
Paul Teewen

nr 140
Integral Design Method in the Context of Sustainable Building Design
Perica Savanović

nr 141
Household Activity-Travel Behavior: Implementation of Within-Household Interactions
Renni Anggraini

nr 142
Design Research in the Netherlands 2010
Henri Achten

nr 143
Modelling Life Trajectories and Transport Mode Choice Using Bayesian Belief Networks
Marloes Verhoeven

nr 144
Assessing Construction Project Performance in Ghana
William Gyadu-Asiedu

nr 145
Empowering Seniors through Domotic Homes
Masi Mohammadi

nr 146
An Integral Design Concept for Ecological Self-Compacting Concrete
Martin Hunger

nr 147
Governing Multi-Actor Decision Processes in Dutch Industrial Area Redevelopment
Erik Blokhuis

nr 148
A Multifunctional Design Approach for Sustainable Concrete
Götz Hüsken

nr 149
Quality Monitoring in Infrastructural Design-Build Projects
Ruben Favié

nr 150
Assessment Matrix for Conservation of Valuable Timber Structures
Michael Abels

nr 151
Co-simulation of Building Energy Simulation and Computational Fluid Dynamics for Whole-Building Heat, Air and Moisture Engineering
Mohammad Mirsadeghi

nr 152
External Coupling of Building Energy Simulation and Building Element Heat, Air and Moisture Simulation
Daniel Cóstola

nr 153
Adaptive Decision Making In Multi-Stakeholder Retail Planning
Ingrid Janssen

nr 154
Landscape Generator
Kymo Slager

nr 155
Constraint Specification in Architecture
Remco Niemeijer

nr 156
A Need-Based Approach to Dynamic Activity Generation
Linda Nijland

nr 157
Modeling Office Firm Dynamics in an Agent-Based Micro Simulation Framework
Gustavo Garcia Manzato

nr 158
Lightweight Floor System for Vibration Comfort
Sander Zegers

nr 159
Aanpasbaarheid van de Draagstructuur
Roel Gijsbers

nr 160
'Village in the City' in Guangzhou, China
Yanliu Lin

nr 161
Climate Risk Assessment in Museums
Marco Martens

nr 162
Social Activity-Travel Patterns
Pauline van den Berg

nr 163
Sound Concentration Caused by Curved Surfaces
Martijn Vercammen

nr 164
Design of Environmentally Friendly Calcium Sulfate-Based Building Materials: Towards an Improved Indoor Air Quality
Qingliang Yu

nr 165
Beyond Uniform Thermal Comfort on the Effects of Non-Uniformity and Individual Physiology
Lisje Schellen

nr 166
Sustainable Residential Districts
Gaby Abdalla

nr 167
Towards a Performance Assessment Methodology using Computational Simulation for Air Distribution System Designs in Operating Rooms
Mônica do Amaral Melhado

nr 168
Strategic Decision Modeling in Brownfield Redevelopment
Brano Glumac

nr 169
Pamela: A Parking Analysis Model for Predicting Effects in Local Areas
Peter van der Waerden

nr 170
A Vision Driven Wayfinding Simulation-System Based on the Architectural Features Perceived in the Office Environment
Qunli Chen

nr 171
Measuring Mental Representations Underlying Activity-Travel Choices
Oliver Horeni

nr 172
Modelling the Effects of Social Networks on Activity and Travel Behaviour
Nicole Ronald

nr 173
Uncertainty Propagation and Sensitivity Analysis Techniques in Building Performance Simulation to Support Conceptual Building and System Design
Christian Struck

nr 174
Numerical Modeling of Micro-Scale Wind-Induced Pollutant Dispersion in the Built Environment
Pierre Gousseau

nr 175
Modeling Recreation Choices over the Family Lifecycle
Anna Beatriz Grigolon

nr 176
Experimental and Numerical Analysis of Mixing Ventilation at Laminar, Transitional and Turbulent Slot Reynolds Numbers
Twan van Hooff

nr 177
Collaborative Design Support: Workshops to Stimulate Interaction and Knowledge Exchange Between Practitioners
Emile M.C.J. Quanjel

nr 178
Future-Proof Platforms for Aging-in-Place
Michiel Brink

nr 179
Motivate: A Context-Aware Mobile Application for Physical Activity Promotion
Yuzhong Lin

nr 180
Experience the City: Analysis of Space-Time Behaviour and Spatial Learning
Anastasia Moiseeva

nr 181
Unbonded Post-Tensioned Shear Walls of Calcium Silicate Element Masonry
Lex van der Meer

nr 182
Construction and Demolition Waste Recycling into Innovative Building Materials for Sustainable Construction in Tanzania
Mwita M. Sabai

nr 183
Durability of Concrete with Emphasis on Chloride Migration
Przemysław Spiesz

nr 184
Computational Modeling of Urban Wind Flow and Natural Ventilation Potential of Buildings
Rubina Ramponi

nr 185
A Distributed Dynamic Simulation Mechanism for Buildings Automation and Control Systems
Azzedine Yahiaoui

nr 186
Modeling Cognitive Learning of Urban Networks in Daily Activity-Travel Behavior
Şehnaz Cenani Durmazoğlu

nr 187
Functionality and Adaptability of Design Solutions for Public Apartment Buildings in Ghana
Stephen Agyefi-Mensah

nr 188
A Construction Waste Generation Model for Developing Countries
Lilliana Abarca-Guerrero

nr 189
Synchronizing Networks: The Modeling of Supernetworks for Activity-Travel Behavior
Feixiong Liao

nr 190
Time and Money Allocation Decisions in Out-of-Home Leisure Activity Choices
Gamze Zeynep Dane

nr 191
How to Measure Added Value of CRE and Building Design
Rianne Appel-Meulenbroek

nr 192
Secondary Materials in Cement-Based Products: Treatment, Modeling and Environmental Interaction
Miruna Florea

nr 193
Concepts for the Robustness Improvement of Self-Compacting Concrete: Effects of Admixtures and Mixture Components on the Rheology and Early Hydration at Varying Temperatures
Wolfram Schmidt

nr 194
Modelling and Simulation of Virtual Natural Lighting Solutions in Buildings
Rizki A. Mangkuto

nr 195
Nano-Silica Production at Low Temperatures from the Dissolution of Olivine - Synthesis, Tailoring and Modelling
Alberto Lazaro Garcia

nr 196
Building Energy Simulation Based Assessment of Industrial Halls for Design Support
Bruno Lee

nr 197
Computational Performance Prediction of the Potential of Hybrid Adaptable Thermal Storage Concepts for Lightweight Low-Energy Houses
Pieter-Jan Hoes

nr 198
Application of Nano-Silica in Concrete
George Quercia Bianchi

nr 199
Dynamics of Social Networks and Activity Travel Behaviour
Fariya Sharmeen

nr 200
Building Structural Design Generation and Optimisation including Spatial Modification
Juan Manuel Davila Delgado

nr 201
Hydration and Thermal Decomposition of Cement/Calcium-Sulphate Based Materials
Ariën de Korte

nr 202
Republiek van Beelden:
De Politieke Werkingen van het Ontwerp in Regionale Planvorming
Bart de Zwart

nr 203
Effects of Energy Price Increases on Individual Activity-Travel Repertoires and Energy Consumption
Dujuan Yang

nr 204
Geometry and Ventilation:
Evaluation of the Leeward Sawtooth Roof Potential in the Natural Ventilation of Buildings
Jorge Isaac Perén Montero

nr 205
Computational Modelling of Evaporative Cooling as a Climate Change Adaptation Measure at the Spatial Scale of Buildings and Streets
Hamid Montazeri

nr 206
Local Buckling of Aluminium Beams in Fire Conditions
Ronald van der Meulen

nr 207
Historic Urban Landscapes:
Framing the Integration of Urban and Heritage Planning in Multilevel Governance
Loes Veldpaus

nr 208
Sustainable Transformation of the Cities:
Urban Design Pragmatics to Achieve a Sustainable City
Ernesto Antonio Zumelzu Scheel

nr 209
Development of Sustainable Protective Ultra-High Performance Fibre Reinforced Concrete (UHPFRC):
Design, Assessment and Modeling
Rui Yu

nr 210
Uncertainty in Modeling Activity-Travel Demand in Complex Uban Systems
Soora Rasouli

nr 211
Simulation-based Performance Assessment of Climate Adaptive Greenhouse Shells
Chul-sung Lee

nr 212
Green Cities:
Modelling the Spatial Transformation of the Urban Environment using Renewable Energy Technologies
Saleh Mohammadi

nr 213
A Bounded Rationality Model of Short and Long-Term Dynamics of Activity-Travel Behavior
Ifigeneia Psarra

nr 214
Effects of Pricing Strategies on Dynamic Repertoires of Activity-Travel Behaviour
Elaheh Khademi

nr 215
Handstorm Principles for Creative and Collaborative Working
Frans van Gassel

nr 216
Light Conditions in Nursing Homes: Visual Comfort and Visual Functioning of Residents
Marianne M. Sinoo

nr 217
Woonsporen: De Sociale en Ruimtelijke Biografie van een Stedelijk Bouwblok in de Amsterdamse Transvaalbuurt
Hüseyin Hüsnü Yegenoglu

nr 218
Studies on User Control in Ambient Intelligent Systems
Berent Willem Meerbeek

nr 219
Daily Livings in a Smart Home: Users' Living Preference Modeling of Smart Homes
Erfaneh Allameh

nr 220
Smart Home Design: Spatial Preference Modeling of Smart Homes
Mohammadali Heidari Jozam

nr 221
Wonen: Discoursen, Praktijken, Perspectieven
Jos Smeets

nr 222
Personal Control over Indoor Climate in Offices: Impact on Comfort, Health and Productivity
Atze Christiaan Boerstra

nr 223
Personalized Route Finding in Multimodal Transportation Networks
Jianwe Zhang

nr 224
The Design of an Adaptive Healing Room for Stroke Patients
Elke Daemen

nr 225
Experimental and Numerical Analysis of Climate Change Induced Risks to Historic Buildings and Collections
Zara Huijbregts

nr 226
Wind Flow Modeling in Urban Areas Through Experimental and Numerical Techniques
Alessio Ricci

nr 227
Clever Climate Control for Culture: Energy Efficient Indoor Climate Control Strategies for Museums Respecting Collection Preservation and Thermal Comfort of Visitors
Rick Kramer

nr 228
Fatigue Life Estimation of Metal Structures Based on Damage Modeling
Sarmediran Silitonga

nr 229
A multi-agents and occupancy based strategy for energy management and process control on the room-level
Timilehin Moses Labeodan

nr 230
Environmental assessment of Building Integrated Photovoltaics: Numerical and Experimental Carrying Capacity Based Approach
Michiel Ritzen

nr 231
Performance of Admixture and Secondary Minerals in Alkali Activated Concrete: Sustaining a Concrete Future
Arno Keulen

nr 232
World Heritage Cities and Sustainable Urban Development: Bridging Global and Local Levels in Monitoring the Sustainable Urban Development of World Heritage Cities
Paloma C. Guzman Molina

nr 233
Stage Acoustics and Sound Exposure in Performance and Rehearsal Spaces for Orchestras: Methods for Physical Measurements
Remy Wenmaekers

nr 234
Municipal Solid Waste Incineration (MSWI) Bottom Ash: From Waste to Value Characterization, Treatments and Application
Pei Tang

nr 235
Large Eddy Simulations Applied to Wind Loading and Pollutant Dispersion
Mattia Ricci

nr 236
Alkali Activated Slag-Fly Ash Binders: Design, Modeling and Application
Xu Gao

nr 237
Sodium Carbonate Activated Slag: Reaction Analysis, Microstructural Modification & Engineering Application
Bo Yuan

nr 238
Shopping Behavior in Malls
Widiyani

nr 239
Smart Grid-Building Energy Interactions: Demand Side Power Flexibility in Office Buildings
Kennedy Otieno Aduda

nr 240
Modeling Taxis Dynamic Behavior in Uncertain Urban Environments
Zheng Zhong

nr 241
Gap-Theoretical Analyses of Residential Satisfaction and Intention to Move
Wen Jiang

nr 242
Travel Satisfaction and Subjective Well-Being: A Behavioral Modeling Perspective
Yanan Gao

nr 243
Building Energy Modelling to Support the Commissioning of Holistic Data Centre Operation
Vojtech Zavrel

nr 244
Regret-Based Travel Behavior Modeling: An Extended Framework
Sunghoon Jang

nr 245
Towards Robust Low-Energy Houses: A Computational Approach for Performance Robustness Assessment using Scenario Analysis
Rajesh Reddy Kotireddy

nr 246
Development of sustainable and functionalized inorganic binder-biofiber composites
Guillaume Doudart de la Grée

nr 247
A Multiscale Analysis of the Urban Heat Island Effect: From City Averaged Temperatures to the Energy Demand of Individual Buildings
Yasin Toparlar

nr 248
Design Method for Adaptive Daylight Systems for buildings covered by large (span) roofs
Florian Heinzelmann

nr 249
Hardening, high-temperature resistance and acid resistance of one-part geopolymers
Patrick Sturm

nr 250
Effects of the built environment on dynamic repertoires of activity-travel behaviour
Aida Pontes de Aquino

nr 251
Modeling for auralization of urban environments: Incorporation of directivity in sound propagation and analysis of a framework for auralizing a car pass-by
Fotis Georgiou

nr 252
Wind Loads on Heliostats and Photovoltaic Trackers
Andreas Pfahl

nr 253
Approaches for computational performance optimization of innovative adaptive façade concepts
Roel Loonen

nr 254
Multi-scale FEM-DEM Model for Granular Materials: Micro-scale boundary conditions, Statics, and Dynamics
Jiadun Liu

nr 255
Bending Moment - Shear Force Interaction of Rolled I-Shaped Steel Sections
Rianne Willie Adriana Dekker

nr 256
Paralympic tandem cycling and handcycling: Computational and wind tunnel analysis of aerodynamic performance
Paul Fionn Mannion

nr 257
Experimental characterization and numerical modelling of 3D printed concrete: Controlling structural behaviour in the fresh and hardened state
Robert Johannes Maria Wolfs

nr 258
Requirement checking in the building industry: Enabling modularized and extensible requirement checking systems based on semantic web technologies
Chi Zhang

nr 259
A Sustainable Industrial Site Redevelopment Planning Support System
Tong Wang

nr 260
Efficient storage and retrieval of detailed building models: Multi-disciplinary and long-term use of geometric and semantic construction information
Thomas Ferdinand Krijnen

nr 261
The users' value of business center concepts for knowledge sharing and networking behavior within and between organizations
Minou Weijs-Perrée

nr 262
Characterization and improvement of aerodynamic performance of vertical axis wind turbines using computational fluid dynamics (CFD)
Abdolrahim Rezaeiha

nr 263
In-situ characterization of the acoustic impedance of vegetated roofs
Chang Liu

nr 264
Occupancy-based lighting control: Developing an energy saving strategy that ensures office workers' comfort
Christel de Bakker

nr 265
Stakeholders-Oriented Spatial Decision Support System
Cahyono Susetyo

nr 266
Climate-induced damage in oak museum objects
Rianne Aleida Luimes

nr 267
Towards individual thermal comfort: Model predictive personalized control of heating systems
Katarina Katic

nr 268
Modelling and Measuring Quality of Urban Life: Housing, Neighborhood, Transport and Job
Lida Aminian

nr 269
Optimization of an aquifer thermal energy storage system through integrated modelling of aquifer, HVAC systems and building
Basar Bozkaya

nr 270
Numerical modeling for urban sound propagation: developments in wave-based and energy-based methods
Raúl Pagán Muñoz

nr 271
Lighting in multi-user office environments: improving employee wellbeing through personal control
Sanae van der Vleuten-Chraibi

nr 272
A strategy for fit-for-purpose occupant behavior modelling in building energy and comfort performance simulation
Isabella I. Gaetani dell'Aquila d'Aragona

nr 273
Een architectuurhistorische waardestelling van naoorlogse woonwijken in Nederland: Het voorbeeld van de Westelijke Tuinsteden in Amsterdam
Eleonore Henriette Marie Mens

nr 274
Job-Housing Co-Dependent Mobility Decisions in Life Trajectories
Jia Guo

nr 275
A user-oriented focus to create healthcare facilities: decision making on strategic values
Emilia Rosalia Catharina Maria Huisman

nr 276
Dynamics of plane impinging jets at moderate Reynolds numbers – with applications to air curtains
Adelya Khayrullina

nr 277
Valorization of Municipal Solid Waste Incineration Bottom Ash - Chemical Nature, Leachability and Treatments of Hazardous Elements
Qadeer Alam

nr 278
Treatments and valorization of MSWI bottom ash - application in cement-based materials
Veronica Caprai

nr 279
Personal lighting conditions of office workers - input for intelligent systems to optimize subjective alertness
Juliëtte van Duijnhoven

nr 280
Social influence effects in tourism travel: air trip itinerary and destination choices
Xiaofeng Pan

nr 281
Advancing Post-War Housing: Integrating Heritage Impact, Environmental Impact, Hygrothermal Risk and Costs in Renovation Design Decisions
Lisanne Claartje Havinga

nr 282
Impact resistant ultra-high performance fibre reinforced concrete: materials, components and properties
Peipeng Li

nr 283
Demand-driven Science Parks: The Perceived Benefits and Trade-offs of Tenant Firms with regard to Science Park Attributes
Wei Keat Benny Ng

nr 284
Raise the lantern; how light can help to maintain a healthy and safe hospital environment focusing on nurses
Maria Petronella Johanna Aarts

nr 285
Modelling Learning and Dynamic Route and Parking Choice Behaviour under Uncertainty
Elaine Cristina Schneider de Carvalho

nr 286
Identifying indoor local microclimates for safekeeping of cultural heritage
Karin Kompatscher

nr 287
Probabilistic modeling of fatigue resistance for welded and riveted bridge details. Resistance models and estimation of uncertainty.
Davide Leonetti

nr 288
Performance of Layered UHPFRC under Static and Dynamic Loads: Effects of steel fibers, coarse aggregates and layered structures
Yangyueye Cao

nr 289
Photocatalytic abatement of the nitrogen oxide pollution: synthesis, application and long-term evaluation of titania-silica composites
Yuri Hendrix

nr 290
Assessing knowledge adoption in post-disaster reconstruction: Understanding the impact of hazard-resistant construction knowledge on reconstruction processes of self-recovering communities in Nepal and the Philippines
Eefje Hendriks

nr 291
Locating electric vehicle charging stations: A multi-agent based dynamic simulation
Seheon Kim

nr 292
De invloed van Lean Management op de beheersing van het bouwproces
Wim van den Bouwhuijsen

nr 293
Neighborhood Environment and Physical Activity of Older Adults
Zhengying Liu

nr 294
Practical and continuous luminance distribution measurements for lighting quality
Thijs Willem Kruisselbrink

nr 295
Auditory Distraction in Open-Plan Study Environments in Higher Education
Pieternella Elizabeth Braat-Eggen

nr 296
Exploring the effect of the sound environment on nurses' task performance: an applied approach focusing on prospective memory
Jikke Reinten

nr 297
Design and performance of water resistant cementitious materials– Mechanisms, evaluation and applications
Zhengyao Qu

nr 298
Design Optimization of Seasonal Thermal Energy Storage Integrated District Heating and Cooling System: A Modeling and Simulation Approach
Luyi Xu

nr 299
Land use and transport: Integrated approaches for planning and management
Zhongqi Wang

nr 300
Multi-disciplinary optimization of building spatial designs: co-evolutionary design process simulations, evolutionary algorithms, hybrid approaches
Sjonnie Boonstra

nr 301
Modeling the spatial and temporal relation between urban land use, temperature, and energy demand
Hung-Chu Chen

nr 302
Seismic retrofitting of masonry walls with flexible deep mounted CFRP strips
Ömer Serhat Türkmen

nr 303
Coupled Aerostructural Shape and Topology Optimization of Horizontal-Axis Wind Turbine Rotor Blades
Zhijun Wang

nr 304
Valorization of Recycled Waste Glass and Converter Steel Slag as Ingredients for Building Materials: Hydration and Carbonation Studies
Gang Liu

nr 305
Low-Carbon City Development based on Land Use Planning
Gengzhe Wang

nr 306
Sustainable energy transition scenario analysis for buildings and neighborhoods - Data driven optimization
Shalika Saubhagya Wickramarachchi Walker

nr 307
In-between living and manufactured: an exploratory study on biobuilding components for building design
Berrak Kirbas Akyurek

nr 308
Development of alternative cementitious binders and functionalized materials: design, performance and durability
Anna Monika Kaja

nr 309
Development a morphological approach for interactive kinetic façade design: Improving multiple occupants' visual comfort
Seyed Morteza Hosseini

nr 310
PV in urban context: modeling and simulation strategies for analyzing the performance of shaded PV systems
Ádám Bognár

nr 311
Life Trajectory, Household Car Ownership Dynamics and Home Renewable Energy Equipment Adoption
Gaofeng Gu

nr 312
Impact of Street-Scale Built Environment on Walking/Cycling around Metro Stations
Yanan Liu

nr 313
Advances in Urban Traffic Network Equilibrium Models and Algorithms
Dong Wang

nr 314
Development of an uncertainty analysis framework for model-based consequential life cycle assessment: application to activity-based modelling and life cycle assessment of multimodal mobility
Paul Martin Baustert

nr 315
Variable stiffness and damping structural joints for semi-active vibration control
Qinyu Wang

nr 316
Understanding Carsharing-Facilitating Neighborhood Preferences
Juan Wang

nr 317
Dynamic alignment of Corporate Real Estate to business strategies: An empirical analysis using historical data and in-depth modelling of decision making
Howard Cooke

nr 318
Local People Matter: Towards participatory governance of cultural heritage in China
Ji Li

nr 319
Walkability and Walkable Healthy Neighborhoods
Bojing Liao

nr 320
Light directionality in design of healthy offices: exploration of two methods
Parisa Khademagha

nr 321
Room acoustic modeling with the time-domain discontinuous Galerkin method
Huiqing Wang

nr 322
Sustainable insulating lightweight materials for enhancing indoor building performance: miscanthus, aerogel and nano-silica
Yuxuan Chen

nr 323
Computational analysis of the impact of façade geometrical details on wind flow and pollutant dispersion
Xing Zheng

nr 324
Analysis of urban wind energy potential around high-rise buildings in close proximity using computational fluid dynamics
Yu-Hsuan Jang

nr 325
A new approach to automated energy performance and fault detection and diagnosis of HVAC systems: Development of the 4S3F method
Arie Taal

nr 326
Innovative Admixtures for Modifying Viscosity and Volume Change of Cement Composites
Hossein Karimi

nr 327
Towards houses with low grid dependency: A simulation-based design optimization approach
Zahra Mohammadi

The world's energy systems are experiencing a transition towards increased renewable integration. As renewable energy generation (such as wind and solar) fluctuates, energy systems require possibilities to enable flexible operations in power supply and demand. On the demand side, it is required that building energy-management systems adapt the energy consumption to fluctuations in supply – the so-called demand response and demand-side management. One of the greatest challenges of demand-side management is the activation of flexibility resources that depend on the availability of flexibility potentials, the technical implementation and control of flexibility, and market penetration of flexibility services.

This thesis demonstrated the activation of buildings' demand flexibility in real-time power markets through experimental investigations. To activate demand flexibility, optimal control methods were developed and tested for building heating systems including power-to-heat and thermal energy storage. An optimal controller was introduced, which was a Model Predictive Control framework that implemented predictions of time-varying dynamics of building and heating systems, weather forecasting and grid signal support. This made it possible to apply innovative control methods and flexibility services that enable optimal control of buildings' demand flexibility.

DEPARTMENT OF THE BUILT ENVIRONMENT

TU/e EINDHOVEN UNIVERSITY OF TECHNOLOGY